Optimising Prostate Radiation Using Magnetic Resonance Imaging and Hypoxia Biomarkers

Jim Zhong

Submitted in accordance with the requirements for the degree of Doctor of Philosophy

The University of Leeds
Leeds Institute of Medical Research

September 2023

The candidate confirms that the work submitted is his own, except where work which has formed part of jointly-authored publications has been included. The contribution of the candidate and the other authors to this work has been explicitly indicated below. The candidate confirms that appropriate credit has been given within the thesis where reference has been made to the work of others.

The following joint publications have been written as a result of the work in this thesis:

i) Zhong J, Frood R, McWilliam A, Davey A, Shortall J, Swinton M, Hulson O, West CM, Buckley D, Brown S, Choudhury A, Hoskin P, Henry A, Scarsbrook A. Prediction of prostate tumour hypoxia using pre-treatment MRI-derived radiomics: preliminary findings. Radiol Med. 128(6):765-774.

Contribution: J Zhong was responsible for the study design, image segmentation, prediction model creation, data analysis, literature search, manuscript preparation and submission.

Contribution of other authors: A Scarsbrook was the lead supervisor on this study. R Frood contributed to the model creation. A McWilliam, A Davey, J Shortall, M Swinton, O Hulson, CM West, D Buckley, S Brown, A Choudhury, P Hoskin and A Henry all reviewed the manuscript and provided comments

ii) Zhong J, Slevin F, Scarsbrook AF, Serra M, Choudhury A, Hoskin PJ, Brown S, Henry AM. Salvage Reirradiation Options for Locally Recurrent Prostate Cancer: A Systematic Review. Front Oncol. 11:681448.

Contribution: J Zhong was responsible for the creation of the review question, design, literature search, data extraction and analysis and writing of the manuscript

Contribution of other authors: A Henry was lead supervisor. F Slevin was the second author reviewing the literature. AF Scarsbrook, A Henry, M Serra, A Choudhury A, PJ Hoskin and S Brown all reviewed the manuscript and provided comments

iii) Zhong J, Brown S, Serra M, Shuttleworth P, Bownes P, Thompson C, Reed R, Reeves K, Dubec M, McHugh D, Eccles C, Chuter R, Tsang YM, Taylor NJ, West C, Buckley D, Scarsbrook A, Choudhury A, Hoskin P, Henry A. Reirradiation Options

for Previously Irradiated Prostate cancer (RO-PIP): Feasibility study investigating toxicity outcomes following reirradiation with stereotactic body radiotherapy (SBRT) versus high-dose-rate brachytherapy (HDR-BT). BMJ Open. 12(11):e068580.

Contribution: J Zhong was responsible for the literature search, study design, ethics application, study set up, data analysis plan, study coordination and patient recruitment.

Contribution of other authors: A Henry was the lead supervisor. S Brown helped with the study trial design. M Serra, P Shuttleworth, P Bownes, C Thompson helped with the radiotherapy treatment protocols. M Dubec, D McHugh, NJ Taylor and D Buckley helped with the imaging substudy design and MRI sequence optimisation. R Reed, K Reeves, C West and A Choudhury helped with the translational substudy design. A Henry, S Brown, M Serra, P Shuttleworth, P Bownes, C Thompson, R Reed, K Reeves, M Dubec, D McHugh, C Eccles, R Chuter, YM Tsang, NJ Taylor, C West, D Buckley, A Scarsbrook, A Choudhury and P Hoskin all reviewed the manuscript and provided comments

Acknowledgements

This doctoral research fellowship was funded by the Cancer Research UK Leeds-Manchester Stella Erdheim Fund (Grant reference 95653117/ 95653118).

I would like to express utmost gratitude to my supervisors Professor Ann Henry, Professor Sarah Brown, Professor Ananya Choudhury, Professor Peter Hoskin, Professor David Buckley, Professor Catharine West, Professor Andrew Scarsbrook for all their support and guidance throughout the fellowship.

I would like to thank Dr Rachel Hyland, Head of School for Radiology Yorkshire, and Dr Hannah Lambie, Training Programme Director at the West Yorkshire Radiology Academy, for supporting my out of programme research during my Radiology training.

I would like to thank Dr Russell Frood, Dr Jane Shortall and Dr Angela Davey for their wisdom, support and friendship.

I would like to dedicate this thesis to my parents for all they have done and their sacrifices so I could have the opportunities today.

Abstract

Despite radiotherapy (RT) being an effective treatment, prostate cancer recurrence is not uncommon, particularly in high-risk disease. A key biological process driving treatment failure is tumour hypoxia which is associated with radiotherapy resistance. Established methods of detecting hypoxia are invasive and not routinely undertaken. Predicting which patients will recur after RT and those more likely to suffer from RT-related side effects is also challenging. Quantitative analysis of routinely acquired prostate magnetic resonance imaging (MRI) data might help to address these existing dilemmas. The choice of the optimal treatment for recurrent prostate cancer remains uncertain and warrants further investigation. The aims of this PhD thesis were to investigate the role of quantitative MRI and hypoxia biomarkers in optimising prostate RT, predicting oncological outcomes and toxicity, and providing further evidence on the efficacy of prostate reirradiation.

The following five studies were undertaken during this PhD: A model to predict prostate tumour hypoxia using pre-treatment MRI-derived radiomics was developed and compared to an established genomic hypoxic signature using a twin-centre retrospective cohort of patients with prostate cancer. The potential utility of an outcome prediction model integrating radiomic and hypoxia information with clinical data for predicting biochemical recurrence free survival (BCRFS) was explored. An exploratory study of bladder and rectum radiomic feature changes following external beam radiation therapy (EBRT) delivered on a magnetic resonance imaging linear accelerator (MRI-LINAC) was undertaken. A systematic review of the evidence for prostate reirradiation in locally recurrent cancer was undertaken. Finally, a prospective trial Reirradiation Options for Previously Irradiated Prostate cancer (RO-PIP) comparing different radiation treatments for recurrent prostate cancer was designed and set-up.

The key findings from this PhD included: Whole prostate MRI-radiomics has the potential to non-invasively predict tumour hypoxia prior to radiotherapy, which may be helpful for individualised treatment optimisation. The addition of pre-treatment MRI-derived radiomic features to clinical variables improved the accuracy of predicting BCRFS after prostate radiotherapy with or without the addition of hypoxia gene signature. A feasible methodology for collecting longitudinal radiomic changes from the bladder and rectum during MRI-LINAC radiotherapy treatments was designed and preliminary results show potential radiomic changes between the EBRT treatment time points. Published literature evaluating salvage reirradiation of radiorecurrent prostate cancer using stereotactic body radiotherapy (SBRT) or high-dose-rate brachytherapy (HDR-BT) reports similar biochemical control and acceptable late toxicity however data

is mainly retrospective and of low quality and prospective randomised trials are needed. The RO-PIP study, a feasibility study investigating toxicity outcomes following reirradiation with SBRT versus HDR-BT is currently open to recruitment.

Pre-treatment MRI-derived radiomic analysis may help reveal underlying biological processes such as tumour hypoxia and in outcome prediction models. Longitudinal evaluation of radiomic feature changes using an MRI-LINAC potentially provides an innovative way of measuring tissue response during radiotherapy treatments. A feasibility study of reirradiation techniques should help inform the design of a future phase 3 trial, which could be driven by MRI biomarkers.

Table of Contents

List of Tables

List of Figures

Abbreviations

ADC	Apparent diffusion coefficient
ADT	Androgen deprivation therapy
AIC	Akaike Information Criterion
ANOVA	Analysis of Variance
BCR	Biochemical recurrence
BCRFS	Biochemical recurrence-free survival
BOLD	Blood oxygenation level–dependent
BT	Brachytherapy
CAPRA	Cancer of the Prostate Risk Assessment
CaPSURE	Cancer of the Prostate Strategic Urologic Research Endeavor
cGAN	Conditional generative adversarial network
CI	Confidence interval
CLAIM	Checklist for Artificial Intelligence in Medical Imaging
CPG	Cambridge Prognostic Group
CT	Computed Tomography
CTgRT	Computed tomography guided radiotherapy
CTV	Clinical target volume
DCE	Dynamic contrast-enhanced
DMFS	Distant metastasis free survival
DWI	Diffusion-weighted imaging
EBRT	External beam radiation therapy
FFPE	Formalin-fixed paraffin-embedded
GI	Gastrointestinal
GLCM	Grey level co-occurrence matrix

GLDM	Grey level dependence matrix
GLRLM	Grey level run length matrix
GLSZM	Grey level size zone matrix
GTV	Gross tumour volume
GU	Genitourinary
Gy	Gray
HDR	High Dose-Rate
HIF	Hypoxia-inducible factor
HIFU	High-intensity focused ultrasound
IB	Imaging biomarker
IBSI	Image biomarker standardisation initiative
ICC	Intraclass correlation coefficient
ISUP	International Society of Urological Pathology
IVIM	Intravoxel incoherent motion
LAE	Large Area Emphasis
LASSO	Least absolute shrinkage and selection operator
LINAC	Linear accelerator
MCC	Maximal correlation coefficient
MRIgRT	MRI-guided radiotherapy
MRMR	Minimum redundancy maximum relevance
NCCN	National Comprehensive Cancer Network
NICE	National Institute for Health and Care Excellence
NIfTI	Neuroimaging Informatics Technology Initiative
NPV	Negative predictive value
OAR	Organs at risk
PCSM	Prostate cancer-specific mortality

PET	Positron emission tomography
PI-RADS	Prostate Imaging–Reporting and Data System
PPV	Positive predictive value
PROM	Patient reported outcome measure
PSA	Prostate specific antigen
PSMA	Prostate-specific membrane antigen
PTV	Planned treatment volume
PZ	Peripheral zone
RF	Radiomic feature
RFo	Random forest
ROC	Receiver operating characteristic
ROI	Region of interest
RT	Radiation therapy
SABR	Stereotactic Ablative Body Radiotherapy
SBRT	Stereotactic Body Radiation Therapy
SCV	Stratified cross-validation
T2W	T2-weighted
TZ	Transition zone
UK	United Kingdom
USA	United States of America
VEGF	Vascular endothelial growth factor

Chapter 1
Introduction

1.1 Prostate Cancer

Prostate cancer is the most common malignancy in males in the United Kingdom (UK) with approximately 48,500 new diagnoses every year, and the incidence has increased over the last decade [1]. Worldwide, prostate cancer accounts for over 1.4 million new cases per year and causes over 375,000 deaths (3.8% of all deaths caused by cancer in men) [2,3]. Prostate cancer is the most frequently diagnosed cancer in 112 countries, and the leading cause of cancer death in 48 countries [4].

1.1.1 Prostate Cancer Grading Systems

The Gleason grading system, developed by Dr. Donald Gleason in the 1960s, has become the standard method for grading of prostate cancer [5]. It is used to evaluate the aggressiveness of prostate cancer based on the microscopic appearance of tumour tissue and assigns a grade ranging from 1 (least aggressive) to 5 (most aggressive) to different areas within the prostate gland. The most common and second most common patterns are added together to give a Gleason score, ranging from 2 to 10. A higher Gleason score indicates a higher likelihood of aggressive behaviour and a poorer prognosis.

Over the past 40 years, the histologic and clinical diagnosis as well as the treatment of prostate cancer (PCa) have advanced, resulting in revisions to the Gleason grading system in 2005 and further updates in 2014 by the International Society of Urological Pathology (ISUP) [6,7]. The current Gleason grading significantly deviates from the original system as scores 2–5 are no longer used, and some patterns previously categorised as a score of 6 are now classified as 7. Consequently, contemporary Gleason score 6 cancers have a more favourable prognosis compared to historical score 6 cancers.

The ISUP endorsed grading system limits the number of prostate cancer grades, ranging them from 1 to 5 by grouping different Gleason grades together (see Table 1.1).

Table 1.1 International Society of Urological Pathology (ISUP) grading (group) system.

Gleason score	ISUP Grade
2-6	1
7 (3+4)	2
7 (4+3)	3
8 (4+4 or 3+5 or 5+3)	4
9-10 (4+5 or 5+4 or 5+5)	5

1.1.2 Clinically significant Prostate Cancer and risk stratification

The term "clinically significant" is used to distinguish prostate cancer that poses a risk of morbidity or mortality in a particular patient from types of cancer that do not. This differentiation is crucial, because insignificant prostate cancer does not cause harm but remains very common and there is a risk of over-treatment, exposing patients to potentially harmful side effects [8,9].

Pathological factors are often utilised to define insignificant cancer. ISUP grade 1 disease is considered clinically insignificant and associated with a low risk of developing metastasis and disease-specific death [10]. Clinically significant cancer can be considered as ISUP grade group 2 and above.

At diagnosis patients in the UK are categorised into risk categories using the National Institute for Health and Care Excellence (NICE) risk stratification and more recently, the Cambridge Prognostic Groups (CPG) classification[11]. These classification systems, like the National Comprehensive Cancer Network (NCCN) guidelines for staging prostate cancer used in the US, help to guide treatment decisions by providing prognostic information about the risk of cancer progression (Table 1.2) [11,12].

It remains important to consider other factors, including patient preference, pre-existing symptoms, co-morbidity, and increasing age when deciding the most appropriate management strategy. ISUP grade 1, T1-2a and PSA$<$ 10 represents low-risk prostate cancer and the recommended management is active surveillance (AS). Active treatment with either surgery or radiotherapy benefits patients with intermediate- or high-risk prostate cancer and at least 10-year life expectancy. Radiotherapy is preferred in older patients and those with co-morbidity. For those undergoing radiotherapy, additional androgen deprivation is also recommended, 6 months in intermediate risk disease and

Table 1.2 Patient characteristics of men diagnosed with non-metastatic prostate cancer according to the NICE three-tiered risk stratification (2) and the Cambridge Prognostic Group classification (CPG) (4). Abbreviations: PSA = prostate specific antigen; T = tumour stage.

NICE risk group	Criteria	CPG Category	Criteria
Low-risk disease	Gleason score ≤ 6 *AND* PSA < 10 ng/ml *AND* stages T1-T2a	1	Gleason score 6 (Grade Group 1) *AND* PSA < 10 ng/ml *AND* stages T1-T2a
Intermediate-risk disease	Gleason score ≤ 6 **OR** PSA 10-20 ng/ml **OR** Stage T2b	2	Gleason score 3+4=7 (Grade Group 2) **OR** PSA 10-20 ng/ml *AND* Stage T1-T2
		3	Gleason score 3+4=7 (Grade Group 2) *AND* PSA 10-20 ng/ml *AND* Stage T1-T2 **OR** Gleason score 4+3=7 (Grade Group 3) *AND* stages T1-T2
High-risk or locally advanced disease	Gleason score 8-10 **OR** PSA > 20 ng/ml **OR** Stage ≥ T2c	4	**One of:** Gleason score 8 (Grade Group 4) **OR** PSA > 20 ng/ml **OR** Stage T3
		5	**Any Combination of:** Gleason score 8 (Grade Group 4), PSA > 20 ng/ml or Stage T3 **OR** Gleason score 9-10 (Grade Group 5) **OR** Stage T4

2-3 years in high-risk or locally advanced disease. Watchful waiting, where androgen deprivation is commenced if the patient is symptomatic, is offered to patients with co-morbidity and/or frailty likely to result in less than 5-year overall life expectancy [13].

1.1.3 Radiation Therapy

Radiation therapy (RT) is an effective curative treatment for localised and locally advanced non-metastatic prostate cancer. RT can be delivered in two ways: External beam RT (EBRT, where the radiation source is located outside the body), and brachytherapy (BT, where a sealed radioactive source is placed inside the body). EBRT is delivered using a linear accelerator (LINAC) machine, which generates a therapeutic X-ray beam and directs it to the desired target. BT involves placement of radioactive source(s) directly inside the prostate. Due to the physical properties of the radioactive sources (sharp drop off in dose over millimetres) and better certainty in dose delivery, it provides a highly conformal method to deliver high radiation dose to the tumour. Sparing of surrounding normal organs in brachytherapy is ensured by choosing an isotope which generates high radiation energy with limited tissue penetration [14]. These sources can be placed either permanently or temporarily, using appropriate applicators. Improving the efficacy of RT entails maximising the dose to target volumes while minimising the amount of normal tissue irradiated. This is directly affected by the imaging technique used during RT planning and treatment. Enhanced visibility of tumour by functional imaging methods such as magnetic resonance imaging (MRI) and positron emission tomography computed tomography (PET-CT) aids in more accurate delineation of gross tumour volume (GTV). MRI offers superior soft-tissue contrast compared to standard CT imaging and enables more accurate delineation of the tumour target and organs at risk during RT planning (Figure 1.1). The normal anatomy of the prostate gland is shown in Figure 1.2.

Incorporation of imaging on modern LINACs allows verification of target volume before beam delivery, resulting in more precise irradiation and smaller planned treatment volume (PTV) margins (Figure 1.3). Consequent sparing of normal tissues leads to reduction in RT-related morbidity [15]. Another advantage with improved reliability of tumour targeting is the use of hypofractionated RT, whereby larger dose per fraction can be safely delivered using fewer fractions. Such treatment delivered to a highly conformal target volume with a steep dose gradient in a small number of fractions, is referred to as Stereotactic Ablative Body Radiotherapy (SABR). Novel MRI-guided linear accelerator (MRI-LINAC) systems combine MRI with a LINAC for irradiation and offers real-time adaptive treatment opportunities to further optimise RT delivery [16].

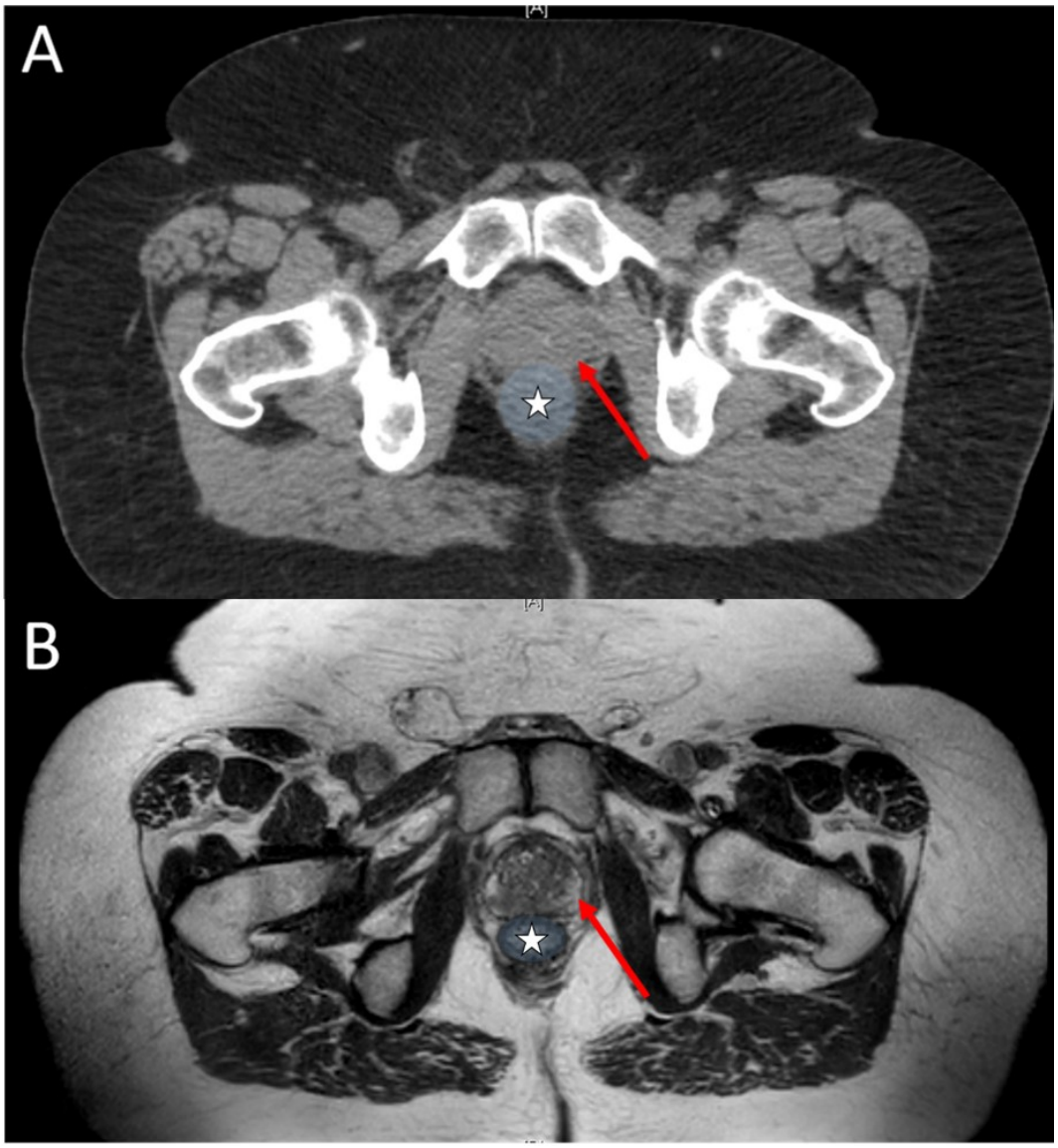

Figure 1.1 A case of prostate cancer treated with radiotherapy showing the standard non-contrast RT planning CT (A) and an axial T2-weighted (T2W) MRI image acquired on an MRI LINAC (B) showing the prostate (red arrow) and rectum (blue circle and star). The tissue boundaries are much clearer on MRI, which allows for a more accurate RT contouring, particularly when highlighting the posterior border of the prostate, which contacts the rectum.

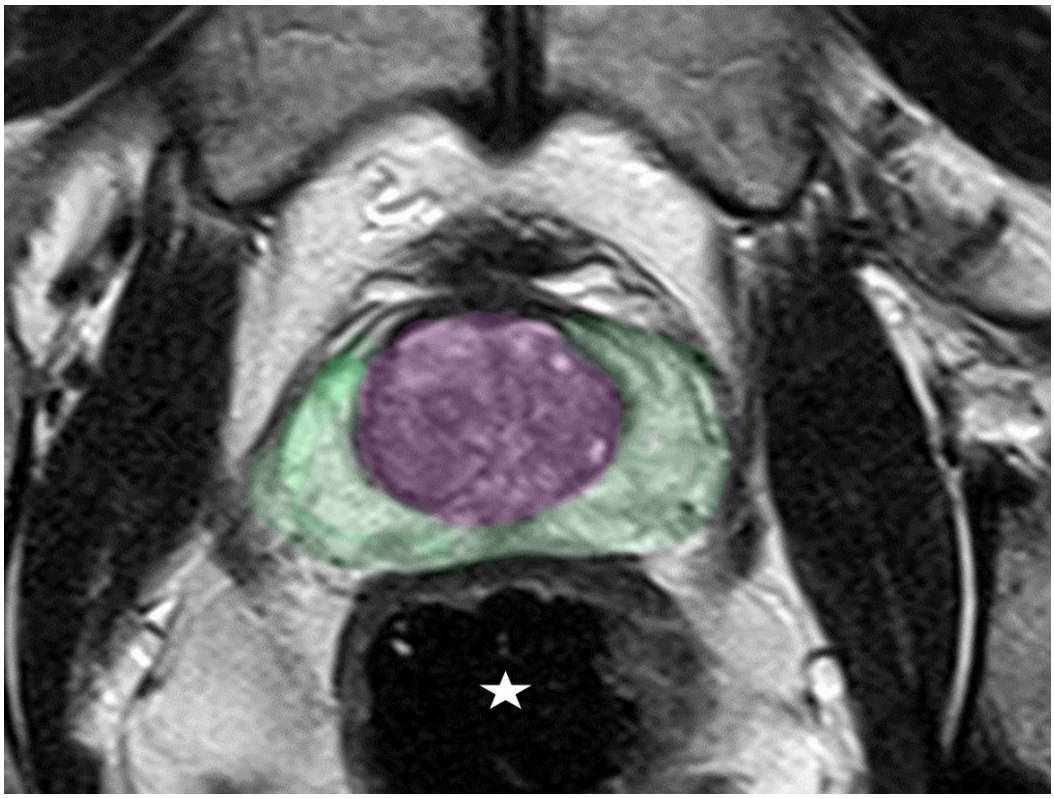

Figure 1.2 Close-up and cropped Axial T2W MRI of a prostate showing the normal anatomy of the peripheral zone (green area), transition zone (purple area) and rectum (star).

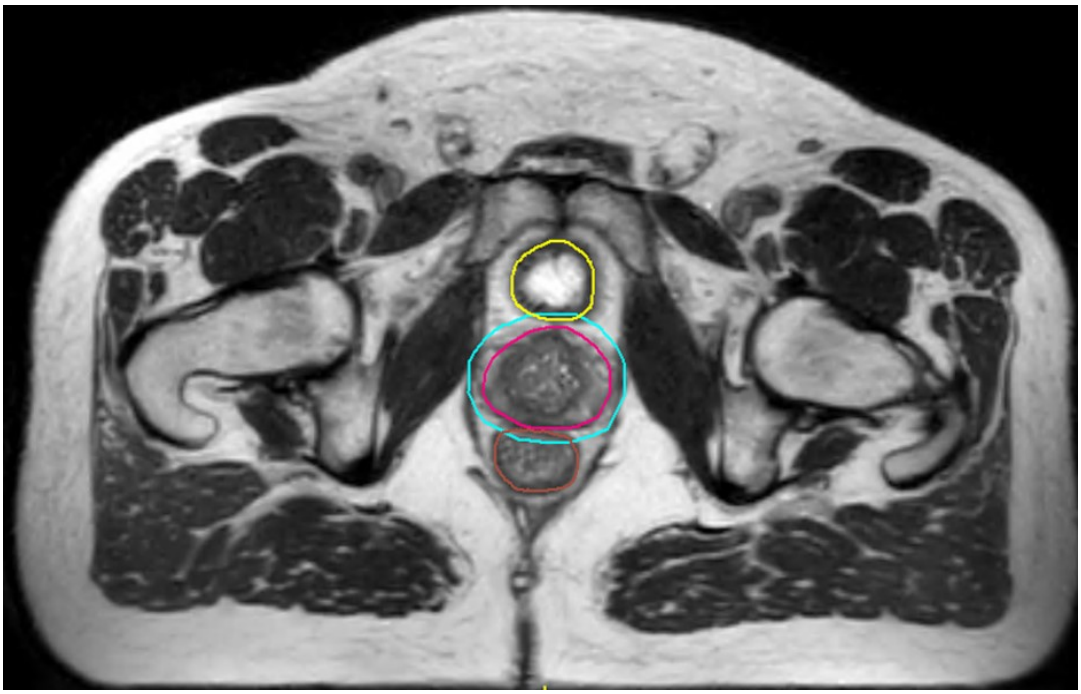

[h]

Figure 1.3 Axial T2W MRI images acquired from the MRI-LINAC showing the clinical target volume (CTV) (pink) which is the prostate gland and any extraprostatic tumour extension, the surrounding planning target volume (PTV) (blue) which is determined by adding a fixed margin to the CTV to account for internal target volume and patient motion. The surrounding organs at risk (OAR), the bladder (yellow) and rectum (brown) are also demarcated.

1.1.4 Biomarkers in Prostate Cancer

A biomarker can be defined as a characteristic that is measured as an indicator of a normal physiological or pathological process or a response to an exposure or intervention [17,18]. Traditionally, biomarkers were biological molecules however with imaging, this offers a further metric that can be measured longitudinally. Few biomarkers have yet to be incorporated into standard clinical practices in order to guide treatment decisions given the rigorous testing and external validation required to show definitive real-life improvements in healthcare with important endpoints such as survival and cost effectiveness [19–22].

Distinguishing between a prognostic and predictive biomarker is paramount. Prognostic biomarkers provide information on the overall patient outcome e.g. survival length or recurrence, irrespective of what treatment they receive. The presence or absence of a prognostic biomarker can aid patient selection for treatment intensification or de-escalation, however it would not predict the response to this treatment. A predictive biomarker on the other hand gives information on the effect of a therapeutic intervention for a patient, which can also be used for patient or treatment selection [23].

A framework for imaging biomarker (IB) validation and qualification was designed by a consensus panel of experts as part of the Imaging Biomarker Roadmap for Cancer Studies in order to accelerate the clinical translation of effective IBs [24].

Prostate cancer biomarkers can be used for diagnosis, risk stratification or treatment response assessment. Such 'biomarkers' may be serum-based, urine-based, tissue-based, imaging markers or risk assessment tools [25,26]. Current established biomarkers include serum prostate specific antigen (PSA) and Gleason grading of biopsy specimens. Risk factors and markers for biochemical recurrence (BCR) following radical radiotherapy include initial tumour stage, PSA value, and pathological Grade group [27,28]. Serum PSA level, a measure of tumour burden, has been widely used to predict prostate cancer incidence among asymptomatic men as well as assessing disease relapse in patients after surgery [29]. Following radiotherapy, where the prostate remains intact, the clinical significance of PSA dynamics is less clear as rising PSA levels could be due to infection/inflammation, recovering normal prostatic tissue, cancer relapse, or a combination of these [30]. Some patients will have a temporary PSA increase followed by spontaneous reduction to the nadir level, the absolute lowest level that the PSA will drop following treatment. This 'PSA bounce' has been associated with better prognosis [31]. It has been postulated this may be secondary to tumour–immune cell dynamics [32]. Imaging therefore has a central role in the problem-solving required in such cases. Given the complex and heterogeneous nature of prostate cancer, a combination of biological and imaging biomarkers may be necessary to guide personalised treatment strategies in order to maximise clinical benefit for patients.

Prostate cancer patients with the same histological and clinical parameters may still have different clinical presentations, molecular profiles, and clinical outcomes. More specific biomarkers are required to identify the patient subsets that may benefit from alternate treatment approaches. Adding genomic markers in combination with clinical and pathological variables could potentially reduce the number of unnecessary biopsies, more accurately stratify low-risk and high-risk tumours and guide personalised treatment decisions but is not yet in widespread clinical use. Large multicentre studies are required to validate their efficacy and cost effectiveness [33].

1.1.5 Treatment Failure

Despite advances in diagnostic imaging, radiotherapy delivery techniques and dose-escalated radiation, treatment failure remains common [34,35]. Over 50% of men with high-risk prostate cancer will develop BCR after EBRT during extended follow-up

of 10-15 years [36]. The definition of BCR after radiotherapy is based on the Phoenix criteria which requires an increase in PSA of at least 2 ng/ml above the post-radiation PSA nadir (the absolute lowest level that the PSA drops after treatment) [37]. In a study of almost 2000 patients with localised prostate cancer, treatment with radiotherapy alone, resulted in an overall survival at 10-years of 57%, which increased to 62% with the addition of 4 months of short-term androgen deprivation therapy (ADT) [38]. Further follow-up of this cohort however demonstrated that the overall survival at approximately 15 years was the same for these two treatment groups at 23% demonstrating that, for the majority, overall survival is driven by deaths from non-prostate cancer causes [39]. Following dose-escalated radiotherapy, the most common site of clinically detectable recurrence is within the prostate itself at the site of the index lesion and the 8-year cumulative incidence of local recurrence of 3.5%, 9.8%, and 14.6% in low, intermediate, and high-risk prostate cancer groups respectively [35]. Older patients and/or those with co-morbidity may be managed with observation only or androgen deprivation therapy. Local recurrence after radiotherapy is amenable to further salvage treatments which are potentially curative however only 15-20% of men undergo local salvage therapy according to the Cancer of the Prostate Strategic Urologic Research Endeavor (CaPSURE) registry [40].

The evidence behind the management of local recurrence after definitive radiotherapy is limited mainly to case-series, and remains controversial with few consensus recommendations [41]. A meta-analysis of six randomized trials found that local failure after radiotherapy for high-grade prostate cancer was significantly associated with overall survival, prostate cancer-specific survival, and distant metastasis-free survival, therefore, some patients with isolated local recurrence may benefit from local salvage treatment [42]. Two systematic reviews evaluating all salvage therapies found higher biochemical control rates for reirradiation treatments (BT and EBRT) compared to surgical and other non-surgical local therapies (high intensity focused ultrasound (HIFU) and cryotherapy) along with potentially lower genitourinary (GU) toxicity [43,44]. As part of this thesis, a focused systematic review was conducted to identify the reirradiation modality that offers the best balance of prostate cancer control and toxicity. More advanced imaging techniques such as prostate-specific membrane antigen positron emission tomography – computed tomography (PSMA PET-CT), aid in salvage treatment selection by identifying non-local failures more confidently so only true isolated local recurrences are treated [45].

Following EBRT, the median time from biochemical failure to disease metastasis was 5.4 years and from biochemical failure to prostate cancer-specific mortality (PCSM) of

10.5 years [36]. Independent predictors for clinical progression after biochemical failure were shorter post-treatment PSA doubling time, higher initial tumour stage (T3b or T4), higher pre-treatment Gleason score (score of 8-10), and a shorter interval from end of radiotherapy to biochemical failure, where an interval of less than 3 years was associated with increased rate of disease metastasis and PCSM [36]. These clinical and biochemical factors may be surrogates for underlying genomic and epigenomic aberrations which could drive the cancer's progression. Further understanding the biology of prostate cancer progression will improve the ability to predict clinical outcomes following treatment and enable potential interventions to improve patient outcomes.

1.1.6 Hypoxia in Prostate Cancer

Hypoxia, defined as poor oxygenation, within solid tumours is associated with poor local control and early biochemical and local recurrence in prostate cancer [46–48]. Hypoxia is a feature of many tumours and is involved in the modulation of clinical behaviour and treatment response, mediated via genomic and molecular changes that promote tumour aggressiveness and metastatic spread [49]. The rapid proliferation of cancer cells without sufficient neo-vascularisation induces a state of tumour hypoxia [50]. Hypoxia plays a particularly key role in prostate cancer cells which are metabolically dependent on enhanced glucose transport and glycolysis for expansion therefore reliant on neovascularisation to enable diffusion of oxygen and glucose [51,52]. There are two types of tumour hypoxia, chronic and acute, which highlight the complexity and dynamic changes in oxygenation that occur within tumours [53]. Chronic or diffusion-limited hypoxia is due to the oxygen diffusion distance, which affects cells that do not have access to a blood vessel within approximately 100 micrometres. Acute or perfusion-limited hypoxia is caused by temporary blood flow changes.

Hypoxia-inducible factors (HIFs) are critical mediators of cellular response to hypoxia, for example HIF-1 which remains central in controlling the upregulation and expression of genes encoding proteins involved in angiogenesis, erythropoiesis, energy metabolism, cell growth, and survival influencing the intratumoural hypoxia state [54]. Furthermore, hypoxia may cause biological resistance to radiotherapy due to the lack of oxygen [55,56]. Radiation causes DNA strand breaks which are caused by reactive oxygen species following water radiolysis and this induces tumour cell death[57]. In a hypoxic environment, formation of these reactive oxygen species is however limited and tumour cells are also able to remove hydrogen from free sulfhydryl groups and can repair DNA damage [58].

In the primary treatment setting for prostate cancer with radiotherapy, angiogenic and hypoxia biomarkers have been found to be predictive of biochemical relapse free survival (BRFS) and distant metastasis free survival (DMFS) [59]. The increased expression of intrinsic markers of tumour hypoxia and angiogenesis, such as HIF-1 and vascular endothelial growth factor (VEGF) in localised prostate cancer have been shown in two separate large randomised control trial cohorts to predict biochemical failure, independent of tumour stage, Gleason score and initial PSA level [60].

Developing transcriptomic and/or imaging hypoxia biomarkers would help stratify patients according to the degree of tumour hypoxia, potentially offer adapted or intensified radiotherapy schedules and help monitor their response to therapy. Several hypoxia-associated gene signatures for prostate cancer have been shown to be of independent prognostic value for prostate cancer patients [61,62]. The effect of radiotherapy on these genomic signatures has not been studied therefore the role of it in the salvage treatment setting remains unclear. Ionising radiation has already been found to cause distinctive mutational genomic signatures and has a role in the development of second malignancies from within a treated radiotherapy field [63]. In a study of 190 paired primary and recurrent and over 3000 post-treatment metastatic brain tumours, a high radiation-associated deletion burden was associated with worse clinical outcomes, suggesting that effective repair of radiation-induced DNA damage was also detrimental to patient survival. This highlights the importance of studying the impact of radiotherapy on prognostic genomic signatures in prostate cancer as identifying these changes could help with predicting response to treatment for recurrent cancer [64].

1.1.7 Prostate Magnetic Resonance Imaging

Multiparametric MRI (mpMRI) is central to the detection, and assessment of prostate cancer [65]. Imaging protocols typically include T1-weighted (T1W) and T2-weighted (T2W) anatomical sequences along with functional sequences, particularly diffusion-weighted imaging (DWI) and dynamic contrast-enhanced MRI (DCE-MRI) mpMRI is routinely used before prostate biopsy in the work-up for a patient with elevated PSA following recommendations from international guidelines [66]. The Prostate Imaging–Reporting and Data System (PI-RADS) was designed to help standardise prostate imaging and reduce variation in the prostate MRI acquisition, interpretation, and reporting [67]. The most recent version of PI-RADS is version 2.1 and Figure 1.4 summarises the key differentiating MRI features for each of the PI-RADS categories based on the location of the lesion (Peripheral zone vs Transition zone), and appearances on each sequence (T2W, DWI and DCE-MRI).

For the peripheral zone (PZ), the DWI/ apparent diffusion coefficient (ADC) is the primary determining sequence (dominant technique) to assign the PI-RADS category. Whereas for the transition zone (TZ), the T2W imaging is the primary determining sequence (dominant technique) to assign the PI-RADS assessment category. For TZ lesions, the overall PI-RADS assessment usually follows the T2W score, but scores of 2 or 3 can be upgraded by the DWI sequence if the DWI score is two higher (i.e. 4 or 5, respectively) as this would upgrade the overall PI-RADS assessment by one further point (i.e. from 2 to 3 or 3 to 4, respectively). For PZ lesions which have a DWI score of 3, the presence of dynamic contrast enhancement further upgrades the PI-RADS assessment category to 4. This means the DCE sequences show ALL the following findings: (1) focal enhancement, (2) earlier than or contemporaneous with enhancement of adjacent normal prostatic tissues, (3) enhancement corresponds to a suspicious finding on T2W and/or DWI sequence [67]. In terms of the clinical relevance of using PI-RADS scoring for identifying clinically significant cancer, a recent systematic review by Oerther et al. reported the following cancer detection rates for each PI-RADS group: PI-RADS 1 = 6%, PI-RADS 2 = 9%, PI-RADS 3 = 16%, PI-RADS 4 = 59%, PI-RADS 5 = 85%.

DWI-MRI is a functional imaging technique where image contrast depends on the magnitude and direction of water molecules' Brownian motion in tissue. As this motion is influenced by cellular structures such as cell membranes, the technique provides a non-invasive probe of tissue microstructure. DWI-MRI is often interpreted in terms of cell density, for example with higher cellular density in tumours leading to hindered/restricted diffusion compared with normal, less cellular, tissue. Such hindered/ restricted diffusion results in higher signal intensity on DWI sequences, corresponding to a lower apparent diffusion coefficient (ADC), a quantitative value derived from DWI.

DCE-MRI involves the acquisition of T1W fast spoiled-gradient echo images before, during, and after intravenous injection of a low molecular-weight gadolinium chelate. In tumours, contrast enhancement followed by wash-out tends to occur more rapidly than in normal tissue, reflecting the higher perfusion of the tumour. Pharmacokinetic analysis of DCE-MRI data models the transfer of the contrast agent between the vascular space and the extravascular extracellular space [68]. It generates parameters related to perfusion including the volume transfer constant, Ktrans, and the rate constant, kep, which are associated with tumour response to RT for prostate tumours [69].

Imaging also offers a non-invasive method to image tumour hypoxia [70]. Previous work evaluating the use of MRI to measure tumour hypoxia has highlighted blood oxygenation level–dependent (BOLD) and intravoxel incoherent motion (IVIM) sequences as having

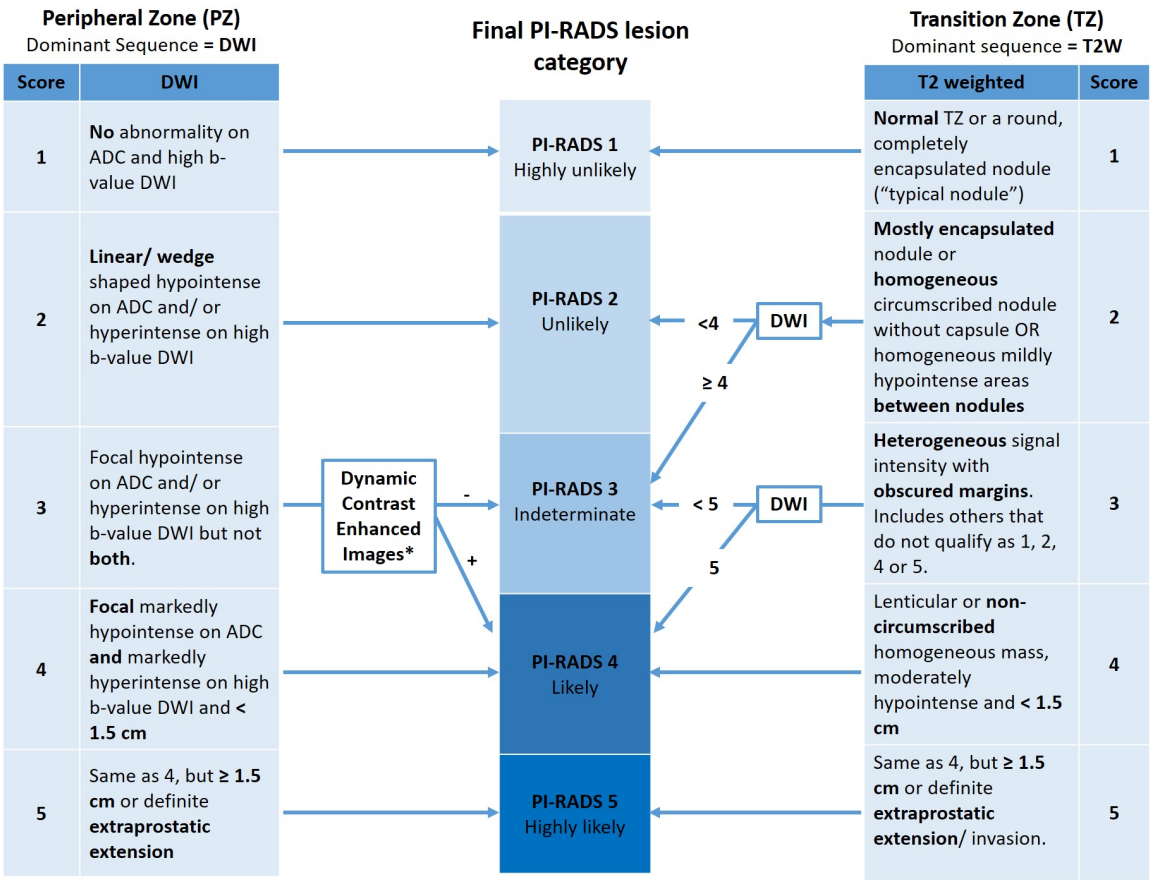

Figure 1.4 PI-RADS version 2.1 schematic summarising key differentiating MRI features for each of the PI-RADS categories (1-5) for both the peripheral zone (PZ) and transition zone (TZ) and a scoring flow chart showing the potential up-scoring or down-scoring based functional imaging. Abbreviations: ADC = apparent diffusion coefficient, DWI = diffusion-weighted imaging, DCE = dynamic contrast-enhanced.

For Dynamic Contrast Enhanced (DCE) Images: (-) means no early or contemporaneous enhancement OR diffuse multifocal enhancement NOT corresponding to a focal finding on T2W and/ or DWI OR focal enhancement corresponding to benign prostatic hypertrophy. (+) means focal AND earlier enhancement AND corresponds to suspicious finding on TWI and/ or DWI imaging.

potential for clinical translation to measure hypoxia specifically in prostate cancer [52,71]. Intrinsic susceptibility weighted or BOLD MRI (R2* biomarker) exploits the difference in magnetic susceptibility of oxyhaemoglobin and deoxyhaemoglobin to generate contrast and identify regions of hypoxia [72,73]. IVIM is a DWI-MRI technique which provides information about tissue perfusion as well as diffusion [74]. By modelling diffusion data with a perfusion component, a surrogate for tissue perfusion can be calculated (perfusion fraction or f). Early increases in f are associated with good response [75], and recent work provides evidence linking IVIM parameters to tumour hypoxia [52].

Prospectively evaluating the use of hypoxia imaging in the setting of clinical trials and research studies is required to help cross the 'translational gaps' through validation and qualification as highlighted by the Imaging Biomarker Roadmap [24]. An example schematic of a hypoxia imaging biomarker (IB) roadmap is shown in Figure 1.5 where the technical, biological and clinical validation of the IB occurs simultaneously and alongside each other. It is important to link the IB with pathophysiology and provide biological validation in order for it to cross the first translational gap. Cost-effectiveness is also a key consideration as it impacts the development of an IB and how realistic it can be incorporated into clinical practice through availability of imaging equipment and the requirement for any specialist personnel. Standard operating procedures (SOPs) are also required to help with setting up IB driven multicentre clinical trials and facilitate more widespread adoption.

1.1.8 Current Clinical Methods of Predicting Recurrence after Radiotherapy

IIn order to predict prostate cancer recurrence following treatment, mathematical models or "nomograms" have been developed to help clinicians make treatment decisions. The D'Amico nomogram used pre-treatment PSA, clinical stage and biopsy Gleason score to categorise patients into three risk categories (low, intermediate and high risk) and found men at high risk of early biochemical failure (within 2 years post-treatment) could be identified [76]. Recently, a new tool called the Candiolo nomogram [77] predicts the risk of biochemical recurrence using five pre-treatment parameters; age, PSA at diagnosis, stage, Gleason score and percentage of biopsy positive cores. This nomogram potentially better identifies patients with high and very high risk disease along with greater numbers of low risk patients compared to D'Amico classification [78]. Similar tools have been employed in assessing biochemical recurrence following prostatectomy, namely the Cancer of the Prostate Risk Assessment (CAPRA) score which integrates additional factors such

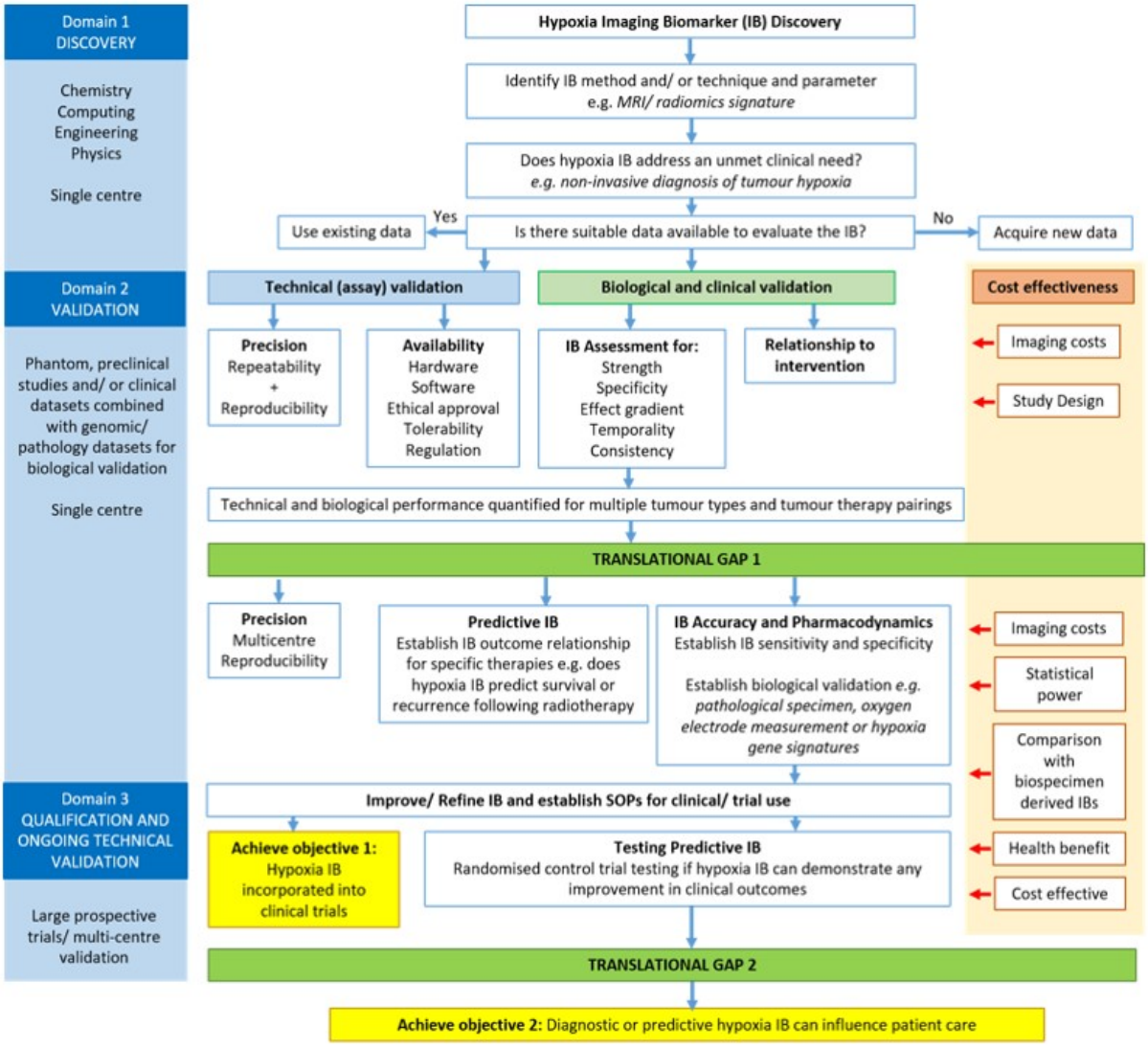

Figure 1.5 Example of a hypoxia imaging biomarker roadmap from discovery to clinical translation (Adapted from the Imaging Biomarker Roadmap [17])

as surgical margin status, extracapsular extension, seminal vesicle invasion, and lymph node involvement [79,80].

In the UK, the 'Predict Prostate' tool is a commonly used and free online tool that can be used for men with non-metastatic prostate cancer to help decide between conservative and radical management regimes based on their unique characteristics [81]. This tool was constructed using a dataset of over 10,000 men with prostate cancer, using Cox regression and fractional polynomial models to build a model able to predict overall survival using routinely collected baseline data about patient and tumour characteristics. This risk prediction model was able to predict overall survival with a high degree of accuracy in a UK validation dataset and a further additional Singaporean dataset of over 2,500 men,

with concordance indices up to 0.84 showing the potential benefit for widespread clinical adoption. The clinical impact of this tool for men regarding perception of disease in terms of uncertainty, anxiety and perception of survival along with their decision making regarding treatment has been evaluated in a randomised control trial, where participants were given standard of care information with or without an additional presentation of the Predict Prostate tool [82]. This study found that the tool was helpful for patients when deciding what treatment to undertake, with 36% of men being less likely to select radical treatment and over half of the men reporting that the tools estimates for prostate cancer-specific mortality being lower than expected.

These prediction models currently fail to account for tumour molecular heterogeneity. In the last decade, there has been increased interest in the utility of genomic signatures for predicting outcomes following treatment, helping with treatment selection and also determining if definitive treatment is required at all [61,83–85]. Imaging also offers a non-invasive method to characterise disease and recently, radiomic features extracted from mpMRI have helped define texture patterns that allow characterisation of tumour phenotypes which may help with prostate cancer stratification [86–89]. To date, few risk prediction tools, either pre- or post-biopsy calculators, have incorporated MRI findings [90–92]. Integrating imaging derived biomarkers into predictive nomograms could help to better prognosticate prostate cancer outcomes. Rayn et al [93] reported that combining mpMRI with clinical nomograms could improve the prediction of adverse pathology at radical prostatectomy which would enable urologists to better counsel patients about the risks of future therapy [93].

A recent study using an integrated nomogram, combining deep learning-based imaging predictions, PI-RADS scoring of prostate MRI scans, along with clinical variables was able to accurately risk stratify patients from their biparametric MRI and identify patients who would benefit from adjuvant therapy [90].

1.1.9 MRI Changes Following Radiotherapy

The European Association of Urology (EAU) prostate cancer guidelines state that imaging should only be performed at biochemical recurrence if the result will affect treatment planning however no general recommendation is made in terms of specific imaging modalities [94]. Specifically in the context of follow-up in men with non-metastatic disease on ADT, the EAU recommends imaging with bone scan and CT when PSA progression suggests Castration-resistant prostate cancer and treatment modification is considered to restage the patient however the diagnostic yield from these

common imaging techniques is low [95]. International clinical guidelines recommend both nuclear medicine imaging (PET-CT) and MRI imaging to assess local and distant metastases [96]. The majority of recurrences following definitive radiotherapy occur locally within the prostate, usually at the original tumour site as previously mentioned, and prostate MRI still has a role in post-treatment evaluation particularly for the assessment of local recurrence and/or pelvic disease however the availability of other imaging techniques such as PSMA PET-CT can offer further information and help clarify the situation of salvageable local disease recurrence by searching for distant metastatic disease in the setting of biochemical failure [97].

A recent narrative review highlighted several studies that found PSMA-PET to be superior to conventional imaging (e.g. CT, bone scintigraphy and MRI) in terms of higher accuracy and sensitivity in localising biochemical recurrences [98]. Most false positive results were within the prostate region which can be due to treated benign tissue or potentially indolent tumour remnants [99]. The ideal time interval from radiotherapy to PSMA-PET to ensure post-treatment changes have settled is still unclear however a minimum interval of 6 months has been suggested [98].

Prostate mpMRI may still have value in characterising any local recurrences given the better spatial resolution however with the background radiotherapy changes to the prostate gland anatomy this can be challenging [35,36,100]. Following radiotherapy (EBRT or BT), the entire prostate appears hypointense on T2W imaging, with loss of prostatic zonal differentiation. Detecting local recurrence on T2W imaging is challenging since tumour is usually hypointense therefore additional DWI +/- DCE sequences are required [101]. On DWI, the signal characteristics of recurrent tumour are similar to the primary setting, with a focal hypointensity on the ADC map and hyperintensity on high b-value imaging corresponding to a nodular area that may be seen on T2W imaging [102]. Similarly, on DCE MRI, recurrent tumour displays early enhancement due to the abnormal vascular network [103]. An example of a post-radiation local recurrence is shown in Figure 1.5.

Following EBRT, the seminal vesicles will atrophy and the muscles appear relatively hyperintense compared to pre-treatment [104,105]. The imaged pelvic bone marrow will also be hypointense on T2W imaging, as a result of sclerosis from the effect of radiation.

Prostate changes following BT are similar, with the addition of the retained radioactive seeds if LDR-BT has been used, which are metallic and appear as low signal foci within the prostate on MRI (Figure 3). Imaging shortly after any type of BT could be subject

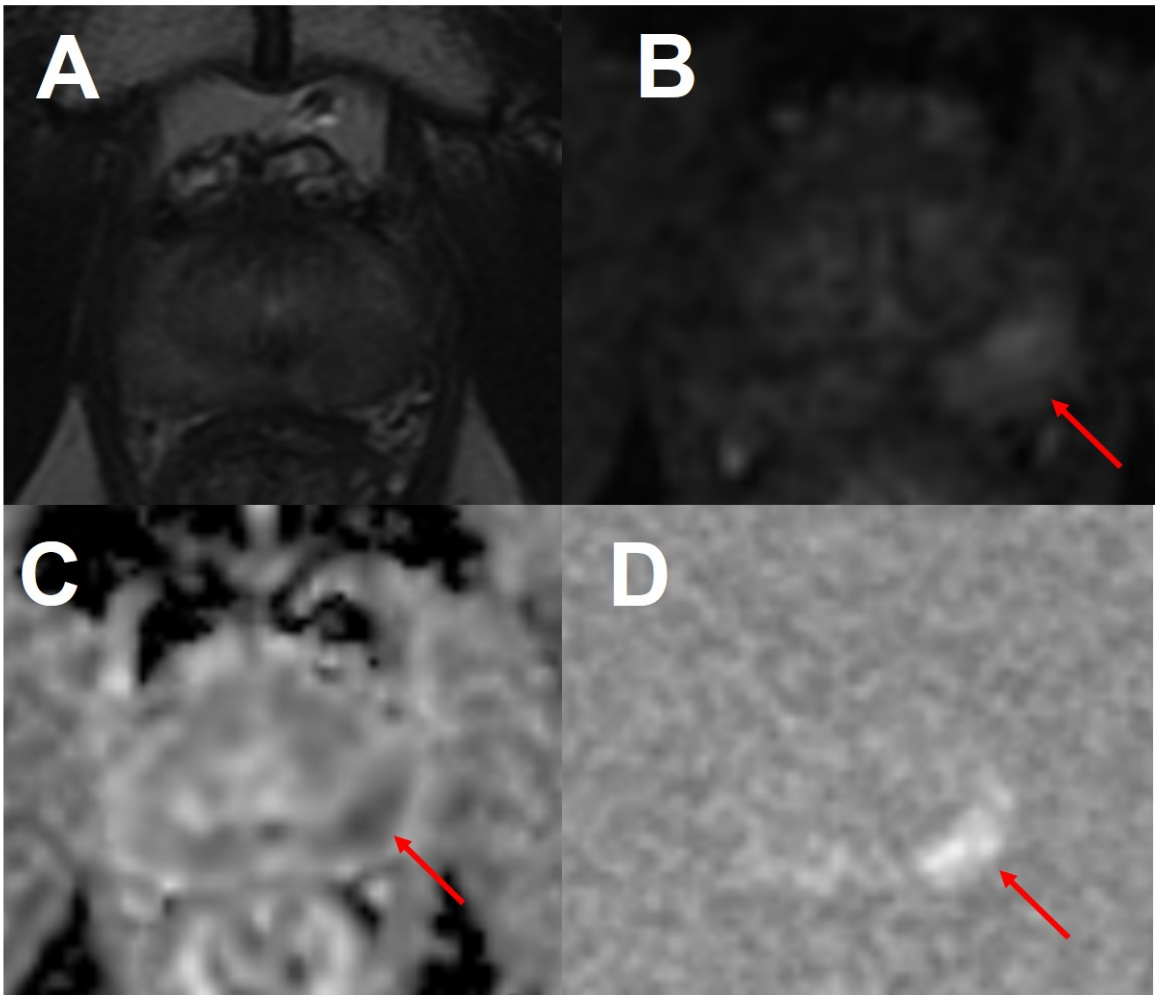

Figure 1.6 Post-EBRT case with local recurrence. (A) T2W sequence showing diffuse T2 hypointensity in the peripheral zone (PZ), with loss of zonal differentiation, consistent with previous radiation treatment. (B) DCE-MRI shows early lenticular enhancement in the left mid PZ region. Hypointense focal area (red arrow) on ADC map (C) corresponding to hyperintense focus on DWI (D) representing true restricted diffusion in the same area of enhancement seen on DCE supportive of residual/recurrent tumour diagnosis. Capsular bulging is present and extra-capsular extension is likely with a close association to the left neurovascular bundle. Images courtesy of Professor Tristan Barrett, University of Cambridge.

to potential diagnostic pitfalls from haemorrhage. In addition to radiation treatment, hormonal therapy also causes prostate atrophy, reduction in gland vascularity and overall reduction in ADC values [106,107].

Despite prostate MRI being accurate for detecting local recurrence after RT, no optimal acquisition and reporting protocols are available and standardisation is needed. Experts from the European Society of Urogenital Radiology, the European Society of Urologic

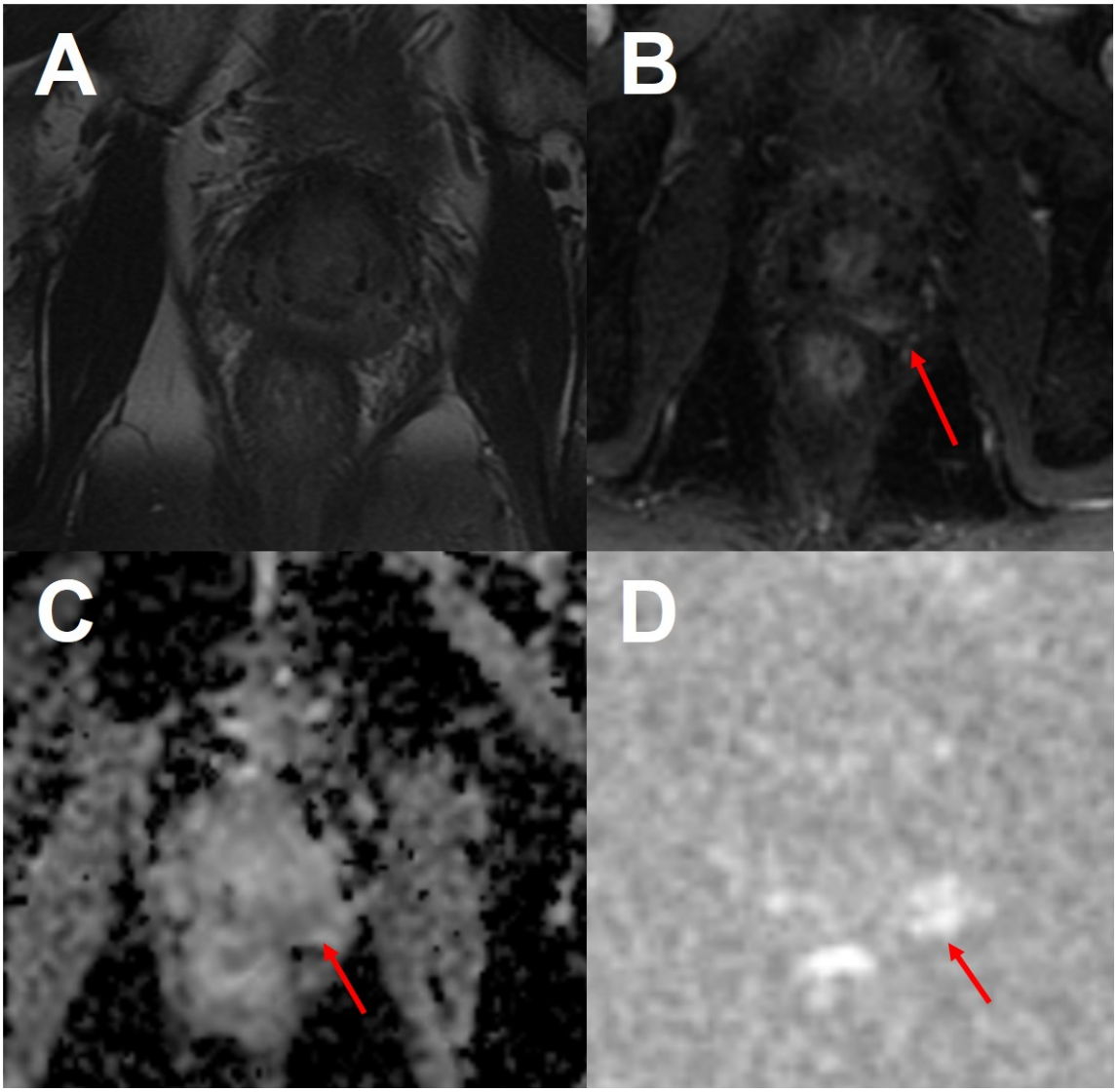

Figure 1.7 Post-brachytherapy case with local recurrence. (A) Artefact noted from brachytherapy seeds with hypointense foci seen throughout the prostate on T2W sequence along with diffuse T2 hypointensity in the peripheral zone (PZ), with loss of zonal differentiation, consistent with previous radiation treatment. (B) DCE-MRI shows early enhancement in the left mid PZ region. Residual hypointense focal area (red arrow) on ADC map (C) corresponding to hyperintense focus on DWI (D) representing true restricted diffusion in the same area of enhancement seen on DCE supportive of residual/recurrent tumour diagnosis. Images courtesy of Professor Tristan Barrett, University of Cambridge.

Imaging, and members of the PI-RADS group established a set of guidelines for MRI to assess local pelvic recurrence of prostate cancer – the Prostate Imaging for Recurrence Reporting (PI-RR) system [108]. Like with PI-RADS, PI-RR combines criteria for TWI, DWI and DCE sequences to assess the likelihood of relapse (See Table 1.3) and also helps standardise MR image acquisition, interpretation, and reporting in local recurrence after RT and prostatectomy.

Table 1.3 Prostate Imaging for Recurrence Reporting (PI-RR) system scoring categories based on each MRI sequence (T2W, DWI, and DCE) pattern changes for the overall risk assessment of local recurrence after radiation therapy. Abbreviations: ADC = apparent diffusion coefficient, BPH = Benign Prostatic Hypertrophy, DCE = dynamic contrast-enhanced, DWI = diffusion-weighted imaging, T2W = T2 weighted.

Sequence	Score	MRI Pattern changes
T2W	1	**No abnormal** signal intensity compared to the background
	2	**Linear, wedge-shaped**, or **diffuse** moderate hypointensity or residual BPH nodules
	3	Focal or mass-like mild hypointensity **NOT** at the primary tumour site; includes others that do not qualify as 2, 4, or 5
	4	Focal or mass-like moderate hypointensity **NOT** at the same site as the primary tumour, or location of primary tumour not known
	5	Focal or mass-like marked hypointensity at the **same site as the primary tumour**
DWI	1	**No abnormality** on high b-value DWI and ADC map
	2	**Diffuse** moderate hyperintensity on high b-value DWI and/or diffuse moderate hypointensity on the ADC map
	3	**Focal marked hyperintensity** on high b-value DWI or focal marked hypointensity on the ADC map, but not on both
	4	**Focal marked hyperintensity** on high b-value DWI and marked hypointensity on the ADC map **NOT** at the same site as the primary tumour, or site of the primary tumour not known
	5	**Focal marked hyperintensity** on high b-value DWI and marked hypointensity on the ADC map at the **same site as the primary tumour**
DCE	1	**No enhancement**
	2	**Diffuse** or **heterogeneous** enhancement
	3	**Focal** or **mass-like late** enhancement
	4	Focal or mass-like **early** enhancement **NOT** at the same site as the primary tumour, or tumour site not known
	5	Focal or mass-like **early** enhancement at the **same site as the primary tumour**

1.2 Radiomics

Tumour heterogeneity at the phenotypic, physiologic and genomic level influences tumour aggressiveness and response to therapy [109,110]. Medical imaging contains mineable high dimensional data, which is not routinely used or seen by the radiologist. Radiomics refers to the process by which quantitative features are extracted from medical images. This involves a workflow including mapping, extraction, analysis and modelling of imaging data to predict a clinical outcome or target [111,112]. It has great potential as a source of quantitative biomarkers and can be used to build both descriptive and predictive clinical models that relate imaging features to intratumoural heterogeneity and biology phenotypes. The hope of radiomics would be that such quantitative imaging features could serve as a biomarker to help characterise diseases or allow prediction of treatment response to aid decision making in patient management.

Given that the calculated number of radiomic features often far exceeds the number of patients, a robust approach is needed to avoid false discovery. Comprehensive work by the Image Biomarker Standardization Initiative (IBSI) attempts to address the main challenges in radiomics, including the lack of reproducibility and validation of radiomics studies, and aims at standardising the workflow, nomenclature, and implementation steps [113]. The key processing steps in MRI radiomic analysis will be described in further detail.

1.2.1 Image Acquisition

MRI offers both anatomical and functional information to help characterise soft tissue. High diagnostic quality prostate MRI is vital to help the radiologist in the detection or exclusion of prostate cancer. Multiple factors affect image quality in prostate MRI which is highly variable across centres and requires standardisation of technical acquisition parameters [114,115]. Using a multiparametric approach which includes T2W, DWI), and DCE-MRI sequences may help to reduce the risk of bias from features extracted from only one sequence [116]. Voxel size and post-processing steps vary between institutions, different MRI scanner vendors and protocols. This means that appropriate image harmonisation is required to account for these changes in order to compare imaging features across these different platforms.

1.2.2 Segmentation

Selecting the region(s) of interest (ROI) from the imaging is an important first step in the radiomics workflow. This may include the whole organ of interest, a whole tumour,

part of a tumour e.g. subregions or habitats, and/ or peri-tumoral areas where the choice of ROI is guided by the initial research hypothesis. Radiotherapy tumour volume data used for treatment planning can also be used as segmentations. Ensuring that these structures are accurately identified and segmented i.e. delineated/ highlighted, ensures that the subsequent radiomics feature data are correctly derived as these are based on the voxels from the selected ROI [117]. Segmentation techniques used for defining the ROI therefore have tremendous impact on the reproducibility of the radiomic features extracted. Manual delineation is a straightforward solution, but may be time-consuming and susceptible to intra-observer and inter-observer variability [118–120]. When ROIs have been manually segmented, radiomic feature stability should be assessed by performing multiple segmentations of the same tumour with either the same or a different reader performing the delineation.

1.2.3 Feature Extraction

Radiomic features can be grouped into four major categories:

1. Size and shape 'morphologic' features – volume, surface area, compactness.
2. First-order histogram – distribution of the intensities of voxels.
3. Second-order histogram or textural features – spatial distribution of voxel intensities.
4. Transform-based features – by imposing kernel functional transformation of the segmentation, repetitive or non-repetitive spatial patterns can be identified.

A complete list of features is found in the reference manual of the IBSI [113].

First-order features describe statistical properties of voxel intensities within a ROI including location of the distribution (mean, median, mode), a measure of the spread of the distribution (variance, interquartile range), a measure of the shape of the distribution (skewness, kurtosis), and features linked to properties of the voxel intensity heterogeneity (entropy and energy). Second-order features describe local spatial relationships (texture) within the ROI and quantify heterogeneity, for example, gray-level co-occurrence matrix (GLCM) features measure the signal intensities of pairs of pixels separated by a given distance and direction, while gray-level size-zone matrix (GLSZM) features consider the sizes of contiguous regions that share the same signal intensity after discretisation. Intensity discretisation involves assigning pixels within a given intensity range to a single value or "bin" and is used before calculation of second-order features.

1.2.4 Resampling

Prior to extraction, the voxels within the segmented area are resampled into uniform sizes by a process called relative discretization which is a type of image pre-processing technique used to reduce the number of intensity levels in an image while preserving the relative relationships between the intensity values i.e. without changing the structure or features of the image. The size and shape of voxels can have a major impact on the radiomic data extracted [121]. Voxel intensities are 'normalised' by resampling the values to lie between 0 and 1 [112,122]. Voxels of similar intensities are then grouped into 'bins'. The number of bins (bin number) or the size of each bin (bin width) can be specified. Reducing the bin number (or increasing the bin width) will lead to a loss of image detail but will remove noise. On the other hand, increasing the bin number (or decreasing the bin width) will preserve more image detail but will also retain image noise. By normalising the values this way, overall noise is reduced but this also impacts on the features extracted [109,123]. As MRI data has intensity units that are arbitrary, fixing the number of bins (rather than the bin width) is recommended for radiomic analysis however bin width can be used when the image data is on an intensity scale that is quantitative such as ADC maps [113]. Similarly, image interpolation and resampling to obtain isotropic voxels, meaning uniform dimensions in all directions, should be performed with caution and must depend on variations in slice thickness and voxel sizes.

1.2.5 Reproducibility and Repeatability

The identification of a clinically useful IB of disease or for response prediction relies on the basic requirement that such a biomarker must be stable between two separate measurements i.e. at different time points, if the conditions remain unchanged. This means that the biomarker should remain stable despite scanner noise and normal anatomical or physiological variation. Reproducibility refers to the ability to obtain consistent results or features when extracted using different equipment, software or image acquisition parameters when the same experiment or methodology is followed. Investigating the "reproducibility" of IBs is a fundamental step in its technical (assay) validation and has been recommended as an essential early part of IB development by a consensus panel [24]. The terms "repeatability" [124–126] and "stability" [127–129] have also been used to describe this attribute of radiomic features.

Repeatability refers to how stable a feature is or how consistent measurements are when the same experiment is repeated under the same conditions by the same operator or using the same equipment. This may be imaging the same subject multiple times (using the same acquisition methods). It assesses the variation in measurements obtained from

the same sample or subject, typically over a short period of time. Essentially, repeatability measures how reliably the same experiment can be reproduced within a controlled environment [130]. Schwier et al found that prostate MRI radiomic feature repeatability was highly sensitive to processing parameters such as image normalisation methods, different pre-filtering and different bin widths for image discretisation [131]. A recent systematic review assessing the quality of prostate MRI radiomics studies found these to be lacking in sufficient quality to allow their introduction in to clinical practice, with the most critical limitations being lack of feature robustness testing strategies and external validation datasets [132].

1.2.6 Harmonisation

A major challenge in validating radiomic models across different institutions is the heterogeneous imaging data generated from different scanners using varied MRI reconstruction protocols, given that radiomics features are highly sensitive to these acquisition and reconstruction parameters. MRI generates images with arbitrary intensity scaling, and if this is not consistent for all patients included in the research study it will be necessary to apply image standardisation or harmonisation techniques before calculating first-order features. These processes help to adjust the image data to reduce variation in imaging appearances caused by differences in imaging protocols, equipment, and acquisition parameters which ultimately affect the radiomic features [133,134]. This can involve post-processing steps such as image normalisation, intensity normalisation, and image registration, which aim to make images from different sources more similar in appearance and more comparable, which can facilitate pooling of data from multiple sources for analysis. Features such as skewness are unaffected by harmonisation methods because they depend on the shape of the distribution of intensity values rather than their absolute values.

There is no consensus within radiomic studies regarding the best MRI image intensity normalisation method. Histogram normalisation approaches have been shown to reduce MRI scanner-dependent variability of radiomic features [133]. This technique also maintains the interpretability of the radiomic features [135]. The Nyúl method, a histogram intensity-based normalisation technique was used on the prostate MRI data in this thesis to render the dynamic signal intensity ranges comparable prior to radiomic feature extraction [136,137].

Different harmonisation methods exist that can be applied to the extracted radiomic features. Ideally harmonisation should occur prospectively (with standardisation of

acquisition protocols and reconstruction settings) to ensure scans are comparable between centres, most techniques have been applied to retrospective data sets which rely on statistically standardising the numeric radiomic feature values to pool the data together for the modelling step.

One technique called ComBat (Combatting batch effects when combining batches of microarray data) harmonisation, a batch-effect correction tool initially proposed for genomic studies [138], has shown promise in the setting of multicentre PET-CT and MRI radiomic studies [139–141]. This statistical technique is easily accessible, practical, and fast to implement, with the additional advantage that it is based on patient data only with no requirement for phantom experiments. ComBat uses an empirical Bayes framework to estimate a normalised value for a feature for a specific ROI and scanner protocol [142]. ComBat then determines and applies a transformation for each feature based on the effect of the scanner protocol on the individual features [143]. Limitations of ComBat include losing the original physical meaning of harmonised features due to the data being manipulated in order to account for all samples [142]. In order for a ComBat based radiomics model to be applied to a different institution, all the available radiomic features must be available to use which although is important for transparency, practically can be challenging [140].

Emerging techniques for MRI harmonisation have included more image-based approaches rather than statistical approaches such as deep learning based models [144]. One supervised deep learning approach using a U-net convolutional neural network required two separate MRI scans per patient making the model training process time intensive and expensive, limiting clinical applicability [145]. Conditional generative adversarial networks (cGANs), an unsupervised deep learning-based generative model, are able to synthesise new images with a set contrast (e.g. to that of a target scanner) which in theory should be indistinguishable from real images from the training dataset [144]. cGANs cannot distinguish the image content from contrast which can result in alteration of anatomical information and geometrical distortion to become more like data from the target scanner. These changes would not be acceptable in clinical practice where the accuracy of anatomical detail is vital to ensure accurate treatment planning and delivery. One recent study used ‘style blind auto-encoders’ which learns to compress imaging data into a ‘latent representation’ that was scanner contrast independent using an encoder neural network and decompress it before reconstructing the original image using a decoder [146]. This scanner-independent approach with no target contrast domain avoided issues with anatomical distortion and was able to harmonise brain images from multiple different MRI scanners, including images from

scanners unseen to the neural network during training. This approach outperformed other harmonisation methods in terms of the number of statistically indistinguishable radiomic features post-harmonisation and the preservation of anatomical content.

1.2.7 Modelling

Model creation involves splitting the data into training, testing and validation sets. The radiomic and clinical features should be first analysed on the training set and any highly correlated features reduced, to prevent the impact of individual parameters being underestimated in the model. Feature reduction helps to reduce the risk of model overfitting. A typical model uses a combination of clinical and radiomic features, in addition to outcome data that the model aims to predict, such as disease recurrence or survival. A variety of machine learning based feature-reduction and feature selection methods can be used, with no consensus on the best approach however the choice of method still affects the performance of the final model [147]. Following the model-training stage, the radiomics based model is usually tested on an unseen dataset (which could be an internal dataset that has been kept away from the model at the training stage) before being externally validated on a further dataset, usually from another institution, however this is not always possible. This is to assess the performance and generalizability of a model by validating the model on new test data. Splitting single-institution data into training, testing and validation sets is often more practical. This could be done randomly, through a temporal approach (by using the most recent cases as validation data), or through stratified sampling by ensuring similar class proportion (e.g. benign versus malignant or hypoxic versus normoxic) in the training and validation groups [148]. The disadvantage of the temporal approach is due to the time-sensitive data that will be influenced by the length of follow-up for example the time to BCR or time to progression which will vary depending on the choice patient cohort i.e. a more historic cohort will have a greater proportion of patients that will have progressed due to the longer follow-up compared to a more contemporary group. In addition, the MRI protocols may have changed over time affecting the imaging data quality and this would affect how comparable the data is even allowing for harmonisation techniques.

1.2.8 Machine Learning

Depending on the endpoint of interest, various machine learning (ML) classification methods can be used to develop a radiomics-based prediction model (98). This thesis

will focus on both binary outcome prediction for hypoxia status and survival outcome prediction.

Logistic regression models, support vector machine (SVM) and random forests, are among the ML classifiers that have been used in radiomic studies of prostate cancer that are focused on clinically significant cancer diagnosis and lesion characterisation tasks [149–151]. These techniques may vary between using established statistical methods for binary classification tasks (e.g. logistic regression) to using supervised learning methods that require the ground truth needs to be defined, labelled and linked to the image (e.g. hypoxic or not hypoxic tumour), prior to the ML algorithm being trained and tested [152].

Support vector machines (SVMs) are supervised learning methods used for classification and regression tasks. SVMs are effective for high-dimensional data, where the number of features or variables is greater than the number of observations, such as in the case of radiomics where there can be thousands of features for a limited patient sample size. SVMs are however prone to over-fitting which makes selecting the appropriate kernel functions and other parameters such as regularisation terms very crucial [153].

Random forest is another commonly used machine learning algorithm that uses an ensemble of multiple decision trees, a collection of specific questions organised hierarchically, for regression and classification tasks [154]. By combining the outputs for each of these trees, the algorithm delivers a more accurate and comprehensive result e.g. for classification tasks, the output of the random forest model is the class selected by most trees and for regression tasks, the average prediction of the individual trees determines the result. Random forest models can be particularly effective when being trained on large datasets and can accurately identify important variables that contribute to classification without overfitting from having more features due to the ability to create random trees with different sub-features [154]. Limitations of using random forest include the high computational power required to build numerous trees, which can lead to prolonged training times. The ensemble of decision trees can however affect the interpretability of the data and significance of each predictive variable.

1.2.9 Radiogenomics

Imaging-based radiogenomics combines the areas of advanced image texture analysis (radiomics) and molecular characteristics (genomics) with clinical outcome prediction and provides biological validation to radiomic imaging biomarkers by integrating

information on histopathological or molecular/gene signatures [155]. Radiomic signatures have been shown to accurately predict molecular subtypes of cancers associated with a more invasive phenotype [156].The application of ML to radiogenomic studies provides novel insights into tumour biology and has been evaluated in multiple tumour types [157–159]. A recent systematic review found that up until 31st January 2022 there had been 45 published radiogenomic studies, which by the authors definition had used genetics to validate their radiomics predictive model and clinical outcomes in oncology patient cohorts [160]. Over half these studies were published in the last two years, highlighting the novelty of this area of research. CT was the most common imaging modality used for the radiomic feature extraction (47%), followed by MRI (44%). Brain tumours were the most commonly studied site in these studies and there was only one prostate cancer radiogenomic study included[87].

If imaging biomarkers, could provide surrogate information on genetic data then this would offer a non-invasive and cost-effective alternative given that genomic signatures are usually acquired from tumour biopsy specimens. Utilising imaging also enables the whole tumour to be analysed compared to the biopsy-based approach, which only samples specific areas of the tumour without accounting for intratumoural heterogeneity. Radiogenomic signatures could offer further measurable longitudinal metrics that might help guide RT treatment planning, post-treatment surveillance and allow for more accurate survival predictions. Evidence for the clinical utility of using radiogenomic signatures specifically associated with hypoxia (imaging features linked to hypoxia-associated genes or gene signatures) in terms of predicting clinical outcomes are emerging for tumour sites including glioblastoma and renal cell cancer [161,162]. Beig et al. reported that radiomic features extracted from different ROIs on MRIs in 180 patients with glioblastoma such as, enhancing tumour, necrotic tumour, and peri-tumoral regions were predictive of a hypoxia enrichment score based on 21 genes implicated in the hypoxia pathway of glioblastoma [163]. The top eight features most associated with the hypoxia enrichment score included radiomic features which quantified structural heterogeneity and their imaging-based radiogenomic hypoxic signature was associated with patient survival [163]. Gao et al. derived a hypoxia-gene related radiogenomic signature using radiomic features extracted from contrast-enhanced CT and found that this was significantly associated with prognosis in patients with renal cell cancer validating this in an independent cohort [162]. Such validation and insight into the biological characteristics of tumours from imaging modalities is vital and needs to be replicated for prostate cancer pathways, which the current thesis attempts to address.

1.3 Role of Quantitative MRI in Radiotherapy

1.3.1 MRI-guided Radiotherapy

MRI-guided radiotherapy (MRIgRT) for prostate cancer provides excellent visualisation of the prostate gland and tumour extent, resulting in more precise delineation compared to when using CT for planning and also allows margin reduction resulting in reduced rectal irradiation. This is particularly important with the increasing use of SABR for prostate cancer [164,165]. Visualising normal organs and structures is also superior therefore identifying and sparing the neurovascular bundle may help to preserve erectile function [165,166]. MRI can be used for RT planning and functional MRI has been used to select patients for different types of dose escalation in clinical trials such as PIVOTALboost, a phase III randomised controlled trial of prostate and pelvis versus prostate alone radiotherapy with or without prostate boost (HDR brachytherapy or focal dose escalation with intensity-modulated radiation therapy are used as options) [167]. MRIgRT also provides real-time prostate imaging therefore invasive fiducial markers are not required [165]. Daily plan re-optimisation allows compensation for interfraction prostate motion caused by rectal and bladder filling [165,168].

Published studies of MRIgRT for treating prostate cancers report a low incidence of acute gastrointestinal (GI) and genitourinary (GU) toxicity. The first prospective phase II study of prostate MRIgRT by Bruynzeel et al. found grade 2 acute GI and GU toxicity rates (both clinician- and patient-reported outcome measurements) of 5% and 24% [169]. This low incidence of acute GI toxicity, despite including the seminal vesicles in 96% of patients, was likely a direct benefit of using MRIgRT due to the smaller clinical target volume (CTV) to planned target volume (PTV) margins, which can only be made possible by the superior tissue contrast and ability for online CTV monitoring and daily plan re-optimization. Despite the routine plan re-optimization with selective relative sparing of the urethra, incidence of acute GU toxicity was still 24% but this was still lower than other trials that involved similar hypofractionation RT schedules using CT-guided radiotherapy (CTgRT) rather than MRIgRT and reported GU toxicities of 46-61% [170,171]. At 1-year follow-up, the majority of these described GI and GU symptoms had resolved with no grade 3 toxicity observed [172]. A further prospective observational study by Alongi et al. found lower grade 2 or higher acute GI and GU toxicity rates of 4% and 12%, respectively with no grade 3 toxicity [173].

The MIRAGE trial, the first phase 3 randomized clinical trial comparing MRIgRT to CT-guided RT for prostate cancer, found that MRIgRT was superior to CT-guided RT in terms of acute toxicity and patient-reported quality of life [15]. With MRIgRT, margins

were reduced to 4mm with an incidence of acute grade 2+ urinary adverse effects of 24% vs 43% for standard CT-guided RT with margins of 6mm, while acute grade 2+ GI toxicity was 0% vs 10.5%. This benefit was reflected in lower proportion of patients reporting clinically significant worsening of bowel symptoms (25% vs 50%) as well as urinary symptoms (7% vs 19%). However, reduction in RT margins also raises concerns of under coverage of the target. Extended follow-up data for these trials is needed to evaluate long-term cancer control and toxicity outcomes although this would need to be a large phase 3 multicentre study and challenging to organise. In the UK National Health Service (NHS), there remains the pertinent issue of resource and equipment availability and delivery of MRIgRT throughout the UK is likely to be challenging and of uncertain clinical significance. Additionally, MRIgRT takes longer to deliver thereby reducing patient throughput and requires additional clinician input and/or upskilling of the therapeutic radiographer workforce. Currently the use of acute toxicity as a primary end point, as in the MIRAGE trial, remains debatable when the overall cumulative incidence of late toxicity symptoms remains low (5-10%) for modern SABR prostate treatments. There are also potential biases for both the patient, in terms of knowing they are receiving a "more targeted" treatment and may therefore feel their side effects are more tolerable, and the unblinded physician who is scoring and collecting the toxicity data and may be influenced knowing if the patient received the MRIgRTarm.

Quantitative MRI highlights different tissue characteristics and provides a means of non-invasively probing the microenvironment of prostate tumours and surrounding organs at risk (OAR). A range of functional MRI techniques can be used to investigate tissue characteristics such as cellular microstructure, perfusion, and oxygenation status, and these techniques can yield quantitative imaging biomarkers [24]. Such biomarkers may be sensitive to early treatment-induced changes in prostate tumours and OARs, providing a quantitative assessment of treatment response. In addition, spatial and temporal heterogeneity in such biomarkers may be used to identify and track aggressive tumour sub-regions, which could be targeted with an increased dose [174]. Quantitative MR may therefore inform future RT treatment planning, an example of biological image-guided adaptive radiotherapy (BIGART) [175]. Escalating dose to the tumour regions of highest cellularity in theory could improve local control rates, providing a rationale for using DWI-MRI to guide treatment planning [176]. Early increases in tumour ADC values following prostate RT has been associated with good treatment response, highlighting the potential value of DWI-MRI in monitoring RT response [177]. BIGART also has the potential to target hypoxic areas once appropriate MRI sequences can be implemented onto MRI-LINAC machines. This approach could also utilise

imaging radiogenomic signatures (imaging features linked to hypoxia gene-signatures) by offering MRI-guided focal boosting of hypoxic tumours if specific hypoxia associated radiogenomic signatures are identified and may further improve clinical outcomes given that hypoxic cells are more resistant to radiation than normoxic ones [48,178,179].

1.3.2 Outcome Prediction

Identifying quantitative changes in the prostate and organs at risk on functional mpMRI could provide a non-invasive way of assessing early RT response allowing clinicians to adapt treatment and minimise toxicity. DWI can quantify variation in tissue function and cellular density during RT, but correlation with clinical outcomes have not been shown [180]. Wu et al found significant reductions in prostate cancer DCE-MRI derived perfusion and permeability parameters at 3 months following EBRT in a study of 55 men, and further reductions at 12 months [181]. This may represent a decrease in tumour microcirculation and neovascularisation following effective radiotherapy, and potentially allows for quantitative follow-up with DCE-MRI [181,182]. A further small study of 47 men investigating the quantitative MRI changes in the prostate during weekly ultra-hypofractionated EBRT found statistically significant increases in median ADC values of the tumour for men who did not receive hormonal therapy, and a minority of patients also displayed persistent T2W signal changes [183]. Adjuvant hormone therapy appears to attenuate the differences in ADC values of normal and malignant tissue during EBRT and therefore may limit the utility of ADC when androgen deprivation therapy (ADT) is given [184]. ADT has also been shown to have a potential anti-angiogenic effect which affects the DCE parameters with a differential response seen on DWI [185]. This small study (n=23) found after 3 months of ADT, the tumour DCE MRI parameters all reduced however areas of normal PZ showed no significant change. Interestingly after ADT, no significant change in tumour ADC values were seen, however the ADC values of normal PZ significantly decreased [185].

Longer-term follow-up and larger sample sizes are required to relate these MRI changes to clinical outcomes before this can be used for treatment personalisation. The predictive value of radiomics on the response to prostate radiotherapy has been studied in a small retrospective study of 79 patients treated with standard fractionation EBRT for biopsy confirmed high risk prostate cancer, where T2W radiomic features correlated with biochemical recurrence after radiotherapy [186].

1.3.3 Toxicity Prediction

A comprehensive tool for reporting treatment-related adverse events in oncological care is vital to ensure the relevant toxicity effects after radiotherapy are captured. One commonly used grading system is the Common Terminology Criteria for Adverse Events (CTCAE) [187]. Based on CTCAE, the definition of an adverse event (AE) is "any unfavourable and unintended sign (including an abnormal laboratory finding), symptom, or disease temporally associated with the use of a medical treatment or procedure that may or may not be considered related to the medical treatment or procedure".

The CTCAE uses a grading system of 1 to 5: Grade 1 is asymptomatic or mild symptoms that do not require any intervention. Grade 2 is moderate symptoms that require local or non-invasive intervention indicated (e.g. oral pain relief medication). Grade 3 is severe or medically significant but not immediately life-threatening issues that require invasive intervention, hospitalisation or prolongation of hospitalisation (e.g. surgery for urinary fistula after radiotherapy). Grade 4 is life-threatening consequences requiring urgent intervention (e.g. multi-organ failure). Grade 5 is Death related to the AE.

Imaging biomarkers allow non-invasive assessment of the prostate and surrounding tissue, along with temporal changes associated with radiotherapy treatment. Previous work has demonstrated that pre-radiation MR imaging/ radiomic biomarkers can predict urinary and rectal toxicity [188,189]. This could potentially guide tailoring of treatment strategies and radiation dose in patients. There has been no prospective assessment of predictive imaging biomarkers for toxicity in the primary or salvage radiotherapy setting and correlating this with toxicity symptoms and patient reported outcomes would allow a more comprehensive assessment of the impact of radiotherapy. This is increasingly relevant with the advent of MR-only radiotherapy treatment pathways which will allow for improved soft tissue contrast and online adaptive planning allowing for greater accuracy of fraction delivery [165].

1.3.4 Hypothesis

The central hypothesis of the thesis is that prostate radiation could be optimised using magnetic resonance imaging and hypoxia biomarkers because radiomic data extracted from imaging potentially enables quantitative assessment of intra and inter-tumoural and genomic heterogeneity that may confer worse disease prognosis and could be used to tailor radiotherapy intensification and guide treatment monitoring based on prediction of toxicity and disease recurrence risks.

1.3.5 Summary

This firsts chapter introduces the key concepts in the diagnosis, management and follow-up in prostate cancer, focusing on the radiotherapy techniques used, tumour hypoxia, outcome prediction tools and the role of imaging biomarkers, and advanced quantitative imaging methods. It provides the necessary background for linking the subsequent thesis chapters that address different components of the central question which is how we can optimise prostate radiation using MRI and hypoxia biomarkers.

1.4 Aims

The aims of this thesis were:

- To develop a machine-learning model to predict prostate tumour hypoxia using pre-treatment MRI-derived radiomics
- To develop a clinical outcome prediction model for prostate cancer by integrating hypoxia-associated gene signature and radiomic information with clinical data.
- To investigate longitudinal radiomic feature changes in the bladder wall and rectum during radiotherapy for prostate cancer
- To systematically review the evidence for reirradiation of the prostate for locally radiorecurrent cancer
- To design a randomised controlled trial evaluating the feasibility of patient recruitment to a trial comparing high dose-rate brachytherapy and external beam radiotherapy for recurrent prostate cancer

1.5 References

1. Cancer Research UK. Cancer Incidence from Cancer Intelligence Statistical Information Team at Cancer Research UK. 2019. Available from: https://www.cancerresearchuk.org/health-professional/cancer-statistics/statistics-by-cancer-type/prostate-cancer [Accessed 22/09/2023]
2. Bray F, Ferlay J, Soerjomataram I, Siegel RL, Torre LA, Jemal A. Global cancer statistics 2018: GLOBOCAN estimates of incidence and mortality worldwide for 36 cancers in 185 countries. CA Cancer J Clin . 2018;68:394–424.

3. Wang L, Lu B, He M, Wang Y, Wang Z, Du L. Prostate Cancer Incidence and Mortality: Global Status and Temporal Trends in 89 Countries From 2000 to 2019. Front Public Heal. 2022;10.

4. Sung H, Ferlay J, Siegel RL, Laversanne M, Soerjomataram I, Jemal A, *et al.* Global Cancer Statistics 2020: GLOBOCAN Estimates of Incidence and Mortality Worldwide for 36 Cancers in 185 Countries. CA Cancer J Clin. 2021;71(3):209–49.

5. Gleason DF. Classification of prostatic carcinomas. Cancer Chemother reports. 1966;50(3):125–8.

6. Epstein JI, Allsbrook WC, Amin MB, Egevad LL. The 2005 International Society of Urological Pathology (ISUP) Consensus Conference on Gleason Grading of Prostatic Carcinoma. Am J Surg Pathol. 2005;29(9):1228–42.

7. Epstein JI, Egevad L, Amin MB, Delahunt B, Srigley JR, Humphrey PA. The 2014 International Society of Urological Pathology (ISUP) Consensus Conference on Gleason Grading of Prostatic Carcinoma. Am J Surg Pathol. 2016;40(2):244–52.

8. Bell KJL, Del Mar C, Wright G, Dickinson J, Glasziou P. Prevalence of incidental prostate cancer: A systematic review of autopsy studies. Int J Cancer. 2015;137(7):1749–57.

9. Moyer VA. Screening for Prostate Cancer: U.S. Preventive Services Task Force Recommendation Statement. Ann Intern Med. 2012;157(2):120.

10. Anderson BB, Oberlin DT, Razmaria AA, Choy B, Zagaja GP, Shalhav AL, et al. Extraprostatic Extension Is Extremely Rare for Contemporary Gleason Score 6 Prostate Cancer. Eur Urol. 2017;72(3):455–60.

11. Gnanapragasam VJ, Bratt O, Muir K, Lee LS, Huang HH, Stattin P, *et al.* The Cambridge Prognostic Groups for improved prediction of disease mortality at diagnosis in primary non-metastatic prostate cancer: a validation study. BMC Med. 2018;16(1):31.

12. National Comprehensive Cancer Network. Prostate Cancer (Version 2.2023). 2023. Available from: https://www.nccn.org/guidelines/recently-published-guidelines [Last Accessed 20/09/2023].

13. Mottet N, Bastian P, Bellmunt J, van den Bergh R, Bolla M, van Casteren N, et al. EAU - EANM - ESTRO - ESUR - SIOG: Guidelines on Prostate Cancer. Eur Assoc Urol [Internet]. 2020;

14. Vicens RA, Rodriguez J, Sheplan L, Mayo C, Mayo L, Jensen C. Brachytherapy in pelvic malignancies: a review for radiologists. Abdom Imaging. 2015;40(7):2645–59.

15. Kishan AU, Ma TM, Lamb JM, Casado M, Wilhalme H, Low DA, *et al.* Magnetic Resonance Imaging–Guided vs Computed Tomography–Guided Stereotactic Body Radiotherapy for Prostate Cancer. JAMA Oncol. 2023;

16. Chin S, Eccles CL, McWilliam A, Chuter R, Walker E, Whitehurst P, *et al.* Magnetic resonance-guided radiation therapy: A review. J Med Imaging Radiat Oncol. 2020;64(1):163–77.

17. Biomarkers and surrogate endpoints: Preferred definitions and conceptual framework. Clin Pharmacol Ther. 2001;69(3):89–95.

18. Food and Drug Administration and National Institutes of Health. BEST (Biomarkers, Endpoints, and other tools) resource. 2016. Available from: `https://www.ncbi.nlm.nih.gov/books/NBK338448/`. (Last Accessed 20/09/2023).

19. Poste G. Bring on the biomarkers. Nature. 2011;469(7329):156–7.

20. Hayes DF, Allen J, Compton C, Gustavsen G, Leonard DGB, McCormack R, *et al.* Breaking a Vicious Cycle. Sci Transl Med. 2013;5(196):196cm6-196cm6.

21. Macleod MR, Michie S, Roberts I, Dirnagl U, Chalmers I, Ioannidis JPA, *et al.* Biomedical research: increasing value, reducing waste. Lancet. 2014;383(9912):101–4.

22. Salciccia S, Capriotti AL, Laganà A, Fais S, Logozzi M, De Berardinis E, *et al.* Biomarkers in Prostate Cancer Diagnosis: From Current Knowledge to the Role of Metabolomics and Exosomes. Int J Mol Sci. 2021;22(9):4367.

23. Oldenhuis CNAM, Oosting SF, Gietema JA, de Vries EGE. Prognostic versus predictive value of biomarkers in oncology. Eur J Cancer. 2008;44(7):946–53.

24. O'Connor JPB, Aboagye EO, Adams JE, Aerts HJWL, Barrington SF, Beer AJ, *et al.* Imaging biomarker roadmap for cancer studies. Nat Rev Clin Oncol. 2017;14(3):169–86.

25. Porzycki P, Ciszkowicz E. Modern biomarkers in prostate cancer diagnosis. Cent Eur J Urol. 2020;73(3):300–306.

26. Alberts AR, Roobol MJ, Verbeek JFM, Schoots IG, Chiu PK, Osses DF, *et al.* Prediction of High-grade Prostate Cancer Following Multiparametric Magnetic Resonance Imaging: Improving the Rotterdam European Randomized Study of Screening for Prostate Cancer Risk Calculators. Eur Urol. 2019;75(2):310–8.

27. Spratt DE, Pei X, Yamada J, Kollmeier MA, Cox B, Zelefsky MJ. Long-term Survival and Toxicity in Patients Treated With High-Dose Intensity Modulated Radiation Therapy for Localized Prostate Cancer. Int J Radiat Oncol. 2013;85(3):686–92.

28. Rosenbaum E, Partin A, Eisenberger MA. Biochemical Relapse After Primary Treatment for Prostate Cancer: Studies on Natural History and Therapeutic Considerations. J Natl Compr Cancer Netw. 2004;2(3):249–56.

29. Sharma S, Watabe K. Biomarkers and mechanisms associated with recurrent prostate cancer. Front Biosci. 2014;19(2):339–51.

30. Vollmer RT, Montana GS. Tumour and immune cell dynamics explain the PSA bounce after prostate cancer brachytherapy. Clin Cancer Res. 1999;5(12):4119 LP – 4125.

31. Patel C, Elshaikh MA, Angermeier K, Ulchaker J, Klein EA, Chehade N, *et al.* PSA bounce predicts early success in patients with permanent iodine-125 prostate implant. Urology. 2004;63(1):110–3.

32. Yamamoto Y, Offord CP, Kimura G, Kuribayashi S, Takeda H, Tsuchiya S, *et al.* Tumour and immune cell dynamics explain the PSA bounce after prostate cancer brachytherapy. Br J Cancer. 2016;115(2):195–202.

33. Cucchiara V, Cooperberg MR, Dall'Era M, Lin DW, Montorsi F, Schalken JA, *et al.* Genomic Markers in Prostate Cancer Decision Making. Eur Urol. 2018;73(4):572–82.

34. Beckendorf V, Guerif S, Le Prisé E, Cosset JM, Bougnoux A, Chauvet B, *et al.* 70 Gy versus 80 Gy in localized prostate cancer: 5-year results of GETUG 06 randomized trial. Int J Radiat Oncol Biol Phys . 2011;80(4):1056–63.

35. Zumsteg ZS, Spratt DE, Romesser PB, Pei X, Zhang Z, Kollmeier M, *et al.* Anatomical patterns of recurrence following biochemical relapse in the dose

escalation era of external beam radiotherapy for prostate cancer. J Urol . 2015;194(6):1624-1630.

36. Zumsteg ZS, Spratt DE, Romesser PB, Pei X, Zhang Z, Polkinghorn W, *et al.* The Natural History and Predictors of Outcome Following Biochemical Relapse in the Dose Escalation Era for Prostate Cancer Patients Undergoing Definitive External Beam Radiotherapy. Eur Urol. 2015;67(6):1009–16.

37. Jones CU, Hunt D, McGowan DG, Amin MB, Chetner MP, Bruner DW, *et al.* Radiotherapy and Short-Term Androgen Deprivation for Localized Prostate Cancer. N Engl J Med. 2011;365(2):107–18.

38. Jones CU, Pugh SL, Sandler HM, Chetner MP, Amin MB, Bruner DW, *et al.* Adding Short-Term Androgen Deprivation Therapy to Radiation Therapy in Men With Localized Prostate Cancer: Long-Term Update of the NRG/RTOG 9408 Randomized Clinical Trial. Int J Radiat Oncol. 2022;112(2):294–303.

39. Cooperberg MR, Vickers AJ, Broering JM, Carroll PR. Comparative risk-adjusted mortality outcomes after primary surgery, radiotherapy, or androgen-deprivation therapy for localized prostate cancer. Cancer . 2010;116:5226–5234.

40. Valle LF, Lehrer EJ, Markovic D, Elashoff D, Levin-Epstein R, Karnes RJ, *et al.* A Systematic Review and Meta-analysis of Local Salvage Therapies After Radiotherapy for Prostate Cancer (MASTER). Eur Urol. 2020;1(310):1–13.

41. Kishan AU, Chu F-I, King CR, Seiferheld W, Spratt DE, Tran P, *et al.* Local Failure and Survival After Definitive Radiotherapy for Aggressive Prostate Cancer: An Individual Patient-level Meta-analysis of Six Randomized Trials. Eur Urol. 2020;77(2):201–8.

42. Ingrosso G, Becherini C, Lancia A, Caini S, Ost P, Francolini G, *et al.* Nonsurgical Salvage Local Therapies for Radiorecurrent Prostate Cancer: A Systematic Review and Meta-analysis. Eur Urol Oncol . 2019;3(2):183–97.

43. Chade DC, Eastham J, Graefen M, Hu JC, Karnes RJ, Klotz L, *et al.* Cancer control and functional outcomes of salvage radical prostatectomy for radiation-recurrent prostate cancer: A systematic review of the literature. Eur Urol . 2012;61(5):961–71.

44. Tan N, Bavadian N, Calais J, Oyoyo U, Kim J, Turkbey IB, *et al.* Imaging of Prostate Specific Membrane Antigen Targeted Radiotracers for the Detection of

Prostate Cancer Biochemical Recurrence after Definitive Therapy: A Systematic Review and Meta-Analysis. J Urol. 2019;202(2):231–40.

45. Adams GE. The clinical relevance of tumour hypoxia. European Journal of Cancer and Clinical Oncology. 1990.

46. Marignol L, Coffey M, Lawler M, Hollywood D. Hypoxia in prostate cancer: A powerful shield against tumour destruction? Cancer Treat Rev. 2008;34(4):313–27.

47. Milosevic M, Warde P, Ménard C, Chung P, Toi A, Ishkanian A, *et al.* Tumor Hypoxia Predicts Biochemical Failure following Radiotherapy for Clinically Localized Prostate Cancer. Clin Cancer Res. 2012;18(7):2108–14.

48. Bristow RG, Hill RP. Hypoxia, DNA repair and genetic instability. Nat Rev Cancer. 2008;8(3):180–92.

49. Gilkes DM, Semenza GL, Wirtz D. Hypoxia and the extracellular matrix: drivers of tumour metastasis. Nat Rev Cancer. 2014;14(6):430–9.

50. Fraga A, Ribeiro R, Príncipe P, Lopes C, Medeiros R. Hypoxia and Prostate Cancer Aggressiveness: A Tale With Many Endings. Clin Genitourin Cancer. 2015;13(4):295–301.

51. Hompland T, Hole KH kon, Ragnum HB, Aarnes EK, Vlatkovic L, Kathrine Lie A, *et al.* Combined mr imaging of oxygen consumption and supply reveals tumor hypoxia and aggressiveness in prostate cancer patients. Cancer Res . 2018;78(16):4774–85.

52. Bayer C, Shi K, Astner ST, Maftei C-A, Vaupel P. Acute Versus Chronic Hypoxia: Why a Simplified Classification is Simply Not Enough. Int J Radiat Oncol. 2011;80(4):965–8.

53. Abu el Maaty MA, Terzic J, Keime C, Rovito D, Lutzing R, Yanushko D, *et al.* Hypoxia-mediated stabilization of HIF1A in prostatic intraepithelial neoplasia promotes cell plasticity and malignant progression. Sci Adv. 2022;8(29).

54. Stewart GD, Ross JA, McLaren DB, Parker CC, Habib FK, Riddick ACP. The relevance of a hypoxic tumour microenvironment in prostate cancer. BJU International. 2010.

55. Bouleftour W, Rowinski E, Louati S, Sotton S, Wozny A-S, Moreno-Acosta P, *et al.* A Review of the Role of Hypoxia in Radioresistance in Cancer Therapy. Med Sci Monit. 2021;27.

56. Pouget J-P, Frelon S, Ravanat J-L, Testard I, Odin F, Cadet J. Formation of modified DNA bases in cells exposed either to gamma radiation or to high-LET particles. Radiat Res. 2002;157(5):589–95.

57. Brown JM, Wilson WR. Exploiting tumour hypoxia in cancer treatment. Nat Rev Cancer. 2004;4(6):437–47.

58. Bhattacharya IS, Taghavi Azar Sharabiani M, Alonzi R, Hoskin PJ. Hypoxia and angiogenic biomarkers in prostate cancer after external beam radiotherapy (EBRT) alone or combined with high-dose-rate brachytherapy boost (HDR-BTb). Radiother Oncol. 2019;137:38–44.

59. Vergis R, Corbishley CM, Norman AR, Bartlett J, Jhavar S, Borre M, *et al.* Intrinsic markers of tumour hypoxia and angiogenesis in localised prostate cancer and outcome of radical treatment: a retrospective analysis of two randomised radiotherapy trials and one surgical cohort study. Lancet Oncol. 2008;9(4):342–51.

60. Yang L, Roberts D, Takhar M, Erho N, Bibby BAS, Thiruthaneeswaran N, *et al.* Development and Validation of a 28-gene Hypoxia-related Prognostic Signature for Localized Prostate Cancer. EBioMedicine . 2018;31:182–9.

61. Ragnum HB, Vlatkovic L, Lie AK, Axcrona K, Julin CH, Frikstad KM, *et al.* The tumour hypoxia marker pimonidazole reflects a transcriptional programme associated with aggressive prostate cancer. Br J Cancer. 2015;112(2):382–90.

62. Behjati S, Gundem G, Wedge DC, Roberts ND, Tarpey PS, Cooke SL, *et al.* Mutational signatures of ionizing radiation in second malignancies. Nat Commun. 2016;7(1):12605.

63. Kocakavuk E, Anderson KJ, Varn FS, Johnson KC, Amin SB, Sulman EP, *et al.* Radiotherapy is associated with a deletion signature that contributes to poor outcomes in patients with cancer. Nat Genet. 2021;53(7):1088–96.

64. Hoeks CMA, Barentsz JO, Hambrock T, Yakar D, Somford DM, Heijmink SWTPJ, *et al.* Prostate Cancer: Multiparametric MR Imaging for Detection, Localization, and Staging. Radiology. 2011;261(1):46–66.

65. Bjurlin MA, Carroll PR, Eggener S, Fulgham PF, Margolis DJ, Pinto PA, *et al.* Update of the Standard Operating Procedure on the Use of Multiparametric Magnetic Resonance Imaging for the Diagnosis, Staging and Management of Prostate Cancer. J Urol. 2020;203(4):706–12.

66. Weinreb JC, Barentsz JO, Choyke PL, Cornud F, Haider MA, Macura KJ, *et al.* PI-RADS Prostate Imaging – Reporting and Data System: 2015, Version 2. Eur Urol. 2016;69(1):16–40.

67. Sourbron SP, Buckley DL. On the scope and interpretation of the Tofts models for DCE-MRI. Magn Reson Med . 2011;66(3):735-745.

68. Berman RM, Brown AM, Chang SD, Sankineni S, Kadakia M, Wood BJ, *et al.* DCE MRI of prostate cancer. Abdom Radiol. 2016;41(5):844–53.

69. Horsman MR, Mortensen LS, Petersen JB, Busk M, Overgaard J. Imaging hypoxia to improve radiotherapy outcome. Nat Rev Clin Oncol. 2012;9(12):674–87.

70. Hoskin PJ, Carnell DM, Taylor NJ, Smith RE, Stirling JJ, Daley FM, *et al.* Hypoxia in Prostate Cancer: Correlation of BOLD-MRI With Pimonidazole Immunohistochemistry-Initial Observations. Int J Radiat Oncol Biol Phys . 2007;68(4):1065–71.

71. Taylor NJ, Baddeley H, Goodchild KA, Powell MEB, Thoumine M, Culver LA, *et al.* BOLD MRI of human tumor oxygenation during carbogen breathing. J Magn Reson Imaging. 2001;14(2):156–63.

72. Kooreman ES, van Houdt PJ, Keesman R, Pos FJ, van Pelt VWJ, Nowee ME, *et al.* ADC measurements on the Unity MR-linac – A recommendation on behalf of the Elekta Unity MR-linac consortium. Radiother Oncol. 2020;153:106–13.

73. Iima M, Le Bihan D. Clinical Intravoxel Incoherent Motion and Diffusion MR Imaging: Past, Present, and Future. Radiology. 2016;278(1):13–32.

74. Kato H, Esaki K, Yamaguchi T, Tanaka H, Kajita K, Furui T, *et al.* Predicting Early Response to Chemoradiotherapy for Uterine Cervical Cancer Using Intravoxel Incoherent Motion MR Imaging. Magn Reson Med Sci. 2019;18(4):293–8.

75. D'Amico A V., Whittington R, Malkowicz SB, Fondurulia J, Chen M-H, Kaplan I, *et al.* Pretreatment Nomogram for Prostate-Specific Antigen Recurrence After Radical Prostatectomy or External-Beam Radiation Therapy for Clinically Localized Prostate Cancer. J Clin Oncol. 1999;17(1):168–168.

76. Gabriele D, Jereczek-Fossa BA, Krengli M, Garibaldi E, Tessa M, Moro G, *et al.* Beyond D'Amico risk classes for predicting recurrence after external beam radiotherapy for prostate cancer: the Candiolo classifier. Radiat Oncol. 2016;11(1):23.

77. Gabriele D, Guarneri A, Bartoncini S, Munoz F, Tamponi M, Russo F, *et al.* An external validation of the Candiolo nomogram in a cohort of prostate cancer patients treated by external-beam radiotherapy. Radiat Oncol. 2021;16(1):85.

78. Cooperberg MR, Hilton JF, Carroll PR. The CAPRA-S score. Cancer. 2011;117(22):5039–46.

79. Brajtbord JS, Leapman MS, Cooperberg MR. The CAPRA Score at 10 Years: Contemporary Perspectives and Analysis of Supporting Studies. Eur Urol. 2017;71(5):705–9.

80. Thurtle DR, Greenberg DC, Lee LS, Huang HH, Pharoah PD, Gnanapragasam VJ. Individual prognosis at diagnosis in nonmetastatic prostate cancer: Development and external validation of the PREDICT Prostate multivariable model. Johnstone RW, editor. PLOS Med. 2019;16(3):e1002758.

81. Thurtle D, Jenkins V, Freeman A, Pearson M, Recchia G, Tamer P, *et al.* Clinical Impact of the Predict Prostate Risk Communication Tool in Men Newly Diagnosed with Nonmetastatic Prostate Cancer: A Multicentre Randomised Controlled Trial. Eur Urol. 2021;80(5):661–9.

82. Ross AE, Johnson MH, Yousefi K, Davicioni E, Netto GJ, Marchionni L, *et al.* Tissue-based Genomics Augments Post-prostatectomy Risk Stratification in a Natural History Cohort of Intermediate- and High-Risk Men. Eur Urol. 2016;69(1):157–65.

83. Shi, Bao, Weischenfeldt, Schaefer, Rogowski, Schmidt-Hegemann, *et al.* A Novel Gene Signature-Based Model Predicts Biochemical Recurrence-Free Survival in Prostate Cancer Patients after Radical Prostatectomy. Cancers (Basel). 2019;12(1):1.

84. Lotan TL, Tomlins SA, Bismar TA, Van der Kwast TH, Grignon D, Egevad L, *et al.* Report From the International Society of Urological Pathology (ISUP) Consultation Conference on Molecular Pathology of Urogenital Cancers. I. Molecular Biomarkers in Prostate Cancer. Am J Surg Pathol. 2020;44(7):e15–29.

85. Shiradkar R, Ghose S, Jambor I, Taimen P, Ettala O, Purysko AS, *et al.* Radiomic features from pretreatment biparametric MRI predict prostate cancer biochemical recurrence: Preliminary findings. J Magn Reson Imaging . 2018;48(6):1626–36.

86. Hectors SJ, Cherny M, Yadav KK, Beksaç AT, Thulasidass H, Lewis S, *et al.* Radiomics Features Measured with Multiparametric Magnetic Resonance Imaging Predict Prostate Cancer Aggressiveness. J Urol. 2019;202(3):498–505.

87. Bourbonne V, Vallières M, Lucia F, Doucet L, Visvikis D, Tissot V, *et al.* MRI-derived radiomics to guide post-operative management for high-risk prostate cancer. Front Oncol . 2019;9:807.

88. Abdollahi H, Mofid B, Shiri I, Razzaghdoust A, Saadipoor A, Mahdavi A, *et al.* Machine learning-based radiomic models to predict intensity-modulated radiation therapy response, Gleason score and stage in prostate cancer. Radiol Med. 2019;124(6):555–67.

89. Hiremath A, Shiradkar R, Fu P, Mahran A, Rastinehad AR, Tewari A, *et al.* An integrated nomogram combining deep learning, Prostate Imaging–Reporting and Data System (PI-RADS) scoring, and clinical variables for identification of clinically significant prostate cancer on biparametric MRI: a retrospective multicentre study. Lancet Digit Heal. 2021;3(7):e445–54.

90. Ankerst DP, Straubinger J, Selig K, Guerrios L, De Hoedt A, Hernandez J, *et al.* A Contemporary Prostate Biopsy Risk Calculator Based on Multiple Heterogeneous Cohorts. Eur Urol. 2018;74(2):197–203.

91. Thompson IM, Ankerst DP, Chi C, Goodman PJ, Tangen CM, Lucia MS, *et al.* Assessing Prostate Cancer Risk: Results from the Prostate Cancer Prevention Trial. JNCI J Natl Cancer Inst. 2006;98(8):529–34.

92. Rayn KN, Bloom JB, Gold SA, Hale GR, Baiocco JA, Mehralivand S, *et al.* Added Value of Multiparametric Magnetic Resonance Imaging to Clinical Nomograms for Predicting Adverse Pathology in Prostate Cancer. J Urol. 2018;200(5):1041–7.

93. Mottet N, van den Bergh RCN, Briers E, Van den Broeck T, Cumberbatch MG, De Santis M, et al. EAU-EANM-ESTRO-ESUR-SIOG Guidelines on Prostate Cancer—2020 Update. Part 1: Screening, Diagnosis, and Local Treatment with Curative Intent. Eur Urol. 2021;79(2):243–62.

94. Cornford P, van den Bergh RCN, Briers E, Van den Broeck T, Cumberbatch MG, De Santis M, et al. EAU-EANM-ESTRO-ESUR-SIOG Guidelines on Prostate Cancer. Part II—2020 Update: Treatment of Relapsing and Metastatic Prostate Cancer. Eur Urol. 2021;79(2):263–82.

95. Lowrance WT, Breau RH, Chou R, Chapin BF, Crispino T, Dreicer R, et al. Advanced Prostate Cancer: AUA/ASTRO/SUO Guideline PART I. J Urol. 2021;205(1):14–21.

96. Slevin F, Beasley M, Cross W, Scarsbrook A, Murray L, Henry A. Patterns of Lymph Node Failure in Patients With Recurrent Prostate Cancer Postradical Prostatectomy and Implications for Salvage Therapies. Adv Radiat Oncol . 2020;5(6):1126-1140.

97. Bukavina L, Luckenbaugh AN, Hofman MS, Hope T, Kamran SC, Murphy DG, *et al.* Incorporating Prostate-specific Membrane Antigen Positron Emission Tomography in Management Decisions for Men with Newly Diagnosed or Biochemically Recurrent Prostate Cancer. Eur Urol. 2023;83(6):521–33.

98. Fendler WP, Calais J, Eiber M, Simko JP, Kurhanewicz J, Santos RD, *et al.* False positive PSMA PET for tumor remnants in the irradiated prostate and other interpretation pitfalls in a prospective multi-center trial. Eur J Nucl Med Mol Imaging. 2021;48(2):501–8.

99. Arrayeh E, Westphalen AC, Kurhanewicz J, Roach M, Jung AJ, Carroll PR, *et al.* Does Local Recurrence of Prostate Cancer After Radiation Therapy Occur at the Site of Primary Tumor? Results of a Longitudinal MRI and MRSI Study. Int J Radiat Oncol. 2012;82(5):e787–93.

100. Kim CK, Park BK, Park W, Kim SS. Prostate MR imaging at 3T using a phased-arrayed coil in predicting locally recurrent prostate cancer after radiation therapy: preliminary experience. Abdom Imaging. 2010;35(2):246–52.

101. Patel P, Mathew MS, Trilisky I, Oto A. Multiparametric MR Imaging of the Prostate after Treatment of Prostate Cancer. RadioGraphics. 2018;38(2):437–49.

102. Franiel T, Lüdemann L, Taupitz M, Böhmer D, Beyersdorff D. MRI before and after external beam intensity-modulated radiotherapy of patients with prostate cancer: The feasibility of monitoring of radiation-induced tissue changes using a dynamic contrast-enhanced inversion-prepared dual-contrast gradient echo sequen. Radiother Oncol. 2009;93(2):241–5.

103. Chan TW, Kressel HY. Prostate and seminal vesicles after irradiation: MR appearance. J Magn Reson Imaging. 1991;1(5):503–11.

104. Coakley F V., Teh HS, Qayyum A, Swanson MG, Lu Y, Roach M, *et al.* Endorectal MR Imaging and MR Spectroscopic Imaging for Locally Recurrent

Prostate Cancer after External Beam Radiation Therapy: Preliminary Experience. Radiology. 2004;233(2):441–8.

105. Hötker AM, Mazaheri Y, Zheng J, Moskowitz CS, Berkowitz J, Lantos JE, *et al.* Prostate Cancer: assessing the effects of androgen-deprivation therapy using quantitative diffusion-weighted and dynamic contrast-enhanced MRI. Eur Radiol. 2015;25(9):2665–72.

106. Kim AY, Kim CK, Park SY, Park BK. Diffusion-Weighted Imaging to Evaluate for Changes From Androgen Deprivation Therapy in Prostate Cancer. Am J Roentgenol. 2014;203(6):W645–50.

107. Panebianco V, Villeirs G, Weinreb JC, Turkbey BI, Margolis DJ, Richenberg J, et al. Prostate Magnetic Resonance Imaging for Local Recurrence Reporting (PI-RR): International Consensus -based Guidelines on Multiparametric Magnetic Resonance Imaging for Prostate Cancer Recurrence after Radiation Therapy and Radical Prostatectomy. Eur Urol Oncol. 2021;1–9.

108. Yip SSF, Aerts HJWL. Applications and limitations of radiomics. Phys Med Biol. 2016;61(13):R150–66.

109. Yang F, Young L, Grigsby P. Predictive Value of Standardized Intratumoral Metabolic Heterogeneity in Locally Advanced Cervical Cancer Treated With Chemoradiation. Int J Gynecol Cancer. 2016;26(4):777–84.

110. Kumar V, Gu Y, Basu S, Berglund A, Eschrich SA, Schabath MB, *et al.* Radiomics: The process and the challenges. Magn Reson Imaging . 2012;30(9):1234–48.

111. Lambin P, Leijenaar RTH, Deist TM, Peerlings J, De Jong EEC, Van Timmeren J, *et al.* Radiomics: The bridge between medical imaging and personalized medicine. Nat Rev Clin Oncol . 2017;4(12):749-762.

112. Zwanenburg A, Vallières M, Abdalah MA, Aerts HJWL, Andrearczyk V, Apte A, *et al.* The Image Biomarker Standardization Initiative: Standardized Quantitative Radiomics for High-Throughput Image-based Phenotyping. Radiology. 2020;295(2):328–38.

113. Barentsz JO, Richenberg J, Clements R, Choyke P, Verma S, Villeirs G, *et al.* ESUR prostate MR guidelines 2012. Eur Radiol. 2012;22(4):746–57.

114. Brizmohun Appayya M, Adshead J, Ahmed HU, Allen C, Bainbridge A, Barrett T, *et al.* National implementation of multi-parametric magnetic resonance imaging for

prostate cancer detection – recommendations from a UK consensus meeting. BJU Int . 2018;122(1):13–25.

115. Zhang B, Tian J, Dong D, Gu D, Dong Y, Zhang L, *et al.* Radiomics Features of Multiparametric MRI as Novel Prognostic Factors in Advanced Nasopharyngeal Carcinoma. Clin Cancer Res. 2017;23(15):4259–69.

116. Smith CP, Czarniecki M, Mehralivand S, Stoyanova R, Choyke PL, Harmon S, *et al.* Radiomics and radiogenomics of prostate cancer. Abdom Radiol. 2019;44(6):2021–9.

117. Hoeks CMA, Hambrock T, Yakar D, Hulsbergen–van de Kaa CA, Feuth T, Witjes JA, *et al.* Transition Zone Prostate Cancer: Detection and Localization with 3-T Multiparametric MR Imaging. Radiology. 2013;266(1):207–17.

118. Eminowicz G, McCormack M. Variability of clinical target volume delineation for definitive radiotherapy in cervix cancer. Radiother Oncol. 2015;117(3):542–7.

119. Isebaert S, Van den Bergh L, Haustermans K, Joniau S, Lerut E, De Wever L, *et al.* Multiparametric MRI for prostate cancer localization in correlation to whole-mount histopathology. J Magn Reson Imaging. 2013;37(6):1392–401.

120. Shafiq-Ul-Hassan M, Zhang GG, Latifi K, Ullah G, Hunt DC, Balagurunathan Y, *et al.* Intrinsic dependencies of CT radiomic features on voxel size and number of gray levels. Med Phys . 2017;44(3):1050–62.

121. Larue RTHM, Defraene G, De Ruysscher D, Lambin P, Van Elmpt W. Quantitative radiomics studies for tissue characterization: A review of technology and methodological procedures. Br J Radiol . 2017;90(1070).

122. Leijenaar RTH, Nalbantov G, Carvalho S, Van Elmpt WJC, Troost EGC, Boellaard R, *et al.* The effect of SUV discretization in quantitative FDG-PET Radiomics: The need for standardized methodology in tumor texture analysis. Sci Rep . 2015;5(November 2014):1–10.

123. Zhao B, James LP, Moskowitz CS, Guo P, Ginsberg MS, Lefkowitz RA, *et al.* Evaluating Variability in Tumor Measurements from Same-day Repeat CT Scans of Patients with Non–Small Cell Lung Cancer. Radiology. 2009;252(1):263–72.

124. Sadinski M, Medved M, Karademir I, Wang S, Peng Y, Jiang Y, *et al.* Short-term reproducibility of apparent diffusion coefficient estimated from diffusion-weighted MRI of the prostate. Abdom Imaging. 2015;40(7):2523–8.

125. Alonzi R, Taylor NJ, Stirling JJ, D'Arcy JA, Collins DJ, Saunders MI, *et al.* Reproducibility and correlation between quantitative and semiquantitative dynamic and intrinsic susceptibility-weighted MRI parameters in the benign and malignant human prostate. J Magn Reson Imaging. 2010;32(1):155–64.

126. Aerts HJWL, Velazquez ER, Leijenaar RTH, Parmar C, Grossmann P, Cavalho S, *et al.* Decoding tumour phenotype by noninvasive imaging using a quantitative radiomics approach. Nat Commun . 2014;3(5):4006.

127. Leijenaar RTH, Carvalho S, Velazquez ER, van Elmpt WJC, Parmar C, Hoekstra OS, *et al.* Stability of FDG-PET Radiomics features: An integrated analysis of test-retest and inter-observer variability. Acta Oncol (Madr). 2013;52(7):1391–7.

128. Bologna M, Corino VDA, Montin E, Messina A, Calareso G, Greco FG, *et al.* Assessment of Stability and Discrimination Capacity of Radiomic Features on Apparent Diffusion Coefficient Images. J Digit Imaging. 2018;31(6):879–94.

129. Reproducibility and Replicability in Science [Internet]. Washington, D.C.: National Academies Press; 2019.

130. Schwier M, van Griethuysen J, Vangel MG, Pieper S, Peled S, Tempany C, *et al.* Repeatability of Multiparametric Prostate MRI Radiomics Features. Sci Rep . 2019;9(1):1–16.

131. Stanzione A, Gambardella M, Cuocolo R, Ponsiglione A, Romeo V, Imbriaco M. Prostate MRI radiomics: A systematic review and radiomic quality score assessment. Eur J Radiol. 2020;129(April):109095.

132. Um H, Tixier F, Bermudez D, Deasy JO, Young RJ, Veeraraghavan H. Impact of image preprocessing on the scanner dependence of multi-parametric MRI radiomic features and covariate shift in multi-institutional glioblastoma datasets. Phys Med Biol. 2019;64(16):165011.

133. Moradmand H, Aghamiri SMR, Ghaderi R. Impact of image preprocessing methods on reproducibility of radiomic features in multimodal magnetic resonance imaging in glioblastoma. J Appl Clin Med Phys. 2020;21(1):179–90.

134. Chatterjee A, Vallieres M, Dohan A, Levesque IR, Ueno Y, Saif S, *et al.* Creating Robust Predictive Radiomic Models for Data From Independent Institutions Using Normalization. IEEE Trans Radiat Plasma Med Sci. 2019;3(2):210–5.

135. Carré A, Klausner G, Edjlali M, Lerousseau M, Briend-Diop J, Sun R, *et al.* Standardization of brain MR images across machines and protocols: bridging the gap for MRI-based radiomics. Sci Rep. 2020;10(1):12340.

136. Nyul LG, Udupa JK, Xuan Zhang. New variants of a method of MRI scale standardization. IEEE Trans Med Imaging. 2000;19(2):143–50.

137. Johnson WE, Li C, Rabinovic A. Adjusting batch effects in microarray expression data using empirical Bayes methods. Biostatistics. 2007;8(1):118–27.

138. Lucia F, Visvikis D, Vallières M, Desseroit M-C, Miranda O, Robin P, *et al.* External validation of a combined PET and MRI radiomics model for prediction of recurrence in cervical cancer patients treated with chemoradiotherapy. Eur J Nucl Med Mol Imaging. 2019;46(4):864–77.

139. Orlhac F, Boughdad S, Philippe C, Stalla-Bourdillon H, Nioche C, Champion L, *et al.* A Postreconstruction Harmonization Method for Multicenter Radiomic Studies in PET. J Nucl Med. 2018;59(8):1321–8.

140. Orlhac F, Lecler A, Savatovski J, Goya-Outi J, Nioche C, Charbonneau F, *et al.* How can we combat multicenter variability in MR radiomics? Validation of a correction procedure. Eur Radiol. 2021;31(4):2272–80.

141. Da-ano R, Masson I, Lucia F, Doré M, Robin P, Alfieri J, *et al.* Performance comparison of modified ComBat for harmonization of radiomic features for multicenter studies. Sci Rep . 2020;10(1):1–12.

142. Orlhac F, Frouin F, Nioche C, Ayache N, Buvat I. Validation of a method to compensate multicenter effects affecting CT radiomics. Radiology . 2019;291(1):53–9.

143. Gebre RK, Senjem ML, Raghavan S, Schwarz CG, Gunter JL, Hofrenning EI, *et al.* Cross–scanner harmonization methods for structural MRI may need further work: A comparison study. Neuroimage. 2023;269:119912.

144. Dewey BE, Zhao C, Reinhold JC, Carass A, Fitzgerald KC, Sotirchos ES, *et al.* DeepHarmony: A deep learning approach to contrast harmonization across scanner changes. Magn Reson Imaging. 2019;64:160–70.

145. Fatania K, Clark A, Frood R, Scarsbrook A, Al-Qaisieh B, Currie S, *et al.* Harmonisation of scanner-dependent contrast variations in magnetic resonance

imaging for radiation oncology, using style-blind auto-encoders. Phys Imaging Radiat Oncol. 2022;22:115–22.

146. Parmar C, Grossmann P, Bussink J, Lambin P, Aerts HJWL. Machine Learning methods for Quantitative Radiomic Biomarkers. Sci Rep . 2015;5(13087).

147. Shur JD, Doran SJ, Kumar S, ap Dafydd D, Downey K, O'Connor JPB, *et al.* Radiomics in Oncology: A Practical Guide. RadioGraphics. 2021;41(6):1717–32.

148. Wang J, Wu C-J, Bao M-L, Zhang J, Wang X-N, Zhang Y-D. Machine learning-based analysis of MR radiomics can help to improve the diagnostic performance of PI-RADS v2 in clinically relevant prostate cancer. Eur Radiol. 2017;27(10):4082–90.

149. Bonekamp D, Kohl S, Wiesenfarth M, Schelb P, Radtke JP, Götz M, *et al.* Radiomic Machine Learning for Characterization of Prostate Lesions with MRI: Comparison to ADC Values. Radiology. 2018;289(1):128–37.

150. Wu M, Krishna S, Thornhill RE, Flood TA, McInnes MDF, Schieda N. Transition zone prostate cancer: Logistic regression and machine-learning models of quantitative ADC, shape and texture features are highly accurate for diagnosis. J Magn Reson Imaging. 2019;50(3):940–50.

151. Willemink MJ, Koszek WA, Hardell C, Wu J, Fleischmann D, Harvey H, *et al.* Preparing Medical Imaging Data for Machine Learning. Radiology. 2020;295(1):4–15.

152. Gholami R, Fakhari N. Support Vector Machine: Principles, Parameters, and Applications. In: Handbook of Neural Computation. Elsevier; 2017. p. 515–35.

153. Uddin S, Khan A, Hossain ME, Moni MA. Comparing different supervised machine learning algorithms for disease prediction. BMC Med Inform Decis Mak. 2019;19(1):281.

154. Bodalal Z, Trebeschi S, Nguyen-Kim TDL, Schats W, Beets-Tan R. Radiogenomics: bridging imaging and genomics. Abdom Radiol. 2019;44(6):1960–84.

155. Binder ZA, Thorne AH, Bakas S, Wileyto EP, Bilello M, Akbari H, *et al.* Epidermal Growth Factor Receptor Extracellular Domain Mutations in Glioblastoma Present Opportunities for Clinical Imaging and Therapeutic Development. Cancer Cell. 2018;34(1):163-177.e7.

156. Kirienko M, Sollini M, Corbetta M, Voulaz E, Gozzi N, Interlenghi M, *et al.* Radiomics and gene expression profile to characterise the disease and predict outcome in patients with lung cancer. Eur J Nucl Med Mol Imaging. 2021;48(11):3643–55.

157. Fjeldbo CS, Hompland T, Hillestad T, Aarnes E-K, Günther C-C, Kristensen GB, *et al.* Combining imaging- and gene-based hypoxia biomarkers in cervical cancer improves prediction of chemoradiotherapy failure independent of intratumour heterogeneity. EBioMedicine. 2020;57:102841.

158. Fan M, Xia P, Clarke R, Wang Y, Li L. Radiogenomic signatures reveal multiscale intratumour heterogeneity associated with biological functions and survival in breast cancer. Nat Commun. 2020;11(1):4861.

159. Mirón Mombiela R, Arildskov AR, Bruun FJ, Hasselbalch LH, Holst KB, Rasmussen SH, *et al.* What Genetics Can Do for Oncological Imaging: A Systematic Review of the Genetic Validation Data Used in Radiomics Studies. Int J Mol Sci. 2022;23(12):6504.

160. Tomaszewski MR, Gillies RJ. The Biological Meaning of Radiomic Features. Radiology. 2021;298(3):505–16.

161. Gao J, Ye F, Han F, Wang X, Jiang H, Zhang J. A Novel Radiogenomics Biomarker Based on Hypoxic-Gene Subset: Accurate Survival and Prognostic Prediction of Renal Clear Cell Carcinoma. Front Oncol. 2021;11.

162. Beig N, Bera K, Prasanna P, Antunes J, Correa R, Singh S, *et al.* Radiogenomic-based survival risk stratification of tumor habitat on Gd-T1w MRI is associated with biological processes in glioblastoma. Clin Cancer Res . 2020;26(8):1866–76.

163. Pathmanathan AU, Schmidt MA, Brand DH, Kousi E, As NJ, Tree AC. Improving fiducial and prostate capsule visualization for radiotherapy planning using <scp>MRI</scp>. J Appl Clin Med Phys. 2019;20(3):27–36.

164. Tocco BR, Kishan AU, Ma TM, Kerkmeijer LGW, Tree AC. MR-Guided Radiotherapy for Prostate Cancer. Front Oncol . 2020;10:1–11.

165. Spratt DE, Lee JY, Dess RT, Narayana V, Evans C, Liss A, *et al.* Vessel-sparing Radiotherapy for Localized Prostate Cancer to Preserve Erectile Function: A Single-arm Phase 2 Trial. Eur Urol. 2017;72(4):617–24.

166. Syndikus I, Cruickshank C, Staffurth J, Tree A, Henry A, Naismith O, et al. PIVOTALboost: A phase III randomised controlled trial of prostate and pelvis versus prostate alone radiotherapy with or without prostate boost (CRUK/16/018). Clin Transl Radiat Oncol. 2020;25:22–8.

167. Tetar SU, Bruynzeel AME, Lagerwaard FJ, Slotman BJ, Bohoudi O, Palacios MA. Clinical implementation of magnetic resonance imaging guided adaptive radiotherapy for localized prostate cancer. Phys Imaging Radiat Oncol. 2019;9:69–76.

168. Bruynzeel AME, Tetar SU, Oei SS, Senan S, Haasbeek CJA, Spoelstra FOB, *et al.* A Prospective Single-Arm Phase 2 Study of Stereotactic Magnetic Resonance Guided Adaptive Radiation Therapy for Prostate Cancer: Early Toxicity Results. Int J Radiat Oncol. 2019;105(5):1086–94.

169. Dearnaley DP, Jovic G, Syndikus I, Khoo V, Cowan RA, Graham JD, *et al.* Escalated-dose versus control-dose conformal radiotherapy for prostate cancer: Long-term results from the MRC RT01 randomised controlled trial. Lancet Oncol . 2014;15(4):464–73.

170. Aluwini S, Pos F, Schimmel E, van Lin E, Krol S, van der Toorn PP, *et al.* Hypofractionated versus conventionally fractionated radiotherapy for patients with prostate cancer (HYPRO): acute toxicity results from a randomised non-inferiority phase 3 trial. Lancet Oncol. 2015;16(3):274–83.

171. Tetar SU, Bruynzeel AME, Oei SS, Senan S, Fraikin T, Slotman BJ, *et al.* Magnetic Resonance-guided Stereotactic Radiotherapy for Localized Prostate Cancer: Final Results on Patient-reported Outcomes of a Prospective Phase 2 Study. Eur Urol Oncol. 2021;4(4):628–34.

172. Alongi F, Rigo M, Figlia V, Cuccia F, Giaj-Levra N, Nicosia L, *et al.* 1.5 T MR-guided and daily adapted SBRT for prostate cancer: feasibility, preliminary clinical tolerability, quality of life and patient-reported outcomes during treatment. Radiat Oncol. 2020;15(1):69.

173. Ling CC, Humm J, Larson S, Amols H, Fuks Z, Leibel S, *et al.* Towards multidimensional radiotherapy (MD-CRT): biological imaging and biological conformality. Int J Radiat Oncol. 2000;47(3):551–60.

174. van Houdt PJ, Yang Y, van der Heide UA. Quantitative Magnetic Resonance Imaging for Biological Image-Guided Adaptive Radiotherapy. Front Oncol. 2021;10.

175. Fredén E, Tilly D, Ahnesjö A. Adaptive dose painting for prostate cancer. Front Oncol. 2022;12.

176. Liu L, Wu N, Ouyang H, Dai J-R, Wang W-H. Diffusion-weighted MRI in early assessment of tumour response to radiotherapy in high-risk prostate cancer. Br J Radiol. 2014;87(1043):20140359.

177. Lalonde E, Ishkanian AS, Sykes J, Fraser M, Ross-Adams H, Erho N, *et al.* Tumour genomic and microenvironmental heterogeneity for integrated prediction of 5-year biochemical recurrence of prostate cancer: a retrospective cohort study. Lancet Oncol. 2014;15(13):1521–32.

178. Datta A, West C, O'Connor JPB, Choudhury A, Hoskin P. Impact of hypoxia on cervical cancer outcomes. Int J Gynecol Cancer. 2021;31(11):1459–70.

179. Decker G, Mürtz P, Gieseke J, Träber F, Block W, Sprinkart AM, *et al.* Intensity-modulated radiotherapy of the prostate: Dynamic ADC monitoring by DWI at 3.0T. Radiother Oncol. 2014;113(1):115–20.

180. Wu X, Reinikainen P, Kapanen M, Vierikko T, Ryymin P, Kellokumpu-Lehtinen P-L. Monitoring radiotherapy induced tissue changes in localized prostate cancer by multi-parametric magnetic resonance imaging (MP-MRI). Diagn Interv Imaging. 2019;100(11):699–708.

181. Verma S, Turkbey B, Muradyan N, Rajesh A, Cornud F, Haider MA, *et al.* Overview of Dynamic Contrast-Enhanced MRI in Prostate Cancer Diagnosis and Management. Am J Roentgenol. 2012;198(6):1277–88.

182. van Schie MA, van Houdt PJ, Ghobadi G, Pos FJ, Walraven I, de Boer HCJ, *et al.* Quantitative MRI Changes During Weekly Ultra-Hypofractionated Prostate Cancer Radiotherapy With Integrated Boost. Front Oncol . 2019;9(December).

183. McPartlin A, Kershaw L, McWilliam A, Taylor M Ben, Hodgson C, van Herk M, *et al.* Changes in prostate apparent diffusion coefficient values during radiotherapy after neoadjuvant hormones. Ther Adv Urol. 2018;10(12):359–64.

184. Gnep K, Fargeas A, Gutiérrez-Carvajal RE, Commandeur F, Mathieu R, Ospina JD, *et al.* Haralick textural features on T 2 -weighted MRI are associated with

biochemical recurrence following radiotherapy for peripheral zone prostate cancer. J Magn Reson Imaging. 2017;45(1):103–17.

185. National Cancer Institute. Common Terminology Criteria for Adverse Events (CTCAE) version 5.0. NIH Publ [Internet]. 2020;

186. Abdollahi H, Mahdavi SR, Mofid B, Bakhshandeh M, Razzaghdoust A, Saadipoor A, *et al.* Rectal wall MRI radiomics in prostate cancer patients: prediction of and correlation with early rectal toxicity. Int J Radiat Biol . 2018;94:829–837.

187. Abdollahi H, Tanha K, Mofid B, Razzaghdoust A, Saadipoor A, Khalafi L, *et al.* MRI Radiomic Analysis of IMRT-Induced Bladder Wall Changes in Prostate Cancer Patients: A Relationship with Radiation Dose and Toxicity. J Med Imaging Radiat Sci . 2019;50:252–260.

Chapter 2
Prediction of Prostate Tumour Hypoxia Using Pre-treatment MRI-derived Radiomics – Preliminary Findings

2.1 Abstract

2.1.1 Purpose

To develop a machine learning (ML) model based on radiomic features (RF) extracted from whole prostate gland magnetic resonance imaging (MRI) for prediction of tumour hypoxia pre-radiotherapy.

2.1.2 Methods

Consecutive patients with high-grade prostate cancer and pre-treatment MRI treated with radiotherapy between 01/12/2007-31/08/2013 at two cancer centres were included. Cancers were dichotomised as normoxic or hypoxic using a biopsy-based 32-gene hypoxia signature (Ragnum signature). Prostate segmentation was performed on axial T2 weighted (T2W) sequences using RayStation (v9.1). Histogram standardisation was applied prior to RF extraction. PyRadiomics (v3.0.1) was used to extract RFs for analysis. The cohort was split 80:20 into training and test sets. Six different ML classifiers for distinguishing hypoxia were trained and tuned using five different feature selection models and five-fold cross validation with 20 repeats. The model with highest mean validation area under the curve (AUC) receiver operating characteristic (ROC) curve was tested on the unseen set and AUCs were compared via DeLong test with 95% confidence interval (CI).

2.1.3 Results

195 patients were included with 97 (49.7%) having hypoxic tumours. The hypoxia-prediction model with best performance was derived using ridge regression and had a test AUC of 0.69 (95% CI: 0.14). The test AUC for the clinical-only model was lower (0.57) but this was not statistically significant ($p = 0.35$). The five selected RFs included textural and wavelet-transformed features.

2.1.4 Conclusion

Whole prostate MRI-radiomics has the potential to non-invasively predict tumour hypoxia prior to radiotherapy which may be helpful for individualised treatment optimisation.

2.2 Background

Prostate cancer is the commonest malignancy in men and a major cause of cancer-related death[1]. Radiation therapy (RT), including external beam radiation therapy (EBRT) and brachytherapy (BT), is an effective treatment for localised prostate cancer[2]. Despite advances in diagnostic imaging and RT delivery techniques, treatment failure remains common with biochemical failure occurring in almost half of high risk patients at 10 years [3–5].

Tumour hypoxia, a low oxygen environment, is associated with RT resistance and metastatic disease in prostate cancer [6–9]. Identifying tumour hypoxia may help with patient selection for radiation boosting. Current methods of assessing hypoxia, such as using prostate biopsy samples to identify gene-based hypoxia biomarkers, or oxygen electrodes, are invasive and hindered by sampling errors due to multi-focal tumours and intra-tumoral heterogeneity[10]. Positron emission tomography (PET) based hypoxia imaging using PET tracers based on 2-Nitroimidazole, originally developed as a radiosensitiser for hypoxic cells, have shown promise as imaging-based hypoxia biomarkers [11]. This includes the tracers Fluorine-18 (^{18}F)fluoroimidazole (^{18}F-FMISO) and ^{18}F-FAZA [1-(5-fluoro-5-deoxy-α-D-arabinofuranosyl)-2-nitroimidazole)], the latter of which is a second-generation drug which has improved pharmacokinetic properties allowing for better hypoxia-normoxia contrast at earlier time points [11]. Issues remain regarding the reproducibility of PET-based hypoxia imaging, availability of such tracers and identifying appropriate hypoxia thresholds for different tumour types. Magnetic resonance imaging (MRI) offers a potential non-invasive method of assessing hypoxia that allows the whole prostate to be measured and assessed over time, i.e. before, during and following treatment to monitor response.

Radiomics is a quantitative method of imaging analysis using data-characterisation algorithms to derive imaging biomarkers[12]. Imaging-based radiogenomics offers promise in bridging the gap between medical imaging and histopathological or molecular/gene signatures, by integrating data generated from complementary data sources to improve the accuracy of predictive models[13]. Machine learning (ML) models based on radiomic features (RF) extracted from T2 weighted (T2W) prostate MRI have demonstrated good performance for detecting clinically significant cancer[14]. Radiomic signatures have also been shown to accurately predict molecular subtypes of cancers associated with a more invasive phenotype[14]. The application of ML to radiogenomic studies provides novel insights into tumour biology and has been evaluated in multiple tumour types[15–17]. Identifying hypoxia on T2W prostate MRI also has

treatment implications given the role of MRI-guided RT, which already incorporates a T2W sequence into the standard workflow, therefore there is potential for dose escalation based on an imaging radiogenomic approach.

The aim of this study was to develop a ML model based on RFs extracted from whole gland prostate MRI for prediction of tumour hypoxia pre-radiotherapy.

2.3 Materials and Methods

2.3.1 Dataset and Study Population

This retrospective study was approved by the United Kingdom North West Research Ethics Committee (Validation and qualification of a multiplex hypoxia biomarker for radiotherapy individualisation in prostate cancer study (IRAS 15/NW/0559)). Informed consent was obtained from all patients.

The study cohort consisted of 195 consecutive patients with histologically confirmed high-risk prostate cancer treated between 01/12/2007-31/08/2013 at either St James's University Hospital (Leeds, UK) with EBRT (74 Gray (Gy) in 37 fractions) (N=100) or at The Christie (Manchester, UK) with EBRT (57 Gy in 19 fractions) or EBRT (37.5 Gy in 15 fractions) plus high dose rate (HDR) brachytherapy (BT) boost (single fraction 15 Gy) (N=95).

Inclusion criteria were: (a) male patients with prostate cancer aged at least 18 years; (b) primary radiotherapy to treat their prostate cancer (either BT or EBRT); (c) available pre-treatment MRI and hypoxia gene signature data; (d) available clinical features (patient age, International Society of Urological Pathology (ISUP) grade, prostate specific antigen (PSA) and T-stage).

2.3.2 MRI Acquisition

All patients underwent prostate MRI on 1.5T MRI scanners which included a minimum of an axial T2W sequence encompassing the whole prostate. Imaging was performed using multiple different MRI scanners. Specific scanner acquisition parameters are listed in Supplementary Material Table S2.1.

2.3.3 Hypoxia Gene Signature

All patients were grouped into normoxia and hypoxia groups based on their pre-treatment prostate biopsy which was used as the ground truth for hypoxia status. The ribonucleic acid (RNA) from formalin-fixed, paraffin-embedded prostate biopsy specimens was extracted and samples were processed using Affymetrix GeneChip (Clariom S Array) to calculate the expression of a 32-gene prostate hypoxia signature, based on pimonidazole staining (Ragnum signature)[10]. The gene enrichment analysis and construction of the gene signature is described by Ragnum et al. [10]. The normoxia and hypoxia split was based on a previously validated threshold[19].

2.3.4 Study Pipeline

Adherence was made to the Checklist for Artificial Intelligence in Medical Imaging (CLAIM) (Supplementary Material), a tool for assessing the quality of multivariate prediction models involving ML techniques[20].

2.3.5 Image Seqmentation

All imaging data was de-identified using a data masking method. The whole prostate gland and prostate tumour (if visible) were manually segmented by an experienced radiologist and confirmed by a specialist Uroradiologist. Segmentation was performed using RayStation (v9.1). The prostate tumour region of interest was used to calculate the tumour volume only and was not used to generate radiomic features. Exported DICOM images were converted to Neuroimaging Informatics Technology Initiative (NIfTI) files and exported into PyRadiomics (v3.0.1) for analysis[21]. The Nyúl method, a histogram intensity-based normalisation technique was applied to MRI data to render the dynamic signal intensity ranges comparable prior to RF extraction [22,23].

A flowchart illustrating the methodological pipeline for RF-derived hypoxia prediction from segmentation through to ML model construction is shown in Figure 2.1.

2.3.6 Feature Extraction

Eight RF classes[20] were extracted from each segmented region of interest (ROI) using PyRadiomics (v3.0.1) (https://pyradiomics.readthedocs.io/en/latest/index.html, accessed 09/02/2023). All RFs extracted and filters applied are detailed in Supplementary Material. Different numbers of bins (8, 16, 32, 64, 128, 256) and isotropic voxel sizes (1, 2, 3) were tested to assess the most robust quantisation/rebinning setting and confirm the number of bins with the largest set of

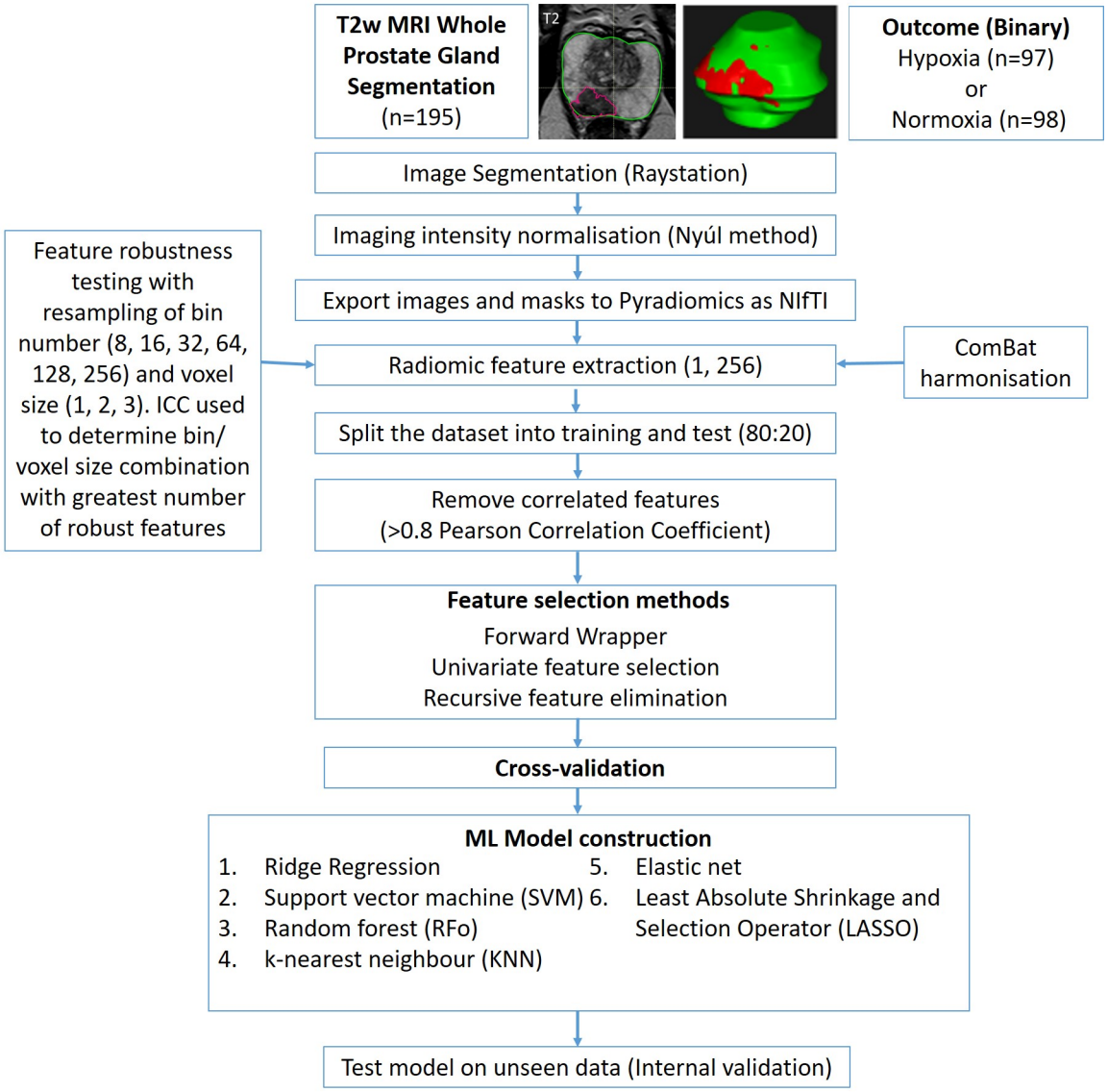

Figure 2.1 Flowchart demonstrating the methodological pipeline for the T2W MRI whole prostate gland radiomic model for predicting hypoxia. Legend: NIfTI = Neuroimaging Informatics Technology Initiative, ICC = intraclass correlation coefficient, ComBat = imaging harmonisation method, LASSO = Least Absolute Shrinkage and Selection Operator, RFo = Random Forest.

robust features. To determine the most robust features against bin number and voxel size, approximately 10% of the total cohort was also re-segmented (n=21). This created separate ROIs from which RFs were extracted and compared using interclass correlation coefficient (ICC).

The Image Biomarkers Standardization Initiative (IBSI) was adhered to, which provides a comprehensive review of each step involved in radiomic analyses, including nomenclature of RFs and required calibration datasets[23]. Number of bins was favoured over the bin width given the arbitrary nature of MRI intensity units. The ComBat Harmonisation method (https://github.com/Jfortin1/ComBatHarmonization, accessed 09/02/2023) (v0.2.10) was applied to extracted RFs to account for variation in scanner models, acquisition protocols and reconstruction settings by which RFs are affected [31,32].

2.3.7 Feature Selection

First, an unsupervised method of feature selection was applied to reduce the dataset using Pearson's correlation coefficient. For each feature pair, correlations were assessed, a threshold of 0.8 was used to highlight highly correlated pairs and the feature in the pair with the largest average correlation to all other features was removed. Additional feature selection steps were performed using three different methods: a forward wrapper method (mlxtend 0.18.0); a univariate analysis method (scikit-learn v0.24.2); and a recursive feature extraction method (where applicable) (scikit-learn v0.24.2). The top 5 ranked features were chosen as these were the most robust.

2.3.8 Machine Learning (ML) Model Construction and Statistical Analysis

The dataset was split into training and test sets stratified around MRI scanner vendor and ISUP, with an 80:20 split using scikit-learn (v0.24.2) `https://scikit-learn.org/stable/whats_new/v0.24.html,accessed09/02/2023`). Six predictive ML methods (as listed under ML model construction in Figure 2.1) were implemented with the Python library scikit-learn (v23.0) in order to incorporate the selected RFs into a binary classifier for distinguishing patients grouped as hypoxia or normoxia [25]. Methods used included ridge regression, random forest (RFo), elastic net, k-nearest neighbour (KNN), support vector machine (SVM), and least absolute shrinkage and selection operator (LASSO) regression. These models were trained to build classification models based on whole prostate T2W RFs, respectively.

Training of ML models and tuning of hyperparameters was performed using a Bayes Search method (scikit-optimize v0.8.1), with five-fold cross validation stratified around hypoxia status (normoxia or hypoxia) with 25 repeats. The area under the curve (AUC) of the receiver operating characteristic (ROC) curve was calculated with confidence intervals and the DeLong method was used to compare AUCs, to assess how accurately the radiomic and clinical-only models could classify a tumour's hypoxia status[25]. RFs and hyperparameters with the highest mean validation AUC which was within 0.05 of the mean training AUC were selected. A 0.05 cut-off was chosen to try and minimise selection of an overfitted model. The model which had the highest mean validation AUC overall was tested once on the unseen test set. The overall evaluation of clinical variables between the training and testing groups to ensure balanced groups was compared using the independent t-test (continuous variables) and Chi-square test (categorical variables). The statistically significant level was set at 0.05.

2.4 Results

The demographics, pathology information and hypoxia status of the prostate tumours in the final study cohort, split by training and test cohort, are described in Table 2.1.

2.4.1 Machine Learning Model Building

The best performing model with clinical variables alone was a ridge regression model (Figure 2.2) which included age and tumour stage variables. Mean training AUC was 0.61 (Standard Deviation (SD) 0.02) and mean training validation AUC was 0.60 (SD 0.08). Mean test AUC was 0.57 (95% confidence interval (CI) 0.14). The ML models with added RFs outperformed the clinical only model. Mean training and validation AUCs for the best performing radiomics-based ML models along with hyperparameters and selected RFs are shown in Table 2.2.

Table 2.1 Demographics of the training and test cohort. PSA = Prostate Specific Antigen, ISUP = International Society of Urological Pathology, T-stage = Tumour stage. *Median values (IQR = interquartile range) presented for Age and PSA.

Characteristics	Training Cohort (n=156) N (%)	Test Cohort (n=39) N (%)	p-value
Age* (years)	69.9 (IQR = 8.4)	68.0 (IQR = 10.0)	0.48
PSA (ng/mL)*	19.5 (IQR = 18.5)	21.0 (IQR = 17.0)	0.45
ISUP			
1	4 (2.5)	1 (2.4)	
2	60 (38.8)	15 (31.7)	
3	27 (20.6)	10 (12.2)	0.69
4	17 (8.1)	2 (14.6)	
5	48 (30.0)	11 (39.0)	
T-stage			
T1	4 (2.6)	1 (2.6)	
T2	30 (19.2)	9 (23.1)	0.91
T3	121 (77.6)	29 (74.4)	
T4	1 (0.6)	0	
Hypoxia			
Yes	78 (50.0)	19 (48.7)	0.89
No	78 (50.0)	20 (51.3)	

Table 2.2 Mean training and validation scores for the best performing machine learning models along with hyperparameters and radiomic features selected. Key: AUC = area under the curve, SVM = support vector machine, KNN = k-nearest neighbour, LASSO = Least Absolute Shrinkage and Selection Operator, GLSZM = logarithm grey level size zone matrix, LAE = Large Area Emphasis, GLCM = Grey Level Co-occurrence Matrix, MCC = Maximal Correlation Coefficient (MCC), GLDM = Grey Level Dependence Matrix, NGTDM = Neighbouring Grey Tone Difference Matrix, SD = standard deviation

Machine learning model	Hyperparameters	Radiomic features selected	AUC mean training (SD)	AUC mean validation (SD)
Ridge Regression	C: 0.03, penalty: l2, solver: saga	Logarithm GLSZM Large Area Emphasis, wavelet-LLH GLCM ClusterProminence, wavelet-HLL GLCM MCC, wavelet-HLH_firstorder_Median, wavelet-HHH GLCM MCC	0.73 (0.02)	0.71 (0.10)
SVM	C: 3.6, degree: 6, ga2mma: 0.13, kernel: rbf	Exponential GLDM Small Dependence Low Grey Level Emphasis, wavelet-HLL first-order Mean, wavelet-HLL GLCM MCC, wavelet-HHH first-order Mean	0.88 (0.01)	0.70 (0.07)
KNN	algorithm: kd_tree, metric: manhattan, n_neighbors: 13, weights: uniform	Original firstorder 90th percentile, wavelet-LLH GLCM Autocorrelation, wavelet-LHH first-order Maximum, wavelet-HHL first-order Skewness, wavelet-HHH GLCM MCC	0.78 (0.02)	0.70 (0.09)
Random forest	bootstrap: false, max_depth: 1, max_features: log2, min_samples_leaf: 5, min_samples_split: 32, n_estimators: 416	Original GLDM Large Dependence Low Grey Level Emphasis, exponential NGTDM strength, gradient first-order 10th percentile', wavelet-LLH GLCM autocorrelation, wavelet-LHL GLCM correlation, wavelet-LHH first-order Entropy	0.79 (0.02)	0.69 (0.08)
Elastic net	C: 1e-06, l1 ratio: 1.25e-05, penalty: elastic net, solver: saga	Gradient first-order 10th percentile, wavelet-LLH GLCM autocorrelation, wavelet-LHL GLCM Correlation, wavelet-LHH GLCM MCC, wavelet-HLL first-order entropy, wavelet-HLL GLCM MCC, wavelet-HLH first-order entropy, wavelet-HLH first-order Median, wavelet-HHH GLCM MCC	0.70 (0.03)	0.61 (0.10)
LASSO	C: 0.08, penalty: l1, solver: liblinear	wavelet-HLL GLCM MCC and wavelet-HHH GLCM MCC	0.69 (0.03)	0.62 (0.10)

The model within the highest mean validation AUC was a ridge regression model created using radiomic and clinical features. The best performing ML model is shown in Figure 2.3 with a mean training AUC of 0.73 (SD 0.02), mean training validation AUC of 0.71 (SD 0.10) and mean test AUC of 0.69 (95% CI 0.14). The 5 selected RFs were logarithm grey level size zone matrix (GLSZM), Large Area Emphasis (LAE) and the following 3-dimensional wavelet features; LLH grey level co-occurrence matrix (GLCM) Cluster Prominence, HLL GLCM maximal correlation coefficient (MCC), HLH first order Median, HHH GLCM MCC. No clinical features were selected despite integrating all clinical variables into the model.

For the combined model with the highest AUC, performance metrics were: overall model accuracy 0.72, sensitivity 0.74, specificity 0.70, positive predictive value (PPV) 0.70, and negative predictive value (NPV) 0.74. The best performing clinical model had an overall accuracy of 0.56, sensitivity of 0.67, specificity of 0.53, PPV of 0.3, and NPV of 0.84. Confusion matrices are presented in Tables 2.3 and 2.4 respectively (Table 2.3)(Table 2.4). The radiomics and clinical only models showed no significant difference according to DeLong's testing ($p = 0.35$) (Figure 2.4).

Table 2.3 Confusion matrix for clinical-based ridge regression hypoxia prediction model. Key: Positive = Hypoxia tumour status, Negative = Normoxia tumour status, Predicted Positive = predicted to be hypoxic, Predicted Negative = predicted to be normoxic.

Prediction	Negative	Positive
Predicted Negative	16	3
Predicted Positive	14	6

Table 2.4 Confusion matrix for radiomics-based ridge regression hypoxia prediction model. Key: Positive = Hypoxia tumour status, Negative = Normoxia tumour status, Predicted Positive = predicted to be hypoxic, Predicted Negative = predicted to be normoxic.

Prediction	Negative	Positive
Predicted Negative	14	5
Predicted Positive	6	14

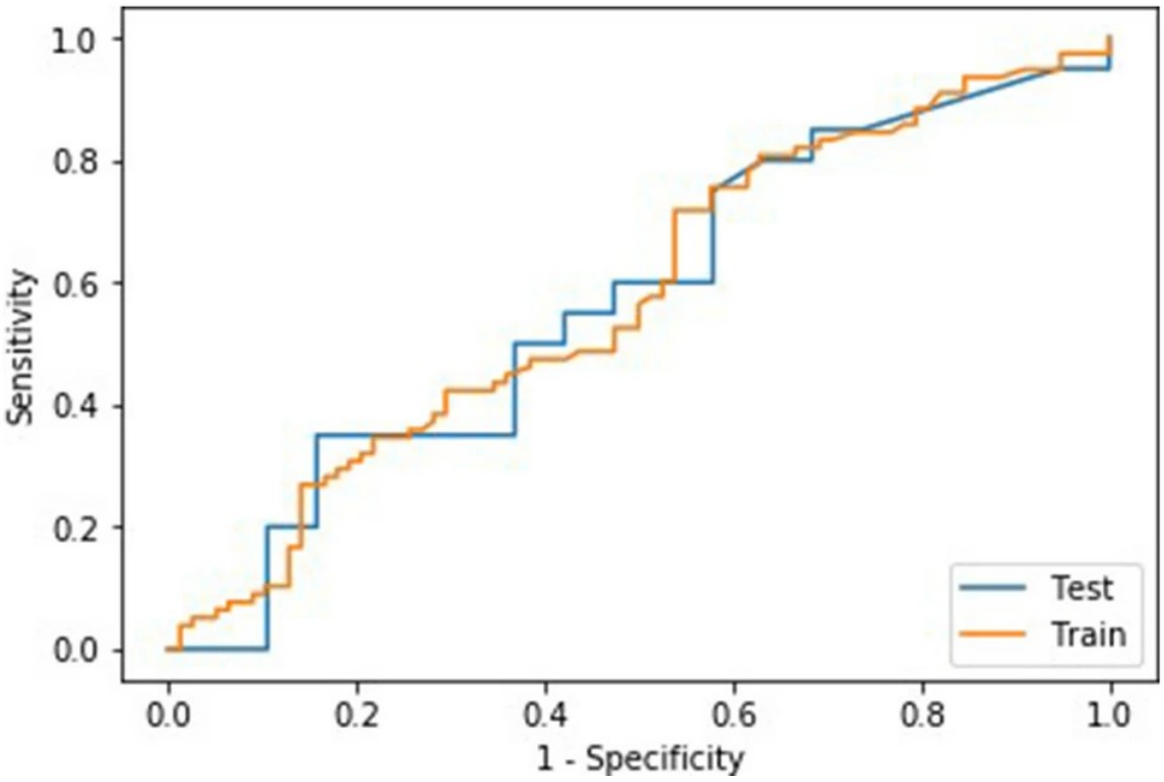

Figure 2.2 ROC curve of the best performing ridge regression hypoxia prediction model (test and training performance) using clinical features. Mean training AUC 0.61 (SD 0.02), mean training validation AUC 0.60 (SD 0.08). Mean test AUC 0.57 (95% CI 0.14)

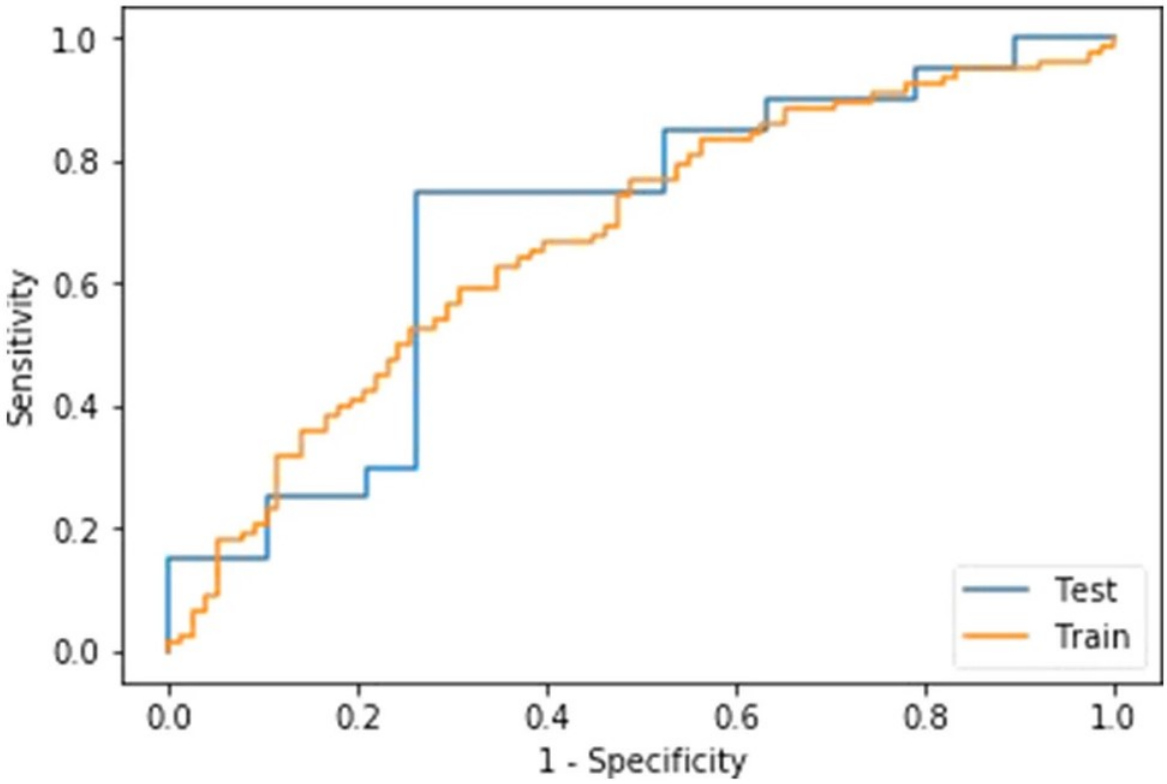

Figure 2.3 ROC curve of the best performing ridge regression hypoxia prediction model (test and training performance) using radiomic features. Mean training AUC 0.73 (SD 0.02). Mean training validation AUC 0.71 (SD 0.10). Mean test AUC 0.69 (95% CI 0.14).

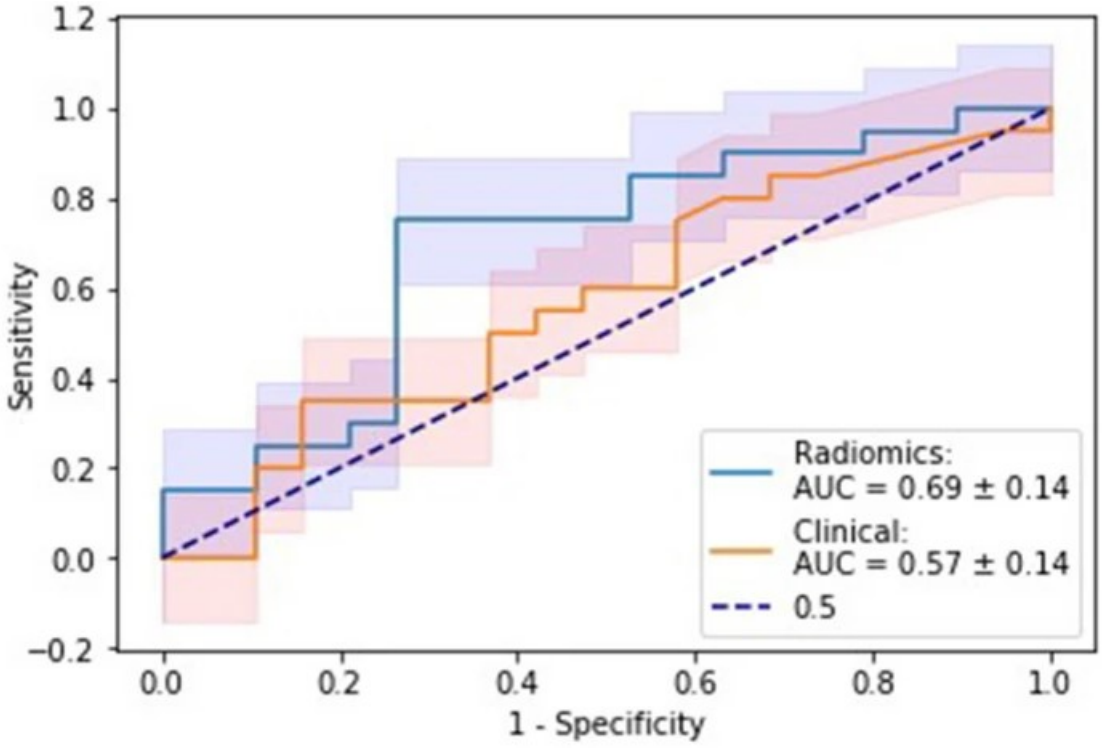

Figure 2.4 Mean ROC curves of the best performing radiomics and clinical-based ridge regression hypoxia prediction models with 95% confidence intervals highlighted

2.5 Discussion

The aim of this study was to develop a ML model based on RFs extracted from whole prostate gland T2W MRI for non-invasive prediction of tumour hypoxia identified in biopsies using a 32-gene signature [9]. The results showed that the integration of RFs from MRI helped improve the prediction of hypoxia in patients with prostate cancer, with the best ML model (ridge regression) having an AUC of 0.69 for the unseen internal test cohort compared to 0.57 for a model derived from only clinical variables. Although this change did not reach statistical significance, it still highlights the potential use of MRI to non-invasively assess hypoxia status in prostate cancer.

The benchmark for tumour hypoxia determination in this study was a hypoxia-associated gene expression (Ragnum) signature. This intrinsic molecular biomarker reflected the transcriptional profile associated with pimonidazole staining, an extrinsic marker of hypoxia, and was validated for prognostic significance in independent datasets [9]. Whole-mount prostate specimens were not available in the current cohort where all patients only received RT. By using the gene signature as the ground truth, we were able to provide a biological basis for the observed hypoxia-associated RFs selected by the ML models.

MRI-guided EBRT focal boosting to intra-prostatic lesions has been demonstrated to be safe and Level 1 evidence shows it improves biochemical control when compared to whole prostate EBRT [26]. Incorporating imaging radiogenomics into MRI-guided focal boosting of hypoxic tumours may further improve clinical outcomes given that hypoxic cells are three times more radioresistant than normoxic ones [8,28]. Most prostate cancer patients undergo MRI routinely as part of diagnostic work-up, and T2W imaging is the most utilised sequence thereby potentially facilitating use of a T2W MRI hypoxia radiomics based approach in the clinic. Despite the role of adaptive RT, there is no routine clinical use of any imaging methods to identify hypoxic regions. However, in the era of MRI-guided RT using MRI linear accelerators, there is potential to develop a radiomics-based hypoxia targeted radiotherapy methodological framework. This approach would also require robust harmonisation algorithms to account for the difference in field strength and MRI parameters on MR linear accelerators.

After prostate RT, the only validated biomarker for disease recurrence is PSA [29,30]. The results of this preliminary study suggest that imaging biomarkers and RFs could potentially offer further measurable longitudinal metrics that may help guide post-treatment surveillance and survival predictions. This aligns with evidence from other tumours such as glioblastoma and renal cell cancer, which provide a biological basis for RFs[31,32]. Beig et al. reported that RFs extracted from different regions of interest in 180 patients with glioblastoma such as, enhancing tumour, necrotic tumour, and peri-tumoral regions were predictive of a hypoxia enrichment score based on 21 genes implicated in the hypoxia pathway of glioblastoma [33]. The top eight features most associated with the hypoxia enrichment score included RFs which quantified structural heterogeneity and their imaging-based radiogenomic hypoxic signature was associated with survival[33]. Gao et al. derived a hypoxia-gene related radiogenomic signature using RFs extracted from contrast-enhanced CT and found that this was significantly associated with prognosis in patients with renal cell cancer validating this in an independent cohort [32]. Such validation and insight into the biological characteristics of tumours is vital and needs to be replicated for prostate cancer pathways, which the current study attempts to address.

Previous research investigating the association between MRI and transcriptomic profiles in prostate cancer have suffered from low patient numbers, limiting transferability of results[34,35]. To develop imaging biomarkers of prostate hypoxia, the availability of 'ground truth' data such as pathology or genomic profiling is critical to ensure the translational gap can be crossed allowing integration into routine care[36]. Leech et al. found that a radiomics model extracted from 88 T2W prostate MRIs (single axial slice

used rather than a volume) could predict tumour hypoxia measured using pimonidazole stained prostatectomy specimens[37]. Their ML model used elastic net regularization and repeated cross validation to yield an AUC of 0.60 (SD 0.2) without a validation dataset but further demonstrates the feasibility of building a radiomics hypoxia model using T2W MRI. The RFs selected by their ML model were mainly shape-based features but also included the textural feature grey level size zone matrix (GLSZM) which was also one of the features selected by the best performing ML model in the current study. GLSZM quantifies grey level zones in an image, and GLSZM large area emphasis (LAE), one of the selected RFs in the best ML model in our study, measures the distribution of 'large area size zones', where a larger value indicates bigger zones with more coarse textures. Another RF selected was grey level co-occurrence matrix (GLCM) which reflects the spatial relationship among pixels and defines how frequently a combination of pixels are present. This potentially suggests a heterogeneous appearing prostate with more coarse textures associating with hypoxia.

There are a number of limitations to the study: Genomic profiling and MRIs were performed over several years and scanner technology and imaging protocols have evolved in the interim; imaging data used were all acquired on 1.5T scanners and many did not have functional imaging sequences available as this was not routine at the time of the initial imaging acquisition. Similarly, the transcriptomic data was generated in small, old biopsies. As a result, only T2W imaging was used to develop radiomic models; Whole prostate segmentations were used to extract RFs as not all cases had a visible tumour on anatomical imaging, and it was not possible to match the site of biopsy taken. Previous work has linked normal background prostate tissue with high risk gene expression profiles highlighting the value for evaluating the whole gland[38]. Despite this study including data from two centres, further external validation using data from another site would allow the model to be tested for reproducibility.

Obtaining these radiogenomic datasets with matched clinical, imaging, pathology and genomic data remains challenging and requires further collaboration and formation of consortia with standardized methods for RF extraction. Establishing more multi-institutional collaborations with the potential to utilise novel transfer learning techniques will help expand our knowledge of genomics and imaging phenotypes in prostate cancer[39]. A general drawback to retrospective imaging research is the lack of imaging protocol standardization, which differ significantly across institutions. In this study, ComBat harmonisation was used to minimize issues related to MRI data acquired on multiple scanners [39,40]. Exploring the added role of functional MRI sequences in imaging hypoxia is vital to develop more sensitive diagnostic pathways. Hompland et al.

investigated a novel MRI technique called intravoxel incoherent motion (IVIM) as an indirect measure of tumour hypoxia and validated this against the exogenous hypoxia marker pimonidazole[42]. Similarly, R2* maps from blood oxygen level-dependent (BOLD) MRI sequences have been found to have a high sensitivity for defining intraprostatic tumour hypoxia[11]. A major barrier to clinical translation of these advanced imaging techniques is the poor spatial resolution that is required to fully sample the tumour microenvironment [42]. Utilising routinely acquired T2W MR data yields higher resolution prostate images allowing for better appreciation of structural differences. It is also less prone to artefacts compared to functional sequences such as diffusion weighted imaging. Validating imaging biomarkers and RFs using gene expression signatures provides a biological basis but the external validation of any radiogenomic signature followed by further testing in the setting of a prospective randomised trial is essential to demonstrate value in clinical translation[44].

2.6 Conclusion

In conclusion, the current study suggests that whole prostate MRI-radiomics has the potential to non-invasively predict tumour hypoxia prior to radiotherapy. Further external validation of the hypoxia associated radiomics-model in predicting biochemical recurrence and clinical outcomes are required to determine the benefit of using the integrated information for patient stratification.

2.7 References

1. Cronin KA, Lake AJ, Scott S, Sherman RL, Noone A-M, Howlader N, *et al.* Annual Report to the Nation on the Status of Cancer, part I: National cancer statistics. Cancer. 2018;124(13):2785–800.

2. Mottet N, Bellmunt J, Bolla M, Briers E, Cumberbatch MG, De Santis M, *et al.* EAU-ESTRO-SIOG Guidelines on Prostate Cancer. Part 1: Screening, Diagnosis, and Local Treatment with Curative Intent. Eur Urol [Internet]. 2017;71(4):618–29.

3. Beckendorf V, Guerif S, Le Prisé E, Cosset JM, Bougnoux A, Chauvet B, *et al.* 70 Gy versus 80 Gy in localized prostate cancer: 5-year results of GETUG 06 randomized trial. Int J Radiat Oncol Biol Phys [Internet]. 2011;80(4):1056–63.

4. Zumsteg ZS, Spratt DE, Romesser PB, Pei X, Zhang Z, Kollmeier M, *et al.* Anatomical patterns of recurrence following biochemical relapse in the dose escalation era of external beam radiotherapy for prostate cancer. J Urol [Internet]. 2015;194(6):1624-1630.

5. Jones CU, Hunt D, McGowan DG, Amin MB, Chetner MP, Bruner DW, *et al.* Radiotherapy and Short-Term Androgen Deprivation for Localized Prostate Cancer. N Engl J Med. 2011;365(2):107–18.

6. Turaka A, Buyyounouski MK, Hanlon AL, Horwitz EM, Greenberg RE, Movsas B. Hypoxic Prostate/Muscle Po2 Ratio Predicts for Outcome in Patients With Localized Prostate Cancer: Long-Term Results. Int J Radiat Oncol. 2012;82(3):e433–9.

7. Lalonde E, Ishkanian AS, Sykes J, Fraser M, Ross-Adams H, Erho N, *et al.* Tumour genomic and microenvironmental heterogeneity for integrated prediction of 5-year biochemical recurrence of prostate cancer: a retrospective cohort study. Lancet Oncol. 2014;15(13):1521–32.

8. Milosevic M, Warde P, Ménard C, Chung P, Toi A, Ishkanian A, *et al.* Tumor Hypoxia Predicts Biochemical Failure following Radiotherapy for Clinically Localized Prostate Cancer. Clin Cancer Res. 2012;18(7):2108–14.

9. Ragnum HB, Vlatkovic L, Lie AK, Axcrona K, Julin CH, Frikstad KM, *et al.* The tumour hypoxia marker pimonidazole reflects a transcriptional programme associated with aggressive prostate cancer. Br J Cancer. 2015;112(2):382–90.

10. Hoskin PJ, Carnell DM, Taylor NJ, Smith RE, Stirling JJ, Daley FM, et al. Hypoxia in Prostate Cancer: Correlation of BOLD-MRI With Pimonidazole Immunohistochemistry-Initial Observations. Int J Radiat Oncol Biol Phys [Internet]. 2007;68(4):1065–71.

11. Huang Y, Fan J, Li Y, Fu S, Chen Y, Wu J. Imaging of Tumor Hypoxia With Radionuclide-Labeled Tracers for PET. Front Oncol. 2021;11.

12. Lambin P, Leijenaar RTH, Deist TM, Peerlings J, De Jong EEC, Van Timmeren J, *et al.* Radiomics: The bridge between medical imaging and personalized medicine. Nat Rev Clin Oncol [Internet]. 2017;4(12):749-762.

13. Bodalal Z, Trebeschi S, Nguyen-Kim TDL, Schats W, Beets-Tan R. Radiogenomics: bridging imaging and genomics. Abdom Radiol. 2019;44(6):1960–84.

14. Hectors SJ, Chen C, Chen J, Wang J, Gordon S, Yu M, *et al.* Magnetic Resonance Imaging Radiomics-Based Machine Learning Prediction of Clinically Significant Prostate Cancer in Equivocal PI-RADS 3 Lesions. J Magn Reson Imaging. 2021;54(5):1466–73.

15. Binder ZA, Thorne AH, Bakas S, Wileyto EP, Bilello M, Akbari H, *et al.* Epidermal Growth Factor Receptor Extracellular Domain Mutations in Glioblastoma Present Opportunities for Clinical Imaging and Therapeutic Development. Cancer Cell. 2018;34(1):163-177.e7.

16. Kirienko M, Sollini M, Corbetta M, Voulaz E, Gozzi N, Interlenghi M, *et al.* Radiomics and gene expression profile to characterise the disease and predict outcome in patients with lung cancer. Eur J Nucl Med Mol Imaging. 2021;48(11):3643–55.

17. Fjeldbo CS, Hompland T, Hillestad T, Aarnes E-K, Günther C-C, Kristensen GB, *et al.* Combining imaging- and gene-based hypoxia biomarkers in cervical cancer improves prediction of chemoradiotherapy failure independent of intratumour heterogeneity. EBioMedicine. 2020;57:102841.

18. Fan M, Xia P, Clarke R, Wang Y, Li L. Radiogenomic signatures reveal multiscale intratumour heterogeneity associated with biological functions and survival in breast cancer. Nat Commun. 2020;11(1):4861.

19. Yang L, Roberts D, Takhar M, Erho N, Bibby BAS, Thiruthaneeswaran N, *et al.* Development and Validation of a 28-gene Hypoxia-related Prognostic Signature for Localized Prostate Cancer. EBioMedicine [Internet]. 2018;31:182–9.

20. Mongan J, Moy L, Kahn CE. Checklist for Artificial Intelligence in Medical Imaging (CLAIM): A Guide for Authors and Reviewers. Radiol Artif Intell. 2020;2(2):e200029.

21. van Griethuysen JJM, Fedorov A, Parmar C, Hosny A, Aucoin N, Narayan V, *et al.* Computational Radiomics System to Decode the Radiographic Phenotype. Cancer Res. 2017;77(21):e104–7.

22. Carré A, Klausner G, Edjlali M, Lerousseau M, Briend-Diop J, Sun R, *et al.* Standardization of brain MR images across machines and protocols: bridging the gap for MRI-based radiomics. Sci Rep. 2020;10(1):12340.

23. Nyul LG, Udupa JK, Xuan Zhang. New variants of a method of MRI scale standardization. IEEE Trans Med Imaging. 2000;19(2):143–50.

24. Zwanenburg A, Vallières M, Abdalah MA, Aerts HJWL, Andrearczyk V, Apte A, *et al.* The Image Biomarker Standardization Initiative: Standardized Quantitative Radiomics for High-Throughput Image-based Phenotyping. Radiology. 2020;295(2):328–38.

25. Pedregosa, F., Varoquaux, G., Gramfort, A., Michel, V., Thirion, B., Grisel, O., Blondel, M., Prettenhofer, P., Weiss, R., Dubourg, V. and Vanderplas J. Scikit-learn: Machine Learning in Python. J Mach Learn Res [Internet]. 2011;12:2825-2830.

26. DeLong ER, DeLong DM, Clarke-Pearson DL. Comparing the areas under two or more correlated receiver operating characteristic curves: a nonparametric approach. Biometrics. 1988;44(3):837–45.

27. Poon DMC, Yuan J, Yang B, Kerkmeijer LGW, Kishan AU, Murthy V, *et al.* Magnetic Resonance Imaging–guided Focal Boost to Intraprostatic Lesions Using External Beam Radiotherapy for Localized Prostate Cancer: A Systematic Review and Meta-analysis. Eur Urol Oncol. 2022;

28. Bristow R, Berlin A, Dal Pra A. An arranged marriage for precision medicine: hypoxia and genomic assays in localized prostate cancer radiotherapy. Br J Radiol. 2014;87(1035):20130753.

29. Amaro A, Esposito AI, Gallina A, Nees M, Angelini G, Albini A, *et al.* Validation of proposed prostate cancer biomarkers with gene expression data: a long road to travel. Cancer Metastasis Rev. 2014;33(2–3):657–71.

30. Stamey TA, Yang N, Hay AR, McNeal JE, Freiha FS, Redwine E. Prostate-Specific Antigen as a Serum Marker for Adenocarcinoma of the Prostate. N Engl J Med. 1987;317(15):909–16.

31. Tomaszewski MR, Gillies RJ. The Biological Meaning of Radiomic Features. Radiology. 2021;298(3):505–16.

32. Gao J, Ye F, Han F, Wang X, Jiang H, Zhang J. A Novel Radiogenomics Biomarker Based on Hypoxic-Gene Subset: Accurate Survival and Prognostic Prediction of Renal Clear Cell Carcinoma. Front Oncol. 2021;11.

33. Beig N, Bera K, Prasanna P, Antunes J, Correa R, Singh S, *et al.* . Radiogenomic-based survival risk stratification of tumor habitat on Gd-T1w MRI is associated with biological processes in glioblastoma. Clin Cancer Res [Internet]. 2020;26(8):1866–76.

34. Ferro M, de Cobelli O, Vartolomei MD, Lucarelli G, Crocetto F, Barone B, *et al.* Prostate Cancer Radiogenomics—From Imaging to Molecular Characterization. Int J Mol Sci. 2021;22(18):9971.

35. Sun Y, Williams S, Byrne D, Keam S, Reynolds HM, Mitchell C, *et al.* Association analysis between quantitative MRI features and hypoxia-related genetic profiles in prostate cancer: a pilot study. Br J Radiol. 2019;92(1104):20190373.

36. O'Connor JPB, Aboagye EO, Adams JE, Aerts HJWL, Barrington SF, Beer AJ, *et al.* Imaging biomarker roadmap for cancer studies. Nat Rev Clin Oncol. 2017;14(3):169–86.

37. Leech M, Leijennar RTH, Hompland T, Gaffney J, Lyng H, Marignol L. Exploring Hypoxia in Prostate Cancer With T2-weighted Magnetic Resonance Imaging Radiomics and Pimonidazole Scoring. Anticancer Res. 2023;43(1):351–7.

38. Stoyanova R, Takhar M, Tschudi Y, Ford JC, Solórzano G, Erho N, *et al.* Prostate cancer radiomics and the promise of radiogenomics. Transl Cancer Res [Internet]. 2016;5(4):432-447.

39. Hanczar B, Bourgeais V, Zehraoui F. Assessment of deep learning and transfer learning for cancer prediction based on gene expression data. BMC Bioinformatics. 2022;23(1):262.

40. Orlhac F, Lecler A, Savatovski J, Goya-Outi J, Nioche C, Charbonneau F, *et al.* How can we combat multicenter variability in MR radiomics? Validation of a correction procedure. Eur Radiol. 2021;31(4):2272–80.

41. Da-ano R, Masson I, Lucia F, Doré M, Robin P, Alfieri J, *et al.* Performance comparison of modified ComBat for harmonization of radiomic features for multicenter studies. Sci Rep [Internet]. 2020;10(1):1–12.

42. Hompland T, Hole KH kon, Ragnum HB, Aarnes EK, Vlatkovic L, Kathrine Lie A, *et al.* Combined mr imaging of oxygen consumption and supply reveals tumor hypoxia and aggressiveness in prostate cancer patients. Cancer Res [Internet]. 2018;78(16):4774–85.

43. Cao X, Rao Allu S, Jiang S, Jia M, Gunn JR, Yao C, *et al.* Tissue pO2 distributions in xenograft tumors dynamically imaged by Cherenkov-excited phosphorescence during fractionated radiation therapy. Nat Commun. 2020;11(1):573.

44. Sun R, Limkin EJ, Vakalopoulou M, Dercle L, Champiat S, Han SR, *et al.* A radiomics approach to assess tumour-infiltrating CD8 cells and response to anti-PD-1 or anti-PD-L1 immunotherapy: an imaging biomarker, retrospective multicohort study. Lancet Oncol. 2018;19(9):1180–91.

2.8 Supplementary Material

Table S2.1 MRI acquisition parameters of the 4 different 1.5T MRI Scanners used to acquire T2 weighted axial prostate MRI data.

1.5T MRI Scanner	Repetition time/ echo time (ms)	Flip Angle (°)	Field of view (mm)	Matrix size (mm)	Slice thickness (mm)
GE Signa	5020/122	90	250	384 x 224	3
Philips Achieva	3500/ 90	90	220	256 x 192	3
Siemens Aera	3540/ 99	160	220	320 × 256	3
Siemens Sola	4500/ 88	150	200	320 × 256	3

2.8.1 Extracted Radiomic Features and Filters

Radiomic feature classes that were extracted from the T2-weighted MRI whole prostate gland segmentations. All feature classes listed below, with the exception of the shape-based features can be calculated on the original image and/or a derived image, such as applying one of several filters which is how the wavelet features were generated.

Individual feature description can be found at: https://pyradiomics.readthedocs.io/en/latest/features.html

First-order

- 10th Percentile
- 90th Percentile
- Energy
- Entropy
- Interquartile Range
- Kurtosis
- Maximum
- Mean Absolute Deviation
- Mean

- Median
- Minimum
- Range
- Robust Mean Absolute Deviation
- Root Mean Squared
- Skewness
- Total Energy
- Uniformity
- Variance

Shape-based (3D)

- Mesh Volume
- Voxel Volume
- Surface Area
- Surface Area to Volume ratio
- Sphericity
- Maximum 3D diameter
- Maximum 2D diameter (Slice)
- Maximum 2D diameter (Column)
- Maximum 2D diameter (Row)
- Major Axis Length
- Minor Axis Length Least Axis Length
- Elongation
- Flatness

Gray Level Co-occurrence Matrix (GLCM)

- Autocorrelation
- Cluster Prominence
- Cluster Shade
- Cluster Tendency
- Contrast
- Correlation
- Difference Average
- Difference Entropy
- Difference Variance
- ID: Inverse Difference
- IDM: Inverse Difference Moment
- IDMN: Inverse Difference Moment Normalized
- IDN: Inverse Difference Normalized
- IMC1: Informational Measure of Correlation 1
- IMC2: Informational Measure of Correlation 1
- Inverse Variance
- Joint Average
- Joint Energy
- Joint Entropy
- MCC: Maximal Correlation Coefficient
- Maximum Probability
- Sum Average
- Sum Entropy
- Sum Squares

Gray Level Dependence Matrix (GLDM)

- Dependence Entropy
- Dependence NonUniformity
- Dependence NonUniformity Normalized
- Dependence Variance
- Gray Level NonUniformity
- Gray Level Variance
- High Gray Level Emphasis
- Large Dependence Emphasis
- Large Dependence High Gray Level Emphasis
- Large Dependence Low Gray Level Emphasis
- Low Gray Level Emphasis
- Small Dependence Emphasis
- Small Dependence High Gray Level Emphasis
- Small Dependence Low Gray Level Emphasis

Gray Level Run Length Matrix (GLRLM)

- Gray Level NonUniformity
- Gray Level NonUniformity Normalized
- Gray Level Variance
- High Gray Level Run Emphasis
- Long Run Emphasis
- Long Run High Gray Level Emphasis
- Long Run Low Gray Level Emphasis
- Low Grey Level Run Emphasis

- Run Entropy
- Run Length NonUniformity
- Run Length NonUniformity Normalized
- Run Percentage
- Run Variance
- Short Run Emphasis
- Short Run High Gray Level Emphasis
- Short Run Low Gray Level Emphasis

Gray Level Size Zone Matrix (GLSZM)

- Gray Level NonUniformity
- Gray Level NonUniformity Normalized
- Gray Level Variance
- High Gray Level Zone Emphasis
- Large Area Emphasis
- Large Area High Gray Level Emphasis
- Large Area Low Gray Level Emphasis
- Low Gray Level Zone Emphasis
- Size Zone Non-Uniformity
- Size Zone Non-Uniformity Normalized
- Small Area Emphasis
- Small Area High Gray Level Emphasis
- Small Area Low Gray Level Emphasis
- Zone Entropy
- Zone Percentage

- Zone Variance

Neighboring Gray-Tone Difference Matrix (NGTDM)

- Busyness
- Coarseness
- Complexity
- Contrast
- Strength

CLAIM: Checklist for Artificial Intelligence in Medical Imaging

This checklist is in reference to the main manuscript of "*Prediction of prostate tumour hypoxia using pre-treatment MRI-derived radiomics – preliminary findings*".

Section / Topic	No.	Item	
TITLE / ABSTRACT			**Page number**
	1	Identification as a study of AI methodology, specifying the category of technology used (e.g., deep learning)	**P1**
	2	Structured summary of study design, methods, results, and conclusions	**P1**
INTRODUCTION			
	3	Scientific and clinical background, including the intended use and clinical role of the AI approach	**P2-3**
	4	Study objectives and hypotheses	**P3**
METHODS			
Study Design	**5**	Prospective or retrospective study	**P3**
	6	Study goal, such as model creation, exploratory study, feasibility study, non-inferiority trial	**P3**
Data	**7**	Data sources	**P3**
	8	Eligibility criteria: how, where, and when potentially eligible participants or studies were identified (e.g., symptoms, results from previous tests, inclusion in registry, patient-care setting, location, dates)	**P3**
	9	Data pre-processing steps	**P4-5**
	10	Selection of data subsets, if applicable	**P5**
	11	Definitions of data elements, with references to Common Data Elements	**P6**
	12	De-identification methods	**P4**
	13	How missing data were handled	**N/A**
Ground Truth	**14**	Definition of ground truth reference standard, in sufficient detail to allow replication	**P3**
	15	Rationale for choosing the reference standard (if alternatives exist)	**P3**
	16	Source of ground-truth annotations; qualifications and preparation of annotators	**P3**
	17	Annotation tools	**P4**
	18	Measurement of inter- and intrarater variability; methods to mitigate variability and/or resolve discrepancies	**P4**

Data Partitions	**19**	Intended sample size and how it was determined	**P4**
	20	How data were assigned to partitions; specify proportions	**P5**
	21	Level at which partitions are disjoint (e.g., image, study, patient, institution)	**P5**
Model	**22**	Detailed description of model, including inputs, outputs, all intermediate layers and connections	**P5-6/ Tables**
	23	Software libraries, frameworks, and packages	**P4-5**
	24	Initialization of model parameters (e.g., randomization, transfer learning)	**Table 2**
Training	**25**	Details of training approach, including data augmentation, hyperparameters, number of models trained	**P9/ Table 2**
	26	Method of selecting the final model	**P5-6**
	27	Ensembling techniques, if applicable	**N/A**
Evaluation	**28**	Metrics of model performance	**Table 2**
	29	Statistical measures of significance and uncertainty (e.g., confidence intervals)	**P6**
	30	Robustness or sensitivity analysis	**P6**
	31	Methods for explainability or interpretability (e.g., saliency maps), and how they were validated	**P6**
	32	Validation or testing on external data	**P6**
RESULTS			
Data	**33**	Flow of participants or cases, using a diagram to indicate inclusion and exclusion	**P3/ Fig 1**
	34	Demographic and clinical characteristics of cases in each partition	**Table 1**
Model performance	**35**	Performance metrics for optimal model(s) on all data partitions	**Table 2**
	36	Estimates of diagnostic accuracy and their precision (such as 95% confidence intervals)	**P6/ Tables**
	37	Failure analysis of incorrectly classified cases	**N/A**
DISCUSSION			
	38	Study limitations, including potential bias, statistical uncertainty, and generalizability	**P8-9**
	39	Implications for practice, including the intended use and/or clinical role	**P7-9**
OTHER INFORMATION			
	40	Registration number and name of registry	**N/A**
	41	Where the full study protocol can be accessed	**N/A**
	42	Sources of funding and other support; role of funders	**Disclosure**

Chapter 3
Adding MRI Radiomics and Hypoxia Gene Signature Scores to Clinical Variables Improves Prediction of Biochemical Recurrence-Free Survival After Prostate Radiotherapy

3.1 Abstract

3.1.1 Purpose

To investigate the value of combining MRI radiomic and hypoxia-associated gene signature information with clinical data for predicting biochemical recurrence-free survival (BCRFS) after radiotherapy for prostate cancer.

3.1.2 Methods

Patients with biopsy-proven prostate cancer, hypoxia-associated gene signature (Ragnum) scores and pre-treatment MRI who received radiotherapy between 01/12/2007 and 31/08/2013 at two cancer centres were included in a retrospective cohort analysis. Prostate segmentation was performed on axial T2-weighted sequences using RayStation (v9.1). Histogram standardisation was applied prior to radiomic feature (RF) extraction. PyRadiomics (v3.0.1) was used to extract RFs for analysis. A multivariable Cox proportional hazards model including clinical variables (age, PSA, International Society of Urological Pathology (ISUP) grade, T-stage, tumour volume, treatment) was used to model BCRFS. Cross-validation was used to test different feature selection methods. Internal validation (bootstrapping) was used to evaluate model performance of the final combined models incorporating RFs and/or hypoxia scores in terms of concordance index (c-index) [confidence intervals (CI)]. Akaike Information Criterion (AIC) was used to assess model fit.

3.1.3 Results

187 patients were included. The combined clinical/RF/hypoxia score (c-index 0.73 [0.68-0.75]) and clinical/RF models (c-index 0.72 [0.68-0.74]) had similar performance surpassing clinical-only (c-index 0.67 [0.62-0.70]) and clinical/hypoxia score (c-index of 0.68 [0.62-0.69) models. The selected features of the combined clinical-radiomics model included age, ISUP grade, tumour stage, tumour volume, radiotherapy modality and wavelet-derived RFs. Based on AIC, inclusion of RFs improved model performance ($p=0.013$), whereas adding hypoxia score did not ($p=0.079$), unless also combined with RFs ($p=0.005$).

3.1.4 Conclusion

A model combining pre-treatment prostate MRI-derived radiomic features and clinical variables improves accuracy of predicting BCRFS after prostate radiotherapy, with or without the addition of a hypoxia gene signature.

3.2 Introduction

Prostate cancer is the most common malignancy in men and a major cause of cancer-related death [1]. Radiation therapy (RT), including external beam radiation therapy (EBRT) and brachytherapy (BT), is an effective treatment for localised prostate cancer [2]. Despite advances in diagnostic imaging and RT delivery techniques, 30-50% of men with high-risk disease experience biochemical recurrence (BCR) within 10 years of treatment, most commonly due to intraprostatic relapse [3-6]. BCR is regarded as an indicator of three important outcomes in prostate cancer: local recurrence, distant metastasis, and death specifically related to prostate cancer [7]. Predicting the progression of prostate cancer would help oncologists to personalise treatment plans and prioritise follow-up appointments to monitor patients with higher predicted recurrence risk. This would allow earlier detection of disease progression or recurrence and facilitate timely interventions.

Currently, risk stratification in prostate cancer predominantly relies on pathological findings from biopsies and standard imaging evaluation to determine spread of disease. Using information on the serum prostate specific antigen (PSA) level, tumour stage (T-stage) and Gleason grade allows for risk stratification into three major groups (low-risk, intermediate-risk and high-risk) of localised disease based on the probability of biochemical recurrence after local therapy [8]. Early efforts to incorporate genomics into risk prediction tools have been promising, with Spratt et al. proposing a system integrating existing genomic and clinical information to improve risk stratification [9]. The combined clinical–genomic risk system better predicted metastasis than using the standard National Comprehensive Cancer Network (NCCN) clinical risk group alone, and also reclassified 30% of patients.

Hypoxia, a state of low oxygen, is a common micro-environmental feature in most solid tumours, which activates multiple biological processes such as glycolysis and angiogenesis, inducing the expression (mRNA abundance) of multiple genes involved in these pathways and changes in transcriptomic profiles (10). High-throughput expression profiling technologies that can measure RNA expression have allowed the development of hypoxia-associated gene signatures, which were prognostic in prostate cancer cohorts and associated with RT resistance and metastatic disease in prostate cancer cohorts [11-15].

Traditionally, measuring oxygen levels in tumours has been performed using needle electrodes, however this is invasive, technically demanding, and not representative of the whole prostate [16]. Magnetic resonance imaging (MRI) has an essential role in prostate

cancer in diagnosis and treatment planning, and has the potential for monitoring after therapy to assess local recurrence [17]. When combined with radiomics, a quantitative image analysis technique used to derive imaging biomarkers [18], MRI-based radiomic prognostic models have shown improved prediction of survival outcomes for multiple cancer types compared with clinical information alone [19-21]. Additionally, combining MR-imaging, which has potential to image genetic features associated with more aggressive prostate disease [22], with gene-based biomarkers shows further potential in aiding the prediction of clinical outcomes such as survival or treatment resistance [23-24].

Current research has demonstrated potential association between radiomic features (RF) derived from imaging and pimonidazole-based hypoxia biomarkers, showing it may be feasible to develop a radiomics hypoxia model using T2-weighted (T2W) MR images [25], however there is limited evidence on the role in combining imaging and hypoxia-associated genomic biomarkers for outcome prediction. To the best of our knowledge, only a single study (in cervical cancer) has evaluated integrated imaging and gene expression signatures for non-invasive assessment of hypoxia-related treatment resistance [24]. Identifying imaging "radiogenomic" (combined radiomics and genomics) hypoxia signatures would potentially offer a non-invasive way to analyse the whole prostate in order to predict outcome.

This study investigates the value of combining prostate MRI radiomic and hypoxia-associated gene signature information with clinical data for the prediction of biochemical recurrence-free survival (BCRFS) following radiotherapy in prostate cancer patients treated with primary radiotherapy.

3.3 Materials and Methods

3.3.1 Dataset and Study Population

Prostate cancer patients treated with primary radiotherapy between 01/12/2007 and 31/08/2018 at two UK NHS hospitals were included in this retrospective cohort study. The study was approved by the United Kingdom North West Research Ethics Committee (IRAS 15/NW/0559).

Inclusion criteria were: (a) male patients with organ-confined or locally invasive prostate cancer (with no detected distant metastatic or nodal disease), aged at least 18 years; (b) biopsy-confirmed high-risk prostate cancer; (c) primary radiotherapy to treat their prostate cancer (either BT, EBRT or combination); (d) available pre-treatment MRI;

(e) available formalin-fixed, paraffin-embedded (FFPE) biopsy to enable Ragnum hypoxia gene signature evaluation; (f) available clinical features (patient age, International Society of Urological Pathology (ISUP) grade, PSA and T-stage) and clinical outcome data.

Diagnostic MR images, patient and tumour characteristics (ISUP grade and T-stage), and hypoxia gene signature were collected for all patients. Adherence was made to the Checklist for Artificial Intelligence in Medical Imaging (CLAIM) (Supplementary Material), a tool for assessing the quality of multivariate prediction models involving imaging and machine learning (ML) techniques [26].

3.3.2 MRI Acquisition

All patients underwent prostate imaging on 1.5T MRI scanners which included a minimum of an axial T2W sequence encompassing the whole prostate. Imaging was performed using multiple different MRI scanners. Specific scanner acquisition parameters are listed in Supplementary Material Table S3.1.

3.3.3 Hypoxia-associated Gene Signature

RNA from FFPE prostate biopsy specimens was extracted and processed using Affymetrix GeneChip (Clariom S Array) to calculate the expression of a 32-gene prostate hypoxia signature, based on pimonidazole staining (Ragnum signature) which generates a hypoxia score [27]. The gene enrichment analysis and construction of the gene signature is described by Ragnum et al. [27].

3.3.4 Image Segmentation

The whole prostate gland and prostate tumour (if visible) were manually segmented by an experienced radiologist and confirmed by a specialist Uroradiologist. All segmentation was performed on axial T2W sequences using RayStation (v9.1). Exported DICOM images were converted to Neuroimaging Informatics Technology Initiative (NIfTI) files and exported into PyRadiomics (v3.0.1) for analysis [28]. Histogram standardisation of all MR-images was applied using the Nyúl method prior to RF extraction to render dynamic signal intensity ranges comparable [29, 20].

A flowchart illustrating the methodological pipeline is shown in Figure 3.1.

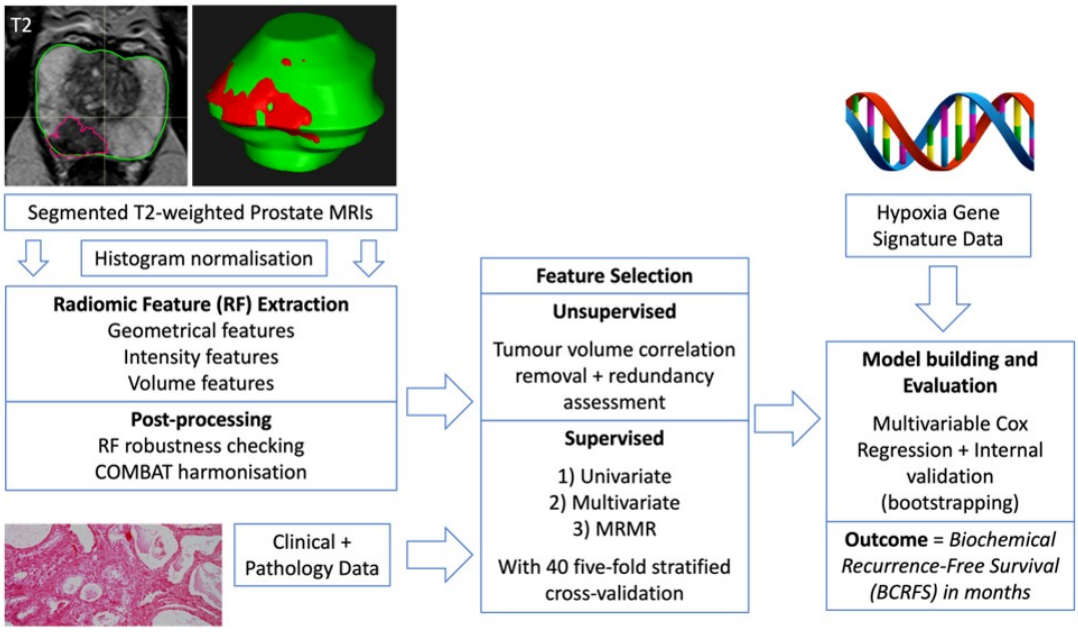

Figure 3.1 Flowchart showing study pipeline from image segmentation, image normalisation, radiomic feature extraction, image post-processing, feature selection steps to model building integrating hypoxia and radiomic data with clinical data.

3.3.5 Feature Extraction

Eight RF classes [28] were extracted from each segmented region of interest (ROI) using PyRadiomics (v3.0.1)[31]. PyRadiomics deviates from the image biomarker standardisation initiative (IBSI) by default applying a fixed bin width from 0 and not the minimum segmentation value, and the PyRadiomics kurtosis is not corrected, yielding a value 3 higher than the IBSI kurtosis however these parameters can be manually adjusted. Otherwise, PyRadiomics adheres to IBSI guidelines, which provides a comprehensive review of each step involved in radiomic analyses, including radiomics nomenclature and required calibration datasets [32]. All RFs extracted and filters applied are detailed in Supplementary Material.

Different numbers of bins (8, 16, 32, 64, 128, 256) and isotropic voxel sizes (1, 2, 3) were tested to assess the most robust quantisation/re-binning setting based on the combination of bin number and voxel size that yielded the largest set of radiomic features. An intraclass correlation coefficient (ICC) threshold of > 0.8 was also used to eliminate inter-correlated features. Number of bins was favoured over the bin width given the arbitrary nature of MRI intensity units. The ComBat harmonisation method (v0.2.10) was applied to extracted RFs to account for variation in scanner models, acquisition protocols and reconstruction settings which affect RFs [33-35].

3.3.6 Feature Selection

3.3.6.0.1 Unsupervised feature selection For each RF, correlation with tumour volume was assessed with Spearman rank correlation coefficient (p) and features with a p-value>0.5 were removed. RFs were assessed for redundancy (linear correlation to other RFs) using Pearson correlation coefficient. If the correlation coefficient was 0.5 or higher between two RFs then they were deemed to be correlated and the feature in the correlated pair with the highest mean correlation to other RFs was removed.

3.3.6.0.2 Supervised feature selection Following the same approach published in Davey et al. [36], supervised feature selection was performed using three different techniques for comparison. The methods implemented selected features that: (1) are significantly associated with outcome in a univariable Cox regression model ($p < 0.05$), (2) significantly improve a multivariable Cox regression model of clinical variables in a likelihood-ratio (LR) test ($p < 0.05$), and (3) have a positive contribution based on minimum redundancy maximum relevance (MRMR) ranking [37].

Each feature selection method was implemented independently over 200 samples created from 40 five-fold stratified cross-validation (SCV) runs with event-matching for number of biochemical recurrences, meaning that the data was partitioned into 5 sub-sets, 4 for training and 1 held for testing with the number of events balanced between the subsets. The training was repeated 5 times with each subset being held as the test set independently. The separation of the subsets was repeated 40 times, with a total of 200 cases to test model performance. In each cross-validation training run, selected features were combined with clinical variables (age, ISUP grade, PSA, T-stage, tumour volume and treatment) to form a clinical-radiomics multivariable Cox model. This model was then applied to the test data. Including the clinical variables for the other feature selection methods (univariable, MRMR) made the comparison to the multivariable feature selection technique fair. The Harrell's concordance index (C-index) was calculated for both training and test models with the median and 95% CI across SCV runs recorded. The feature selection technique was selected based on calculating the performance ranking from the median C-index across all clinical-radiomic models for both the training (Ctrain) and test (Ctest) data [38]. For the chosen technique, the selected features from each training run were recorded and ranked by occurrence. The top ranking features up to the median number of features selected across all runs were recorded.

3.3.7 Model Building

Using the feature results from the chosen MRMR technique four different multivariable Cox proportional hazards models were constructed for comparison: 1) clinical only, 2) clinical + hypoxia, 3) clinical + radiomics, and 4) clinical + hypoxia + radiomics. The Akaike Information Criterion (AIC) was extracted, and an Analysis of Variance (ANOVA) test was used to compare if there was a significant difference in regression model performance for each model 2 to 4, in comparison to model 1 (clinical only model as baseline). To evaluate the added benefit of radiomics to clinical and hypoxia variables, AIC of model 4 was also compared to model 2. AIC provides a mathematical method to evaluate how well a model fits a dataset and the smaller the AIC value, the better the model fit for outcome prediction [39].

For internal validation, the median and 95% CIs of the C-index for each model across 500 bootstrap resamples was calculated. C-index was calculated and each of these bootstrap models was fitted to the original data. For the purpose of analysis, T-stage was grouped into T1/2 group and T3 groups. The radiomic features were scaled to have a mean of 0, and a unit variance of 1.

Statistical analysis was performed in R (v.4.0.2). Two-tailed tests were used with statistical significance defined as $p < 0.05$.

3.4 Results

3.4.1 Clinical Characteristics

A total of 187 patients with histologically confirmed prostate cancer were treated at either St James's University Hospital (Leeds, UK) with EBRT (74 Gy in 37 fractions) (n=94), or at The Christie (Manchester, UK) with EBRT (57 Gy in 19 fractions) (n=55) or EBRT (37.5 Gy in 15 fractions) plus high dose rate (HDR) brachytherapy (BT) boost (single fraction 15 Gy) (n=38), between 01/12/2007 and 31/08/2013.

The clinical and treatment characteristics for all patients are listed in Table 3.1. Median follow-up was 84 months (range 3-140). BCR rate was 32% (n=60). Median BCRFS was 74 months (range 2-132).

Table 3.1 Demographics of the study cohort. Abbreviations: PSA = prostate specific antigen, ISUP = International Society of Urological Pathology, EBRT = external beam radiotherapy, HDR-BT = High Dose Rate Brachytherapy. Statistics presented: Median (range) for Age, PSA, Tumour Volume and Hypoxia Score; n(%) for ISUP and T-stage;

Characteristic	
Age (years)	69 (52 - 80)
PSA (ng/mL)	20 (2 - 234)
ISUP	
1	5 (2.7%)
2	70 (37%)
3	36 (19%)
4	17 (9.1%)
5	59 (32%)
T-stage	
T1	5 (2.7%)
T2	37 (19.8%)
T3	145 (77.5%)
Tumour Volume (cc)	5 (0 - 97)
Treatment	
EBRT	149 (80%)
HDR-BT	38 (20%)
Hypoxia Score (Ragnum Signature)	0.00 (-0.43 - 0.47)
	N = 187

3.4.2 Radiomic Feature Selection

The combination of bin number 256 and voxel size 1 yielded the most number of robust radiomic features (Supplementary Information). A total of 1314 radiomic features were extracted, 1068 remained after volume correlation, and 55 remained after removals for redundancy. The median number of radiomic features selected was 7 in MRMR, 3 in multivariable, and 2 in univariable. All features selected on the multivariable and univariable techniques were also captured by the MRMR technique. The MRMR technique also had the best model performance across training and test data with a test c-index of 0.73 (0.59-0.83) compared to Multivariable (c-index 0.70 (0.53-0.82)) and

univariable models (0.70 (0.55-0.83)).

Figure 3.2 shows the frequency (%) that each feature was selected across all cross-validation runs (out of 200). The higher the frequency the more stable that feature is in the feature selection process.

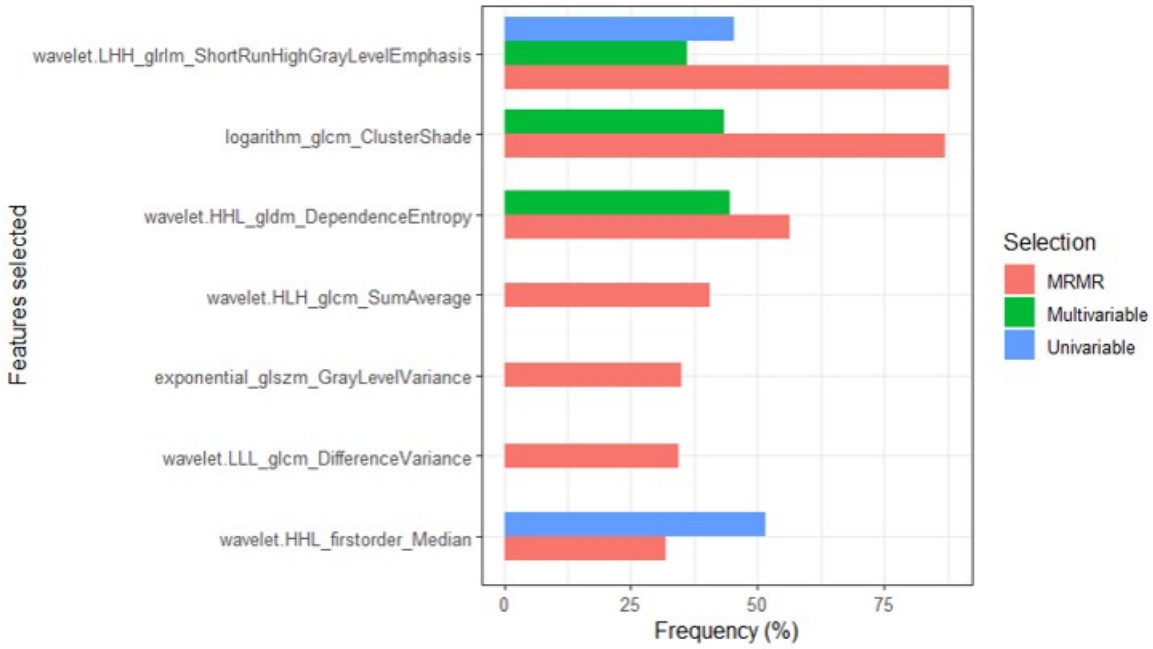

Figure 3.2 Bar chart showing the frequency (%) that each radiomic feature was selected across all cross-validation runs (out of 200) for each feature selection method. Abbreviations: LHH, HHL, HLH, LLL = 3D wavelet radiomic features, GLRLM = Grey level run length matrix, GLCM = Grey level co-occurrence matrix, GLDM = Grey Level Dependence Matrix, GLSZM = Grey level size zone matrix.

3.4.3 Prediction Model Performance

When evaluated on the complete dataset, the median C-index and confidence intervals (CI) of all 4 prediction models are shown in Figure 3.3.
Based on the C-index estimate, the combined clinical-radiomics-hypoxia model and clinical-radiomics model had the highest model performance (C-index 0.73 and 0.72 respectively). The clinical-only model (C-index of 0.67 [0.62-0.69]) and clinical-hypoxia model (C-index of 0.68 [0.64-0.69) had lower model performance.

Each model and overall model fit based on AIC are presented in Table 3.2. The combined clinical, radiomic and hypoxia model has the lowest AIC (AIC = 536.79) and best model fit.

Table 3.2 Selected features for each of the four models (clinical only, clinical with hypoxia, clinical with radiomics and combined clinical, hypoxia and radiomics) and overall model performance score (AIC Statistic). The radiomic features are scaled to mean zero and unit variance. Abbreviations: EBRT = external beam radiotherapy, HDR-BT = high dose-rate brachytherapy, HHL, HLH, LHH, LLL = 3D wavelet radiomic features, GLDM = Grey Level Dependence Matrix, GLCM = Grey level co-occurrence matrix, GLRLM = Grey level run length matrix, GLSZM = Grey level size zone matrix, AIC = Akaike Information Criterion.

	Clinical Model		**Clinical + Hypoxia**		**Clinical + Radiomics**		**Clinical + Hypoxia + Radiomics**	
	HR (95% CI)	**P-value**	**HR (95% CI)**	**P-value**	**HR (95% CI)**	**P-value**	**HR (95% CI)**	**P-value**
Age (years)	0.96 *(0.92-1.00)*	**0.028**	0.96 *(0.92-1.00)*	**0.047**	0.95 *(0.91-0.99)*	**0.019**	0.95 *(0.91-0.99)*	**0.020**
PSA (ng/mL)	1.01 *(1.00-1.01)*	**0.037**	1.01 *(1.00-1.02)*	**0.017**	1.01 *(1.00-1.01)*	0.155	1.01 *(1.00-1.01)*	0.093
ISUP Grade	1.28 *(1.05-1.57)*	**0.013**	1.28 *(1.05-1.57)*	**0.014**	1.25 *(1.02-1.54)*	**0.030**	1.27 *(1.03-1.56)*	**0.026**
T-stage (T1/2 vs T3)	2.28 *(1.08-4.81)*	**0.031**	2.46 *(1.16-5.22)*	**0.019**	2.73 *(1.19-6.25)*	**0.018**	3.05 *(1.31-7.10)*	**0.010**
Tumour volume (cc)	1.01 *(0.98-1.03)*	0.668	1.00 *(0.98-1.02)*	0.846	0.99 *(0.96-1.02)*	0.664	0.99 *(0.96-1.02)*	0.537
Treatment (EBRT vs HDR-BT)	1.67 *(0.87-3.20)*	0.123	1.59 *(0.83-3.03)*	0.163	1.90 *(0.90-4.02)*	0.095	1.75 *(0.83-3.71)*	0.142
Hypoxia Score (Ragnum signature)			4.55 *(0.84-24.6)*	0.079			6.66 *(1.04-42.8)*	**0.046**
Wavelet HHL GLDM Dependence Entropy					1.41 *(1.06-1.88)*	**0.017**	1.49 *(1.11-2.00)*	**0.008**
Wavelet HLH GLCM Sum Average					1.07 *(0.82-1.38)*	0.627	1.08 *(0.84-1.40)*	0.557
Wavelet LHH GLRLM Short Run High Gray Level Emphasis					0.75 *(0.57-0.99)*	**0.042**	0.77 *(0.58-1.02)*	0.071
Logarithm GLCM Cluster Shade					1.31 *(0.91-1.87)*	0.144	1.32 *(0.92-1.90)*	0.137
Wavelet HHL First Order Median					0.81 *(0.59-1.11)*	0.186	0.81 *(0.59-1.11)*	0.190
Exponential GLSZM Gray Level Variance					1.19 *(0.90-1.57)*	0.215	1.11 *(0.84-1.47)*	0.467
Wavelet LLL GLCM Difference Variance					0.76 *(0.55-1.06)*	0.104	0.77 *(0.56-1.06)*	0.110
AIC Statistic **Comparison to clinical model* ***Comparison to clinical+hypoxia model*	*542.54*		*538.85* **P = 0.079*		*541.45* **P = 0.013*		*536.79* **P = 0.005* ***P = 0.044*	

Figure 3.3 C-index and confidence interval (CI) of all 4 models showing best models were Clinical + Radiomics + Hypoxia (0.73) and Clinical + Radiomics (0.72).

When statistically comparing the combined model AICs to the clinical only model using an ANOVA test, the clinical and radiomics model was significantly better (p=0.013). Including hypoxia information alone (clinical + hypoxia model) did not improve model performance (p=0.079), unless it was also combined with radiomic features (p=0.005) (clinical + radiomics + hypoxia). When comparing the AIC of the clinical and hypoxia model vs the combined clinical, radiomic and hypoxia model, there was a statistically significant improvement in model performance for the combined clinical, radiomic and hypoxia model (p=0.044).

3.5 Discussion

In this study, the addition of pre-treatment T2W MRI-derived radiomic features to standard clinical variables improved the accuracy of predicting BCRFS after prostate radiotherapy with or without the addition of hypoxia gene signature scores.

The utility of MRI-based radiomic analysis has been studied in the setting of prostate cancer diagnosis and prediction of Gleason score with satisfactory early results [40-43]. More recently prediction models using prostate MRI radiomics have been reported assessing the risk of BCR after radiotherapy. Gnep et al. demonstrated that T2W MRI-derived Haralick textural features, which quantify spatial relationships between neighbouring voxels, were associated with BCR occurrence [44]. Few studies have investigated the role of MRI-derived radiomics in assessing progression-free survival in prostate cancer, however an initial report combining radiomics and clinical data into a hybrid prediction model yielded excellent performance and showed promise as a non-invasive diagnostic tool for risk stratification [19]. The current study also supports the notion that whole prostate gland radiomic features can provide additional information to help predict survival outcomes.

It is already known that hypoxic tumours are associated with worse outcomes after radiotherapy and using biopsy-based hypoxia-associated gene signatures has demonstrated prognostic significance in prostate cancer cohorts [14, 15]. Both imaging and genomic biomarkers have different strengths, however, there has been a paucity of studies investigating how they relate to each other in prostate cancer and their impact on survival outcomes to understand how to fully exploit any synergistic potential. In cervical cancer, a multifactorial prediction model combining both imaging and gene expression signatures was studied to assess hypoxia-related treatment resistance [24]. The results found a combined model allowed better prediction of progression-free survival. The current research confirms the same finding in prostate cancer and highlights further study of multifactorial prediction models would be worthwhile.

Addition of RFs derived from pre-treatment prostate MRI provided more prognostic information that use of a gene signature. An explanation for this finding is that imaging permits a more comprehensive prostate assessment compared to a biopsy-derived hypoxia gene signature, which is limited to the sampled region/s of the prostate and does not capture the overall spatial and temporal heterogeneity of the tumour or whole gland [45]. It is known that regional differences in hypoxia exist across the entire tumour volume and this heterogeneity may limit the use of gene signatures derived from only limited parts of the tumour [46]. This may help in understanding why the addition

of the hypoxia-associated gene signature alone to the clinical model did not further increase the performance of the outcome prediction model in this study however the same issue may not apply to tumour ISUP grade despite it being biopsy derived because it remained prognostic in the current study (47). ISUP grades are categorical and a study by De Nunzio et al. found the rate of discrepancy between biopsy pathology and the prostatectomy specimen to be low meaning the 5 tier ISUP system was highly specific (91%) for correctly defining the tumour aggressiveness (48).

The predictive prostate RFs observed in this study may already be a surrogate for tumour aggressiveness and hypoxia. Wavelet transformation of RFs further separates out the spatial and frequency distributions of low and high frequency signals within the region of interest to delineate such changes [49]. Differentiating these properties may improve the overall performance of the hybrid radiomic prediction model, as demonstrated by the current study where the best performing radiomic features were all wavelet ones.

Imaging features could be linked to underlying biological changes. Recent work has reported associations between T2W MRI radiomic features of the whole prostate gland or index lesion and tumour hypoxia, demonstrating the feasibility of building a radiomics hypoxia model from anatomical MRI [25, 50]. A study of 15 patients found bi-parametric prostate MRI RFs associated with increased expression of hypoxia-related genes was associated with unfavourable survival outcomes [51]. Similarly, Beig et al. reported in 180 glioblastoma patients that RFs extracted from the enhancing tumour, necrotic tumour, and peri-tumoral regions were predictive of a hypoxia enrichment score based on 21 genes implicated in the hypoxia pathway of glioblastoma [52]. An imaging radiogenomics study in renal cell cancer identified a contrast-enhanced CT-based radiomic signature associated with increased levels of hypoxia-associated gene expression that was able to accurately predict survival outcomes [53]. This radiogenomic model achieved good survival prediction performance in the training set and an independent external validation cohort, highlighting the potential for using such biomarkers for assisting in treatment decisions.

The hypoxia score was borderline significant ($p=0.046$) on the combined clinical, radiomics and hypoxia model but not significant on the clinical and hypoxia model ($p=0.079$). Potential reasons for this include overfitting due to the number of events per variable with the combined model but further investigation and external validation is required to determine the additive benefit of combining hypoxia markers with imaging-based radiomic features. If there are imaging features that may act as a surrogate marker for hypoxia, as previously highlighted in another exploratory study [45], then there may be less benefit to

including the hypoxia gene signature information.

In the future, using a radiogenomics- or hypoxia-driven approach in radiotherapy planning, through accurate delivery of focal radiation boosts to more 'hypoxic' parts of a tumour, could help to improve oncological outcomes and avoid rectal and urinary bladder toxicity in men treated with hypo-fractionated external beam radiotherapy for localised cancers [54].This would require additional investigation to correlate genomic and imaging-based hypoxia signatures with functional MRI sequences to generate radiology hypoxia maps and enable detection of hypoxic regions.

3.6 Limitations

There are a number of limitations to the study: Our study was retrospective with MRI data acquired from several scanners across different institutions, which is why an image harmonisation method was applied to minimise bias. The dataset is unique given the paired imaging and genomic data available from two centres. Only one hypoxia-associated gene signature was used which has its own limitations as the Ragnum signature is essentially a combination of genes whose expression correlates with pimonidazole-generated scores, another hypoxia biomarker. As this gene signature requires expression profiling platforms measuring relative mRNA abundance, it is affected by the biopsy sample preservation technique (e.g. fresh-frozen or FFPE), age of the FFPE blocks and by technical batch effect which limits comparison of these hypoxia scores between different institution cohorts.

Only T2W imaging was used due to the historic nature of the MRIs available for the study participants. Studies in cervical cancer have found that a radiomics signature derived from diffusion-weighted imaging (DWI) outperformed a model using T2W MRI-derived radiomic features for predicting survival [20]. In prostate cancer, a combined DWI and T2W survival prediction model outperformed models using only one of these sequences when predicting 3-year progression-free survival [19]. It is reasonable to assume DWI would add to the prognostic information offered by the T2W sequence, which is mainly used for detailing anatomy, whereas DWI measures underlying tumour cell density and water diffusion which can provide additional information on the cellular microenvironment and even hypoxia [46]. Future work will integrate other functional sequences such as DWI and dynamic contrast-enhanced (DCE) imaging to the prediction model in order to further improve its performance.

Three supervised feature selection techniques were used prior to the implementation of

the Cox regression model. This approach performs similarly to more complex ML models such as those using boosting trees, boosting gradient linear models and random forest based methods given that the feature selection part is the most error-prone stage [55]. No adjustment for multiple testing was incorporated in the statistical analysis, reflecting the exploratory nature of the study.

Finally, the choice of outcome metric remains debateable as biochemical recurrence was not a surrogate endpoint for overall survival in recurrent prostate cancer in the NRG Oncology/RTOG 9601 phase III trial [56]. Due to loss of follow-up in this patient cohort, assigning overall survival, cancer specific mortality or determining metastasis-free survival would not be reliable. Biochemical recurrence may be due to local or systemic relapse, both of which hypoxia predisposes to and hypoxia-associated gene signatures have been identified as independent risk factors for metastasis-free survival in prostate cancer [56], therefore evaluating the prediction of other survival endpoints may be more widely accepted by the clinical oncology community.

3.7 Conclusions

Adding pre-treatment prostate MRI-derived radiomic features to clinical variables improves the accuracy of predicting BCRFS after prostate radiotherapy, with or without the addition of a hypoxia gene signature. The overall best-fit model was the combined clinical, radiomic and hypoxia model. Further multicentre and subsequent prospective validation of this radiogenomic signature is required to demonstrate that it is reproducible and stable prior to clinical implementation.

3.8 References

1. Cronin KA, Lake AJ, Scott S, Sherman RL, Noone AM, Howlader N, *et al.* Annual Report to the Nation on the Status of Cancer, part I: National cancer statistics. Cancer. 2018 Jul 1;124(13):2785–800.

2. Mottet N, Bellmunt J, Bolla M, Briers E, Cumberbatch MG, De Santis M, *et al.* EAU-ESTRO-SIOG Guidelines on Prostate Cancer. Part 1: Screening, Diagnosis, and Local Treatment with Curative Intent. Eur Urol. 2017;71(4):618–29.

3. Beckendorf V, Guerif S, Le Prisé E, Cosset JM, Bougnoux A, Chauvet B, *et al.* 70 Gy versus 80 Gy in localized prostate cancer: 5-year results of GETUG 06 randomized trial. Int J Radiat Oncol Biol Phys. 2011;80(4):1056–63.

4. Zumsteg ZS, Spratt DE, Romesser PB, Pei X, Zhang Z, Kollmeier M, *et al.* Anatomical patterns of recurrence following biochemical relapse in the dose escalation era of external beam radiotherapy for prostate cancer. Journal of Urology. 2015;194(6):1624-1630.

5. Jones CU, Hunt D, McGowan DG, Amin MB, Chetner MP, Bruner DW, *et al.* Radiotherapy and Short-Term Androgen Deprivation for Localized Prostate Cancer. New England Journal of Medicine. 2011 Jul 14;365(2):107–18.

6. Jereczek-Fossa BA, Marvaso G, Zaffaroni M, Gugliandolo SG, Zerini D, Corso F, *et al.* Salvage stereotactic body radiotherapy (SBRT) for intraprostatic relapse after prostate cancer radiotherapy: An ESTRO ACROP Delphi consensus. Cancer Treat Rev. 2021 Jul;98:102206.

7. Paller CJ, Antonarakis ES. Management of biochemically recurrent prostate cancer after local therapy: evolving standards of care and new directions. Clin Adv Hematol Oncol. 2013 Jan;11(1):14–23.

8. Mohler JL, Antonarakis ES, Armstrong AJ, D'Amico A V., Davis BJ, Dorff T, *et al.* Prostate Cancer, Version 2.2019, NCCN Clinical Practice Guidelines in Oncology. Journal of the National Comprehensive Cancer Network. 2019 May;17(5):479–505.

9. Spratt DE, Zhang J, Santiago-Jiménez M, Dess RT, Davis JW, Den RB, *et al.* Development and Validation of a Novel Integrated Clinical-Genomic Risk Group Classification for Localized Prostate Cancer. Journal of Clinical Oncology. 2018 Feb 20;36(6):581–90.

10. Harris AL. Hypoxia–a key regulatory factor in tumour growth. Nat Rev Cancer. 2002 Jan;2(1):38–47.

11. Turaka A, Buyyounouski MK, Hanlon AL, Horwitz EM, Greenberg RE, Movsas B. Hypoxic Prostate/Muscle Po2 Ratio Predicts for Outcome in Patients With Localized Prostate Cancer: Long-Term Results. International Journal of Radiation Oncology*Biology*Physics. 2012 Mar;82(3):e433–9.

12. Lalonde E, Ishkanian AS, Sykes J, Fraser M, Ross-Adams H, Erho N, *et al.* Tumour genomic and microenvironmental heterogeneity for integrated prediction of 5-year biochemical recurrence of prostate cancer: a retrospective cohort study. Lancet Oncol. 2014 Dec;15(13):1521–32.

13. Milosevic M, Warde P, Ménard C, Chung P, Toi A, Ishkanian A, *et al.* Tumor Hypoxia Predicts Biochemical Failure following Radiotherapy for Clinically Localized Prostate Cancer. Clinical Cancer Research. 2012 Apr 1;18(7):2108–14.

14. Yang L, Roberts D, Takhar M, Erho N, Bibby BAS, Thiruthaneeswaran N, *et al.* Development and Validation of a 28-gene Hypoxia-related Prognostic Signature for Localized Prostate Cancer. EBioMedicine. 2018 May;31:182–9.

15. Ragnum HB, Vlatkovic L, Lie AK, Axcrona K, Julin CH, Frikstad KM, *et al.* The tumour hypoxia marker pimonidazole reflects a transcriptional programme associated with aggressive prostate cancer. Br J Cancer. 2015 Jan 2;112(2):382–90.

16. Hockel M, Schlenger K, Aral B, Mitze M, Schaffer U, Vaupel P. Association between tumor hypoxia and malignant progression in advanced cancer of the uterine cervix. Cancer Res. 1996 Oct 1;56(19):4509–15.

17. Fernandes MC, Yildirim O, Woo S, Vargas HA, Hricak H. The role of MRI in prostate cancer: current and future directions. Magnetic Resonance Materials in Physics, Biology and Medicine. 2022 Mar 16;35(4):503–21.

18. Lambin P, Leijenaar RTH, Deist TM, Peerlings J, De Jong EEC, Van Timmeren J, *et al.* Radiomics: The bridge between medical imaging and personalized medicine. Nat Rev Clin Oncol. 2017;4(12):749-762.

19. Jia Y, Quan S, Ren J, Wu H, Liu A, Gao Y, *et al.* MRI radiomics predicts progression-free survival in prostate cancer. Front Oncol. 2022 Aug 30;12.

20. Zheng R ru, Cai M ting, Lan L, Huang XW, Yang YJ, Powell M, *et al.* An MRI-based radiomics signature and clinical characteristics for survival prediction in early-stage cervical cancer. Br J Radiol. 2022 Jan 1;95(1129).

21. Geraghty BJ, Dasgupta A, Sandhu M, Malik N, Maralani PJ, Detsky J, *et al.* Predicting survival in patients with glioblastoma using MRI radiomic features extracted from radiation planning volumes. J Neurooncol. 2022 Feb 3;156(3):579–88.

22. Norris JM, Simpson BS, Parry MA, Allen C, Ball R, Freeman A, *et al.* Genetic Landscape of Prostate Cancer Conspicuity on Multiparametric Magnetic Resonance Imaging: A Systematic Review and Bioinformatic Analysis. Eur Urol Open Sci. 2020 Jul;20:37–47.

23. Sanduleanu S, Jochems A, Upadhaya T, Even AJG, Leijenaar RTH, Dankers FJWM, *et al.* Non-invasive imaging prediction of tumor hypoxia: A novel developed and externally validated CT and FDG-PET-based radiomic signatures. Radiotherapy and Oncology. 2020 Dec;153:97–105.

24. Fjeldbo CS, Hompland T, Hillestad T, Aarnes EK, Günther CC, Kristensen GB, *et al.* Combining imaging- and gene-based hypoxia biomarkers in cervical cancer improves prediction of chemoradiotherapy failure independent of intratumour heterogeneity. EBioMedicine. 2020 Jul;57:102841.

25. Leech M, Leijenaar RTH, Hompland T, Gaffney J, Lyng H, Marignol L. Exploring Hypoxia in Prostate Cancer With T2-weighted Magnetic Resonance Imaging Radiomics and Pimonidazole Scoring. Anticancer Res. 2023 Jan;43(1):351–7.

26. Mongan J, Moy L, Kahn CE. Checklist for Artificial Intelligence in Medical Imaging (CLAIM): A Guide for Authors and Reviewers. Radiol Artif Intell. 2020 Mar 1;2(2):e200029.

27. Ragnum HB, Vlatkovic L, Lie AK, Axcrona K, Julin CH, Frikstad KM, *et al.* The tumour hypoxia marker pimonidazole reflects a transcriptional programme associated with aggressive prostate cancer. Br J Cancer. 2015 Jan 2;112(2):382–90.

28. van Griethuysen JJM, Fedorov A, Parmar C, Hosny A, Aucoin N, Narayan V, *et al.* Computational Radiomics System to Decode the Radiographic Phenotype. Cancer Res. 2017 Nov 1;77(21):e104–7.

29. Carré A, Klausner G, Edjlali M, Lerousseau M, Briend-Diop J, Sun R, *et al.* Standardization of brain MR images across machines and protocols: bridging the gap for MRI-based radiomics. Sci Rep. 2020 Dec 23;10(1):12340.

30. Nyul LG, Udupa JK, Xuan Zhang. New variants of a method of MRI scale standardization. IEEE Trans Med Imaging. 2000;19(2):143–50.

31. van Griethuysen JJM, Fedorov A, Parmar C, Hosny A, Aucoin N, Narayan V, *et al.* Computational Radiomics System to Decode the Radiographic Phenotype. Cancer Res. 2017 Nov 1;77(21):e104–7.

32. Zwanenburg A, Vallières M, Abdalah MA, Aerts HJWL, Andrearczyk V, Apte A, *et al.* The Image Biomarker Standardization Initiative: Standardized Quantitative Radiomics for High-Throughput Image-based Phenotyping. Radiology. 2020 May;295(2):328–38.

33. Fortin JP, Cullen N, Sheline YI, Taylor WD, Aselcioglu I, Cook PA, *et al.* Harmonization of cortical thickness measurements across scanners and sites. Neuroimage. 2018 Feb;167:104–20.

34. Johnson WE, Li C, Rabinovic A. Adjusting batch effects in microarray expression data using empirical Bayes methods. Biostatistics. 2007 Jan 1;8(1):118–27.

35. Fortin JP, Parker D, Tunç B, Watanabe T, Elliott MA, Ruparel K, *et al.* Harmonization of multi-site diffusion tensor imaging data. Neuroimage. 2017 Nov;161:149–70.

36. Davey A, van Herk M, Faivre-Finn C, Brown S, McWilliam A. Optimising use of 4D-CT phase information for radiomics analysis in lung cancer patients treated with stereotactic body radiotherapy. Phys Med Biol. 2021 Jun 7;66(11):115012.

37. De Jay N, Papillon-Cavanagh S, Olsen C, El-Hachem N, Bontempi G, Haibe-Kains B. mRMRe: an R package for parallelized mRMR ensemble feature selection. Bioinformatics. 2013 Sep 15;29(18):2365–8.

38. Rabasco Meneghetti A, Zwanenburg A, Leger S, Leger K, Troost EGC, Linge A, *et al.* Definition and validation of a radiomics signature for loco-regional tumour control in patients with locally advanced head and neck squamous cell carcinoma. Clin Transl Radiat Oncol. 2021 Jan;26:62–70.

39. Akaike Hirotogu. Information theory and an extension of the maximum likelihood principle. New York: Springer New York; 1998. 199–213 p.

40. Toivonen J, Montoya Perez I, Movahedi P, Merisaari H, Pesola M, Taimen P, *et al.* Radiomics and machine learning of multisequence multiparametric prostate MRI: Towards improved non-invasive prostate cancer characterization. PLoS One. 2019 Jul 8;14(7):e0217702.

41. Li M, Chen T, Zhao W, Wei C, Li X, Duan S, *et al.* Radiomics prediction model for the improved diagnosis of clinically significant prostate cancer on biparametric MRI. Quant Imaging Med Surg. 2020 Feb;10(2):368–79.

42. Wibmer A, Hricak H, Gondo T, Matsumoto K, Veeraraghavan H, Fehr D, *et al.* Haralick texture analysis of prostate MRI: utility for differentiating non-cancerous prostate from prostate cancer and differentiating prostate cancers with different Gleason scores. Eur Radiol. 2015 Oct 21;25(10):2840–50.

43. Chaddad A, Niazi T, Probst S, Bladou F, Anidjar M, Bahoric B. Predicting Gleason Score of Prostate Cancer Patients Using Radiomic Analysis. Front Oncol. 2018 Dec 18;8.

44. Gnep K, Fargeas A, Gutiérrez-Carvajal RE, Commandeur F, Mathieu R, Ospina JD, *et al.* Haralick textural features on T 2 -weighted MRI are associated with biochemical recurrence following radiotherapy for peripheral zone prostate cancer. Journal of Magnetic Resonance Imaging. 2017 Jan;45(1):103–17.

45. Hoskin PJ, Carnell DM, Taylor NJ, Smith RE, Stirling JJ, Daley FM, *et al.* Hypoxia in Prostate Cancer: Correlation of BOLD-MRI With Pimonidazole Immunohistochemistry-Initial Observations. Int J Radiat Oncol Biol Phys. 2007;68(4):1065–71.

46. Hompland T, Hole KH, Ragnum HB, Aarnes EK, Vlatkovic L, Lie AK, *et al.* Combined MR Imaging of Oxygen Consumption and Supply Reveals Tumor Hypoxia and Aggressiveness in Prostate Cancer Patients. Cancer Res. 2018 Aug 15;78(16):4774–85.

47. Offermann A, Hohensteiner S, Kuempers C, Ribbat-Idel J, Schneider F, Becker F, *et al.* Prognostic Value of the New Prostate Cancer International Society of Urological Pathology Grade Groups. Front Med (Lausanne). 2017 Sep 29;4.

48. De Nunzio C, Pastore AL, Lombardo R, Simone G, Leonardo C, Mastroianni R, *et al.* The new Epstein gleason score classification significantly reduces upgrading in prostate cancer patients. Eur J Surg Oncol. 2018 Jun;44(6):835-839.

49. Wang Y, Che X, Ma S. Nonlinear filtering based on 3D wavelet transform for MRI denoising. EURASIP J Adv Signal Process. 2012 Dec 21;2012(1):40.

50. Zhong J, Frood R, McWilliam A, Davey A, Shortall J, Swinton M, *et al.* Prediction of prostate tumour hypoxia using pre-treatment MRI-derived radiomics: preliminary findings. Radiol Med. 2023 May 17;128(6):765–74.

51. Ogbonnaya CN, Alsaedi BSO, Alhussaini AJ, Hislop R, Pratt N, Nabi G. Radiogenomics Reveals Correlation between Quantitative Texture Radiomic Features of Biparametric MRI and Hypoxia-Related Gene Expression in Men with Localised Prostate Cancer. J Clin Med. 2023 Mar 30;12(7):2605.

52. Beig N, Bera K, Prasanna P, Antunes J, Correa R, Singh S, *et al.* Radiogenomic-Based Survival Risk Stratification of Tumor Habitat on Gd-T1w MRI Is Associated with Biological Processes in Glioblastoma. Clinical Cancer Research. 2020 Apr 15;26(8):1866–76.

53. Gao J, Ye F, Han F, Wang X, Jiang H, Zhang J. A Novel Radiogenomics Biomarker Based on Hypoxic-Gene Subset: Accurate Survival and Prognostic Prediction of Renal Clear Cell Carcinoma. Front Oncol. 2021 Oct 7;11.

54. Her EJ, Haworth A, Sun Y, Williams S, Reynolds HM, Kennedy A, *et al.* Biologically Targeted Radiation Therapy: Incorporating Patient-Specific Hypoxia Data Derived from Quantitative Magnetic Resonance Imaging. Cancers (Basel). 2021 Sep 29;13(19):4897.

55. Leger S, Zwanenburg A, Pilz K, Lohaus F, Linge A, Zöphel K, *et al.* A comparative study of machine learning methods for time-to-event survival data for radiomics risk modelling. Sci Rep. 2017 Oct 16;7(1):13206.

56. Shipley WU, Seiferheld W, Lukka HR, Major PP, Heney NM, Grignon DJ, *et al.* Radiation with or without Antiandrogen Therapy in Recurrent Prostate Cancer. New England Journal of Medicine. 2017 Feb 2;376(5):417–28.

57. Xia H, Wang J, Guo X, Lv Z, Liu J, Yan Q, *et al.* Identification of a Hypoxia-Related Gene Signature for Predicting Systemic Metastasis in Prostate Cancer. Front Cell Dev Biol. 2021 Oct 13;9.

3.9 Supplementary Material

Table S3.1 MRI acquisition parameters of the 4 different 1.5T MRI Scanners used to acquire T2 weighted axial prostate MRI data.

1.5T MRI Scanner	Repetition time/ echo time (ms)	Flip Angle (°)	Field of view (mm)	Matrix size (mm)	Slice thickness (mm)
GE Signa	5020/122	90	250	384 x 224	3
Philips Achieva	3500/ 90	90	220	256 x 192	3
Siemens Aera	3540/ 99	160	220	320 × 256	3
Siemens Sola	4500/ 88	150	200	320 × 256	3

3.9.1 Extracted Radiomic Features and Filters

Radiomic feature classes that were extracted from the T2-weighted MRI whole prostate gland segmentations. All feature classes listed below, with the exception of the shape-based features can be calculated on the original image and/or a derived image, such as applying one of several filters which is how the wavelet features were generated. Individual feature description can be found at: https://pyradiomics.readthedocs.io/en/latest/features.html

First-order

- 10th Percentile
- 90th Percentile
- Energy
- Entropy
- Interquartile Range
- Kurtosis
- Maximum
- Mean Absolute Deviation
- Mean
- Median

- Minimum
- Range
- Robust Mean Absolute Deviation
- Root Mean Squared
- Skewness
- Total Energy
- Uniformity
- Variance

Shape-based (3D)

- Mesh Volume
- Voxel Volume
- Surface Area
- Surface Area to Volume ratio
- Sphericity
- Maximum 3D diameter
- Maximum 2D diameter (Slice)
- Maximum 2D diameter (Column)
- Maximum 2D diameter (Row)
- Major Axis Length
- Minor Axis Length Least Axis Length
- Elongation
- Flatness

Gray Level Co-occurrence Matrix (GLCM)

- Autocorrelation
- Cluster Prominence
- Cluster Shade
- Cluster Tendency
- Contrast
- Correlation
- Difference Average
- Difference Entropy
- Difference Variance
- ID: Inverse Difference
- IDM: Inverse Difference Moment
- IDMN: Inverse Difference Moment Normalized
- IDN: Inverse Difference Normalized
- IMC1: Informational Measure of Correlation 1
- IMC2: Informational Measure of Correlation 1
- Inverse Variance
- Joint Average
- Joint Energy
- Joint Entropy
- MCC: Maximal Correlation Coefficient
- Maximum Probability
- Sum Average
- Sum Entropy
- Sum Squares

Gray Level Dependence Matrix (GLDM)

- Dependence Entropy
- Dependence NonUniformity
- Dependence NonUniformity Normalized
- Dependence Variance
- Gray Level NonUniformity
- Gray Level Variance
- High Gray Level Emphasis
- Large Dependence Emphasis
- Large Dependence High Gray Level Emphasis
- Large Dependence Low Gray Level Emphasis
- Low Gray Level Emphasis
- Small Dependence Emphasis
- Small Dependence High Gray Level Emphasis
- Small Dependence Low Gray Level Emphasis

Gray Level Run Length Matrix (GLRLM)

- Gray Level NonUniformity
- Gray Level NonUniformity Normalized
- Gray Level Variance
- High Gray Level Run Emphasis
- Long Run Emphasis
- Long Run High Gray Level Emphasis
- Long Run Low Gray Level Emphasis
- Low Grey Level Run Emphasis

- Run Entropy
- Run Length NonUniformity
- Run Length NonUniformity Normalized
- Run Percentage
- Run Variance
- Short Run Emphasis
- Short Run High Gray Level Emphasis
- Short Run Low Gray Level Emphasis

Gray Level Size Zone Matrix (GLSZM)

- Gray Level NonUniformity
- Gray Level NonUniformity Normalized
- Gray Level Variance
- High Gray Level Zone Emphasis
- Large Area Emphasis
- Large Area High Gray Level Emphasis
- Large Area Low Gray Level Emphasis
- Low Gray Level Zone Emphasis
- Size Zone Non-Uniformity
- Size Zone Non-Uniformity Normalized
- Small Area Emphasis
- Small Area High Gray Level Emphasis
- Small Area Low Gray Level Emphasis
- Zone Entropy
- Zone Percentage

- Zone Variance

Neighboring Gray-Tone Difference Matrix (NGTDM)

- Busyness
- Coarseness
- Complexity
- Contrast
- Strength

CLAIM: Checklist for Artificial Intelligence in Medical Imaging

This checklist is in reference to the main manuscript of "*Adding MRI radiomics and hypoxia gene signature scores to clinical variables improves prediction of biochemical recurrence-free survival after prostate radiotherapy*".

Section / Topic	No.	Item	
TITLE / ABSTRACT			**Page number**
	1	Identification as a study of AI methodology, specifying the category of technology used (e.g., deep learning)	**P1**
	2	Structured summary of study design, methods, results, and conclusions	**P1**
INTRODUCTION			
	3	Scientific and clinical background, including the intended use and clinical role of the AI approach	**P3-4**
	4	Study objectives and hypotheses	**P5**
METHODS			
Study Design	**5**	Prospective or retrospective study	**P5**
	6	Study goal, such as model creation, exploratory study, feasibility study, non-inferiority trial	**P5**
Data	**7**	Data sources	**P5**
	8	Eligibility criteria: how, where, and when potentially eligible participants or studies were identified (e.g., symptoms, results from previous tests, inclusion in registry, patient-care setting, location, dates)	**P5**
	9	Data pre-processing steps	**P5-6**
	10	Selection of data subsets, if applicable	**P5**
	11	Definitions of data elements, with references to Common Data Elements	**P5-6**
	12	De-identification methods	**P5**
	13	How missing data were handled	**N/A**
Ground Truth	**14**	Definition of ground truth reference standard, in sufficient detail to allow replication	**P7**
	15	Rationale for choosing the reference standard (if alternatives exist)	**P15**
	16	Source of ground-truth annotations; qualifications and preparation of annotators	**P5-7**
	17	Annotation tools	**P5**
	18	Measurement of inter- and intrarater variability; methods to mitigate variability and/or resolve discrepancies	**N/A**

Data Partitions	**19**	Intended sample size and how it was determined	**P5**
	20	How data were assigned to partitions; specify proportions	**P7**
	21	Level at which partitions are disjoint (e.g., image, study, patient, institution)	**P7**
Model	**22**	Detailed description of model, including inputs, outputs, all intermediate layers and connections	**P10-12**
	23	Software libraries, frameworks, and packages	**P5-7**
	24	Initialization of model parameters (e.g., randomization, transfer learning)	**P7-8**
Training	**25**	Details of training approach, including data augmentation, hyperparameters, number of models trained	**P8**
	26	Method of selecting the final model	**P8**
	27	Ensembling techniques, if applicable	**N/A**
Evaluation	**28**	Metrics of model performance	**Table 3.2**
	29	Statistical measures of significance and uncertainty (e.g., confidence intervals)	**P12**
	30	Robustness or sensitivity analysis	**P11**
	31	Methods for explainability or interpretability (e.g., saliency maps), and how they were validated	**P11**
	32	Validation or testing on external data	**P11**
RESULTS			
Data	**33**	Flow of participants or cases, using a diagram to indicate inclusion and exclusion	**Fig 1**
	34	Demographic and clinical characteristics of cases in each partition	**Table 3.1**
Model performance	**35**	Performance metrics for optimal model(s) on all data partitions	**Table 3.2**
	36	Estimates of diagnostic accuracy and their precision (such as 95% confidence intervals)	**P6/ Tables**
	37	Failure analysis of incorrectly classified cases	**N/A**
DISCUSSION			
	38	Study limitations, including potential bias, statistical uncertainty, and generalizability	**P15**
	39	Implications for practice, including the intended use and/or clinical role	**P12-15**
OTHER INFORMATION			
	40	Registration number and name of registry	**N/A**
	41	Where the full study protocol can be accessed	**N/A**
	42	Sources of funding and other support; role of funders	**Disclosure**

Chapter 4
Exploratory Study of Bladder and Rectum Radiomic Feature Changes Following External Beam Radiation Therapy Delivered on a Magnetic Resonance Imaging Linear Accelerator (MRI-LINAC)

4.1 Abstract

4.1.1 Purpose

To investigate longitudinal radiomic feature changes in bladder wall and rectum during radiotherapy for prostate cancer and report preliminary findings on impact of dose-fractionation and relation with acute gastrointestinal (GI) and genitourinary (GU) toxicity.

4.1.2 Methods

All men with prostate cancer treated on a 1.5T Elekta Unity MRI-LINAC between July-2020 and May-2021 at a single institution were included. Whole rectum and bladder wall were contoured by two observers on T2-weighted MRI sequences using RayStation (v9.1) at 5 timepoints: Fraction 1, 5, 10, 15 and 20 for patients treated with conventional external beam radiotherapy (EBRT) (60Gy in 20 fractions) and every fraction for patients treated with stereotactic ablative radiotherapy (SABR) (36.25Gy in 5 fractions). First-order radiomic features (RFs) were extracted from each timepoint using PyRadiomics (v3.0.1). Acute GI and GU toxicity information (CTCAE v5.0) was collected for all patients. Radiomic profiles for patients with and without toxicity were plotted. MR images were qualitatively assessed. Pairwise t-test was used to compare radiomic changes relative to fraction 1.

4.1.3 Results

A total of 21 patients and 105 MRIs were analysed, 10 received EBRT, 11 received SABR. In the EBRT group, 80% experienced acute toxicity (n=8) and 20% had grade 2 toxicity (n=2). For the SABR group, 82% had GU toxicity (n=9) and 36% had GI toxicity (n=4), with one patient experiencing grade 2 GI toxicity. Statistically significant changes ($p<0.05$) were seen in the EBRT cohort in 6 rectal RFs as early as fraction 10 over the population. Different RF trends were observed in the EBRT bladder group across 5 time points in patients with and without GU toxicity. Fewer longitudinal changes in the radiomic profiles were observed in the SABR group.

4.1.4 Conclusions

Analysing longitudinal radiomic changes from the bladder and rectum during MRI-LINAC radiotherapy treatments is feasible. Potential changes in RFs were observed across 5 time points in both structures. Differences were seen between patients receiving SABR and EBRT and in patients who experienced acute toxicity.

4.2 Introduction

Prostate cancer is the most common malignancy in men and a major cause of cancer-related death[1]. Radiotherapy (RT) is an effective treatment for controlling prostate cancer progression however despite technological advances including dose escalation with stereotactic ablative radiotherapy (SABR), image-guidance and improved treatment accuracy through increased target conformality, a number of patients will still suffer from significant side effects from radiation-induced damage to the surrounding organs at risk (OAR), namely the bladder and rectum. A recent large multicentre study found severe (Grade 3 or higher) genitourinary (GU) and gastrointestinal (GI) toxicity rates 7 years after SABR were 2.4% and 0.4% respectively, slightly better compared to the toxicity rates reported for historic external beam fractionation regimens (GU 3% and GI 1%) [2,3].

There remains an unmet need for objective and easily accessible ways to assess an individual patients' risk of RT induced toxicity before or during treatment. These metrics would not only enhance patient counselling but also enable timely treatment adjustments or interventions to mitigate side effects. Despite the potential advantages this data could offer, there is a paucity of research into developing such measures.

With the establishment of magnetic resonance imaging - linear accelerator (MRI-LINAC) treatment platforms, there is an opportunity to obtain more information before and during RT and facilitate adaptive, real-time treatment planning[2]. This allows in theory the monitoring of imaging changes within the prostate, bladder wall and rectum during RT to assess and potentially predict RT side effects and treatment response. Radiomics offers a systematic approach, aided by high-throughput software, to mine and quantify imaging data, facilitating the discovery of predictive and prognostic imaging biomarkers. These biomarkers encompass both macroscopic and microscopic characteristics of tumours or normal tissue, such as their textural patterns (signal intensity and heterogeneity) to unveil additional information on underlying pathophysiology which could provide insight into early radiation-induced toxicity[3]. With the availability of imaging at each RT treatment time point, this allows for the measurement of radiomic feature (RF) changes over time in longitudinal MR images [4].

The use of MRI-LINAC presents a valuable advantage by enabling repeated and non-invasive collection of qualitative and quantitative data over time[5]. MR imaging is particularly appealing for longitudinal radiomic assessments due to its superior spatial resolution and ability to delineate soft tissues effectively.

The purpose of this exploratory study was to design a methodological pipeline for analysing the longitudinal radiomic profiles of OAR (bladder wall and rectum) for patients undergoing RT for prostate cancer using T2 weighted (T2W) MR images acquired on a 1.5 Tesla (T) MRI-LINAC. A secondary objective was to investigate if changes in OAR radiomic metrics varied between conventional external beam radiotherapy (EBRT) and SABR treatment groups and in patients experiencing radiotherapy toxicity side-effects(Grade 2 or higher). Treatment response within the prostate tumour has not been presented in this chapter as this forms a separate study which will be future work.

4.3 Methods

4.3.1 Dataset and Study Population

A total of 21 patients who had MRI and dose data available were included. 10 patients received EBRT (60Gy in 20 fractions over four weeks) and 11 received SABR (36.25Gy in 5 fractions over two weeks) respectively. All patients were treated and imaged on a 1.5T Elekta Unity MRI-LINAC system and were recruited as part of an ongoing prospective observational imaging clinical trial (NCT30500081). All patients had intermediate risk localised disease, and all received androgen deprivation therapy (ADT) prior to radiotherapy. All patients provided informed written consent. Images were obtained between July 2020 and May 2021.

Inclusion criteria were: (a) male patients with prostate cancer aged at least 18 years; (b) radiotherapy delivered on the MRI-LINAC; (c) available MRI for each radiotherapy fraction; (d) available clinical features and toxicity data. Toxicity side-effect information was collected one month post-treatment by the clinical research nursing team during a routine follow-up outpatient clinic (virtual) using the Common Terminology Criteria for Adverse Events (CTCAE) version 5.0 [6]. The cut-off for patients with and without GU and GI toxicity was defined as Grade 2 or higher for this study.

4.3.2 Organs at Risk Contouring

Treatment localisation scans were transferred from the treatment planning system (Monaco v5.40, Elekta, Crawley UK) to RayStation (v9.1, RaySearch Laboratories). The whole rectum (up to the level of the peritoneal reflection) and whole bladder were contoured by two individuals (MK and LB) following a live demonstration and tutorial on contouring pelvic organs on MRI using RayStation, provided by a board-certified

radiologist with over 7 years' experience (JZ). All contours were independently checked and adapted by the radiologist. Contours were completed using the T2 weighted (T2W) MRI sequences obtained at fraction 1 (pre-treatment), 2,3,4 and 5 for the SABR cases and at fraction 1 (pre-treatment), 5, 10, 15 and 20 for the conventional fractionation cases. A total of 105 MRIs were analysed. Examples of the different contours are shown in Figure 4.1.

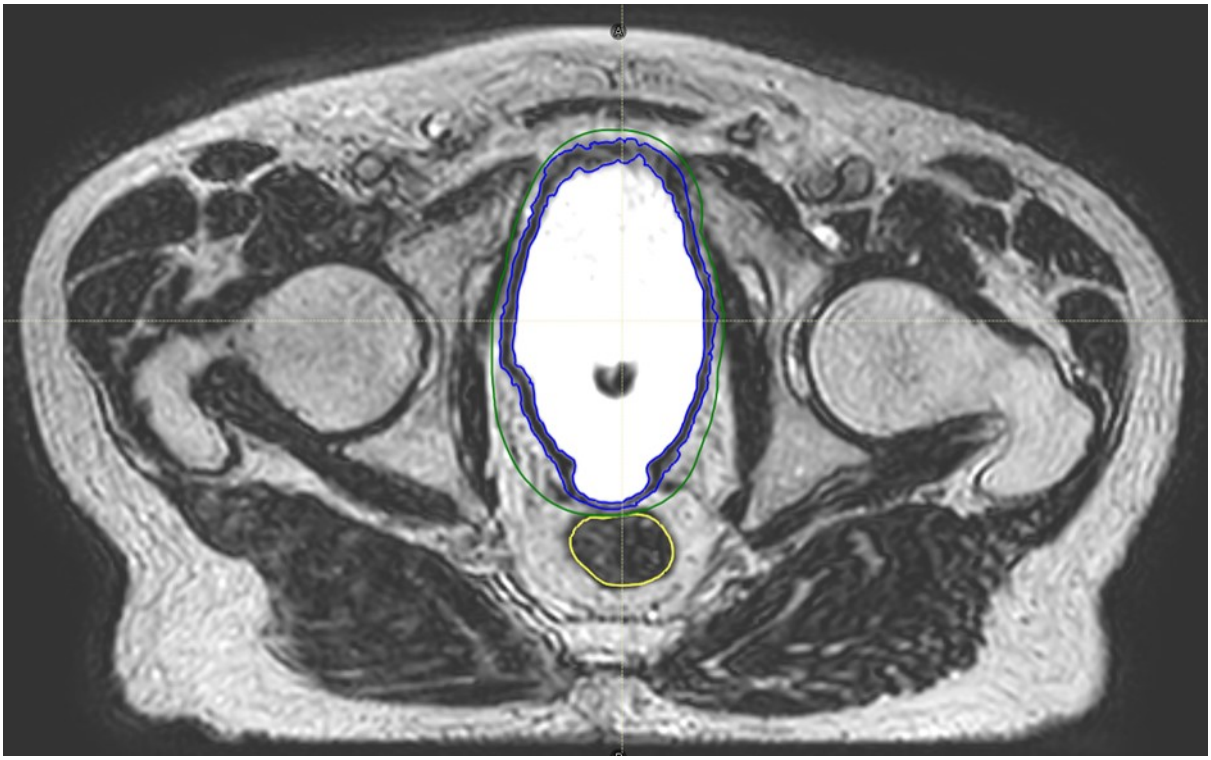

Figure 4.1 Examples of the different rectal and bladder wall contouring steps from manual contour of the entire organ to semi-automated thresholding techniques used for identifying the bladder or rectal wall. Yellow = manual rectal contour, Blue = manual bladder wall contour, Green = Whole bladder contour which thresholding was applied to generate a second bladder wall contour.

The rectum contour was uniformly contracted by 2 and 3 mm to produce a rectal wall contour. For the bladder contours, all cases had a manual contour of the bladder wall and a contour of the whole bladder which then had a thresholding technique applied to it to auto contour the bladder wall (i.e. remove the urine contents and external pelvic fat from the whole bladder contour). This thresholding technique involved calculating the mean signal intensity within the whole bladder contour (wall and bladder contents) before applying the mean value to threshold the bladder wall, i.e., thresholding within the bladder contour only to remove the bladder contents (bright on T2). This was a patient specific and dynamic thresholding approach to account for inter- and intra-patient variation in

the bladder signal. All image post-processing was performed using an in-house medical image processing software, WorldMatch. Binary masks of all segmentations – bladder (manual segmentation and whole bladder contour for thresholding) and rectal wall (2 mm and 3mm) – high, intermediate, and low dose regions were saved.

The daily adapted radiotherapy dose was available for all fractions. The mean dose across all treatment fractions for each patient was calculated to define regions of "high dose" vs "intermediate" vs "low" dose. The following dose thresholds were used: For the EBRT group, the RT dose cut-offs were >50 (High), 30-50 (intermediate) and <30 Gy (low) and for the SABR group, >30 (high), 20-30 (Intermediate) and <20 Gy (low). These EBRT and SABR doses are converted equivalent doses. These dose regions were used to segment out the respective parts of the bladder and rectum contours. Figure 4.2 shows an example of the radiotherapy doses overlaid onto the T2W MRL images with the contours to highlight the different dose thresholds for the conventional fractionation and SABR cases.

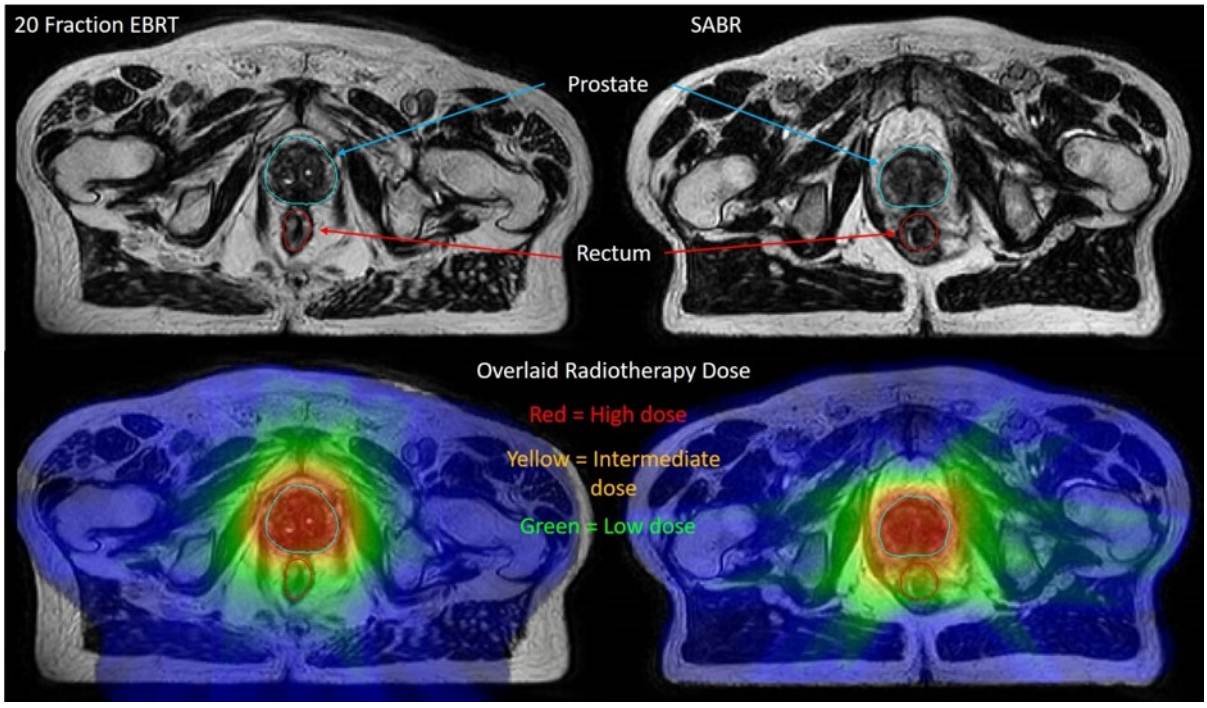

Figure 4.2 Axial T2W MRIs of a conventional 20 fraction EBRT and a SABR case showing the prostate and rectum contours and the overlaid radiotherapy dose showing the high dose (red), intermediate dose (yellow) and low dose (green) regions.

Histogram standardisation of all MR-images was applied using the Nyúl method prior to radiomic feature extraction on the contoured imaging datasets [7,8]. This was applied to each image twice - firstly, each image was standardised to the first available image (to

remove any potential scanner variation across treatment) and then to an arbitrary chosen reference patient's first image (to remove inter-patient variation).

PyRadiomics (v3.0.1) was used to extract RFs for analysis from the rectal wall and bladder wall contours. Only first-order RFs (n=19) were extracted because higher order statistics calculations would be affected by the narrow walls of the bladder/ rectum and may be unstable.A previous systematic review found first-order RFs to be more reproducible than shape metrics and textural features [11]. First-order statistics describe the distribution of the intensities of voxels within the image region calculated through histogram analysis (e.g. mean, minimum, maximum, standard deviation, skewness, or kurtosis) however it does not account for the spatial interactions between them. The description of RFs are available from the publicly available Image Biomarkers Standardization Initiative (IBSI) reference document [12]. Unlike the approach taken in the previous radiomics work (Chapter 2 and 3), in this study the intent was to identify radiomic features that significantly changed post-treatment and then to correlate these features with the presence of RT side-effects.

All MR-images were qualitatively assessed by a radiologist (JZ) for any visually perceptible changes between the time points analysed such as presence of rectal/ bladder wall oedema or subjective increase in wall thickness unrelated to bladder filling or rectal contents.

All MR-images were qualitatively assessed by a radiologist (JZ) for any visually perceptible changes between the time points analysed.

4.3.3 Statistical analysis

For each OAR, RF values at each time point were summarised by presenting mean and standard deviation (SD) across all patients. Pairwise t-test was used to compare RF mean values for timepoints 2, 3, 4 and 5 against timepoint 1 for both bladder wall and rectal contours for SABR and EBRT groups. The median and inter-quartile range radiomic metrics of the bladder wall and rectum were plotted on line graphs for each of the 5 time points and split into toxicity and no toxicity groups. The features which showed greatest separation between toxicity and no toxicity were then delineated on a boxplot with the three different dose thresholds. Volume correlation with RFs was assessed using the Pearson correlation coefficient. A coefficient value between 0.50 to 1 represented strong correlation, between 0.30 to 0.49, moderate correlation and below 0.29, low correlation.

All statistical analyses were performed using R (v4.3.1). All p-values were 2-sided and a p value less than 0.05 was considered statistically significant.

4.4 Results

Demographics and characteristics of the study cohort (n=21) are shown in Table 4.1. The median age was 73 years (range 57-77). Median PSA at diagnosis was 8.7 ng/mL (range 5.3-22.0).

In the EBRT group, 8 out of 10 (80%) experienced acute GU toxicity and 8 (80%) had GI toxicity. Two patients (20%) experienced grade 2 or higher GU toxicity and one experienced grade 2 GI toxicity. The patient who had grade 3 GU toxicity had a hypertrophic median lobe protruding into the urinary bladder which will have been treated and therefore a larger volume of bladder will have been treated. For the SABR group, 9 out of 11 (82%) experienced acute GU toxicity and 4 (36%) had GI toxicity. One SABR patient experienced grade 2 GI toxicity.

Supplementary Material Tables S4.1 to 4.4 show the mean and standard deviation (SD) values for each first order radiomic metric for the bladder wall and rectum at each of the 5 time points (1st, 5th, 10th, 15th, 20th fractions) for the conventional fractionation and SABR cohort.

The greatest number of statistically significant changes were seen in the conventional fractionation rectum with 6 different RFs demonstrating significant changes, as early as the 3rd time point (fraction 10). The other groups (conventional fractionation bladder and SABR rectum and SABR bladder) all showed a statistically significant change in the 10th percentile RF values by the 5th time point. Supplementary Material Table S4.5 summarises the Pearson correlation coefficient values for correlation of volume to the first-order RFs extracted from the bladder and rectum for both the SABR and conventional fractionation groups. 72.5% (29/40) of the RFs showed low correlation and 27.5% (11/40) showed moderate correlation.

Figures 4.3-4.6 are line graphs showing the change from fraction 1 in the median and inter-quartile range values in six radiomic metrics (Mean, 10th percentile, 90th percentile, Skewness, Entropy and Kurtosis) at each of the 5 time points for the bladder wall and rectum in the conventional fractionation and SABR groups, with separate lines for the patients with (blue) and without (red) genitourinary or gastrointestinal toxicity. The bladder wall (both conventional fractionation and SABR) graphs, demonstrate separation in the median values for all six radiomic profiles from time point 2 onwards between the patients who had toxicity vs asymptomatic patients. This separation was not seen in the rectum group between the patients with and without toxicity.

Table 4.1 Patient demographics and clinical characteristics for the 5 fraction SABR group and 20 fraction EBRT group. Abbreviations: RT = radiotherapy, PSA=prostate specific antigen, CTCAE = Common Terminology Criteria for Adverse Events GI=gastrointestinal, GU=genitourinary.

Patient	Age (years)	RT Fraction number	T-stage	Gleason Score	PSA at diagnosis (ng/mL)	Acute GI CTCAE Grade	Acute GU CTCAE Grade
1	74	5	2c	4+3	15	1	1
2	69	5	2c	3+4	6	0	1
3	76	5	2a	3+4	8.4	0	1
4	67	5	1c	3+4	11	0	1
5	73	5	2c	3+4	15	0	1
6	72	5	1c	4+3	10	0	1
7	77	5	2c	3+4	8.7	0	1
8	70	5	2c	3+4	10.5	2	1
9	75	5	2a	4+3	7.5	1	0
10	68	5	2c	3+4	6.3	0	0
11	73	5	2a	3+4	13	1	1
12	75	20	3a	4+3	5.3	0	1
13	73	20	2c	4+3	9.2	1	1
14	76	20	1c	3+4	10	1	1
15	71	20	3a	4+3	6.9	1	1
16	72	20	3a	3+4	10	0	0
17	61	20	2c	4+3	5.5	1	1
18	57	20	2a	3+4	5.3	1	0
19	73	20	2c	4+3	8.7	1	1
20	75	20	2a	3+4	7.4	1	3
21	76	20	2a	3+4	22	2	2

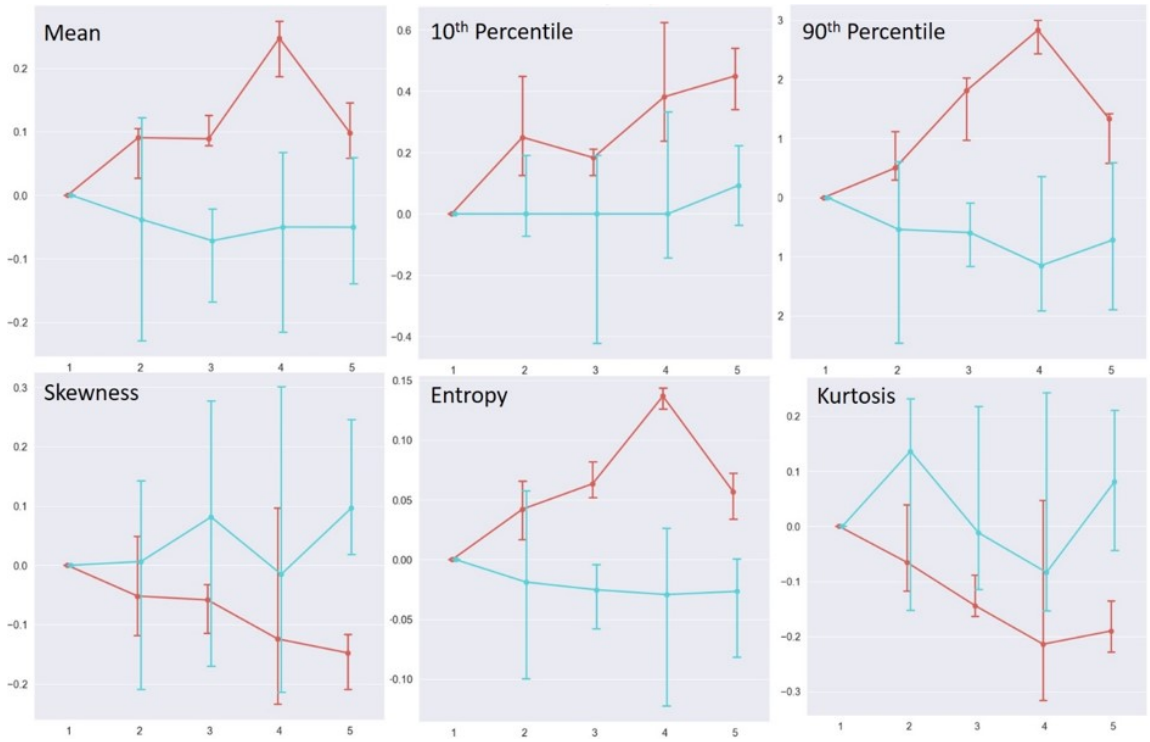

Figure 4.3 Line graphs showing the change from fraction 1 in the median (with inter-quartile range) values of select first order radiomic metrics of the bladder wall (Mean, 10th percentile, 90th percentile, Skewness, Entropy and Kurtosis) for the 20-fraction cohort at each of the 5 time points (1st, 5th, 10th, 15th, 20th fractions) for patients with (blue) and without (red) genitourinary toxicity.

The MR images of a patient who experienced grade 2 acute GI toxicity were evaluated (Figure 4.7). It showed that at the 5th SABR fraction, there was high signal change in the rectal wall which was not seen in the earlier time point. No other patients who experienced toxicity had any qualitative rectal changes on their MRI including the EBRT patient who experienced grade 2 GI toxicity. No qualitative bladder wall changes were seen.

Figures 4.8 and Figure 4.9 illustrate boxplots of median RF intensity values at each of the 5 time points (1st, 5th, 10th, 15th, 20th fractions) for the rectum and bladder (conventional fractionation groups) split into dose threshold groups to visualise changes in the OAR which may be dose-dependent. The boxplots of the rectum contours show at timepoint 4 and 5 there was a trend towards a higher radiomic intensity value in the intermediate dose group vs the low dose group. The SABR group did not have any high dose regions in the bladder or rectum therefore no boxplots were presented.

On the toxicity plots for the conventional fractionation bladder group, at timepoint 4, the greatest separation in RF values between toxicity vs no toxicity groups was observed but

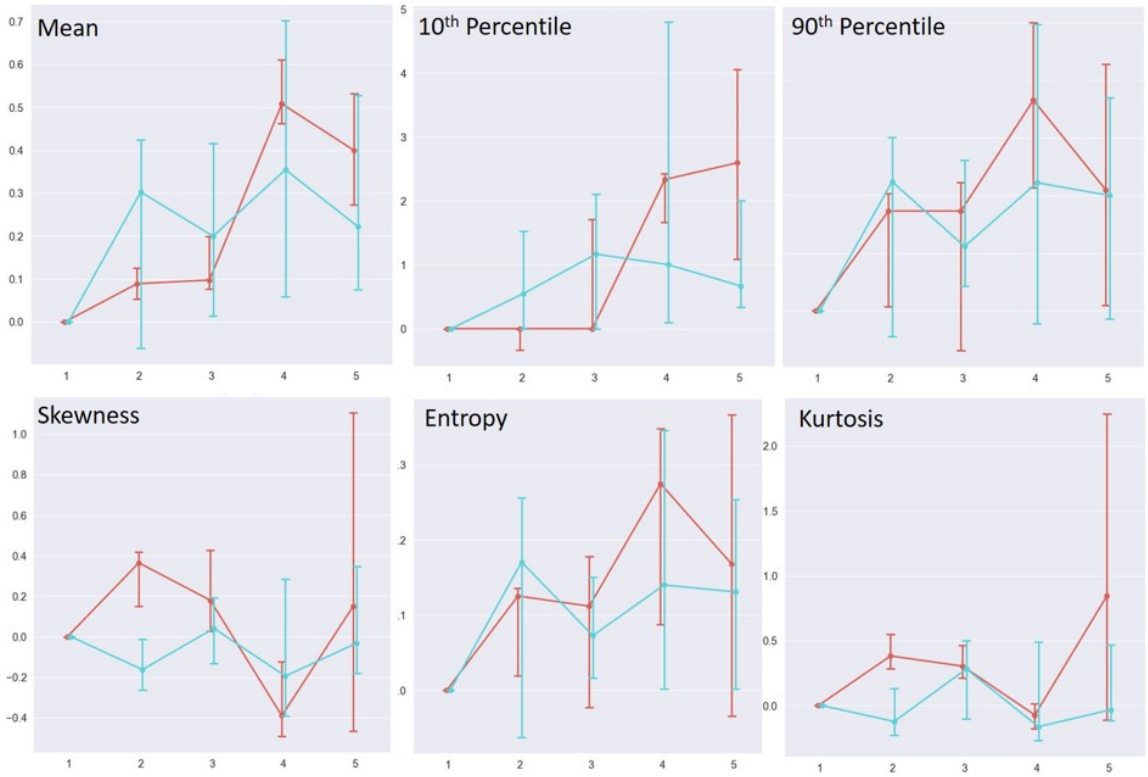

Figure 4.4 Line graph showing the change from fraction 1 in the median (with inter-quartile range) values of the first order radiomic metrics of the rectum (Mean, 10th percentile, 90th percentile, Skewness, Entropy and Kurtosis) for the 20-fraction cohort at each of the 5 time points (1st, 5th, 10th, 15th, 20th fractions) for patients with (blue) and without (red) gastrointestinal toxicity.

no difference in the mean RF intensity values was seen between the 3 dose groups shown in Figure 4.9.

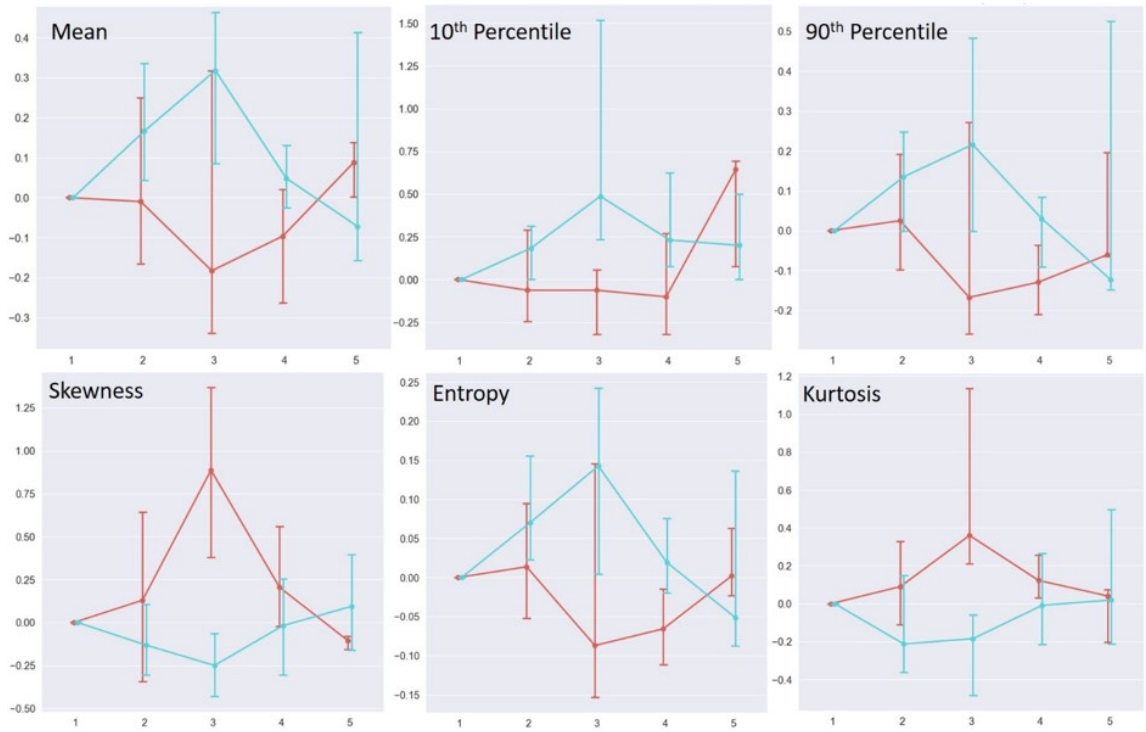

Figure 4.5 Line graph showing the change from fraction 1 in the median (with inter-quartile range) values of the first order radiomic metrics of the bladder wall (Mean, 10th percentile, 90th percentile, Skewness, Entropy and Kurtosis) for the SABR cohort at each of the 5 fractions for patients with (blue) and without (red) genitourinary toxicity.

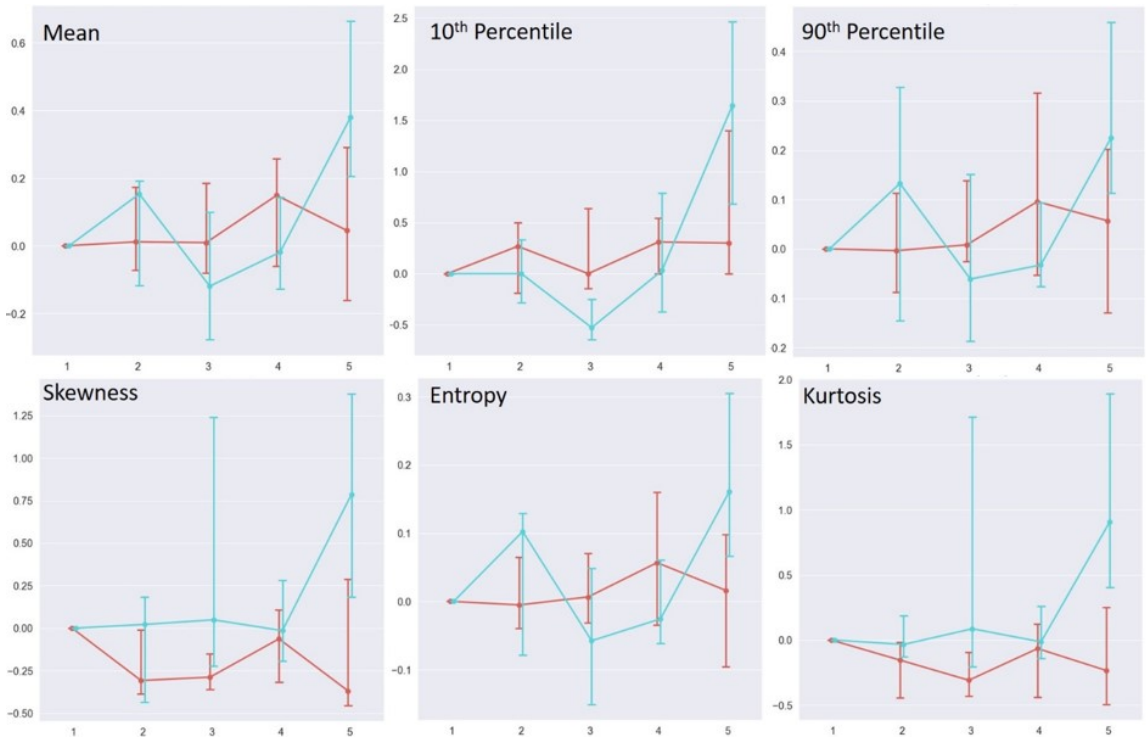

Figure 4.6 Line graph showing the change from fraction 1 in the median (with inter-quartile range) values of the first order radiomic metrics of the rectum (Mean, 10th percentile, 90th percentile, Energy, Entropy and Kurtosis) for the SABR cohort at each of the 5 fractions for patients with (blue) and without (red) gastrointestinal toxicity.

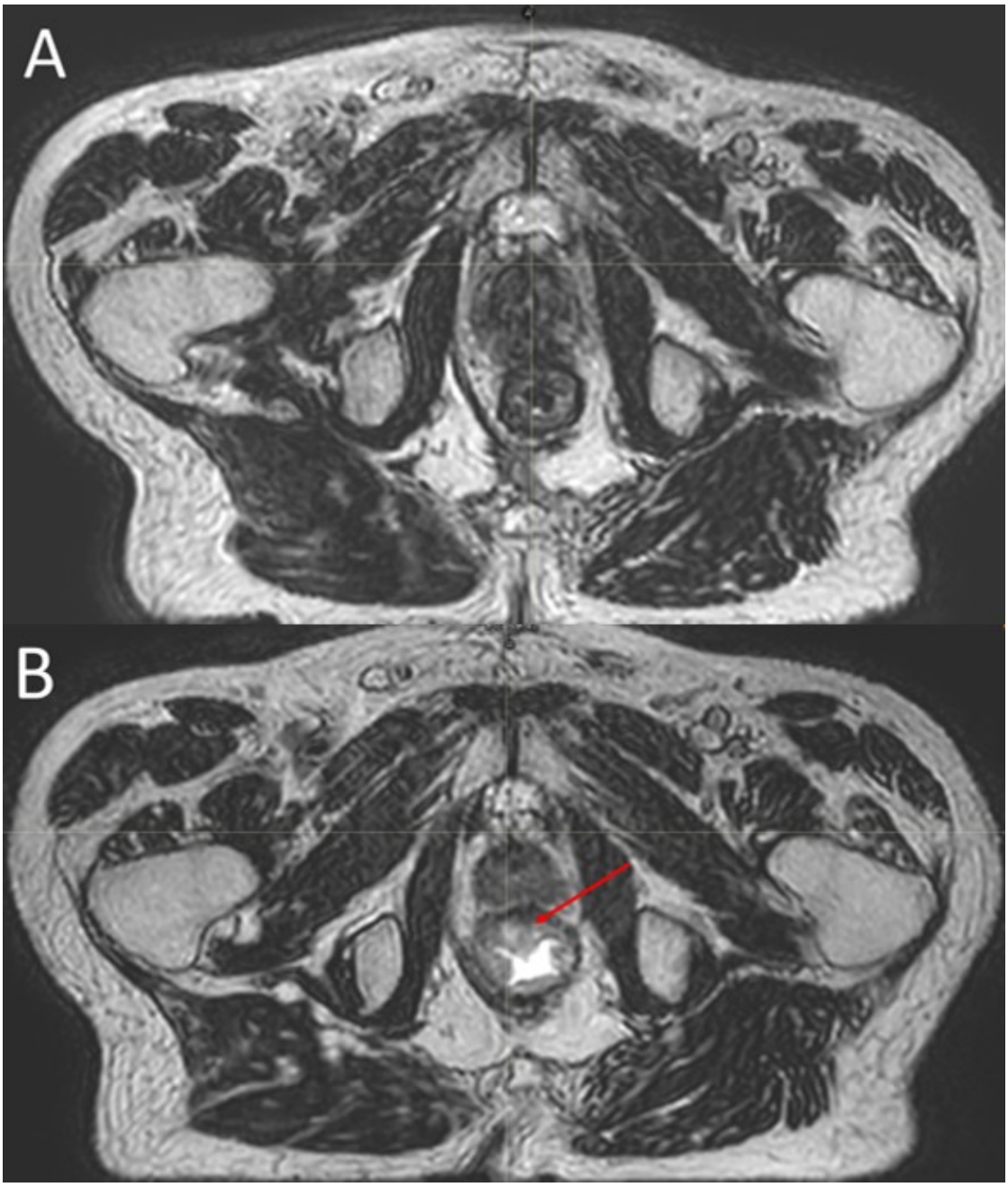

Figure 4.7 Patient 8 treated with SABR who had grade 2 acute GI toxicity (diarrhoea). Baseline T2W MRI (A) and MRI at the 5th fraction (B) 12 days later showing high signal change in the rectal wall (arrow).

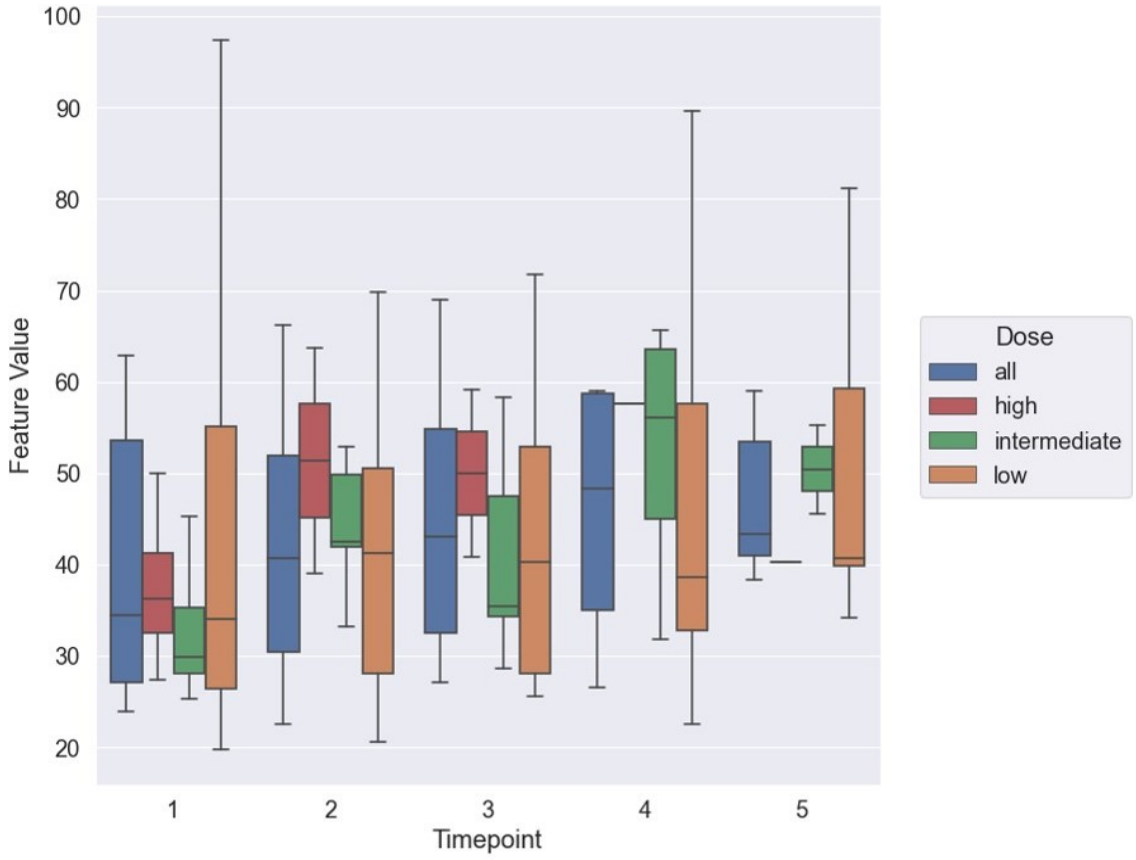

Figure 4.8 Boxplot showing the median and inter-quartile range (25th – 75th centiles) of the mean RF intensity value at each of the 5 time points (1st, 5th, 10th, 15th, 20th fractions) for the rectum contour for different dose levels (All, high, intermediate and low) in the conventional fractionation group.

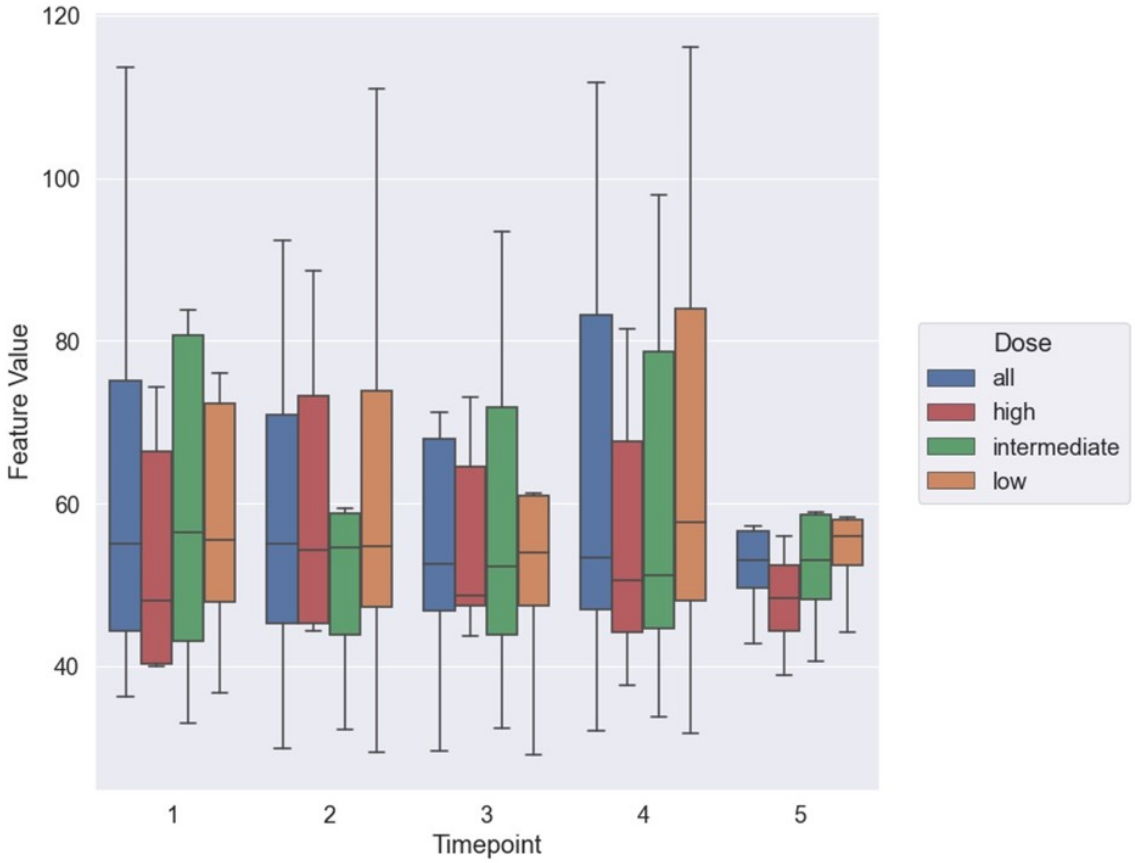

Figure 4.9 Boxplot showing the median and inter-quartile range (25th – 75th centiles) of the mean RF intensity value at each of the 5 time points for the bladder wall for different dose levels (All, high, intermediate and low) in the conventional fractionation group.

4.5 Discussion

This exploratory study demonstrates a feasible methodological approach to extracting longitudinal OAR-derived radiomic data from MR images acquired on a 1.5T MRI-LINAC. The study also discovers potential interesting trends in RF changes within the rectum and bladder wall between radiotherapy fractions that could be influenced by radiation dose/fractionation. In addition, trends in RF changes may be different in patients experiencing radiation toxicity symptoms; however this observation needs to be further evaluated in a larger dataset.

In terms of changes in the first-order RFs, the greatest number of statistically significant changes were seen in the conventional fractionation rectum group with 6 different features demonstrating significant changes, as early as the 3rd time point (fraction 10). The other groups (conventional fractionation bladder and SABR rectum and SABR bladder) all showed a statistically significant change in the 10th percentile RF values by the 5th time point, meaning the bottom 10% of gray level intensity values within the region of interest. The trend towards an increasing intensity value may reflect oedema within the region of interest, either rectum or bladder wall which concurs with visual observations on the relevant timepoint imaging. Evaluating the MR images of a patient who experienced grade 2 acute GI toxicity showed that at the 5th SABR fraction, there was high signal change in the rectal wall which was not seen at earlier time points highlighting the presence of rectal wall oedema. This is likely to contribute to the radiomic changes seen in the rectal wall although these changes are more subtle to visualise in the bladder images given the thin bladder wall.

Regarding the mean RF changes observed at each time point in the rectum for different dose thresholds (conventional fractionation), there was also a general trend towards higher signal intensity values for high and intermediate dose groups compared to the low dose group at all time points which may be secondary to the degree of rectal wall oedema secondary to radiation. With the small patient cohort this was however not statistically evaluated.

To the best of our knowledge, only one other OAR study evaluating RF changes between radiotherapy treatment fractions has been published. This small case series reviewed 4 patients treated on an MRI-LINAC with a minimum of 2 imaging time points. The study found significant variation in mean radiomic values in the bladder wall adjacent to the prostate, termed the prostatic bladder, after the first week of treatment and significant variation in the mean values of the rectal wall adjacent to the prostate by the second week of treatment [10]. Although the evidence remains limited, this provides

a complimentary message that changes in radiomic profiles between treatment fractions might reflect underlying biological changes that could be clinically relevant such as for predicting treatment toxicity. Another study investigated RF changes in the bladder wall in 33 men with prostate cancer treated with EBRT, at baseline and post-treatment timepoints, to identify radiomic changes correlated with GU toxicity [11]. This study reported that in one third of patients experiencing grade 2 or higher GU toxicity, co-occurrence matrix RFs of the bladder wall (which reflect the spatial distribution of the gray levels) showed the greatest change between pre- and post-treatment imaging. Textural features were not included in the current exploratory study which only evaluated first-order intensity values due to the concern with using the bladder wall contours that were very narrow and could cause instability within higher order RFs.

A previous study of 24 men with prostate cancer receiving standard fractionation external beam radiotherapy had MRIs performed at 3 time points (3 days before treatment, halfway during the radiotherapy course and at the end of the treatment) to assess the bladder and rectal wall volumes [12]. The main finding was that the bladder wall volume decreased from pre-treatment to mid-treatment. The rectal wall did not change during treatment. This study however did not assess the bladder and rectal wall signal changes. Future work on the current study cohort could look at using fixed time points (e.g. day 1, day 7 and day 14) which would allow the imaging changes to be more comparable compared to the current time points which do not match up between SABR and EBRT groups i.e. the 20-fraction treatment occurs over 4 weeks and the SABR/ 5-fraction treatment takes only 10-14 days. This may also partly explain the differences observed in the radiomic profiles of the rectum between the two groups. The longer duration may allow any post-radiation inflammatory change to become established, with hyperaemia and oedema affecting the mucosa due to lymphocytic infiltration, a process that can be seen pathologically [13]. Following radiotherapy, it is widely appreciated that prostatic appearances change on T2W MRI [14], with glandular atrophy developing over time and loss of normal zonal anatomy due to the diffuse low T2 signal change in the entire prostate. However, acute MRI changes in OAR are less well understood [15]. With regards to the bladder, radiation cystitis may occur in the acute phase (less than 6 months after radiotherapy), with similar oedematous changes occurring in the bladder wall, or it may occur in the chronic phase (more than 6 months after radiotherapy) where there can be fibrosis, mucosal atrophy, radiation telangiectasia and in severe cases fistula formation [13]. As imaging is not routinely obtained within the acute phase, it is unknown when MRI changes may become visible, and this study adds new information as to the acute physiological changes occurring within the OAR. T2W MRI sequences can demonstrate variable degrees of increased signal in

the bladder wall depending on the severity of the bladder injury [16]. Increased mucosal enhancement may be observed with contrast-enhanced MRI however no functional imaging was available on the MRI-LINAC at the time of this study and would be a future exploratory objective. It is speculated that the RFs that change, particularly the mean and energy features are affected by both changes in vascularity as well as tissue cellularity however comparing this with dynamic contrast enhanced (DCE) imaging or other MR perfusion measurements will help to understand this further.

In terms of overall toxicity, the grade 2 or higher toxicity was low for both conventional fractionation and SABR groups (9-20%). The SABR group had a lower overall GI toxicity rate compared to the conventional group (36% vs 80%), although this is mainly grade 1 only. When compared to the current literature, the PACE-B trial [17], a multi-centre phase 3 randomised control trial (RCT), comparing ultra-hypofractionated radiotherapy/SABR, against conventional hypofractionated radiotherapy found 55% of SABR patients reported at least one grade 2 or higher acute GU toxicity and 41% of conventional fractionation patients reported acute GU toxicity based on CTCAE. For GI toxicity (at least one grade 2 or higher), SABR rate was 35% and conventional fractionation rate was 23%.These rates of grade 2 or higher toxicity are greater than in the current study, which has a small sample size from a single-institution and may not be representative of a larger population, however all patients treated in this study were also treated on an MRI-LINAC which potentially has advantages in terms of improved organ delineation from better soft tissue contrast than CT-based approaches.

The MIRAGE trial, a phase 3 RCT comparing MRI-guided vs CT-guided SABR for prostate cancer reported lower rates of acute GU (24% vs 43%) and GI toxicity (0% vs 11%) favouring the MRI arm. These toxicity improvements were attributed to the significantly reduced planning target volume (PTV) margins which could be achieved due to the ability of MRI guidance to frequently monitor intra-fraction motion and reduced contouring uncertainty. In the CHHiP trial [18], the 60 Gy in 20-fraction treatment arm had a higher rate of acute GI toxicity however this did not translate to higher late GI toxicity, therefore further exploration of this relationship with new hypofractionation schedules is warranted. Identifying patients at the time of treatment who are most at risk of significant late side-effects is beneficial as this could provide an earlier opportunity to intervene and mitigate these symptoms.

The superior soft tissue contrast images available from the MRI-LINAC paired with longitudinal collection of radiomic information offers the opportunity for a more innovative way of measuring tissue response during prostate radiotherapy treatments.

Having a practical method of routinely collecting and analysing this data could help clinical oncologists to make real-time treatment decisions and potential adaptations.

4.5.1 Limitations

Due to the segmentation approach, a significant proportion of both the rectal wall and bladder wall was outside the OAR dose field which means using the median radiomic values for the whole contour may not be optimal given not all the tissue has been exposed to the same radiation dose. Technical limitations included the use of a 2 mm or 3 mm uniform contraction of the rectal contour to define the rectal wall as this may still have included material in the rectum. The bladder thresholding technique may have also still included surrounding peri-vesical fat or bladder contents. Only first-order RFs were included in this initial analysis which focuses on the distribution of voxel intensities however other aspects including second-order features such as shape or texture which may be important features were not analysed.

As this study was exploratory, with a small patient sample, limited conclusions can be drawn about the role of longitudinal radiomics in predicting toxicity. This serves as a hypothesis generating study that can facilitate more extensive data collection with a longer duration of follow-up to allow for late toxicity information to be collected. The relationship between radiation dose and OAR tissue response is not well understood, with no way to account for inter-patient variation in sensitivity to radiation. Future work using dose-surface mapping may help to identify the OAR regions with higher dose that display the greatest radiomic feature changes which are associated with toxicity [19]. A similar radiomics approach could be used on the prostate lesion to predict clinical outcomes such as tumour control. These results serve as preliminary results and further data collection and investigation is required. Full analysis will also account for additional radiomic-based textural features which may give additional information on the tumour microenvironment.

4.6 Conclusions

This exploratory study demonstrates a feasible methodology for collecting longitudinal radiomic profiles from the bladder and rectum during MRI-LINAC radiotherapy treatments. Preliminary results illustrate changes in longitudinal radiomic profiles across 5 time points in both the bladder and rectal wall, differences between patients receiving SABR and conventional fraction radiotherapy and in patients who experienced acute side-effects. Further evaluation in larger datasets are needed to confirm the utility of longitudinal radiomic measurements for toxicity prediction.

4.7 References

1. Cronin KA, Lake AJ, Scott S, Sherman RL, Noone A-M, Howlader N, et al. Annual Report to the Nation on the Status of Cancer, part I: National cancer statistics. Cancer. 2018;124(13):2785–800.

2. Kishan AU, Dang A, Katz AJ, Mantz CA, Collins SP, Aghdam N, et al. Long-term Outcomes of Stereotactic Body Radiotherapy for Low-Risk and Intermediate-Risk Prostate Cancer. JAMA Netw Open. 2019;2(2):e188006.

3. Zelefsky MJ, Levin EJ, Hunt M, Yamada Y, Shippy AM, Jackson A, et al. Incidence of Late Rectal and Urinary Toxicities After Three-Dimensional Conformal Radiotherapy and Intensity-Modulated Radiotherapy for Localized Prostate Cancer. Int J Radiat Oncol. 2008;70(4):1124–9.

4. Pollard JM, Wen Z, Sadagopan R, Wang J, Ibbott GS. The future of image-guided radiotherapy will be MR guided. Br J Radiol. 2017;90(1073):20160667.

5. Desideri I, Loi M, Francolini G, Becherini C, Livi L, Bonomo P. Application of Radiomics for the Prediction of Radiation-Induced Toxicity in the IMRT Era: Current State-of-the-Art. Front Oncol. 2020;10.

6. Kumar V, Gu Y, Basu S, Berglund A, Eschrich SA, Schabath MB, et al. Radiomics: The process and the challenges. Magn Reson Imaging . 2012;30(9):1234–48.

7. Aerts HJWL, Velazquez ER, Leijenaar RTH, Parmar C, Grossmann P, Cavalho S, et al. Decoding tumour phenotype by noninvasive imaging using a quantitative radiomics approach. Nat Commun . 2014;3(5):4006.

8. National Cancer Institute. Common Terminology Criteria for Adverse Events (CTCAE) version 5.0. NIH Publication. 2020.

9. Carré A, Klausner G, Edjlali M, Lerousseau M, Briend-Diop J, Sun R, et al. Standardization of brain MR images across machines and protocols: bridging the gap for MRI-based radiomics. Sci Rep. 2020;10(1):12340.

10. Nyul LG, Udupa JK, Xuan Zhang. New variants of a method of MRI scale standardization. IEEE Trans Med Imaging. 2000;19(2):143–50.

11. Zwanenburg A, Vallières M, Abdalah MA, Aerts HJWL, Andrearczyk V, Apte A, et al. The Image Biomarker Standardization Initiative: Standardized Quantitative Radiomics for High-Throughput Image-based Phenotyping. Radiology. 2020;295(2):328–38.

12. Lorenz JW, Schott D, Rein L, Mostafaei F, Noid G, Lawton C, et al. Serial T2-Weighted Magnetic Resonance Images Acquired on a 1.5 Tesla Magnetic Resonance Linear Accelerator Reveal Radiomic Feature Variation in Organs at Risk: An Exploratory Analysis of Novel Metrics of Tissue Response in Prostate Cancer. Cureus. 2019;

13. Abdollahi H, Tanha K, Mofid B, Razzaghdoust A, Saadipoor A, Khalafi L, et al. MRI Radiomic Analysis of IMRT-Induced Bladder Wall Changes in Prostate Cancer Patients: A Relationship with Radiation Dose and Toxicity. J Med Imaging Radiat Sci . 2019;50:252–260.

14. Tanaka O, Seike K, Taniguchi T, Ono K, Matsuo M. Investigation of the changes in the prostate, bladder, and rectal wall sizes during external beam radiotherapy. Reports Pract Oncol Radiother. 2019;24(2):204–7.

15. Capps GW, Fulcher AS, Szucs RA, Turner MA. Imaging features of radiation-induced changes in the abdomen. RadioGraphics. 1997;17(6):1455–73.

16. McPartlin A, Kershaw L, McWilliam A, Taylor M Ben, Hodgson C, van Herk M, et al. Changes in prostate apparent diffusion coefficient values during radiotherapy after neoadjuvant hormones. Ther Adv Urol. 2018;10(12):359–64.

17. Albano D, Benenati M, Bruno A, Bruno F, Calandri M, Caruso D, et al. Imaging side effects and complications of chemotherapy and radiation therapy: a pictorial review from head to toe. Insights Imaging. 2021;12(1):76.

18. Ganeshan DM, Salem U, Viswanathan C, Balachandran A, Garg N, Silverman P, et al. Complications of oncologic therapy in the abdomen and pelvis: a review. Abdom Imaging. 2013;38(1):1–21.

19. Tree AC, Ostler P, van der Voet H, Chu W, Loblaw A, Ford D, et al. Intensity-modulated radiotherapy versus stereotactic body radiotherapy for prostate cancer (PACE-B): 2-year toxicity results from an open-label, randomised, phase 3, non-inferiority trial. Lancet Oncol. 2022;23(10):1308–20.

20. Dearnaley D, Syndikus I, Mossop H, Khoo V, Birtle A, Bloomfield D, et al. Conventional versus hypofractionated high-dose intensity-modulated radiotherapy for prostate cancer: 5-year outcomes of the randomised, non-inferiority, phase 3 CHHiP trial. Lancet Oncol. 2016;17(8):1047–60.

21. Wortel RC, Witte MG, van der Heide UA, Pos FJ, Lebesque J V., van Herk M, et al. Dose–surface maps identifying local dose–effects for acute gastrointestinal toxicity after radiotherapy for prostate cancer. Radiother Oncol. 2015;117(3):515–20.

4.8 Supplementary Material

Tables S4.1 to S4.4 are showing the mean and standard deviation (SD) values for each first order radiomic metric for the bladder wall and rectum at each of the 5 time points (1st, 5th, 10th, 15th, 20th fractions) for the conventional fractionation EBRT and SABR cohort.

Table S4.5 summarises the Pearson correlation coefficient values for correlation of volume to the first-order RFs extracted from the bladder and rectum for both the SABR and conventional fractionation groups

Table S4.1 Mean and standard deviation (SD) values for each first order radiomic metric for the bladder wall at each of the 5 time points (1st, 5th, 10th, 15th, 20th fractions) for the conventional fractionation cohort. All statistically significant ($p < 0.05$) radiomic feature changes between time points are highlighted in bold and with an asterisk (*).

Radiomic Feature		Timepoint				
	Metric	**1**	**2**	**3**	**4**	**5**
Mean	Mean	71.24	63.29	65.44	70.50	69.36
	SD	44.69	28.39	33.94	42.65	47.80
Variance	Mean	3332.33	2662.87	2922.72	2865.93	2691.24
	SD	2609.55	1731.04	2234.72	2112.00	2072.95
Maximum	Mean	378.50	351.30	354.30	352.80	324.30
	SD	114.80	93.13	77.46	93.61	62.34
10th Percentile	Mean	11.40	10.20	11.00	12.90	**13.00***
	SD	13.78	9.35	10.03	12.55	13.84
90th Percentile	Mean	140.50	131.20	136.10	137.70	134.50
	SD	66.32	56.54	61.57	63.47	62.02
Entropy	Mean	2.65	2.60	2.62	2.63	2.59
	SD	0.56	0.54	0.57	0.58	0.45
Kurtosis	Mean	5.53	5.83	5.22	5.49	5.01
	SD	2.71	3.08	2.46	2.85	1.51
Skewness	Mean	1.25	1.38	1.30	1.22	1.18
	SD	0.86	0.60	0.54	0.78	0.74
Uniformity	Mean	0.21	0.21	0.21	0.21	0.21
	SD	0.08	0.08	0.09	0.08	0.06

Table S4.2 Mean and standard deviation (SD) values for each first order radiomic metric for the rectum at each of the 5 time points (1st, 5th, 10th, 15th, 20th fractions) for the conventional fractionation cohort. All statistically significant ($p < 0.05$) radiomic feature changes between time points are highlighted in bold and with an asterisk (*).

Radiomic Feature		Timepoint				
	Metric	**1**	**2**	**3**	**4**	**5**
Mean	Mean	39.59	41.61	44.96	50.70	**49.77***
	SD	14.90	14.87	15.63	20.51	13.72
Variance	Mean	1984.85	1214.13	1339.22	1257.98	1904.05
	SD	2732.22	802.82	672.06	600.40	1822.15
Maximum	Mean	303.33	304.22	338.33	301.44	331.78
	SD	128.86	83.64	81.59	72.34	87.08
10th Percentile	Mean	3.56	5.00	**7.89***	**11.00***	**9.78***
	SD	1.81	3.20	5.99	9.26	9.35
90th Percentile	Mean	80.44	83.00	86.02	95.22	**93.44***
	SD	29.76	27.34	26.66	31.39	21.16
Entropy	Mean	1.99	2.06	2.14	2.23	**2.26***
	SD	0.48	0.48	0.40	0.44	0.25
Kurtosis	Mean	7.47	7.85	10.95	6.05	8.41
	SD	4.50	4.43	7.28	2.37	4.89
Skewness	Mean	1.66	1.54	1.93	1.21	1.70
	SD	0.85	0.67	1.07	0.53	0.92
Uniformity	Mean	0.33	0.30	0.29	0.26	**0.26***
	SD	0.10	0.11	0.08	0.09	0.05

Table S4.3 Mean and standard deviation (SD) values for each first order radiomic metric for the bladder wall at each fraction for the SABR cohort. All statistically significant ($p < 0.05$) radiomic feature changes between time points are highlighted in bold and with an asterisk (*).

Radiomic Feature		Timepoint				
	Metric	**1**	**2**	**3**	**4**	**5**
Mean	Mean	53.43	53.83	55.31	57.16	64.40
	SD	18.41	13.99	21.40	16.50	23.53
Variance	Mean	2229.47	1981.97	2199.72	2160.64	2633.01
	SD	1877.11	1337.67	1483.32	1354.17	1817.57
Maximum	Mean	335.36	320.17	361.42	355.00	387.45
	SD	111.82	95.81	109.62	130.34	144.58
10th Percentile	Mean	7.64	8.00	7.58	**9.64***	14.45
	SD	4.65	4.92	4.80	5.50	8.64
90th Percentile	Mean	108.49	107.17	113.25	115.36	122.64
	SD	37.14	27.01	43.58	32.66	42.50
Entropy	Mean	2.42	2.43	2.43	2.50	2.59
	SD	0.45	0.34	0.55	0.40	0.50
Kurtosis	Mean	7.88	6.61	7.15	6.32	9.28
	SD	5.36	4.77	3.79	2.41	7.24
Skewness	Mean	1.62	1.40	1.49	1.43	1.75
	SD	0.83	0.82	0.62	0.47	1.01
Uniformity	Mean	0.24	0.23	0.24	0.22	0.21
	SD	0.07	0.06	0.09	0.06	0.08

Table S4.4 Mean and standard deviation (SD) values for each first order radiomic metric for the rectum at each fraction for the SABR cohort. All statistically significant ($p < 0.05$) radiomic feature changes between time points are highlighted in bold and with an asterisk (*).

Radiomic Feature		Timepoint				
	Metric	**1**	**2**	**3**	**4**	**5**
Mean	Mean	74.28	86.47	89.60	79.36	81.71
	SD	23.39	31.64	28.85	31.50	34.35
Variance	Mean	3997.03	6306.66	4987.06	4400.56	5446.26
	SD	2155.20	6011.05	2071.89	3828.26	5318.43
Maximum	Mean	413.27	461.08	455.08	421.36	415.27
	SD	121.44	96.42	82.12	117.75	109.75
10th Percentile	Mean	9.64	11.00	**15.08***	**13.45***	**12.91***
	SD	4.30	5.56	9.14	9.04	7.54
90th Percentile	Mean	154.91	189.25	182.67	165.91	179.64
	SD	40.92	87.33	45.26	67.14	90.58
Entropy	Mean	2.87	3.08	3.11	2.93	2.92
	SD	0.41	0.45	0.43	0.50	0.53
Kurtosis	Mean	5.47	5.50	4.63	4.98	5.42
	SD	3.05	3.33	1.25	1.71	3.73
Skewness	Mean	1.31	1.38	1.18	1.26	1.35
	SD	0.67	0.70	0.47	0.45	0.78
Uniformity	Mean	0.18	0.15	0.15	0.17	0.17
	SD	0.06	0.05	0.05	0.06	0.07

Table S4.5 Radiomic feature with volume correlation analysis using the Pearson correlation coefficient. A coefficient value between 0.50 to 1 represented strong correlation, between 0.30 to 0.49, moderate correlation and below 0.29, low correlation. Abbreviations: SABR = Stereotactic ablative radiotherapy.

Radiomic Feature	Bladder 20 Fraction	Bladder SABR	Rectum 20 Fraction	Rectum SABR
Mean	0.242958	0.142006	0.309641	0.182328
Median	0.251476	0.143499	0.270395	0.231127
10th Percentile	0.316392	0.392947	0.343785	0.271461
90th Percentile	0.214194	0.205098	0.251396	0.164398
Maximum	0.170349	0.192548	0.359846	0.100174
Entropy	0.240824	0.087257	0.263504	0.131732
Kurtosis	0.279224	0.338192	0.341097	0.171977
Skewness	0.261957	0.316048	0.378007	0.256609
Uniformity	0.250408	0.128087	0.213423	0.15595
Variance	0.157033	0.265091	0.354337	0.130763

Chapter 5
Salvage Reirradiation Options for Locally Recurrent Prostate Cancer: A Systematic Review

5.1 Abstract

5.1.1 Background

Reirradiation using brachytherapy (BT) and external beam radiation therapy (EBRT) are salvage strategies with locally radiorecurrent prostate cancer. This systematic review describes the oncologic and toxicity outcomes for salvage BT and EBRT (including Stereotactic Body Radiation Therapy (SBRT)).

5.1.2 Methods

An International Prospective Register of Systematic Reviews (PROSPERO) registered (211875) study was conducted using Preferred Reporting Items for Systematic reviews and Meta-analyses (PRISMA) guidelines. EMBASE and MEDLINE databases were searched from inception to December 2020. For BT, both low dose rate (LDR) and high dose rate (HDR) BT techniques were included. Two authors independently assessed study quality using the 18-item Modified Delphi technique.

5.1.3 Results

A total of 39 eligible studies comprising 1967 patients were included (28 BT and 11 SBRT). In 35 studies (90%), the design was single centre and/or retrospective and no randomised prospective studies were found. Twelve BT studies used LDR only, 11 HDR only, 4 LDR or HDR and 1 pulsed-dose rate only. All EBRT studies used SBRT exclusively, four with Cyberknife alone and 7 using both Cyberknife and conventional linear accelerator treatments.

Median (range) modified Delphi quality score was 15 (6-18). Median (range) follow-up was 47.5 months (13-108) (BT) and 25.4 months (21-44) (SBRT). For the LDR-BT studies, the median (range) 2-year and 5-year bRFS rates were 71% (48-89.5) and 52.5% (20-79). For the HDR-BT studies, the median (range) 2-year and 5-year bRFS rates were 74% (63-89) and 51% (45-65). For the SBRT studies, the median (range) 2-year bRFS for the SBRT group was 54.9% (40-80). Mean (range) acute and late grade 3 GU toxicity rates for LDR-BT/ HDR-BT/ SBRT were 7.4%(0-14)/ 2%(0-14)/ 2.7%(0-8.7) and 13.6%(0-30)/ 7.9%(0-21.3%)/ 2.7%(0-8%). Mean (range) acute and late grade 3 GI toxicity rates for LDR-BT/ HDR-BT/ SBRT were 6.5%(0-19)/ 0%/ 0.5%(0-4%) and

6.4%(0-20)/ 0.1%(0-0.9)/ 0.2%(0-1.5). One third of studies included Patient Reported Outcome Measures (PROMs).

5.1.4 Conclusion

Salvage reirradiation of radiorecurrent prostate cancer using HDR-BT or SBRT provides similar biochemical control and acceptable late toxicity. Salvage LDR-BT is associated with higher late GU/GI toxicity. Challenges exist in comparing BT and SBRT from inconsistencies in reporting with missing data, and prospective randomised trials are needed.

5.2 Introduction

Prostate cancer is the most common male cancer accounting for over 1.2 million new cases per year with >350,000 deaths (3.8% of all male cancer deaths) [1]. Radiation therapy (RT) is a curative treatment option for localised prostate cancer and can be offered to patients from all risk groups [2]. Despite advances in diagnostic imaging, RT delivery techniques and dose-escalated radiation, biochemical progression remains common and occurs in 28-57% of patients with localised disease [3–5]. A recent study of over 16,000 men with prostate cancer who received radiotherapy reported 15-year biochemical recurrence (BCR) rates of 18%, 24% and 36% for low, intermediate and high-risk groups with a median follow-up of 89 months [6].

Multiple salvage options are available for locally recurrent non-metastatic disease including prostatectomy, reirradiation (with brachytherapy (BT) or external beam radiotherapy (EBRT)) and other focal therapies such as high-intensity focused ultrasound (HIFU) and cryotherapy. However, there is limited evidence to support the effectiveness of salvage therapies with concerns regarding the potential for significant toxicity that may impact the long-term quality of life of patients. Due to uncertainty regarding benefits and risks of harm only 15-20% of patients with locally recurrent prostate cancer undergo salvage therapy according to the Cancer of the Prostate Strategic Urologic Research Endeavor (CaPSURE) registry [7].

BT has been preferred for reirradiation as it offers delivery of highly conformal high dose radiation with a steep dose gradient and rapid fall off which minimises dose to surrounding organs at risk [8]. Disadvantages of BT include its invasive nature and the need for a specialist multi-disciplinary team not available in all radiation centres. Previously, EBRT techniques have been associated with high rates of severe late toxicities and poor local control [8]. Stereotactic body radiation therapy (SBRT) involves delivery of a high dose of external beam radiation to a highly conformal target volume with a steep dose gradient in a small number of fractions and is now under investigation for locally recurrent prostate cancer. Advantages of this approach are that it is non-invasive and has the potential to be delivered in more radiation centres than BT [10].

This systematic review collates the most up-to-date evidence for reirradiation of locally recurrent prostate cancer. Two previous systematic reviews which compared all salvage therapies found higher biochemical control rates for BT and EBRT compared to surgical and other non-surgical local therapies (high intensity focused ultrasound (HIFU) and cryotherapy) along with potentially lower genitourinary (GU) toxicity [11,12]. The justification for this systematic review is that the identification of the reirradiation modality that offers optimum prostate cancer control and minimal toxicity is important

to enable patients to make informed decisions and potentially improve outcomes in patients with radiorecurrent prostate cancer. In addition, the evidence base for salvage BT and SBRT continues to expand with a number of new publications in the past 1-2 years.

5.3 Materials and Methods

An International Prospective Register of Systematic Reviews registered (211875) systematic review was conducted.

5.3.1 Study Design

The study followed the Preferred Reporting Items for Systematic Reviews and Meta-analysis (PRISMA) guidelines [13].

Studies were identified by searching the Cochrane library, EMBASE and MEDLINE electronic databases from inception to 14th December 2020.

The search strategy is documented in Supplementary Material and the combination of subject headings and keywords included: 'recurrent or radiorecurrent prostate cancer', 'reirradiation' or 're-irradiation', 'salvage radiotherapy', 'brachytherapy', 'external beam radiotherapy', 'stereotactic body radiation therapy', 'stereotactic ablative radiotherapy', 'radiosurgery'.

5.3.2 Data Extraction

Two authors (JZ and FS) independently reviewed the abstracts and assessed the quality of each study using an 18-item Modified Delphi technique, which has been previously validated for case series [14]. Discordance between reviewers were resolved following arbitration by a third reviewer (AH).

5.3.3 Data Selection

Eligible studies included patients treated with primary EBRT, BT or combination EBRT/BT and salvage therapy for local recurrence with either EBRT or BT. For BT techniques, studies of high-dose rate brachytherapy (HDR-BT), low-dose rate brachytherapy (LDR-BT) and pulse-dose rate brachytherapy (PDR-BT) were included.

Studies that predominantly included patients who had primary treatment with radical prostatectomy, cryotherapy or HIFU were not included in this review as the focus was to collate and present the most up-to-date evidence concerning reirradiation specifically.

Studies with fewer than 20 patients were excluded, along with editorials, letters, abstracts, case reports, conference proceedings and studies not written in English. Where studies had evaluated the same patient cohort as another publication, only the most recent publication was used for analysis unless distinct treatment outcomes or toxicity were described.

5.3.4 Extracted variables

Extracted data included the first author and country in which the study took place, study type (prospective or retrospective), single/ multi-centre status, number of patients, primary disease characteristics, primary treatment modalities, interval between original treatment and salvage treatment, patient age at salvage, pre-salvage prostate specific antigen (PSA), diagnostic imaging prior to salvage treatment, histological confirmation of local recurrence and percentage of biopsy-proven recurrences in study cohort, whole-gland salvage treatment versus focal salvage treatment, type of salvage radiotherapy (HDR-BT, LDR-BT, PDR-BT or EBRT), salvage dose fractionation schedule, percent of patients who received androgen deprivation therapy (ADT) with their salvage treatment, duration of follow up post salvage therapy, treatment outcomes (biochemical control (BC), biochemical recurrence free survival (bRFS), metastasis free survival (MFS), relapse free survival (RFS), cancer specific survival (CSS), overall survival (OS)) and grade 1-4 GU and gastrointestinal (GI) toxicity as classified by the Common Terminology Criteria for Adverse Events (CTCAE) [14] or Radiation Therapy Oncology Group (RTOG) score [16]. Use of any patient recorded outcome measure (PROM) in the study was also collated including the type of tool used. Median (range) values calculated for all collected variables except toxicity rates where mean (range) used to account for the studies which report no toxicity.

5.4 Results

From the initial identification of 2744 articles, a total of 39 studies were included in the final analysis. A PRISMA flowchart of the systematic review is presented in Figure 5.1. The last electronic literature search was performed on 14th December 2020.

The quality assessment tool (modified Delphi 18-item checklist) scores are shown in Table 5.1. The median modified Delphi score was 15 out of 18 (83.3%) (range 6-18).

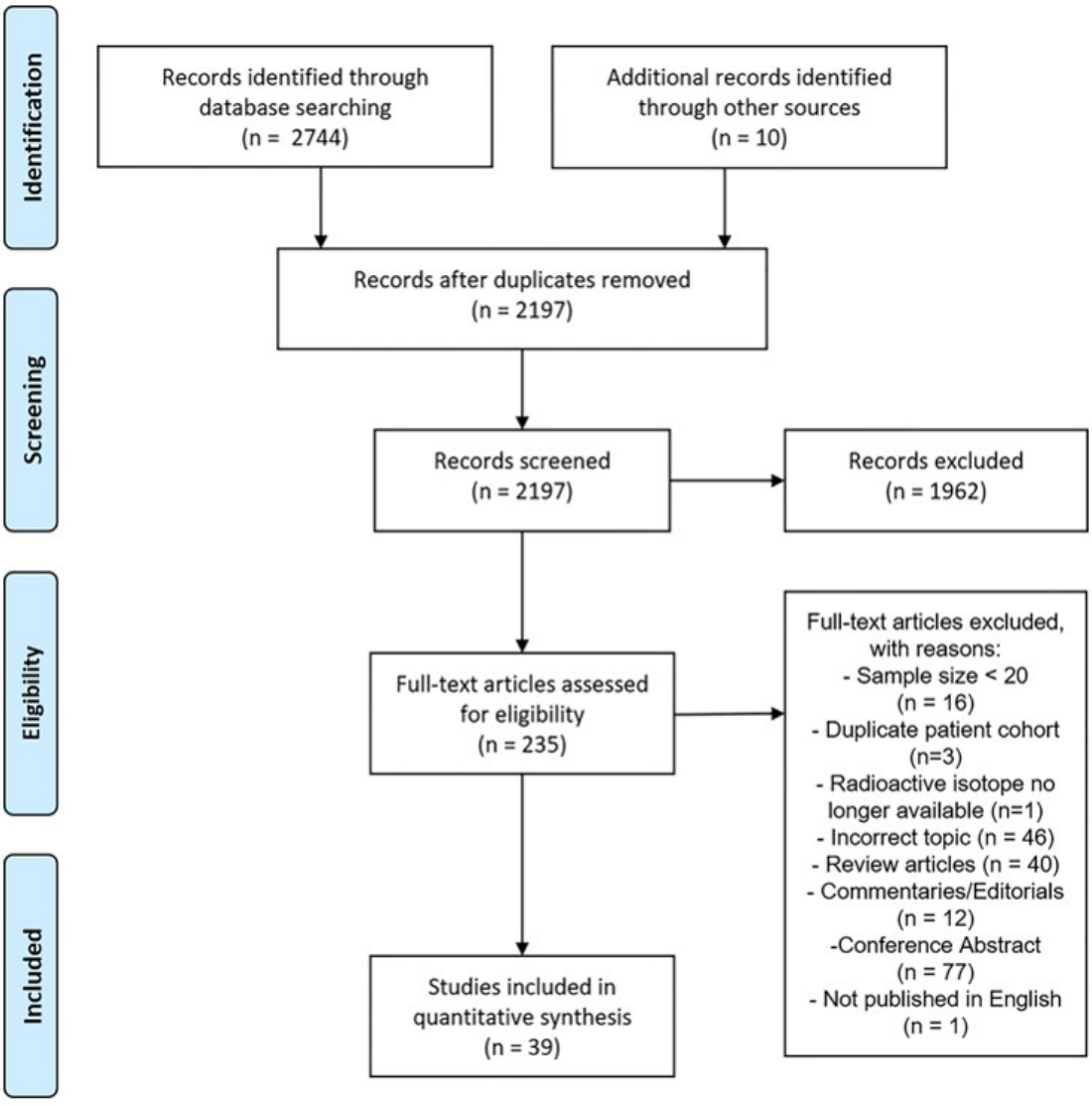

Figure 5.1 PRISMA flow chart of literature search..

Table 5.1 Summary findings from the Modified Delphi checklist for quality assessment applied to all included studies (n=39)

Criterion	Studies, n (%)	
	Yes	No
Study Objective		
1. Is the hypothesis/aim/objective of the study clearly stated in the abstract, introduction, or methods section?	38 (97.4)	1 (2.6)
Study population		
2. Are the characteristics of the participants included in the study described?	39 (100)	0 (0)
3. Were the cases collected in more than 1 Centre?	8 (20.5)	31 (79.5)
4. Are the eligibility criteria (inclusion and exclusion criteria) to entry the study explicit and appropriate?	33 (84.6)	6 (15.4)
5. Were the participants recruited consecutively?	26 (66.7)	13 (33.3)
6. Did participants enter the study at a similar point in the disease?	35 (89.7)	4 (10.3)
Intervention and co-intervention		
7. Was the intervention clearly described in the study?	37 (94.9)	2 (5.1)
8. Were additional interventions (co-interventions) clearly reported in the study?	35 (89.7)	4 (10.3)
Outcome measures		
9. Are the outcome measures clearly defined in the introduction or methods section?	38 (97.4)	1 (2.6)
10. Were relevant outcomes appropriately measured with objective/or subjective methods?	38 (97.4)	1 (2.6)
11. Were outcomes measured before and after intervention?	35 (89.7)	4 (10.3)
Statistical analysis		
12. Were the statistical tests used to assess the relevant outcomes appropriate?	38 (97.4)	1 (2.6)
Results and conclusions		
13. Was the length of follow-up reported?	38 (97.4)	1 (2.6)
14. Was the loss of follow-up reported?	23 (59.0)	16 (41.0)
15. Does the study provide estimates of the random variability in the data analysis of relevant outcomes?	15 (38.5)	24 (61.5)
16. Are adverse events reported?	38 (97.4)	1 (2.6)
17. Are the conclusions of the study supported by results?	38 (97.4)	1 (2.6)
Competing interest and source of support		
18. Are both competing interest and source of support for the study reported?	23 (59.0)	16 (41.0)
Median Modified Delphi score = 15 out of 18 (83.3%) (range 6-18)		

5.4.1 Treatment Details

A summary of patient, disease and treatment characteristics at the time of primary treatment and salvage treatments for BT and EBRT studies is shown in Table 5.2, Table 5.3, Table 5.4 and Table 5.5 respectively. Salvage treatment characteristics for BT and EBRT are shown in Table 5.6 (Part A)/ Table 5.7 (Part B) and Table 5.8 respectively.

Twenty-eight BT studies were included with a total of 1484 patients treated: 22 were retrospective and 6 were prospective. Four were multi-centre and 24 were single centre. Twelve BT studies used LDR only [16,17,26,27,18–25], 11 used HDR only [28,29,38,39,30–37], 4 used LDR or HDR [40–43] and 1 used PDR only [44]. Twenty four studies used whole gland salvage treatments and 4 studies used focal salvage treatments [16,32,34,36]. The number of HDR-BT fractions ranged from 1 to 4 (median of 3 fractions) and the inter-fraction time interval ranged from 4 hours to 3 weeks. The median overall salvage treatment time was 21 days (range 1 to 63 days).

All EBRT studies (n=11) used an SBRT technique with a total of 483 patients treated. Of these studies [9,45,54,46–53], 9 were retrospective and 2 were prospective [46,54]. Two were multi-centre and 9 were single centre. Four studies used Cyberknife delivery only and 7 studies included patients treated with Cyberknife or conventional linear accelerator SBRT techniques. Four studies used whole gland salvage only, 4 focal salvage only, 2 included both whole gland and focal treatments and one did not specify. Of the 11 studies, 8 were published between 2019 and 2020. The median total radiation dose prescribed was 34 Gy (range 34-38 Gy), over a median of 5 fractions (range 3-7). The median overall treatment time was 6 days (range 3-14 days).

The median number (range) of included patients for individual BT and SBRT studies was 44 (21-115) and 42 (23-100) respectively. The median age (range) at salvage treatment was 70 years (59-76) for BT studies and 74 years (64-78) for SBRT studies. The median PSA at primary treatment for the BT and SBRT studies were 10.9 ng/mL (range 7.4-26.4) and 10.3 ng/mL (range 8.7-13.0) respectively. The median PSA at salvage treatment for the BT and SBRT studies were 4.7 ng/mL (range 2.8-11.4) and 3.1 ng/mL (range 2.5-4.1) respectively. The median time from primary treatment to salvage therapy for the BT and SBRT studies were 67 months (range 30-101 months) and 86.5 months (range 60-100 months) respectively.

Table 5.2 Primary disease and treatment characteristics for brachytherapy studies. Key: BT=brachytherapy, HDR=high dose rate, LDR=low dose rate, R=retrospective, P=prospective, Pts=patients, n=number, PSA=prostate specific antigen, NR=not recorded, GS=Gleason score, EBRT=external beam radiotherapy, PBT=proton beam treatment, RP=radical prostatectomy. For PSA, ISUP and GS, the median scores are presented. *Yamada (USA) study cohort included in further publication Kollmeier (USA) however specific treatment characteristics and toxicity were not covered in later paper.)

First author (country)	Year	Salvage BT type	Design	Pts (*n*)	PSA (ng/mL) (range)	ISUP	GS	% GS (≤7)	% GS (≥8)	T stage	% T stage (≤T2a)	% T stage (≥T2b)	Risk Class	Primary treatment
B Lee (USA)	2007	HDR	R	21	NR	1	6	100	0	T2c	48	52	NR	EBRT, BT, protonTx
Lyczek (Poland)	2009	HDR	R	115	13 (2.34-64.5)	NR	NR	NR	NR	T2	58	42	NR	RP+EBRT, EBRT, BT, EBRT+BT
Chen (USA)	2013	HDR	R	52	9.3 (1.2-58)	1	6	87	13	T2	NR	NR	NR	EBRT, BT, EBRT+BT, PBT
Kukielka (Poland)	2014	HDR	R	25	16.3 (6.37-64)	1	<6	88	4	T2c	48	52	Intermediate	EBRT
*Yamada (USA)	2014	HDR	P	42	NR	NR	NR	NR	NR	NR	NR	NR	NR	EBRT
Jiang (Germany)	2016	HDR	R	29	NR	NR	NR	NR	NR	NR	NR	NR	High	EBRT, EBRT+BT
Lacy (USA)	2016	HDR	R	21	NR	NR	NR	NR	NR	NR	NR	NR	Low	BT, EBRT+BT
Wojcieszek (Poland)	2016	HDR	R	83	13.7	1	6	80	4	T2	NR	NR	Intermediate	EBRT, EBRT+BT
Lopez (Spain)	2019	HDR	R	75	8.9 (3.5-42.1)	1	6	75	20	NR	NR	NR	Intermediate	EBRT, BT
	2019	LDR	R	44	14.2 (3.2-167)	1	6	87	11	NR	NR	NR	Intermediate	EBRT
Chitmanee (UK)	2020	HDR	P	50	<10 (46%)	2/3	7	90	10	T2	72	28	Intermediate	EBRT, BT
Slevin (UK)	2020	HDR	R	43	10.5 (3.4-178)	1	6	90	10	T2	73%	27%	Intermediate	EBRT, BT
van Son (Netherlands)	2020	HDR	P	50	13 (2.1-140)	1	6	82	12	T2a	72	28	NR	EBRT, BT
Kollmeier (USA)	2017	HDR/LDR	R	98	≤10 (74%)	2	7	92	8	T2b	68	32	NR	EBRT, BT, EBRT+BT
Baumann (USA)	2017	HDR/LDR	R	33	8.4 (3.8-68.7)	NR	7	79	21	T2	55	45	High	EBRT
Henriquez (Spain)	2014	HDR/LDR	R	56	10.7 (4-121)	1	6	95	5	T2	87	13	Intermediate	EBRT, BT
Grado (USA)	1999	LDR	R	49	26.4 (2.3-95.8)	NR	7 to 10	NR	NR	T2b	NR	NR	NR	EBRT, BT, RP
Koutrouvelis (USA)	2003	LDR	R	31	<10 (32%)	NR	6	77	23	T2b/ T3a	32%	68%	NR	BT
Nguyen (USA)	2007	LDR	P	25	7.4 (4.2-18.4)	1	6	100	0	T1c	NR	NR	NR	EBRT, EBRT+BT
HK Lee (USA)	2008	LDR	R	21	NR	NR	NR	NR	NR	NR	NR	NR	NR	EBRT
Aaronson (USA)	2009	LDR	R	24	9.9 (3.2-69)	3	7	71	12	T1c	NR	NR	NR	EBRT
Burri (USA)	2010	LDR	R	37	10.9 (4.4-81)	NR	6	73	11	NR	19	16	Intermediate	EBRT, BT
Moman (Netherlands)	2010	LDR	R	31	24.3	NR	7	84	6.5	T2	NR	NR	NR	EBRT, BT
Peters (Netherlands)	2014	LDR	R	20	12.9 (5.4-51)	1	6	90	10	T3	NR	NR	High	EBRT, BT
Vargas (USA)	2014	LDR	R	69	<10 (62%)	1	6	80.3	19.7	T2	NR	NR	NR	EBRT
Peters (Netherlands)	2016	LDR	R	62	16.6 (2.6-66.9)	2/3	7	95	5	T2	66	34	NR	EBRT, BT
Crook (Canada)	2019	LDR	P	92	NR	NR	7	100	0	NR	NR	NR	low/ intermediate	EBRT
Smith (USA)	2020	LDR	P	108	9.15 (1.7-116)	1	6	54	10	T2	67	5	Intermediate	EBRT
Schonle (Germany)	2020	PDR	R	82	9 (0.9-170)	2/3	7	74	11	NR	NR	NR	Intermediate	EBRT, BT, RP

Table 5.3 Pre-salvage therapy disease and treatment characteristics for brachytherapy studies. Key: BT=brachytherapy, HDR=high dose rate, LDR=low dose rate, PSA=prostate specific antigen, NR=not recorded, GS=Gleason score, TRS = median time from primary treatment to salvage therapy, mo=months, BCR=biochemical recurrence, ASTRO=American Society for Radiation Oncology, MRI = magnetic resonance imaging, NS=bone scan, CT=computed tomography, US=ultrasound, C-PET=Choline positron emission tomography, PSMA = prostate specific membrane antigen. For TRS, age, PSA, ISUP and GS, the median scores are presented. *Yamada (USA) study cohort included in further publication Kollmeier (USA) however specific treatment characteristics and toxicity were not covered in later paper.

First author (country)	Year	Salvage BT type	TRS (*mo*)(range)	BCR definition	Age (years)(range)	PSA (ng/mL)(range)	ISUP	GS	% GS (≤7)	% GS (≥8)	Imaging for relapse	Biopsy
B Lee (USA)	2007	HDR	63.6 (24-125)	NR	68 (58-81)	5.9 (1.4-9.5)	NR	NR	52	38	MRI	Yes (100%)
Lyczek (Poland)	2009	HDR	49.5	NR	70 (52-82)	NR	1	6	71	12	NR	No
Chen (USA)	2013	HDR	51.6 (10.8-135.6	Phoenix	67.5 (53.9-81.4)	5 (0.4-26.3)	NR	8	48	52	CT	Yes (100%)
Kukielka (Poland)	2014	HDR	NR	Phoenix	71 (62-83)	2.8 (1.04-25.3)	2/3	7	60	20	MRI	Yes (100%)
*Yamada (USA)	2014	HDR	73	Phoenix	72	3.54	NR	7	67	33	MRI, BS	Yes (100%)
Jiang (Germany)	2016	HDR	NR	Phoenix	75.5 (±5.8)	4.05 (2.1-18.6)	NR	NR	NR	NR	C-PET	No
Lacy (USA)	2016	HDR	45 (4-287)	Phoenix	59 (44-72)	6.3 (1-19.1)	NR	NR	NR	NR	CT, BS	Yes (14%)
Wojcieszek (Poland)	2016	HDR	67 (22-124)	NR	70 (57-81)	3.1 (0.1-19.9)	NR	7	46	7	MRI, BS	Yes (100%)
Lopez (Spain)	2019	HDR	> 30	ASTRO/ Phoenix	62.1 (4-75)	4.1 (1.5-16.7)	NR	8 to 10	48	44	CT, MRI, C-PET	Yes (100%)
	2019	LDR	> 30	ASTRO/ Phoenix	60.4 (47-71)	3.6 (1.02-11)	2/3	7	59	9	CT, MRI, C-PET	Yes (100%)
Chitmanee (UK)	2020	HDR	< 5 years	Phoenix	70 (57-82)	<10 (94%)	2/3	7	54	36	MRI, C-PET	Yes (100%)
Slevin (UK)	2020	HDR	70	Phoenix	70 (62-81)	3.1 (1.1-7.5)	2	7	70	30	MRI, PET	Yes (100%)
van Son (Netherlands)	2020	HDR	101 (25-228)	Phoenix	71 (59-83)	5 (0.9-39)	2	7	74	20	PSMA-PET, MRI	Yes (100%)
Kollmeier (USA)	2017	HDR/LDR	72 (12-172)	Phoenix	73.5 (56-88)	3.7 (0-59)	2	7	61	39	CT, MRI, BS	Yes (100%)
Baumann (USA)	2017	HDR/LDR	56.1 (18-118)	Phoenix	75 (57-85)	5 (2-26)	NR	7	55	36	CT, MRI, BS	Yes (100%)
Henriquez (Spain)	2014	HDR/LDR	NR	Phoenix	65 (60-80)	3.7 (1.1-30)	2/3	7	41	14	MRI	Yes (100%)
Grado (USA)	1999	LDR	NR	2 PSA rises>nadir	73.3 (52.9-86.9)	5.6 (1.5-79.1)	NR	NR	NR	NR	CT	Yes (100%)
Koutrouvelis (USA)	2003	LDR	30	nPSA+1.5	65 (51-79)	NR	NR	6	NR	NR	NR	Yes (100%)
Nguyen (USA)	2007	LDR	62.4 (30-153)	ASTRO	65	5.5 (1.4-11.6)	NR	NR	NR	NR	MRI	Yes (100%)
HK Lee (USA)	2008	LDR	85 (±30.1)	Phoenix	72 (±4.8)	3.8	NR	7	NR	NR	NR	Yes (100%)
Aaronson (USA)	2009	LDR	49 (26-109)	Phoenix	66 (54-88)	3.41 (0.3-10)	NR	NR	NR	NR	MRI	Yes (100%)
Burri (USA)	2010	LDR	62 (26-171)	Phoenix	70.2 (51-79)	5.6 (1.7-35)	NR	8	65	32	CT	Yes (100%)
Moman (Netherlands)	2010	LDR	60	ASTRO/ Phoenix	69.3	11.4	NR	8	70.1	12.9	NR	Yes (100%)
Peters (Netherlands)	2014	LDR	79 (42-144)	Phoenix	69 (59-78)	4.7 (0.3-14)	NR	7	65	35	MRI, CT/BS, C-PET	Yes (100%)
Vargas (USA)	2014	LDR	90	Phoenix	72.5 (55-88)	NR	NR	7	73.2	26.8	CT, BS	Yes (100%)
Peters (Netherlands)	2016	LDR	67 (±32)	Phoenix	69 (±5.3)	8.6 (0.1-92.6)	NR	NR	NR	NR	MRI, PET, BS	Yes (100%)
Crook (Canada)	2019	LDR	85 (39-199)	Phoenix	70 (55-82)	4.1 (0.4-9.7)	NR	NR	NR	NR	MRI	Yes (100%)
Smith (USA)	2020	LDR	70 (10-235)	Phoenix	70 (51-87)	5.3 (0.1-38.4)	3	7	65	32	MRI	Yes (100%)
Schonle (Germany)	2020	PDR	87.5 (19-255)	Phoenix	69.9 (51-83)	5.07 (0.28-51)	2/3	7	59	24	MRI	NR

Table 5.4 Primary disease and treatment characteristics for EBRT studies. Key: BT=brachytherapy, HDR=high dose rate, LDR=low dose rate, R=retrospective, P=prospective, Pts=patients, n=number, PSA=prostate specific antigen, NR=not recorded, GS=Gleason score, EBRT=external beam radiotherapy, PBT=proton beam treatment, RP=radical prostatectomy. For PSA, ISUP and GS, the median scores are presented.

First author/ country	Year	Design	Pts (*n*)	PSA (range) (ng/mL)	ISUP	GS	% GS (≤7)	% GS (≥8)	T stage	% T stage (≤T2a)	% T stage (≥T2b)	Risk Class	Primary treatment
Leroy (France)	2017	R	23	10.38 (2.34-57)	2/3	7	82.5	4.3	T2	65.2	30.4	NR	EBRT, BT
Fuller (USA)	2020	P	50	NR	NR	NR	NR	NR	NR	NR	NR	NR	EBRT, BT, RP
Jereczek-Fossa (Italy)	2018	R	64	11.4 (0.5-228.5)	2/3	7	NR	NR	NR	NR	NR	NR	EBRT, BT
Loi (Italy)	2018	R	50	10 (3.1-160)	NR	NR	70	30	NR	NR	NR	High	EBRT, RP+EBRT
D'Agostino (Italy)	2019	R	23	NR	NR	NR	NR	NR	NR	NR	NR	Intermediate	RP+EBRT, EBRT
Pasquier (France)	2019	R	100	10.2 (2.3-120)	1	6	93	7	NR	NR	NR	Intermediate	EBRT
Scher (France)	2019	R	42	10.1 (3-120)	2/3	7	82	18	NR	NR	NR	Intermediate	EBRT, RP+EBRT
Cuccia (Italy)	2020	R	24	NR	3	7	79	21	NR	NR	NR	Intermediate	EBRT, BT
Matrone (Italy)	2020	R	44	8.7 (2.6-46)	2/3	7a	NR	NR	NR	NR	NR	High	EBRT
Caroli (Italy)	2020	R	38	NR	2	7	100	0	T3	42.1	57.9	NR	EBRT, RP+EBRT
Bergamin (Australia)	2020	P	25	13 (4.1-97)	2	7	72	28	T2a	80	20	Intermediate	EBRT, BT

Table 5.5 Pre-salvage therapy disease and treatment characteristics for EBRT studies. Key: BT=brachytherapy, HDR=high dose rate, LDR=low dose rate, PSA=prostate specific antigen, NR=not recorded, GS=Gleason score, TRS = median time from primary treatment to salvage therapy, mo=months, BCR=biochemical recurrence, ASTRO=American Society for Radiation Oncology, MRI = magnetic resonance imaging, NS=bone scan, CT=computed tomography, US=ultrasound, C-PET=Choline positron emission tomography, PSMA = prostate specific membrane antigen. For TRS, age, PSA, ISUP and GS, the median scores are presented.

First author/ country	Year	Design	TRS (*mo*)(range)	BCR definition	Age (years)(range)	PSA (ng/mL)(range)	ISUP	GS	% GS (≤7)	% GS (≥8)	Imaging for relapse	Biopsy
Leroy (France)	2017	R	65 (28-150)	Phoenix	70 (58-82)	2.5 (0-11.7)	NR	NR	NR	NR	C-PET, MRI	Yes (83%)
Fuller (USA)	2020	P	98 (31-241)	Phoenix	74 (50-89)	3.97 (0.1-48.2)	3	7	64	36	MRI	Yes (100%)
Jereczek-Fossa (Italy)	2018	R	99.7 (23-208)	Phoenix	73.2 (52.6-81.7)	3.89 (0.17-51.8)	2/3	7	NR	NR	C-PET, MRI, CT	Yes (44%)
Loi (Italy)	2018	R	76 (9-205)	Phoenix	76 (62-86)	2.6 (1-30)	NR	NR	NR	NR	C-PET, MRI	NR
D'Agostino (Italy)	2019	R	90 (26-138)	NR	78 (69-85)	3.2 (1.2-13.5)	NR	NR	NR	NR	C-PET	No
Pasquier (France)	2019	R	90 (24-216)	Phoenix	71.2 (56-86)	4.3 (2.0-38.3)	3	7	66	34	C-PET, MRI	Yes (100%)
Scher (France)	2019	R	82.5 (29-207)	Phoenix	64 (49-77)	3.1 (0.01-23.7)	NR	NR	NR	NR	C-PET, MRI	Yes (80%)
Cuccia (Italy)	2020	R	69 (29-141)	Phoenix	75 (65-89)	1.79 (0.18-10)	NR	NR	NR	NR	C-PET/ PSMA-PET, MRI	No
Matrone (Italy)	2020	R	60 (16.9-615.5)	Phoenix	76 (56-89)	2.6 (2-7.68)	1	6	NR	NR	MRI, C-PET	Yes (11%)
Caroli (Italy)	2020	R	NR	Phoenix	75 (71-80)	1.1 (0.82-2.59)	NR	NR	NR	NR	PSMA-PET	NR
Bergamin (Australia)	2020	P	99.6 (54-163.2)	Phoenix	72 (62-83)	4.1 (1.1-16.6)	NR	NR	NR	NR	PSMA-PET	Yes (100%)

Table 5.6 Salvage therapy details for BT studies Part A. Key: BT=brachytherapy, HDR=high dose rate, LDR=low dose rate, 125-I=Iodine-125, 103-Pd=Palladium-103, Ir-192=Iridium-192, Gy=Gray, ADT=androgen deprivation therapy, mo=months, BC=biochemical control, bRFS=biochemical recurrence free survival, mFS=metastasis free survival, RFS=relapse free survival, CSS=cancer specific survival, OS=overall survival. Yamada (USA) study cohort included in further publication Kollmeier (USA) however specific treatment characteristics and toxicity were not covered in later paper.

First author (country)	Year	Single-centre (1) or Multi-centre (2)	Patients (n)	BT Technique	Radiation Source	Focal or Whole-gland	Dose (total dose (Gy)/ dose per fraction/ number of fractions)	Duration of treatment	Adjuvant ADT	Follow-up (mo) (range)	BC (%)	Oncologic outcomes
B Lee (USA)	2007	1	21	HDR	Ir-192	Whole	36/6/6	7 days	No	18.7	90.8	2-yr bRFS 89%
Lyczek (Poland)	2009	1	115	HDR	Ir-192	Whole	30 / 10 / 3	9 weeks	NR	NR	46 (PSA<6) vs 18 (PSA>6)	OS 86% (PSA<6) vs 48% (PSA>6)
Chen (USA)	2013	1	52	HDR	Ir-192	Whole	36 / 6 / 6	10 days	NR	59.6 (5.9-154.7)	55.7	5-yr bRFS 51%, 5-yr OS 92%
Kukielka (Poland)	2014	1	25	HDR with interstitial hyperthermia	Ir-192	Whole	37924	63 days	Yes (12%)	13 (4-48)	NR	2-yr bRFS 74%
*Yamada (USA)	2014	1	42	HDR	Ir-192	Whole	32 / 8 / 4	30 hours	Yes (43%)	36 (2-66)	68.5	5-yr OS 90.3%
Jiang (Germany)	2016	1	29	HDR	Ir-192	Whole	30 / 10 / 3	3 weeks	Yes (34.5%)	73 (61-140)	45	5-yr bRFS 45%, 5-yr OS 95.5%
Lacy (USA)	2016	1	21	HDR	Ir-192	Whole	108-144 Gy	–	Yes (14.3%)	61 (10-149)	47.6	NR
Wojcieszek (Poland)	2016	1	83	HDR	Ir-192	Whole	30 / 10 / 3	28-30 days	Yes (53%)	41 (11-76)	67	5-yr CSS 87%
Lopez (Spain)	2019	2	75	HDR	Ir-192	Whole	32 / 7-10 / 2-4	–	Yes (45%)	52	67.5	5-yr bRFS 65%
			44	LDR	NR	Whole	145 Gy	–	Yes (532%)	52	68	5-yr bRFS 79%
Chitmanee (UK)	2020	1	50	HDR	Ir-192	Focal	1 x 19 Gy	–	Yes (8%)	21 (1-53)	46	2-yr bRFS 63%, 3-yr bRFS 46%
Slevin (UK)	2020	1	43	HDR	Ir-192	Focal	1 x 19 Gy	–	Yes (74%)	26 (1-60)	79	3-yr bRFS 41.8%
van Son (Netherlands)	2020	1	50	HDR (MRI Guided ultra-focal)	Ir-192	Ultra-focal	1 x 19 Gy	–	Yes (12%)	31 (13-58)	48	2.5 yr bRFS 51%, mFS 75%, OS 98%

Table 5.7 Salvage therapy details for BT studies Part B. Key: BT=brachytherapy, HDR=high dose rate, LDR=low dose rate, 125-I=Iodine-125, 103-Pd=Palladium-103, Ir-192=Iridium-192, Gy=Gray, ADT=androgen deprivation therapy, mo=months, BC=biochemical control, bRFS=biochemical recurrence free survival, mFS=metastasis free survival, RFS=relapse free survival, CSS=cancer specific survival, OS=overall survival. Yamada (USA) study cohort included in further publication Kollmeier (USA) however specific treatment characteristics and toxicity were not covered in later paper.

First author (country)	Year	Single-centre (1) or Multi-centre (2)	Patients (n)	BT Technique	Radiation Source	Focal or Whole-gland	Dose (total dose (Gy)/ dose per fraction/ number of fractions)	Duration of treatment	Adjuvant ADT	Follow-up (mo) (range)	BC (%)	Oncologic outcomes
Kollmeier (USA)	2017	1	37	LDR	125-I (8%) or 103-Pd (92%)	Whole	125-144 Gy	–	Yes (46%)	31 (2-97)	65	3-yr bRFS 60.2%. 3-yr mFS 78.7%
			61	HDR	Ir-192	Whole	32 / 8 / 4 (n=58), 28 / 7 / 4 (n=1) and 22 / 11 / 2 (n=1)	30 hours	Yes (44%)			
Baumann (USA)	2017	1	33	HDR/LDR	103-Pd (LDR) and Ir-192 (HDR)	Whole	LDR (90-100 Gy) or HDR (30/6/5)	NR	Yes (100%)	61 (7-150)	67	7-yr RFS 67%
Henriquez (Spain)	2014	1	56	HDR/LDR	Ir-192/ 125-I	Whole	HDR: 50.5 / 5.25 / 1-4, LDR: 145 Gy	NR	Yes (26.8%)	48 (25-109)	NR	5-yr bRFS 77%, 5-yr OS 70%
Grado (USA)	1999	1	49	LDR	125-I (76%) or 103-Pd (24%)	Whole	80-180 Gy	–	Yes (16%)	41.7 (21.8-185.2)	34	3-yr bRFS 48%, 5-yr bRFS 34%. LC 98%
Koutrouvelis (USA)	2003	1	31	LDR	125-I (77%) or 103-Pd (23%)	Whole	100-144 Gy	–	No	30 (12-84)	87	3-yr bRFS 83.9%, 5-yr bRFS 41.9%
Nguyen (USA)	2007	1	25	LDR	125-I	Whole	137 Gy	–	No	47 (14-75)	72	4-yr bRFS 70%
HK Lee (USA)	2008	1	21	LDR	103-Pd	Whole	90 Gy	–	Yes (57%)	36	NA	5-yr bRFS 38%, 5-yr OS 81%
Aaronson (USA)	2009	1	24	LDR	125-I or 103-Pd	Whole	146 Gy	–	Yes (29%)	30 (13-65)	87.5	3-yr bRFS 89.5% 3-year CSS 96%
Burri (USA)	2010	1	37	LDR	103-Pd (97%) or 125-I (4%)	Whole	110-135 Gy	–	Yes (84%)	86 (2-156)	NA	5-yr bRFS 65%, 5-yr CSS 94%, 5-yr OS 96%
Moman (Netherlands)	2010	1	31	LDR	125-I	Whole	145 Gy	–	NA	108	19	1-yr bRFS 51%, 5-yr bRFS 20%, 5-yr CSS 74%, 5-yr OS 72%
Peters (Netherlands)	2014	1	20	LDR	125-I	Focal	144 Gy	–	NR	36 (10-45)	71	3-yr bRFS 71%
Vargas (USA)	2014	1	69	LDR	125-I	Whole	100 Gy	–	Yes (90%)	60 (7-164)	68.6	5-yr OS 64%, 5-yr mFS 90%
Peters (Netherlands)	2016	2	62	LDR (Whole Gland)	125-I	Whole	145 Gy	–	Yes (34%)	78 (5-139)	NR	Estimated 10-yr PCaSS 43%, 10-yr OS 34%
Crook (Canada)	2019	2	92	LDR	125-I (92%) or 103-Pd (8%)	Whole	120-140 Gy	–	NR	54	NR	NR
Smith (USA)	2020	2	108	LDR	125-I (1%) or 103-Pd (99%)	Whole	100 Gy	–	Yes (93.5%)	75 (1-228)	NR	5-yr bRFS 63%, 10-yr bRFS 52%
Schonle (Germany)	2020	1	82	PDR	Ir-192	Whole	60 / 30 / 2	4 weeks	Yes (43.9)	49 (12-129)	65.6	5-yr bRFS 65.6%, LC 86.6%

Table 5.8 Salvage therapy details for EBRT studies. Key: SBRT=Stereotactic body radiotherapy, VMAT=Volumetric modulated arc therapy, IMRT= Intensity-modulated radiation therapy, Gy=grey, ADT=androgen deprivation therapy, mo=months, BC=biochemical control, bRFS=biochemical recurrence free survival, mFS=metastasis free survival, RFS=relapse free survival, CSS=cancer specific survival, OS=overall survival, PFS=progression free survival.

First author/ country	Year	Single-centre (1) or Multi-centre (2)	Patients (n)	Treatment Technique	Delivery System	Dose (total dose (Gy)/ dose per fraction/ number of fractions)	Whole or Partial Gland/ Focal	Duration of treatment	Adjuvant ADT	Follow-up (mo) (range)	BC (%)	Oncologic outcomes
Fuller (USA)	2020	2	50	SBRT	Cyberknife	34 / 6.8 / 5	Whole	5 days	Yes (14%)	44 (3-110)	60	2-yr bRFS 76%, 5-yr bRFS 60%
Cuccia (Italy)	2020	1	24	SBRT	VMAT	30/06/05	Whole	5-12 days	Yes (16.7%)	21 (2-68)	54.9	1-yr bRFS 80%, 2-yr bRFS 54.9%, OS 100%
Matrone (Italy)	2020	1	44	SBRT	VMAT	35 / 5 / 7	Focal	7 days	Yes (27%)	25.4 (6.7-81.5)	59	1-yr bRFS 85.9%, 2-yr bRFS 58.3%, 2-yr LC 90.1%, 2-yr OS 100%
Caroli (Italy)	2020	1	38	SBRT	NR	18/ 6/ 3	Focal	3 days	NR	27 (4-35)	NR	bRFS 15 months
Bergamin (Australia)	2020	1	25	SBRT	VMAT	36 / 6 / 6 (72%) *vs* 38/ 6.3/ 6 (28%)	Focal	14 days	Yes (48%)	25 (13-46)	80	2-yr bRFS 80%
D'Agostino (Italy)	2019	1	23	SBRT	VMAT	25/ 5/ 5	Whole	5 days	Yes (43.5%)	33 (5-58)	34.8	2-yr bRFS 41.7%, 2-yr LC 61.1%, OS 100%
Pasquier (France)	2019	2	100	SBRT	Cyberknife (81%)/ VERO-IMRT, RapidArc	36 / 6 / 5	49% Whole *vs* 51% Partial	12 days	Yes (36%)	29.3 (4-91)	NR	bRFS 48 months, 3-yr bRFS 55%, 4-yr OS 94%
Scher (France)	2019	1	42	SBRT	Cyberknife	36 / 6 / 6	Focal	NR	Yes (19%)	21 (3-31)	94	median PFS 11 months, LC 100%
Jereczek-Fossa (Italy)	2018	1	64	SBRT	Cyberknife/ VERO-IMRT	30/ 6/ 5	Whole	5 days	Yes (25%)	26.1 (3.1-82.4)	64	2-yr bRFS 40%, LC 75%, OS 92%
Loi (Italy)	2018	1	50	SBRT	Cyberknife	30/ 6/ 5	NR	5 days	Yes (30%)	21.3 (6.1-49.2)	60	1-yr bRFS 80%, 1-yr mFS 92%
Leroy (France)	2017	1	23	SBRT	Cyberknife	36 / 6 / 6	83% Whole *vs* 17% Partial	14 days	Yes (61%)	22.6 (6-40)	54	2-yr bRFS 54%, OS 100%, 2-yr local dFS 76%

Seventeen studies (44%) used both multi-parametric magnetic resonance imaging (mpMRI) and positron emission tomography-computed tomography (PET-CT) for restaging prior to salvage treatment. Four studies (10%) used prostate-specific membrane antigen (PSMA) PET-CT and 13 studies (33%) used choline/fluciclovine PET-CT for re-staging. Eight studies (all BT) (21%) used computed tomography (CT) or isotope bone scintigraphy for restaging. Ten studies (26%) did not report the imaging modality used for restaging. Among the 28 BT studies, 24 included only patients with biopsy-proven local recurrence. Three of 11 SBRT studies included patients with histological confirmation of recurrence.

For BT studies, median follow up duration (range) was 47.5 months (13-108) compared with 25.4 months (21-44) for SBRT studies. The use of ADT with salvage therapy ranged from 8-100% in the BT study group and 14-61% in the SBRT group.

5.4.2 Oncological Outcomes

For the LDR-BT studies, the median (range) 2-year and 5-year bRFS rates were 71% (48-89.5%) and 52.5% (20-79%). For the HDR-BT studies, the median (range) 2-year and 5-year bRFS rates were 74% (63-89%) and 51% (45-65%). For the SBRT studies, the median (range) 2-year bRFS for the SBRT group was 54.9% (40-80%). A 5-year estimate of bRFS following SBRT was only available for one study and was 60% [46]. For focal gland BT, the median (range) 3-year bRFS was 63% (42-71%). For focal SBRT, the median (range) 3-year bRFS was 69% (58-80%). 3-year bRFS was presented as 2-year bRFS was not reported by the majority of these focal RT studies.

5.4.3 Toxicity

A summary of clinician reported acute and late GU and GI toxicity data for each study is presented in Table 5.9 (BT) and Table 5.10 (SBRT).

In studies that only included LDR-BT, mean (range) grade 3 or higher toxicities were 7.4% (0-14%) (acute GU), 13.6% (0-30%) (late GU), 6.5% (0-19%) (acute GI) and 6.4% (0-20%) (late GI). In studies that only included HDR-BT, mean (range) grade 3 or higher toxicities were 2% (0-14%) (acute GU), 7.9% (0-21.3%) (late GU) and 0.1% (0-0.9%) (late GI). No grade 3 or higher acute GI toxicity was reported. For the SBRT group, mean (range) grade 3 or higher toxicities were 1.8% (0-8.7%) (acute GU), 2.7% (0-8%) (late GU), 0.5% (0-4%) (acute GI) and 0.2% (0-1.5%) (late GI).

Table 5.9 Toxicity details for BT studies. Key: - = 0% reported toxicity, NR=not reported, GU=genitourinary, GI=gastrointestinal, CTCAE = Common Terminology Criteria for Adverse Events, RTOG=Radiation Therapy Oncology Group, NR=not reported, PROMS=patient recorded outcome measures, IPSS= International prostate symptom score, RAND-36=RAND-36 Health Survey, EORTC= European Organisation for Research and Treatment of Cancer Quality of Life questionnaire, IIEF-5=International Index of Erectile Function questionnaire, MSEFS= Mount Sinai Erectile Function Score. Yamada (USA) study cohort included in further publication Kollmeier (USA) however specific treatment characteristics and toxicity were not covered in later paper.

First author (country)	Toxicity Scale	Acute GU toxicity		Acute GI toxicity		Late GU toxicity		Late GI toxicity		Erectile Dysfunction	PROMS
		Grade ≤ 2	Grade ≥ 3	Grade ≤ 2	Grade ≥ 3	Grade ≤ 2	Grade ≥ 3	Grade ≤ 2	Grade ≥ 3		
Kollmeier (USA)	CTCAE v4.0	96.0%	–	96.0%	–	82.0%	9.0%	91.0%	2.0%	NR	Yes (IPSS)
Baumann (USA)	CTCAE v4.0	82.0%	–	9.0%	–	42.0%	12.0%	3.0%	–	NR	Yes (IPSS)
Wojcieszek (Poland)	CTCAE v4.0	87.0%	1.0%	6.0%	–	72.0%	13.0%	6.0%	–	NR	NR
*Yamada (USA)	CTCAE v3.0	78.0%	–	NR	NR	86.0%	10.0%	57.0%	–	Yes	Yes (IPSS)
Peters (Netherlands)	CTCAE v4.0	100.0%	–	55.0%	–	40.0%	5.0%	35.0%	–	Yes (80%)	Yes (RAND-36, EORTC)
Vargas (USA)	NR	5.0%	8.7%	NR	NR	5.0%	8.7%	7.0%	3.0%	NR	NR
Chen (USA)	CTCAE v4.0	98.0%	2.0%	100.0%	–	98.0%	2.0%	100.0%	–	Yes (81%)	NR
Burri (USA)	CTCAE v3.0	35.0%	11.0%	5.0%	NR	35.0%	11.0%	NR	3.0%	Yes (75%)	NR
Moman (Netherlands)	CTCAE v3.0	87.0%	3.0%	55.0%	–	55.0%	19.0%	51.0%	6.0%	NR	NR
Aaronson (USA)	CTCAE v3.0	NR	NR	NR	3.0%	37.0%	4.0%	NR	4.0%	NR	Yes (IPSS, IIEF-5)
HK Lee (USA)	RTOG	29.0%	–	5.0%	–	29.0%	–	5.0%	–	NR	NR
Nguyen (USA)	RTOG	NR	NR	NR	NR	NR	20.0%	NR	20.0%	NR	NR
B Lee (USA)	CTCAE v3.0	86.0%	14.0%	14.0%	–	NR	5.0%	–	–	Yes (95%)	NR
Koutrouvelis (USA)	NR	13.0%	13.0%	13.0%	19.0%	13.0%	13.0%	13.0%	19.0%	NR	NR
Grado (USA)	NR	NR	NR	NR	NR	10.0%	20.0%	4.0%	2.0%	NR	NR
Slevin (UK)	CTCAE v4.0	91.0%	–	14.0%	–	65.0%	2.0%	14.0%	–	NR	NR
Lopez (Spain)	RTOG	33.0%	NR	NR	NR	NR	21.3%	NR	NR	NR	NR
	RTOG	33.0%	NR	NR	NR	NR	27.3%	NR	NR	NR	NR
Crook (Canada)	CTCAE v3.0	NR	14.0%	NR	14.0%	NR	7.0%	NR	4.0%	NR	Yes (IPSS)
Smith (USA)	CTCAE v5.0	NR	NR	NR	NR	NR	15.7%	NR	2.8%	Yes (80%)	Yes (IPSS, MSEFS)
Kukielka (Poland)	CTCAE v4.0	96.0%	–	12.0%	–	41.0%	–	–	–	NR	Yes (IPSS)
Schonle (Germany)	CTCAE v4.0	15.8%	6.1%	2.4%	–	15.8%	6.1%	2.4%	–	NR	NR
Chitmanee (UK)	NR	90.0%	–	32.0%	–	72.0%	10.0%	30.0%	–	Yes (86%)	Yes (IPSS)
Henriquez (Spain)	CTCAE v3.0	NR	NR	NR	NR	NR	23.0%	NR	4.0%	NR	NR
Peters (Netherlands)	CTCAE v4.03	NR	NR	NR	NR	NR	30.0%	NR	10.0%	NR	NR
Jiang (Germany)	CTCAE v4.0	100.0%	–	100.0%	–	90.9%	9.0%	100.0%	–	NR	Yes (IPSS)
van Son (Netherlands)	CTCAE v4.0	65.0%	–	37.0%	–	55.0%	2.0%	37.0%	–	Yes (100%)	Yes (IPSS, RAND-36)
Lacy (USA)	RTOG	9.6%	9.6%	9.6%	9.6%	9.6%	9.6%	9.6%	9.6%	Yes (45.5%)	Yes (IPSS)
Lyczek (Poland)	RTOG	29.6%	2.6%	7.9%	NR	7.0%	12.2%	1.7%	0.9%	NR	NR

Table 5.10 Toxicity details for EBRT studies Key: - = 0% reported toxicity, NR=not reported, GU=genitourinary, GI=gastrointestinal, CTCAE = Common Terminology Criteria for Adverse Events, RTOG=Radiation Therapy Oncology Group, NR=not reported, PROMS=patient recorded outcome measures, IPSS= International prostate symptom score.

First author (country)	Toxicity Scale	Acute GU toxicity		Acute GI toxicity		Late GU toxicity		Late GI toxicity		Erectile Dysfunction	PROMS
		Grade ≤ 2	Grade ≥ 3	Grade ≤ 2	Grade ≥ 3	Grade ≤ 2	Grade ≥ 3	Grade ≤ 2	Grade ≥ 3		
Leroy (France)	CTCAE v4.0	78.2%	8.7%	17.4%	–	NR	NR	NR	NR	NR	NR
Fuller (USA)	CTCAE v3.0	2.2%	–	–	–	17.0%	8.0%	–	–	Yes (70%)	Yes (IPSS)
Jereczek-Fossa (Italy)	RTOG	25.0%	1.5%	9.5%	1.5%	37.0%	1.5%	7.5%	1.5%	NR	No
Loi (Italy)	CTCAE v3.0	20.0%	2.0%	8.0%	–	24.0%	2.0%	6.0%	–	NR	No
D'Agostino (Italy)	CTCAE v4.03	56.5%	4.4%	–	–	17.4%	4.4%	–	–	NR	No
Pasquier (France)	CTCAE v4.03	8.0%	1.0%	–	–	16.0%	1.0%	1.0%	–	NR	No
Scher (France)	CTCAE v4.03	64.0%	2.0%	7.0%	–	21.0%	2.0%	–	–	NR	No
Cuccia (Italy)	CTCAE v4.0	20.8%	–	–	–	12.5%	4.2%	4.2%	–	NR	No
Matrone (Italy)	RTOG	32.0%	–	8.0%	–	32.0%	4.0%	7.0%	–	NR	No
Caroli (Italy)	CTCAE v4.0	31.60%	–	31.60%	–	31.60%	–	31.60%	–	NR	No
Bergamin (Australia)	CTCAE v4.03	28.0%	–	8.0%	4.0%	32.0%	–	8.0%	–	NR	No

5.5 Discussion

This systematic review evaluated the most up-to-date evidence for salvage BT and SBRT and found that both treatment options provide good biochemical control with acceptable late GU/ GI toxicity. However there is considerable heterogeneity between studies for numbers of patients, risk groups of included patients, evaluated treatments, reported endpoints, duration of follow up and methods of toxicity assessment (clinician-assessed versus PROMs). The quality of studies was low and meta-analysis was therefore not conducted due to the significant bias associated with these uncontrolled studies. This highlights the need for further high quality prospective and randomised studies to measure the efficacy and toxicity associated with salvage irradiation.

Consensus national and international recommendations for reirradiation are limited. The European Association of Urology (EAU) guidelines recommend salvage reirradiation using BT or SBRT for locally recurrent prostate cancer should only be undertaken in a clinical trial setting [56]. American Society for Radiation Oncology (ASTRO) and National Comprehensive Cancer Network (NCCN) clinical practice guidelines does not comment on the use of reirradiation for prostate cancer however both the European Society of Radiation Oncology (ESTRO) and American Society of Brachytherapy (ABS) recommendations on prostate HDR-BT highlight the accumulating evidence for salvage HDR-BT in local recurrence as showing great promise [57–59].

There has been increasing interest in the use of salvage therapies for locally recurrent prostate cancer after primary radiation, although concerns have been raised regarding the potential for severe late toxicity [60]. Both BT and SBRT, show durable outcomes in terms of biochemical control with reasonable reported toxicities in the majority of reviewed studies. However, inconsistencies in reporting and missing data preclude accurate comparison between these studies, which are mainly composed of case series. Longer term efficacy data and duration of follow up was available for more BT studies than SBRT but, at short term follow-up, the clinician-reported toxicity following salvage SBRT appear to be infrequent [61]. One additional bias is that HDR-BT requires a general anaesthetic and patients may be younger or fitter and this could translate to better overall survival outcomes.

Two previous meta-analyses which compared salvage therapies in recurrent prostate cancer have been conducted, which included radical prostatectomy, cryotherapy and HIFU in addition to BT and EBRT [11,62]. The meta-analysis by Valle et al.[62] reported that recurrence free survival and toxicity rates were best for salvage radiotherapeutic modalities compared to other salvage treatments, and BT appeared to offer the best balance between

toxicity and efficacy. For example, the estimated recurrence free survival at 2 years for BT was 77-79% compared to 52-72% for cryotherapy, HIFU and salvage radical prostatectomy. In addition, lower grade 3 or higher GU toxicity was observed (5-10% versus 20% for BT compared with other salvage therapies) [62]. The quality of the evidence was not assessed and sub-group and sensitivity analyses to explore potential impact of clinical heterogeneity were also not specified in this meta-analysis [62]. In addition, it was unclear how many studies were excluded from the meta-analysis due to incompatible definitions, outcome measures and follow-up periods. Interestingly, the 2-year bRFS of SBRT (54.9%) appeared to be lower than both LDR- and HDR-BT (71% and 74% respectively). A formal comparison between these modalities is limited by confounding factors, although these data raise an interesting question as to whether salvage SBRT could be inferior to BT in terms of biochemical control. Comparing the SBRT studies to BT remains challenging in view of the heterogeneous populations and shorter follow-up available for SBRT with only one study providing 5-yr bRFS data (although in this study, comparable to outcomes from salvage BT were reported) [48]. No prospective randomised studies exist which compare BT and SBRT as salvage therapies for locally recurrent prostate cancer and this is ultimately what is required.

There may be dosimetric advantages with the use of BT compared with SBRT. A previous planning study in the primary disease setting concluded that HDR-BT was able to achieve higher intraprostatic doses and greater sparing of the rectum than SBRT [63]. It is possible that developments in SBRT planning and delivery might lead to improved outcomes. For example, the superior soft tissue visualisation and functional imaging capabilities of MR guided SBRT might permit better delineation of tumour, greater accuracy of treatment delivery and offer opportunities for dose escalation [64]. Whether this would translate into a clinical benefit at this point remains uncertain. There remains considerable interest in salvage SBRT as evidenced by the fact that 8 of 11 SBRT studies were published in the last two years.

Based on the studies evaluated in this review, salvage LDR-BT appeared to have the potential for higher grade 3+ toxicity compared to HDR-BT [20,25]. In a study which used PROMs, LDR-BT had a higher peak change in IPSS in the early post-implant period and a higher peak urinary symptom flare at 12 months compared with HDR-BT, although the majority of these scores returned to baseline 2-3 years post-treatment [41]. There have been no prospective studies comparing these techniques in the reirradiation setting. In the primary treatment setting however prospective and randomised studies have shown HDR-BT to have better quality of life scores compared to LDR-BT in the acute post-treatment phase, particularly in the urinary health domain, which suggests that HDR

was better tolerated [65,66]. Similarly, evidence from registries and randomised trials of LDR/ EBRT combination therapy and HDR/EBRT combination therapy in the primary disease setting suggest that LDR/EBRT might be associated with higher incidence of significant late GU toxicity although no direct comparison has been performed between the two treatments [67–69].

Based on the available data, grade 3 or higher GU and GI toxicity with SBRT was rare, although follow-up beyond 2 years is limited [10,46,55,47–54]. SBRT has the potential to limit the risk of severe late GU/GI toxicity compared with less conformal EBRT techniques [70]. Careful patient selection remains vital, especially for those at greater risk of excess toxicity following salvage therapy. In a recent observational series of salvage SBRT, grade 3+ GU toxicity was disproportionately observed in patients treated with BT or radical prostatectomy plus salvage RT in the primary disease setting [48]. Furthermore, the use of focal salvage techniques with BT and SBRT appear to have lower toxicity rates and comparable bRFS rates however this is limited to a number of uncontrolled, single-arm case series [17,35,37,39,47,52,54,55].

Appropriate patient selection for salvage RT treatments is vital. The European Society for Radiotherapy and Oncology Advisory Committee on Radiation Oncology Practice (ESTRO ACROP) recently conducted a Delphi consensus of expert opinion on patient selection criteria for salvage RT [71]. Selection criteria with high levels of agreement (>80%) included Eastern Cooperative Oncology Group performance status of 0-1, satisfactory urinary flow with a known IPSS prior to salvage and use of PET-CT to exclude metastatic disease and MRI to define the target. Agreement was reached that concomitant ADT with salvage RT was unnecessary and that previous ADT use was not a contraindication to salvage RT. It was also recommended that the primary RT dose should be taken into account when considering salvage SBRT. In terms of time duration between primary RT and salvage RT, although consensus was not achieved a minimum interval of 2 years reached major agreement (defined as 65-80% agreement).

The impact on quality of life has not been well assessed in the salvage radiotherapy setting with only a third of studies in this systematic review including PROMs. Only one of 11 SBRT (9.1%) studies included PROMs. Without this information, it is likely that reported rates of toxicity are underestimated [72]. Assessment of residual toxicity following primary treatment using validated PROM instruments such as Expanded Prostate Cancer Index (EPIC) could be an important tool for identification of patients at risk of significant toxicity from salvage therapies. Integration of longitudinal PROM assessment into clinical trials is important to ascertain the time-dependent nature of toxicity onset/resolution after

treatment [72,73].

The role of ADT with salvage BT/EBRT remains unclear and no consensus could be reached during a previous Delphi consensus [74]. The use of ADT with salvage radiation therapy in the evaluated studies was highly variable (8-100%) and reporting of ADT duration was incomplete [17,33,37,42,75]. Several BT studies did not report ADT usage or did not use neoadjuvant ADT [25,26,34]. Salvage therapies may delay the need for ADT, with up to 69% patients remaining free of ADT at 5 years following salvage SBRT [48]. Some authors view salvage BT/ SBRT as ADT sparing, which might have the potential to improve quality of life [76].

A recent study found that only 15% of relapses following salvage BT were solely in the prostate [37], suggesting most are likely to be systemic failure therefore accurate and consistent whole body imaging staging is imperative. The optimal combination of re-staging imaging following biochemical failure after primary treatment, and the most clinically relevant PSA level at which to trigger such imaging, remains uncertain [77]. Despite the poor accuracy of CT and isotope bone scintigraphy, 21% of studies in this systematic review used these modalities for restaging and patient selection. It is possible that some patients in these studies could have had undiagnosed metastatic disease, and this could be responsible for some subsequent biochemical failures [76,78]. Less than half of studies used mpMRI and PET-CT for re-staging prior to salvage therapy. mpMRI has the potential to be particularly useful for detecting local recurrence following previous prostate radiotherapy, although studies evaluating its accuracy are limited [79]. The use of novel imaging modalities such as Gallium-68 [68Ga] or Fluorine-18 [18F] labelled PSMA PET-CT, may allow detection of local recurrence at lower PSA levels. While this could lead to a change in management for patients identified with recurrent disease, it was only used in 10% of the studies in this systematic review [80]. 68Ga-PSMA PET-CT has been shown to demonstrate recurrences at prostate-specific antigen (PSA) levels below the Phoenix definition of biochemical failure and it allows for both local staging and exclusion of distant metastatic disease in patients with biochemical failure [81]. The recent proPSMA randomised study reported that PSMA PET-CT had a greater accuracy compared to conventional imaging with CT and bone scan in the primary setting (92% vs 65%) [82]. PSMA PET-CT also has superior performance characteristics for the detection of distant metastasis in the setting of biochemical failure compared to other PET tracers [83]. Nevertheless, the clinical significance of detecting and treating small volume local recurrence at low PSA levels remains uncertain and may risk additional toxicity. Prospective randomised trials comparing BT and SBRT for salvage treatment of locally recurrent prostate cancer are required to determine the efficacy/toxicity of these

interventions

5.5.1 Limitations

The overall quality of evaluated evidence was low. A meta-analysis was not conducted to quantitatively compare the studies as the majority of these were non-comparative retrospective case series with differences in baseline patient demographics, primary and/or salvage treatments, reported endpoints reported and use of ADT. This limits the conclusions that can be drawn about the effectiveness/ toxicity of salvage BT/SBRT. High-quality data from prospective trials are still needed to validate the toxicity and long-term clinical outcomes associated with the salvage treatment of recurrent prostate cancer using BT or EBRT, following previous RT.

5.6 Conclusion

Salvage reirradiation of radiorecurrent prostate cancer using HDR-BT or SBRT provides similar biochemical control and acceptable late toxicity. Salvage LDR-BT is associated with higher late GU/GI toxicity. Challenges exist in comparing BT and SBRT from the current literature due to inconsistencies in reporting and missing data. Prospective randomised trials comparing BT and SBRT and assessing PROMs as well as cancer control outcomes in this setting are needed.

5.7 References

1. Bray F, Ferlay J, Soerjomataram I, Siegel RL, Torre LA, Jemal A. Global cancer statistics 2018: GLOBOCAN estimates of incidence and mortality worldwide for 36 cancers in 185 countries. CA Cancer J Clin [Internet]. 2018;68:394–424.

2. Mottet N, Bellmunt J, Bolla M, Briers E, Cumberbatch MG, De Santis M, et al. EAU-ESTRO-SIOG Guidelines on Prostate Cancer. Part 1: Screening, Diagnosis, and Local Treatment with Curative Intent. Eur Urol [Internet]. 2017;71(4):618–29.

3. Beckendorf V, Guerif S, Le Prisé E, Cosset JM, Bougnoux A, Chauvet B, et al. 70 Gy versus 80 Gy in localized prostate cancer: 5-year results of GETUG 06 randomized trial. Int J Radiat Oncol Biol Phys [Internet]. 2011;80(4):1056–63.

4. Zumsteg ZS, Spratt DE, Romesser PB, Pei X, Zhang Z, Kollmeier M, et al. Anatomical patterns of recurrence following biochemical relapse in the dose escalation era of external beam radiotherapy for prostate cancer. J Urol [Internet]. 2015;194(6):1624-1630.

5. Dearnaley DP, Jovic G, Syndikus I, Khoo V, Cowan RA, Graham JD, et al. Escalated-dose versus control-dose conformal radiotherapy for prostate cancer: Long-term results from the MRC RT01 randomised controlled trial. Lancet Oncol [Internet]. 2014;15(4):464–73.

6. Falagario UG, Abbadi A, Remmers S, Björnebo L, Bogdanovic D, Martini A, et al. Biochemical Recurrence and Risk of Mortality Following Radiotherapy or Radical Prostatectomy. JAMA Netw Open. 2023;6(9):e2332900.

7. Cooperberg MR, Vickers AJ, Broering JM, Carroll PR. Comparative risk-adjusted mortality outcomes after primary surgery, radiotherapy, or androgen-deprivation therapy for localized prostate cancer. Cancer [Internet]. 2010;116:5226–5234.

8. Chatzikonstantinou G, Zamboglou N, Rödel C, Zoga E, Strouthos I, Butt SA, et al. High-dose-rate brachytherapy as salvage modality for locally recurrent prostate cancer after definitive radiotherapy: Asystematic review. Strahlentherapie und Onkol [Internet]. 2017;193:683–691.

9. Zilli T, Benz E, Dipasquale G, Rouzaud M, Miralbell R. Reirradiation of Prostate Cancer Local Failures After Previous Curative Radiation Therapy: Long-Term Outcome and Tolerance. Int J Radiat Oncol Biol Phys [Internet]. 2016;96:218–322.

10. Pasquier D, Martinage G, Janoray G, Rojas DP, Zerini D, Goupy F, et al. Salvage Stereotactic Body Radiation Therapy for Local Prostate Cancer Recurrence After Radiation Therapy: A Retrospective Multicenter Study of the GETUG. Int J Radiat Oncol Biol Phys [Internet]. 2019;105(4):727-734.

11. Ingrosso G, Becherini C, Lancia A, Caini S, Ost P, Francolini G, et al. Nonsurgical Salvage Local Therapies for Radiorecurrent Prostate Cancer: A Systematic Review and Meta-analysis. Eur Urol Oncol [Internet]. 2019;3(2):183–97.

12. Chade DC, Eastham J, Graefen M, Hu JC, Karnes RJ, Klotz L, et al. Cancer control and functional outcomes of salvage radical prostatectomy for radiation-recurrent prostate cancer: A systematic review of the literature. Eur Urol [Internet]. 2012;61(5):961–71.

13. Moher D, Liberati A, Tetzlaff J, Altman DG, Altman D, Antes G, et al. Preferred reporting items for systematic reviews and meta-analyses: The PRISMA statement. PLoS Med [Internet]. 2009;6(7):e1000097.

14. Moga C, Guo B, Harstall C. Development of a Quality Appraisal Tool for Case Series Studies Using a Modified Delphi Technique. Institute of Health Economics (IHE) Publications. 2012.

15. National Cancer Institute. Common Terminology Criteria for Adverse Events (CTCAE) version 5.0. NIH Publ [Internet]. 2020;

16. Cox JD, Stetz JA, Pajak TF. Toxicity criteria of the Radiation Therapy Oncology Group (RTOG) and the European organization for research and treatment of cancer (EORTC). Int J Radiat Oncol Biol Phys [Internet]. 1995;31:1341-1346.

17. Peters M, Maenhout M, Van Der Voort Van Zyp JRN, Moerland MA, Moman MR, Steuten LMG, et al. Focal salvage iodine-125 brachytherapy for prostate cancer recurrences after primary radiotherapy: A retrospective study regarding toxicity biochemical outcome and quality of life. Radiother Oncol [Internet]. 2014;112(1):77–82.

18. Vargas C, Swartz D, Vashi A, Blasser M, Kasraeian A, Cesaretti J, et al. Salvage brachytherapy for recurrent prostate cancer. Brachytherapy [Internet]. 2014;13(1):53–8.

19. Smith WH, Cesaretti J, Chin CP, Terk M, Stock RG. Salvage low dose rate brachytherapy for prostate cancer recurrence following definitive external beam radiation therapy. Radiother Oncol. 2021;155:42–7.

20. Peters M, Van Der Voort Van Zyp JRN, Moerland MA, Hoekstra CJ, Van De Pol S, Westendorp H, et al. Multivariable model development and internal validation for prostate cancer specific survival and overall survival after whole-gland salvage Iodine-125 prostate brachytherapy. Radiother Oncol [Internet]. 2016;119(1):104–10.

21. Burri RJ, Stone NN, Unger P, Stock RG. Long-term outcome and toxicity of salvage brachytherapy for local failure after initial radiotherapy for prostate cancer. Int J Radiat Oncol Biol Phys [Internet]. 2010;77(5):1338–1344.

22. Moman MR, van der Poel HG, Battermann JJ, Moerland MA, van Vulpen M. Treatment outcome and toxicity after salvage 125-I implantation for prostate cancer recurrences after primary 125-I implantation and external beam radiotherapy. Brachytherapy [Internet]. 2010;9(2):119–25.

23. Aaronson DS, Yamasaki I, Gottschalk A, Speight J, Hsu IC, Pickett B, et al. Salvage permanent perineal radioactive-seed implantation for treating recurrence of localized prostate adenocarcinoma after external beam radiotherapy. BJU Int [Internet]. 2009;104(5):600-604.

24. Lee HK, Adams MT, Motta J. Salvage prostate brachytherapy for localized prostate cancer failure after external beam radiation therapy. Brachytherapy [Internet]. 2008;7(1):17-21.

25. Nguyen PL, Chen MH, D'Amico A V., Tempany CM, Steele GS, Albert M, et al. Magnetic resonance image-guided salvage brachytherapy after radiation in select men who initially presented with favorable-risk prostate cancer: A prospective phase 2 study. Cancer [Internet]. 2007;110(7):1485-1192.

26. Koutrouvelis P, Hendricks F, Lailas N, Gil-Montero G, Sehn J, Khawand N, et al. Salvage reimplantation in patient with local recurrent prostate carcinoma after brachytherapy with three dimensional computed tomography-guided permanent pararectal implant. Technol Cancer Res Treat [Internet]. 2003;2(4):339–44.

27. Grado GL, Collins JM, Kriegshauser JS, Balch CS, Grado MM, Swanson GP, et al. Salvage brachytherapy for localized prostate cancer after radiotherapy failure. Urology [Internet]. 1999;53(1):2-10.

28. Crook JM, Zhang P, Pisansky TM, Trabulsi EJ, Amin MB, Bice W, et al. A Prospective Phase 2 Trial of Transperineal Ultrasound-Guided Brachytherapy for Locally Recurrent Prostate Cancer After External Beam Radiation Therapy (NRG Oncology/RTOG-0526). Int J Radiat Oncol Biol Phys [Internet]. 2019;103(3):335-343.

29. Wojcieszek P, Szlag M, Głowacki G, Cholewka A, Gawkowska-Suwińska M, Kellas-Ślęczka S, et al. Salvage high-dose-rate brachytherapy for locally recurrent prostate cancer after primary radiotherapy Prostate cancer salvage brachytherapy failure. Radiother Oncol [Internet]. 2016;119(3):405-410.

30. Yamada Y, Kollmeier MA, Pei X, Kan CC, Cohen GN, Donat SM, et al. A Phase II study of salvage high-dose-rate brachytherapy for the treatment of locally recurrent prostate cancer after definitive external beam radiotherapy. Brachytherapy [Internet]. 2014;13(2):111-116.

31. Ware RE, Matthews JP, Hicks RJ, Porceddu S, Hogg A, Rischin D, et al. Usefulness of fluorine-18 fluorodeoxyglucose positron emission tomography in

patients with a residual structural abnormality after difinitive treatments for squamous cell carcinoma of the head and neck. Head Neck [Internet]. 2004;26(12):1008–17.

32. Łyczek J, Kawczyńska MM, Garmol D, Kasprowicz A, Kulik A, Dąbkowski M, et al. HDR brachytherapy as a solution in recurrences of locally advanced prostate cancer. J Contemp Brachytherapy [Internet]. 2009;1(2):105–108.

33. Chen CP, Weinberg V, Shinohara K, Roach M, Nash M, Gottschalk A, et al. Salvage HDR brachytherapy for recurrent prostate cancer after previous definitive radiation therapy: 5-year outcomes. Int J Radiat Oncol Biol Phys [Internet]. 2013;86(2):324-329.

34. Lee B, Shinohara K, Weinberg V, Gottschalk AR, Pouliot J, Roach M, et al. Feasibility of high-dose-rate brachytherapy salvage for local prostate cancer recurrence after radiotherapy: The University of California-San Francisco experience. Int J Radiat Oncol Biol Phys [Internet]. 2007;67(4):1106–1112,.

35. Slevin F, Hodgson S, Rodda SL, Bownes P, Bottomley D, Adiotomre E, et al. Efficacy and toxicity outcomes for patients treated with focal salvage high dose rate brachytherapy for locally recurrent prostate cancer. Clin Transl Radiat Oncol [Internet]. 2020;23:20-26.

36. Kukiełka AM, Hetnał M, Da browski T, Walasek T, Brandys P, Nahajowski D, et al. Salvage prostate HDR brachytherapy combined with interstitial hyperthermia for local recurrence after radiation therapy failure. Strahlentherapie und Onkol [Internet]. 2014;190(2):165–70.

37. Chitmanee P, Tsang Y, Tharmalingam H, Hamada M, Alonzi R, Ostler P, et al. Single-Dose Focal Salvage High Dose Rate Brachytherapy for Locally Recurrent Prostate Cancer. Clin Oncol [Internet]. 2020;32(4):259-265.

38. Jiang P, van der Horst C, Kimmig B, Zinsser F, Poppe B, Luetzen U, et al. Interstitial high-dose-rate brachytherapy as salvage treatment for locally recurrent prostate cancer after definitive radiation therapy: Toxicity and 5-year outcome. Brachytherapy [Internet]. 2017;16(1):186-192.

39. van Son MJ, Peters M, Moerland MA, Lagendijk JJW, Eppinga WSC, Shah TT, et al. MRI-Guided Ultrafocal Salvage High-Dose-Rate Brachytherapy for Localized Radiorecurrent Prostate Cancer: Updated Results of 50 Patients. Int J Radiat Oncol Biol Phys. 2020;107(1):126–35.

40. Lacy JM, Wilson WA, Bole R, Chen L, Meigooni AS, Rowland RG, et al. Salvage brachytherapy for biochemically recurrent prostate cancer following primary brachytherapy. Prostate Cancer [Internet]. 2016;9561494.

41. Kollmeier MA, McBride S, Taggar A, Anderson E, Lin M, Pei X, et al. Salvage brachytherapy for recurrent prostate cancer after definitive radiation therapy: A comparison of low-dose-rate and high-dose-rate brachytherapy and the importance of prostate-specific antigen doubling time. Brachytherapy [Internet]. 2017;16(6):1091-1098.

42. Baumann BC, Baumann JC, Christodouleas JP, Soffen E. Salvage of locally recurrent prostate cancer after external beam radiation using reduced-dose brachytherapy with neoadjuvant plus adjuvant androgen deprivation. Brachytherapy [Internet]. 2017;16(2):291-298.

43. Henríquez I, Sancho G, Hervás A, Guix B, Pera J, Gutierrez C, et al. Salvage brachytherapy in prostate local recurrence after radiation therapy: Predicting factors for control and toxicity. Radiat Oncol [Internet]. 2014;9:102.

44. Henríquez López I, González-San Segundo C, Vegas JO, Gutierrez C, Hervas A, Cabeza Rodriguez MÁ, et al. Salvage brachytherapy for locally-recurrent prostate cancer after radiation therapy: A comparison of efficacy and toxicity outcomes with high-dose rate and low-dose rate brachytherapy. Radiother Oncol [Internet]. 2019;141:156-163.

45. Schönle N, Strnad V, Lotter M, Kreppner S, Fietkau R. Long-term results of a protocol-based ultrasound-guided salvage brachytherapy as re-irradiation for local recurrent prostate cancer. Radiother Oncol [Internet]. 2020;150:201-205.

46. Leroy T, Lacornerie T, Bogart E, Nickers P, Lartigau E, Pasquier D. Salvage robotic SBRT for local prostate cancer recurrence after radiotherapy: Preliminary results of the Oscar Lambret Center. Radiat Oncol [Internet]. 2017;12(1):95.

47. Bergamin S, Eade T, Kneebone A, Booth J, Hsiao E, Schembri GP, et al. Interim Results of a Prospective Prostate-Specific Membrane Antigen-Directed Focal Stereotactic Reirradiation Trial for Locally Recurrent Prostate Cancer. Int J Radiat Oncol Biol Phys [Internet]. 2020;

48. Fuller D, Wurzer J, Shirazi R, Bridge S, Law J, Crabtree T, et al. Retreatment for Local Recurrence of Prostatic Carcinoma After Prior Therapeutic Irradiation:

Efficacy and Toxicity of HDR-Like SBRT. Int J Radiat Oncol Biol Phys [Internet]. 2020;106(2):291-299.

49. Jereczek-Fossa BA, Patricia Rojas D, Zerini D, Fodor C, Viola A, Fanetti G, et al. reirradiation for isolated local recurrence of prostate cancer: Mono-institutional series of 64 patients treated with salvage stereotactic body radiotherapy (SBrT). Br J Radiol [Internet]. 2019;92(1094):20180494.

50. Loi M, Di Cataldo V, Simontacchi G, Detti B, Bonomo P, Masi L, et al. Robotic Stereotactic Retreatment for Biochemical Control in Previously Irradiated Patients Affected by Recurrent Prostate Cancer. Clin Oncol [Internet]. 2018;30(2):93-100.

51. D'Agostino GR, Di Brina L, Mancosu P, Franzese C, Iftode C, Franceschini D, et al. Reirradiation of Locally Recurrent Prostate Cancer With Volumetric Modulated Arc Therapy. Int J Radiat Oncol Biol Phys [Internet]. 2019;104(3):614-621.

52. Scher N, Bauduceau O, Bollet M, Lamallem H, Charas T, Garaud P, et al. Stereotactic prostate focal reirradiation therapy for local recurrence: preliminary results of Hartmann Oncology Radiotherapy Group. BJR|Open [Internet]. 2019;1(1):20180027.

53. Cuccia F, Nicosia L, Mazzola R, Figlia V, Giaj-Levra N, Ricchetti F, et al. Linac-based SBRT as a feasible salvage option for local recurrences in previously irradiated prostate cancer. Strahlentherapie und Onkol [Internet]. 2020;196(7):628-636.

54. Matrone F, Revelant A, Fanetti G, Polesel J, Chiovati P, Avanzo M, et al. Partial prostate re-irradiation for the treatment of isolated local recurrence of prostate cancer in patients previously treated with primary external beam radiotherapy: short-term results of a monocentric study. Neoplasma [Internet]. 2020;200622N651.

55. Caroli P, Colangione SP, De Giorgi U, Ghigi G, Celli M, Scarpi E, et al. 68Ga-PSMA-11 PET/CT-Guided Stereotactic Body Radiation Therapy Retreatment in Prostate Cancer Patients with PSA Failure after Salvage Radiotherapy. Biomedicines [Internet]. 2020;8(12):536.

56. European Association of Urology. Prostate Cancer Guidelines 2020. 2020.

57. Mohler JL, Antonarakis ES, Armstrong AJ, D'Amico A V., Davis BJ, Dorff T, et al. Prostate Cancer, Version 2.2019, NCCN Clinical Practice Guidelines in Oncology. J Natl Compr Cancer Netw [Internet]. 2019;17(5).

58. Hoskin PJ, Colombo A, Henry A, Niehoff P, Paulsen Hellebust T, Siebert FA, et al. GEC/ESTRO recommendations on high dose rate afterloading brachytherapy for localised prostate cancer: An update. Radiother Oncol [Internet]. 2013;107(3):325-332.

59. Yamada Y, Rogers L, Demanes DJ, Morton G, Prestidge BR, Pouliot J, et al. American Brachytherapy Society consensus guidelines for high-dose-rate prostate brachytherapy. Brachytherapy [Internet]. 2012;11(1):20–32.

60. Golbari NM, Katz AE. Salvage Therapy Options for Local Prostate Cancer Recurrence After Primary Radiotherapy: a Literature Review. Curr Urol Rep [Internet]. 2017;18(8):63.

61. Corkum MT, D'Souza DP, Chin J, Boldt G, Mendez LC, Bauman GS. Salvage Reirradiation using External Beam Radiotherapy for Local Failure in Prostate Cancer: A Systematic Review. Int J Radiat Oncol [Internet]. 2019;

62. Valle LF, Lehrer EJ, Markovic D, Elashoff D, Levin-Epstein R, Karnes RJ, et al. A Systematic Review and Meta-analysis of Local Salvage Therapies After Radiotherapy for Prostate Cancer (MASTER). Eur Urol. 2020;1(310):1–13.

63. Spratt DE, Scala LM, Folkert M, Voros L, Cohen GN, Happersett L, et al. A comparative dosimetric analysis of virtual stereotactic body radiotherapy to high-dose-rate monotherapy for intermediate-risk prostate cancer. Brachytherapy [Internet]. 2013;12(5):428–33.

64. Tocco BR, Kishan AU, Ma TM, Kerkmeijer LGW, Tree AC. MR-Guided Radiotherapy for Prostate Cancer. Front Oncol [Internet]. 2020;10:1–11.

65. Rose T, Garcia E, Bachand F, Kim D, Petrik D, Halperin R, et al. QOL comparison of acute side effects from a high dose rate vs. low dose rate prostate brachytherapy boost combined with external beam radiotherapy. Brachytherapy [Internet]. 2015;14:S36.

66. Hathout L, Mahmoud O, Wang Y, Vergalasova I, Barkati M, Després P, et al. A Phase 2 Randomized Pilot Study Comparing High-Dose-Rate Brachytherapy and Low-Dose-Rate Brachytherapy as Monotherapy in Localized Prostate Cancer. Adv Radiat Oncol [Internet]. 2019;4(4):631-640.

67. Rodda S, Tyldesley S, Morris WJ, Keyes M, Halperin R, Pai H, et al. ASCENDE-RT: An Analysis of Treatment-Related Morbidity for a Randomized Trial Comparing a

Low-Dose-Rate Brachytherapy Boost with a Dose-Escalated External Beam Boost for High- and Intermediate-Risk Prostate Cancer. Int J Radiat Oncol Biol Phys [Internet]. 2017;98(2):286-295.

68. Hoskin PJ, Rojas AM, Ostler PJ, Bryant L, Lowe GJ. Randomised trial of external-beam radiotherapy alone or with high-dose-rate brachytherapy for prostate cancer: Mature 12-year results. Radiother Oncol [Internet]. 2020;154:214-219.

69. Parry MG, Nossiter J, Sujenthiran A, Cowling TE, Patel RN, Morris M, et al. Impact of High-Dose-Rate and Low-Dose-Rate Brachytherapy Boost on Toxicity, Functional and Cancer Outcomes in Patients Receiving External Beam Radiation Therapy for Prostate Cancer: A National Population-Based Study. Int J Radiat Oncol Biol Phys [Internet]. 2020;S0360-3016.

70. Corkum MT, Mendez LC, Chin J, D'Souza D, Boldt RG, Bauman GS. A Novel Salvage Option for Local Failure in Prostate Cancer, Reirradiation Using External Beam or Stereotactic Radiation Therapy: Systematic Review and Meta-Analysis. Adv Radiat Oncol [Internet]. 2020;5(5):965-977.

71. Jereczek-Fossa BA, Marvaso G, Zaffaroni M, Gugliandolo SG, Zerini D, Corso F, et al. Salvage stereotactic body radiotherapy (SBRT) for intraprostatic relapse after prostate cancer radiotherapy: An ESTRO ACROP Delphi consensus. Cancer Treat Rev. 2021;98:102206.

72. Chen RC, Chang P, Vetter RJ, Lukka H, Stokes WA, Sanda MG, et al. Recommended patient-reported core set of symptoms to measure in prostate cancer treatment trials. J Natl Cancer Inst [Internet]. 2014;106(7):dju132.

73. Skolarus TA, Dunn RL, Sanda MG, Chang P, Greenfield TK, Litwin MS, et al. Minimally important difference for the expanded prostate cancer index composite short form. Urology [Internet]. 2015;85(1):101–106.

74. Kaljouw E, Pieters BR, Kovács G, Hoskin PJ. A Delphi consensus study on salvage brachytherapy for prostate cancer relapse after radiotherapy, a Uro-GEC study. Radiother Oncol [Internet]. 2016;118:122-130.

75. Crook J, Malone S, Perry G, Bahadur Y, Robertson S, Abdolell M. Postradiotherapy prostate biopsies: What do they really mean? Results for 498 patients. Int J Radiat Oncol Biol Phys [Internet]. 2000;28(2):355–367.

76. Murgic J, Morton G, Loblaw A, D'Alimonte L, Ravi A, Wronski M, et al. Focal Salvage High Dose-Rate Brachytherapy for Locally Recurrent Prostate Cancer After Primary Radiation Therapy Failure: Results From a Prospective Clinical Trial. Int J Radiat Oncol Biol Phys [Internet]. 2018;102(3):561-567.

77. De Visschere PJL, Standaert C, Fütterer JJ, Villeirs GM, Panebianco V, Walz J, et al. A Systematic Review on the Role of Imaging in Early Recurrent Prostate Cancer. Eur Urol Oncol [Internet]. 2019;2(1):47–76.

78. Hövels AM, Heesakkers RAM, Adang EM, Jager GJ, Strum S, Hoogeveen YL, et al. The diagnostic accuracy of CT and MRI in the staging of pelvic lymph nodes in patients with prostate cancer: a meta-analysis. Clin Radiol [Internet]. 2008;63(4):387–395.

79. Mertan F V., Greer MD, Borofsky S, Kabakus IM, Merino MJ, Wood BJ, et al. Multiparametric magnetic resonance imaging of recurrent prostate cancer. Top Magn Reson Imaging [Internet]. 2016;25:139–147.

80. Afshar-Oromieh A, Avtzi E, Giesel FL, Holland-Letz T, Linhart HG, Eder M, et al. The diagnostic value of PET/CT imaging with the 68Ga-labelled PSMA ligand HBED-CC in the diagnosis of recurrent prostate cancer. Eur J Nucl Med Mol Imaging [Internet]. 2015;42(2):197–209.

81. Hruby G, Eade T, Kneebone A, Emmett L, Guo L, Ho B, et al. Delineating biochemical failure with 68Ga-PSMA-PET following definitive external beam radiation treatment for prostate cancer. Radiother Oncol [Internet]. 2017;122(1):99-102.

82. Hofman MS, Lawrentschuk N, Francis RJ, Tang C, Vela I, Thomas P, et al. Prostate-specific membrane antigen PET-CT in patients with high-risk prostate cancer before curative-intent surgery or radiotherapy (proPSMA): a prospective, randomised, multicentre study. Lancet [Internet]. 2020;395(10231):1208-1216.

83. Slevin F, Beasley M, Cross W, Scarsbrook A, Murray L, Henry A. Patterns of Lymph Node Failure in Patients With Recurrent Prostate Cancer Postradical Prostatectomy and Implications for Salvage Therapies. Adv Radiat Oncol [Internet]. 2020;5(6):1126-1140.

5.8 Supplementary Material

5.8.1 EMBASE and MEDLINE Search Strategies

From inception of databases until December 14th 2020.

EMBASE

- prostat*.mp.
- (external beam* or ebrt or brachytherapy or hypofractionated or stereotactic or sabr or sbrt or re-irradiation or reirradiation or retreatment or radiosurgery).mp.
- (repeat or recurr* or relapse or salvage).mp.
- 1 and 2 and 3

Exclude Medline Journals

MEDLINE

prostat*[tw] AND (external beam*[tw] OR ebrt[tw] OR brachytherapy[tw] OR hypofractionated[tw] OR stereotactic[tw] OR sabr[tw] OR sbrt[tw] OR re-irradiation[tw] OR reirradiation[tw] OR radiosurgery[mh]) AND (repeat[tw] OR recurr*[tw] OR relapse[tw] OR salvage[tw])

Chapter 6
Reirradiation Options for Previously Irradiated Prostate cancer (RO-PIP): Feasibility Study Investigating Toxicity Outcomes Following Reirradiation with Stereotactic Body Radiotherapy (SBRT) vs. High Dose-Rate Brachytherapy (HDR-BT)

6.1 Abstract

6.1.1 Purpose

Radiotherapy is the most common curative treatment for non-metastatic prostate cancer, however up to 13% of patients will develop local recurrence within 10 years. Patients can undergo further and potentially curative treatment including salvage surgery, brachytherapy (BT), external beam radiotherapy (EBRT), high intensity focused ultrasound and cryotherapy. Systematic review shows that high dose rate (HDR) BT and stereotactic body radiotherapy (SBRT) have the best outcomes in terms of biochemical control and lowest side effects. The RO-PIP trial aims to determine the feasibility of recruitment to a trial randomising patients to salvage HDR-BT or SBRT and provide prospective data on patient recorded toxicity outcomes that will inform a future phase III trial.

6.1.2 Methods and Analysis

The primary endpoint of the RO-PIP feasibility study is to evaluate the patient recruitment potential over 2 years to a trial randomising to either SBRT or HDR-BT for patients who develop local recurrence of prostate cancer following previous radiation therapy. The aim is to recruit 60 patients across 3 sites over 2 years and randomise 1:1 to SBRT or HDR-BT. Secondary objectives include recording clinician and patient reported outcome measures (PROMs) to evaluate treatment-related toxicity. In addition, the study aims to identify potential imaging, genomic and proteomic biomarkers that are predictive of toxicity and outcome based on hypoxia status, a prognostic marker of prostate cancer.

6.1.3 Ethics and dissemination

This study has been approved by the Yorkshire and the Humber - Bradford Leeds Research Ethics Committee (Reference: 21/YH/0305, IRAS: 297060, January 2022). The results will be presented in national and international conferences, published in peer-reviewed journals and will be communicated to relevant stakeholders. A plain English report will

be shared with the study participants, patients' organisations and media. Trial registration number: ISRCTN 12238218.

6.2 Introduction

Prostate cancer is the most common cancer in males in the United Kingdom with approximately 48,500 new diagnoses every year and this has increased over the last 10 years [1]. Worldwide, prostate cancer accounts for over 1.2 million new cases and causes over 350,000 deaths (3.8% of all deaths caused by cancer in men) annually [2]. Radiation therapy (RT) is the most common curative treatment for non-metastatic prostate cancer [3,4]. Despite advances in diagnostic imaging, RT delivery techniques and dose-escalation strategies, treatment failure remains common [5–7]. At 10-years, the biochemical failure rate following treatment for localised prostate cancer with RT alone is 41% [8]. Following dose-escalated RT, the most common site of cancer recurrence is in the prostate with 11-year cumulative incidence of local recurrence 7.2%, and 13% in intermediate, and high risk National Comprehensive Cancer Network (NCCN) prostate cancer groups respectively [7].

Multiple salvage options are available for locally recurrent disease including prostatectomy, reirradiation (with brachytherapy (BT) or external beam radiotherapy (EBRT)) and other focal therapies such as high-intensity focused ultrasound (HIFU) and cryotherapy (CRYO). The evidence on the long-term effectiveness and quality of life impact for these treatments are limited, however reirradiation techniques are the safest and most effective out of the currently available salvage treatment options [9–13]. Most of the published literature describes retrospective case-series with heterogeneous methodologies and radiation treatment techniques with no high level evidence for the superiority of any of the re-irradiation approaches or prospective comparative studies. Only a small proportion of patients with locally recurrent prostate cancer following primary radiotherapy (15-20%) undergo local salvage therapy according to the Cancer of the Prostate Strategic Urologic Research Endeavor (CaPSURE) registry [14].

Prostate BT involves the placement of sealed radiation sources into the prostate and offers the ability to deliver highly conformal high dose radiation with a steep dose gradient and rapid fall off in dose which minimises radiation toxicity to surrounding organs at risk, specifically the rectum and bladder [15]. Advances in image-guided targeted BT may allow for more precise and focused treatments [16–18]. BT can be delivered either via a permanent low-dose rate seed implant (LDR-BT), or via high-dose rate BT (HDR-BT) which uses a high-activity radiation source (e.g. iridium-192) that is temporarily introduced into applicators that are placed within the prostate, typically over 1-3 fractions. HDR-BT is less susceptible to issues related to prostate oedema and seed migration that might complicate dosimetry following LDR-BT. Current evidence suggests that HDR-BT

affords lower toxicity, increased tolerability with similar oncological control compared to LDR-BT [19].

Previously, salvage EBRT techniques have been associated with higher rates of severe late toxicities and also poor local control [20]. Stereotactic body radiation therapy (SBRT), involving the delivery of a high dose of radiation to a highly conformal target volume with a steep dose gradient in a small number of fractions may have benefits. Potential advantages include increased sparing of normal tissues than other types of EBRT, and being less invasive compared to BT [21]. BT is also highly specialised and only available in specialist centres.

A prospective trial is required to describe the toxicity profiles for these two most promising options, HDR-BT and SBRT, to allow clinicians and patients to make an informed decision on the most appropriate salvage treatment choice and help inform a larger study with an efficacy endpoint. Strategies to personalise salvage treatment through finding predictive genomic and imaging biomarkers are also required to optimise treatment outcomes.

The RO-PIP trial is the first prospective randomised trial to determine the feasibility of recruitment to a trial comparing SBRT and HDR-BT for locally recurrent prostate cancer and inform power calculations for a definitive RCT. In addition, this feasibility trial will also quantify the impact on patient reported outcome measures (PROMs), quantify longitudinal functional MRI changes and assess proteomic, immune and genomic biomarkers.

6.3 Methods

6.3.1 Study Design

The Standard Protocol Items for Randomized Trials (SPIRIT) checklist was adhered to when drafting the RO-PIP protocol[22]. Completed SPIRIT checklist in Supplementary Material. A schematic overview of the study is shown in Figure 6.1.

6.3.2 Study Setting

The planned study is a prospective two arm (HDR-BT and SBRT) randomised (1:1) feasibility trial aiming to recruit a total of 60 patients with locally recurrent prostate cancer across three tertiary referral oncology sites (Christie Hospital NHS Foundation Trust, Leeds Teaching Hospitals NHS Trust and Mount Vernon Cancer Centre, UK). The study will open for recruitment in September 2022, and the estimated primary recruitment completion date is in September 2024 and study completion date in September 2026.

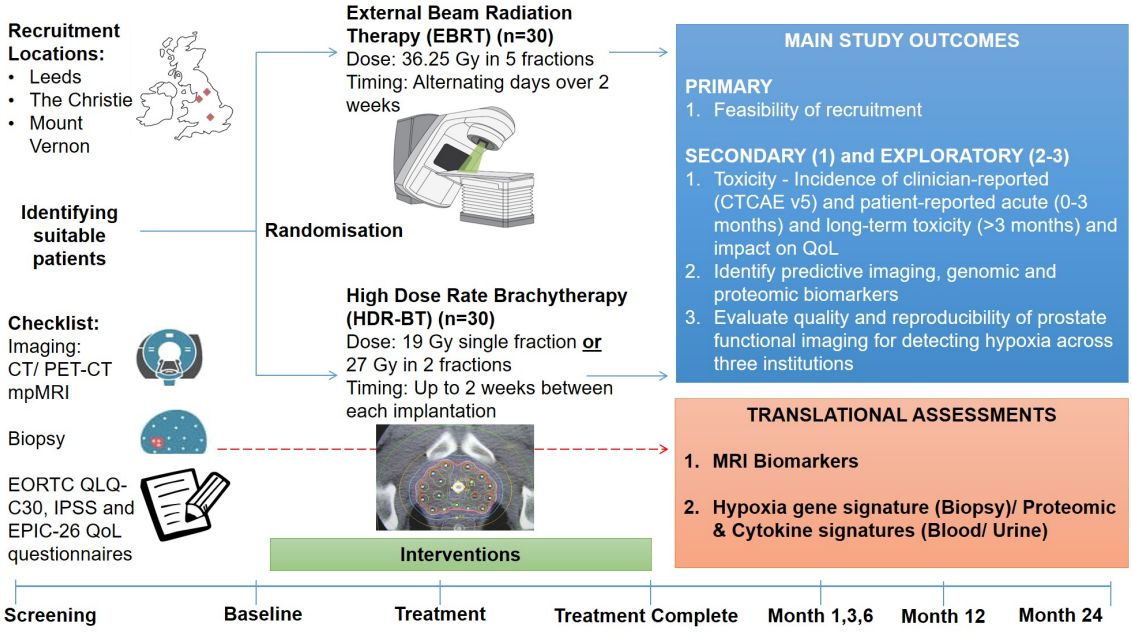

Figure 6.1 Schematic overview of study. Key – CT = Computed Tomography, PET = positron emission tomography, mpMRI = multi-parametric magnetic resonance imaging, EORTC QLQ = European Organization for the Research and Treatment of Cancer Quality of Life Questionnaire, IPSS = international prostate symptom score, EPIC = Expanded Prostate Cancer Index Composite, QoL = quality of life, CTCAE = Common Terminology Criteria for Adverse Events.

6.3.3 Patient and Public Involvement and Engagement (PPIE)

We have sought input from the Leeds Cancer PPIE team and Leeds Radiotherapy user group into the protocol design, lay summary and patient information leaflet and have acted on the information provided.

6.3.4 Consent and Withdrawal

All participants will give written informed consent before entering the study and before any assessments or interventions related to the study are undertaken. Consent will be taken by the direct care clinical oncologist or a member of the RO-PIP research team e.g. clinical research fellow or research nurse. Optional consent will be sought for taking extra blood and urine samples for the translational study component. Participants are free to withdraw at any time, or at the discretion of the chief or principal investigator. In the event of withdrawal, any data collected up until that point will be kept and potentially included in any analyses.

6.3.5 Eligibility Criteria

The inclusion criteria are: (i) Male individuals aged over 18 years; (ii) Histologically confirmed locally recurrent prostate cancer (following previous radiotherapy no less than 2 years ago); (iii) No metastatic disease; (iv) Able and willing to provide an informed consent to participate; (v) World Health Organisation (WHO) performance status 0-2; (vi) Reasonable urinary function (IPSS < 20 and Qmax > 10 ml/second on flow tests); (vii) Greater than 10 year life expectancy.

The exclusion criteria are: (i) Patients who are unfit for a general anaesthetic due to other comorbidities; (ii) Clinical or radiological evidence of metastatic prostate disease; (iii) Any patient with a medical or psychiatric condition that impairs their ability to give informed consent. (iv) contraindication or intolerance of magnetic resonance scanning; (v) Prior prostatectomy; (vi) History of inflammatory bowel disease; (vii) large volume gland not amenable for HDR-BT; (viii) Rectal fistulation; (ix) No rectal access for ultrasound (e.g. previous abdominal perineal resection).

6.3.6 Assignment of Interventions

The treatment decision for the radiation option will been taken at the time of randomisation. Following confirmation of written consent and eligibility, participants will be randomised into the trial by the Leeds Clinical Trials Research Unit (CTRU). Patients will be randomised on a 1:1 basis to receive either HDR-BT or SBRT. Patients will be

randomised using stratified permuted blocks, stratified by recruiting site and previous ADT therapy. Randomisation will be performed centrally using the CTRU 9-5 telephone randomisation system. Authorisation codes and personal identification numbers (PINs), provided by the CTRU, will be required to access the randomisation system

6.3.7 Interventions

6.3.7.1 HDR Brachytherapy

One of two HDR-BT treatment schedules will be decided by the local treatment centre. This will be either a single fraction 19Gy treatment or 27Gy in 2 fractions approximately 2 weeks apart.

Gross tumour volume (GTV) will be delineated based on the intra-prostatic lesion defined on the multi-parametric MRI with or without additional diagnostic PET-CT information; the clinical target volume (CTV) is generated by applying an isotropic 3mm margin constrained by the urethra (where applicable) and rectum. The CTV and planning target volume (PTV) are considered to be the same structures. The rectum, urethra and bladder should be contoured as organs at risk as per the ESTRO guidelines [23].

6.3.7.2 Stereotactic Body Radiation Therapy (SBRT)

Patients will receive 5 fractions of 7.25Gy per fraction which will be delivered on alternate days over no more than 2 weeks to provide a total dose of 36.25Gy. Radiotherapy may be delivered using CyberKnife, linear accelerator or MR-linear accelerator. Implanted prostate markers and SpaceOAR may be used as per centre standard of care.

Gross tumour volume (GTV) will be delineated based on the intra-prostatic lesion defined on the multiparametric MRI with or without additional diagnostic PET-CT information; a clinical target volume (CTV) will be delineated comprising either the whole prostate or for focal treatment the GTV with a 3mm margin constrained to the prostate boundaries. The CTV will then be grown by 3-5mm (dependent on departmental policy and image guidance technique) to generate a PTV. The rectum, bladder, bowel loops (where appropriate) and femoral heads will be contoured as organs at risk.

6.3.8 Additional Interventions

Androgen deprivation therapy (ADT) may be initiated at the discretion of the treating oncologist but this must be started by the time of the first salvage radiotherapy treatment (at first fraction of SBRT or at HDR-BT).

6.3.9 Toxicity Assessment

Clinician reported treatment toxicity will be summarised at each time point as the proportion of patients experiencing each toxicity, summarised by maximum grade experienced as per Common Terminology Criteria for Adverse Events (CTCAE) version 5.0.

6.3.10 PROMs Assessment

Changes in patient reported Health-Related Quality of life (HRQoL)/ PROMs will be assessed using the following validated questionnaires: EPIC-26 (prostate cancer related QoL and functional outcomes), EORTC QLQ-C30 (general QoL score) and IPSS (urinary and sexual functional outcomes). The specific time points for these evaluations are:

- Baseline assessment (prior to salvage treatment)
- 1 month post treatment completion
- 3 months post treatment completion
- 6 months post treatment completion
- 12 months post treatment completion
- 24 months post treatment completion

The PROMs and Quality of Life assessments will not require a separate face to face meeting as these will be posted out to the participants. Follow-up after 2 years will be according to local policy.

6.3.11 Translational MRI Assessment

All patients will have three multiparametric MRIs (including standard anatomical sequences and functional sequences) which will be paired with PROMs assessments at the same time points (at baseline and then post-treatment at 1 month and 1 year). The purpose of this imaging component is four fold:

- To optimise a multiparametric MRI scanning protocol across three institutions incorporating intravoxel incoherent motion (IVIM), dynamic contrast enhanced (DCE) imaging and blood oxygenation level dependent (BOLD) sequences
- To evaluate image quality and reproducibility of prostate functional imaging for detecting tissue perfusion and hypoxia
- To investigate prostate and pelvic anatomical and functional imaging changes related to prostate reirradiation and how this relates to patient reported toxicity side effects (determined by PROMs).
- To study the hypoxia MRI changes seen in the prostate in association with biopsy derived hypoxia-associated gene signature.

MRI scans done within the research study will be stored on the Leeds Teaching Hospitals Picture Archive and Communication System (PACS) server and on the local hospital PACS server where the images were obtained.

6.3.12 Translational Biological Assessment

The aim of this study component is to collect biological parameters that are prognostic and predictive markers of radiotherapy response and correlate this with imaging. From a biological stance the following sample collection will be relevant for assessing this:

- Tissue collection (prostate biopsy including original diagnostic and local recurrence sample) to measure the presence of a hypoxia-associated gene signature.
- Urine collection to measure the inflammatory response via damage-associated molecular patterns.
- Blood sample collection (20-30ml) to measures changes in cytokine response following reirradiation and other proteomics analyses.

The long-term storage arrangement for the research data arising from these biological samples will follow The University of Manchester Biobank (site of processing for biological samples) good practice for research guidance on clinical samples. Participants will have the option to consent to making their biological samples available for future research. The biological sample research data will be stored for 20 years once the study has ended.

6.3.13 Baseline and Follow-up Evaluation

Table 1 shows the full schedule of events

Table 6.1 RO-PIP schedule of events.

Time-point / Item	Baseline	During RT	1 month FU	3 month FU	6 month FU	12 month FU	18 month FU	24 month FU
Informed consent	x							
Registration	x							
Testosterone	x							
Confirmation of eligibility	x							
Randomisation to BT or SBRT	x							
Pre-treatment Prostate Biopsy sample requested and stored	x							
Collection of clinical history and outcome data	x							x
Radiotherapy (BT or SBRT) details	x	x						
PSA test	x			x	x	x	x	x
Functional prostate mpMRI	x		x			x		
PROM assessment (EPIC-26, EORTC QLQ-C30 and IPSS)	x		x	x	x	x		x
Research blood test/ Urine	x		x	x	x			
Clinician reported adverse events		x	x	x	x	x	x	x

6.4 Outcomes

6.4.1 Primary outcome

1. Recruitment rates for the whole 24-month recruitment period will be reported overall and per recruiting site. The average recruitment rate per month and in total over the formal monitoring period will be reported.
The study recruitment period is 24 months. To show that patient recruitment targets for a phase III RCT can be met within an adequate timeframe, a "steady state" of recruitment should be observed. In this feasibility study, formal monitoring of recruitment will begin from the start of the patient recruitment where an average of two patients per month must be randomised over the remaining recruitment period in order to demonstrate a "steady state" of recruitment.

6.4.2 Secondary outcomes

1. Incidence of patient reported acute (0-3 months) and long-term toxicity (>3 months) and impact on QoL determined by EPIC-26 (prostate cancer related QoL and functional outcomes), EORTC QLQ-C30 (general QoL score) and international prostate symptom score (IPSS) (urinary and sexual functional outcomes) measurements (Key secondary endpoint).

2. Incidence of clinician-reported treatment toxicity as per Common Terminology Criteria for Adverse Events (CTCAE) version 5.0.

3. Other feasibility endpoints include screening log summaries, treatment and questionnaire compliance, withdrawal rate and reasons for non-recruitment.

6.4.3 Exploratory outcomes

1. MRI biomarkers at 1 month and 1 year post-treatment predictive of toxicity based on PROMs.

2. Hypoxia levels based on a hypoxia associated gene signature obtained from the pre-salvage RT biopsy correlated with MRI biomarkers.

3. Changes in the levels of inflammatory cytokine signatures from urine and blood obtained at baseline and after reirradiation in relation to PROMs.

4. Multiple measures of image quality and reproducibility of prostate functional imaging (e.g. diffusion coefficient values from IVIM sequences) for measuring tumour biology will be summarised.

6.5 Sample size

This is an exploratory feasibility study, and there is no informative data in the published literature on which to base a sample size calculation. Therefore, a formal statistical power calculation has not been performed. Feasibility studies are not usually sufficiently powered to provide estimates of effect size, but instead aim to determine the feasibility of specific study aspects and to enable estimation of sample size parameters to inform future studies. For this feasibility study, we plan to recruit 60 patients in total (i.e. 30 to each treatment arm) from three UK hospitals (Leeds Cancer Centre, The Christie and Mount Vernon Cancer Centre), all of which are high-volume tertiary prostate cancer treatment centres. This sample size has been informed by the National Institute of Health Research (NIHR) guidance on feasibility sample sizes and the toxicity outcome data from a recent systematic review[13,24]. Few studies have evaluated PROMs feasibility, establishing the need for this trial[25]. It is estimated that this number of participants will provide an adequate sample to estimate the toxicity rates for the key secondary endpoint in each arm (i.e. 30 per arm)[26,27]. Recruiting 60 patients over 2 years, across 3 centres, would mean an average recruitment rate of less than 1 patient per centre per month. This information, combined with the estimated toxicity rates from the study, will be used to determine feasibility of a subsequent larger scale RCT.

6.6 Recruitment

Sixty patients will be recruited over a 24-month period, approximately 2-3 patients per month (across 3 sites).

6.7 Reporting

No formal interim analysis will take place however a study report will be produced for review by the independent data monitoring and ethics committee (DMEC) approximately midway through the study. The aim of the report is to evaluate and monitor the key study objectives (i.e. recruitment rates, number of participants taking up their treatment allocation), as well as expected adverse events (AEs) and serious adverse events (SAEs) and the delivery time of HDR-BT or SBRT post-randomisation.

6.8 Withdrawal of Participants

Participants who withdraw their consent to the study will be taken off the study. The research team will keep any tissue, blood, urine samples and imaging data already collected

and continue analysis (unless the patient requests the destruction of samples and data). Patients will be consented from the outset to continue collecting follow-up data even if patients are withdrawn from the trial, cannot tolerate MRI scans, unable to continue treatment or do not complete all PROMs time points.

6.9 Data Management

Study data will be managed by the trial coordinator and research fellow under the supervision of the chief investigator and the study statistician.

Data stored on hospital computers will be password protected and in locked rooms in the local hospital radiotherapy and/or radiology (imaging data) departments, only accessible by the local research team. Each patient is assigned a unique patient study ID number at enrolment (based on site and trial number allocated during randomisation step) which will be used on all trial documentation. This pseudoanonymisation step will prevent the patient from being identified by those outside the local research team. The local investigator will keep a subject enrolment and identification log that contains the key to the code, i.e. a record of the personal identification data linked to each patient study ID number.

In compliance with Good Clinical Practice guidelines and in accordance with the University of Leeds Code of Conduct and Research Ethics, the chief or local principal investigator will maintain all records regarding the conduct of the RO-PIP study. These will be securely archived for up to 20 years if required.

6.10 Statistical Analysis

As this is a feasibility study, it will not involve hypothesis testing to identify whether the intervention has had an impact. Instead, data analysis will be descriptive and involve summary statistics. The analysis of all primary endpoint and all secondary endpoints relating to recruitment and withdrawals from the trial will take place at the end of the 24-month recruitment period. Final analysis of all other endpoint data will be carried out 6 months after the final participant has been randomised.

6.11 Future Work

Demonstrating feasibility will facilitate a larger randomised study comparing salvage re-irradiation options with ADT alone, the usual management option. This study would have

primary endpoints of survival (overall and metastasis free). This is the first time that a hypoxia gene expression signature will be studied with hypoxia imaging in a prospective cohort of patients with radiorecurrent prostate cancer and could lead to the further studies investigating the introduction in clinical practice of tumour hypoxia testing (from biopsy and/ or imaging) and the biological individualisation of radiotherapy. Given the large number of prostate cancer patients who undergo radiotherapy each year, this would have a significant impact on personalised medicine in the UK.

6.12 Trial Oversight

A trial management group will be convened for the study, consisting of the chief investigator, principal investigators (for each site), research fellow, trial administrator, and research nurse. The group will meet monthly. The study sponsor (University of Leeds) will monitor the conduct of the trial. A trial report will be produced by the DMEC midway through the study

6.13 Ethics and Dissemination

This study has been approved by the Yorkshire and The Humber - Bradford Leeds Research Ethics Committee (Reference: 21/YH/0305, IRAS: 297060, January 2022) (Appendix A).

The results will be presented in national and international conferences, published in peer-reviewed journals, publicised via social media channels such as twitter, and will be communicated to relevant stakeholders. A plain English report will be shared with the study participants, patients' organisations, PPIE groups and media.

6.14 References

1. Cancer Research UK. Cancer Incidence from Cancer Intelligence Statistical Information Team at Cancer Research UK [Internet]. 2019.

2. Bray F, Ferlay J, Soerjomataram I, Siegel RL, Torre LA, Jemal A. Global cancer statistics 2018: GLOBOCAN estimates of incidence and mortality worldwide for 36 cancers in 185 countries. CA Cancer J Clin [Internet]. 2018;68:394–424.

3. Mottet N, Bellmunt J, Bolla M, Briers E, Cumberbatch MG, De Santis M, *et al.* EAU-ESTRO-SIOG Guidelines on Prostate Cancer. Part 1: Screening, Diagnosis, and Local Treatment with Curative Intent. Eur Urol [Internet]. 2017;71(4):618–29.

4. Cancer Research UK . Prostate cancer treatment statistics [Internet]. 2017.

5. Beckendorf V, Guerif S, Le Prisé E, Cosset JM, Bougnoux A, Chauvet B, *et al.* 70 Gy versus 80 Gy in localized prostate cancer: 5-year results of GETUG 06 randomized trial. Int J Radiat Oncol Biol Phys [Internet]. 2011;80(4):1056–63.

6. Zumsteg ZS, Spratt DE, Romesser PB, Pei X, Zhang Z, Kollmeier M, *et al.* Anatomical patterns of recurrence following biochemical relapse in the dose escalation era of external beam radiotherapy for prostate cancer. J Urol [Internet]. 2015;194(6):1624-1630.

7. Ma TM, Chu F-I, Sandler H, Feng FY, Efstathiou JA, Jones CU, *et al.* Local Failure Events in Prostate Cancer Treated with Radiotherapy: A Pooled Analysis of 18 Randomized Trials from the Meta-analysis of Randomized Trials in Cancer of the Prostate Consortium (LEVIATHAN). Eur Urol. 2022;

8. Jones CU, Hunt D, McGowan DG, Amin MB, Chetner MP, Bruner DW, *et al.* Radiotherapy and Short-Term Androgen Deprivation for Localized Prostate Cancer. N Engl J Med. 2011;365(2):107–18.

9. Mbeutcha A, Chauveinc L, Bondiau PY, Chand ME, Durand M, Chevallier D, *et al.* Salvage prostate re-irradiation using high-dose-rate brachytherapy or focal stereotactic body radiotherapy for local recurrence after definitive radiation therapy. Radiat Oncol [Internet]. 2017;

10. Ingrosso G, Becherini C, Lancia A, Caini S, Ost P, Francolini G, *et al.* Nonsurgical Salvage Local Therapies for Radiorecurrent Prostate Cancer: A Systematic Review and Meta-analysis. Eur Urol Oncol [Internet]. 2019;3(2):183–97.

11. Chade DC, Eastham J, Graefen M, Hu JC, Karnes RJ, Klotz L, *et al.* Cancer control and functional outcomes of salvage radical prostatectomy for radiation-recurrent prostate cancer: A systematic review of the literature. Eur Urol [Internet]. 2012;61(5):961–71.

12. Valle LF, Lehrer EJ, Markovic D, Elashoff D, Levin-Epstein R, Karnes RJ, *et al.* A Systematic Review and Meta-analysis of Local Salvage Therapies After Radiotherapy for Prostate Cancer (MASTER). Eur Urol. 2020;1(310):1–13.

13. Zhong J, Slevin F, Scarsbrook AF, Serra M, Choudhury A, Hoskin PJ, *et al.* Salvage Reirradiation Options for Locally Recurrent Prostate Cancer: A Systematic Review. Front Oncol. 2021;11.

14. Cooperberg MR, Vickers AJ, Broering JM, Carroll PR. Comparative risk-adjusted mortality outcomes after primary surgery, radiotherapy, or androgen-deprivation therapy for localized prostate cancer. Cancer [Internet]. 2010;116:5226–5234.

15. Chatzikonstantinou G, Zamboglou N, Rödel C, Zoga E, Strouthos I, Butt SA, *et al.* High-dose-rate brachytherapy as salvage modality for locally recurrent prostate cancer after definitive radiotherapy: Asystematic review. Strahlentherapie und Onkol [Internet]. 2017;193:683–691.

16. Chitmanee P, Tsang Y, Tharmalingam H, Hamada M, Alonzi R, Ostler P, *et al.* Single-Dose Focal Salvage High Dose Rate Brachytherapy for Locally Recurrent Prostate Cancer. Clin Oncol [Internet]. 2020;32(4):259-265.

17. Murgic J, Morton G, Loblaw A, D'Alimonte L, Ravi A, Wronski M, *et al.* Focal Salvage High Dose-Rate Brachytherapy for Locally Recurrent Prostate Cancer After Primary Radiation Therapy Failure: Results From a Prospective Clinical Trial. Int J Radiat Oncol Biol Phys [Internet]. 2018;102(3):561-567.

18. Slevin F, Hodgson S, Rodda SL, Bownes P, Bottomley D, Adiotomre E, *et al.* Efficacy and toxicity outcomes for patients treated with focal salvage high dose rate brachytherapy for locally recurrent prostate cancer. Clin Transl Radiat Oncol [Internet]. 2020;23:20-26.

19. Hathout L, Mahmoud O, Wang Y, Vergalasova I, Barkati M, Després P, *et al.* A Phase 2 Randomized Pilot Study Comparing High-Dose-Rate Brachytherapy and Low-Dose-Rate Brachytherapy as Monotherapy in Localized Prostate Cancer. Adv Radiat Oncol [Internet]. 2019;4(4):631-640.

20. Zilli T, Benz E, Dipasquale G, Rouzaud M, Miralbell R. Reirradiation of Prostate Cancer Local Failures After Previous Curative Radiation Therapy: Long-Term Outcome and Tolerance. Int J Radiat Oncol Biol Phys [Internet]. 2016;96:218–322.

21. Pasquier D, Martinage G, Janoray G, Rojas DP, Zerini D, Goupy F, *et al.* Salvage Stereotactic Body Radiation Therapy for Local Prostate Cancer Recurrence After Radiation Therapy: A Retrospective Multicenter Study of the GETUG. Int J Radiat Oncol Biol Phys [Internet]. 2019;105(4):727-734.

22. Chan A-W, Tetzlaff JM, Altman DG, Laupacis A, Gøtzsche PC, Krleža-Jerić K, *et al.* SPIRIT 2013 Statement: Defining Standard Protocol Items for Clinical Trials. Ann Intern Med. 2013;158(3):200.

23. Salembier C, Villeirs G, De Bari B, Hoskin P, Pieters BR, Van Vulpen M, *et al.* ESTRO ACROP consensus guideline on CT- and MRI-based target volume delineation for primary radiation therapy of localized prostate cancer. Radiother Oncol. 2018;127(1):49–61.

24. Hooper R. Justifying sample size for a feasibility study (NIHR Guidance) [Internet]. 2021. Available from: https://www.rds-london.nihr.ac.uk/resources/justify-sample-size-for-a-feasibility-study/

25. Skolarus TA, Dunn RL, Sanda MG, Chang P, Greenfield TK, Litwin MS, *et al.* Minimally important difference for the expanded prostate cancer index composite short form. Urology [Internet]. 2015;85(1):101–106.

26. Lancaster GA, Dodd S, Williamson PR. Design and analysis of pilot studies: recommendations for good practice. J Eval Clin Pract. 2004;10(2):307–12.

27. Billingham SA, Whitehead AL, Julious SA. An audit of sample sizes for pilot and feasibility trials being undertaken in the United Kingdom registered in the United Kingdom Clinical Research Network database. BMC Med Res Methodol. 2013;13(1):104.

6.15 Supplementary Material

6.15.1 Multi-parametric Prostate MRI Protocol for RO-PIP Study

6.15.1.1 Additional Exclusion Criteria for patients consenting to MRI

- Patients must be able to tolerate/ comply with imaging protocol (i.e. be able to lie still and not have non-MRI compatible devices e.g. pacemaker).
- Patients must have an estimated glomerular filtration rate of greater than 30 mL/min

6.15.1.2 Key points

- All patients enrolled on this study will require a pre-salvage treatment MRI and post-treatment MRI (at 1 and 12 months).
- This will be done at the same time as the radiotherapy planning scan where possible
- The following protocol has been designed using the European Society of Urogenital Radiology (ESUR) 2012 guidelines [1] and UK consensus meeting guidelines [2].
- MRIs will be performed using 1.5- and 3.0-T scanners at 3 sites (Leeds Cancer Centre, The Christie and Mount Vernon Cancer Centre).
- This adapted radiorecurrent prostate cancer MRI protocol has an estimated acquisition time of approximately 45-60 minutes.
- It includes standard multi-parametric sequences such as T1- and T2-weighted, dynamic contrast enhanced (DCE) and diffusion-weighted imaging (DWI) covering the pelvic region (this is likely to be scanner and hospital-site dependent).
- Additional sequences/ parameters to image hypoxia will be added, which are the blood oxygenation level-dependent (BOLD) and intravoxel incoherent motion (IVIM) techniques. Both these sequences will be performed in the axial plane and before contrast injection.

6.15.1.3 Preparation

- The patient should be consented and screened for MRI safety as per departmental local rules.
- The patient's weight in kilograms (kg) should be recorded for specific Absorption Rate (SAR) level and intravenous contrast administration purposes.

- Patients will be changed into a hospital gown as per local departmental rules.
- Intravenous injection of gadolinium will be required for all MRI scans. The dose of gadolinium (Dotarem or Gadovist) recommended is 0.1mmol/kg.
- Prior to entering the scan room all patients should be asked to use the toilet to empty their rectum of stool and bowel gas when possible.
- All patients will be offered an enema in order to help with clearance of air and stool from the rectum to improve the quality of the prostate MRI. Use will be at the discretion of the team.
- Patients should be consented and screened to assess their suitability to administer intravenously/intramuscularly an anti-peristaltic drug to reduce bowel motion (e.g. Buscopan or Glucagon). Unless contraindicated (For Buscopan this would include heart disease and for Glucagon this would be diabetes), this drug can be administered once the patient is comfortable on the MRI scanner.
- A phased array body coil or coil bridge may be used.

6.15.1.4 Positioning

The patient should be positioned supine on the scan table. If after the first localizer view the rectum is still filled with air, then consideration to scan the patient prone to decompress the rectum is advised.

6.15.1.5 Sequences

Minimum axial MRI sequences (in scanning order) to include:

- T2 (3D acquisition)
- BOLD (3D)
- DWI/ ADC
- IVIM
- T1 (large field of view) (2D or 3D)
- DCE

6.15.1.6 Archive

The reconstructed MR data will be archived locally and shared only with the central research team.

6.15.1.7 Reporting

Each site's MRI scans will be centrally reviewed for quality before recruitment. The MRI scans will be interpreted by 2 radiologists who have experience in reporting prostate MRI scans. A reporting template will be used to help standardise the extracted information

6.15.1.8 Additional Image Acquisition Points

- Acquire MRI using the femoral heads as bony landmarks to achieve true orthogonal axial and coronal images of the prostate (rather than along the prostate gland base to apex axes)
- Anatomic coverage for all three planes includes; superiorly the bladder neck, all of the seminal vesicles through the prostate gland to inferiorly the prostate apex. Laterally the medial aspects of the femoral heads and posteriorly the anterior rectum and all of the seminal vesicles. Anteriorly the symphysis pubis should also be included
- BOLD sequence – a radiologist will select the axial slices that contains the maximum tumour dimension for the BOLD imaging. Multiple gradient-recalled echo images will be acquired at the tumour location with varying TE, from 5 to 75 ms in 10-ms intervals (example parameters: TR=100 ms, flip angle =40°, field of view=200 mm, 256x256 matrix, SL=8 mm) from which R2* maps will be calculated (5-6 minutes)
- IVIM imaging– This will involve acquiring diffusion weighted imaging with several additional b-values between 0 and 1000 s/mm2 in addition to the standard b-values obtained
- Planned b-values (Diagnostic Scanner) of 0, 50, 100, 200, 300, 400, 500, 600, 700, 800, 900, and 1,000 s/mm2 and (MR-Linac) 0, 50, 100, 200, 300, 400 and 500
- DCE-MRI sequence will require high temporal resolution (<10 s) and consists of a series of axial T1WI gradient echo sequences covering the entire prostate before, during and after IV bolus injection (2–3 mL/s) of gadolinium contrast (4 second

temporal resolution). Variable flip angles will be used to allow for quantitative analysis.

6.15.1.9 Data Transfer

Anonymised imaging, radiotherapy and clinical data will be shared between Mount Vernon, The Christie, Leeds Teaching Hospitals NHS Trust and University of Leeds for patients within the study to allow a more complete analysis. This will be explicit in the consent form. Following de-identification of the imaging data at the local site, anonymised data will be sent to the research team using the secure and encrypted NHS Egress platform (https://lft.nhs.net). All imaging will be stored securely in a RO-PIP trial specific folder on the Leeds Teaching Hospitals NHS Server which can only be accessed by the study chief investigator, principal investigators and members of the research team.

6.15.1.10 Data Analysis

This feasibility study is intended to be hypothesis generating for future studies. Therefore, it is not designed to demonstrate statistical significance and no formal sample size calculation will be performed. Quantitative perfusion maps will be derived from the T2* BOLD sequences. Quantitative DCE-MRI analysis will be undertaken using Platform for Research in Medical Imaging (PMI) or Madym Open Source Software. BOLD and IVIM data will be analysed using in-house developed software and DIPY (a 3D/4D+ imaging library in Python – https://dipy.org/). The whole prostate and lesion will be contoured in Raystation (v11.1). DICOM images and contour structures will be imported in WorldMatch (v9.0) to generate masks for whole prostate, lesion, and background prostate gland (with lesion subtracted away from the whole prostate). These masks will be used to calculate volume (mm3) for the lesion and background prostate. WorldMatch will be used to generate re-sampled masks to apply to parameter maps from quantitative imaging sequences. Correlations with radiotherapy isodoses and toxicity endpoints will be investigated. Descriptive statistics will be presented, including the median and inter-quartile range (IQR) values obtained for the lesion and background prostate.

6.15.1.11 References

1. Barentsz JO, Richenberg J, Clements R, Choyke P, Verma S, Villeirs G, Rouviere O, Logager V, Fütterer JJ; European Society of Urogenital Radiology. ESUR prostate MR guidelines 2012. Eur Radiol. 2012 Apr;22(4):746-57.

2. Brizmohun Appayya M, Adshead J, Ahmed HU, Allen C, Bainbridge A, Barrett T, Giganti F, Graham J, Haslam P, Johnston EW, Kastner C, Kirkham APS, Lipton A, McNeill A, Moniz L, Moore CM, Nabi G, Padhani AR, Parker C, Patel A, Pursey J, Richenberg J, Staffurth J, van der Meulen J, Walls D, Punwani S. National implementation of multi-parametric magnetic resonance imaging for prostate cancer detection - recommendations from a UK consensus meeting. BJU Int. 2018 Jul;122(1):13-25.

SPIRIT

STANDARD PROTOCOL ITEMS: RECOMMENDATIONS FOR INTERVENTIONAL TRIALS

SPIRIT 2013 Checklist: Recommended items to address in a clinical trial protocol and related documents*

Section/item	ItemNo	Page No	Description
			Administrative information
Title	1	1	Descriptive title identifying the study design, population, interventions, and, if applicable, trial acronym
Trial registration	2a	2	Trial identifier and registry name. If not yet registered, name of intended registry
	2b	2	All items from the World Health Organization Trial Registration Data Set
Protocol version	3	1	Date and version identifier
Funding	4		Sources and types of financial, material, and other support
Roles and responsibilities	5a	1	Names, affiliations, and roles of protocol contributors
	5b	1	Name and contact information for the trial sponsor
	5c	1	Role of study sponsor and funders, if any, in study design; collection, management, analysis, and interpretation of data; writing of the report; and the decision to submit the report for publication, including whether they will have ultimate authority over any of these activities
	5d	1	Composition, roles, and responsibilities of the coordinating centre, steering committee, endpoint adjudication committee, data management team, and other individuals or groups overseeing the trial, if applicable (see Item 21a for data monitoring committee)
Introduction			
Background and rationale	6a	4	Description of research question and justification for undertaking the trial, including summary of relevant studies (published and unpublished) examining benefits and harms for each intervention

	6b	4	Explanation for choice of comparators
Objectives	7	2	Specific objectives or hypotheses
Trial design	8	2	Description of trial design including type of trial (eg, parallel group, crossover, factorial, single group), allocation ratio, and framework (eg, superiority, equivalence, noninferiority, exploratory)
			Methods: Participants, interventions, and outcomes
Study setting	9	6	Description of study settings (eg, community clinic, academic hospital) and list of countries where data will be collected. Reference to where list of study sites can be obtained
Eligibility criteria	10	6	Inclusion and exclusion criteria for participants. If applicable, eligibility criteria for study centres and individuals who will perform the interventions (eg, surgeons, psychotherapists)
Interventions	11a	7	Interventions for each group with sufficient detail to allow replication, including how and when they will be administered
	11b	6	Criteria for discontinuing or modifying allocated interventions for a given trial participant (eg, drug dose change in response to harms, participant request, or improving/worsening disease)
	11c	7	Strategies to improve adherence to intervention protocols, and any procedures for monitoring adherence (eg, drug tablet return, laboratory tests)
	11d	7	Relevant concomitant care and interventions that are permitted or prohibited during the trial
Outcomes	12	10/11	Primary, secondary, and other outcomes, including the specific measurement variable (eg, systolic blood pressure), analysis metric (eg, change from baseline, final value, time to event), method of aggregation (eg, median, proportion), and time point for each outcome. Explanation of the clinical relevance of chosen efficacy and harm outcomes is strongly recommended
Participant timeline	13	9/10	Time schedule of enrolment, interventions (including any run-ins and washouts), assessments, and visits for participants. A schematic diagram is highly recommended (see Figure)

Sample size	14	12	Estimated number of participants needed to achieve study objectives and how it was determined, including clinical and statistical assumptions supporting any sample size calculations
Recruitment	15	12	Strategies for achieving adequate participant enrolment to reach target sample size
			Methods: Assignment of interventions (for controlled trials)
Allocation:			
Sequence generation	16a	12	Method of generating the allocation sequence (eg, computer-generated random numbers), and list of any factors for stratification. To reduce predictability of a random sequence, details of any planned restriction (eg, blocking) should be provided in a separate document that is unavailable to those who enrol participants or assign interventions
Allocation concealment mechanism	16b	12	Mechanism of implementing the allocation sequence (eg, central telephone; sequentially numbered, opaque, sealed envelopes), describing any steps to conceal the sequence until interventions are assigned
Implementation	16c	12	Who will generate the allocation sequence, who will enrol participants, and who will assign participants to interventions
Blinding (masking)	17a	n/a	Who will be blinded after assignment to interventions (eg, trial participants, care providers, outcome assessors, data analysts), and how
	17b	n/a	If blinded, circumstances under which unblinding is permissible, and procedure for revealing a participant's allocated intervention during the trial
			Methods: Data collection, management, and analysis

Data collection methods	18a	12/13	Plans for assessment and collection of outcome, baseline, and other trial data, including any related processes to promote data quality (eg, duplicate measurements, training of assessors) and a description of study instruments (eg, questionnaires, laboratory tests) along with their reliability and validity, if known. Reference to where data collection forms can be found, if not in the protocol
	18b	13	Plans to promote participant retention and complete follow-up, including list of any outcome data to be collected for participants who discontinue or deviate from intervention protocols
Data management	19	13	Plans for data entry, coding, security, and storage, including any related processes to promote data quality (eg, double data entry; range checks for data values). Reference to where details of data management procedures can be found, if not in the protocol
Statistical methods	20a	13	Statistical methods for analysing primary and secondary outcomes. Reference to where other details of the statistical analysis plan can be found, if not in the protocol
	20b	14	Methods for any additional analyses (eg, subgroup and adjusted analyses)
	20c	13/14	Definition of analysis population relating to protocol non-adherence (eg, as randomised analysis), and any statistical methods to handle missing data (eg, multiple imputation)
			Methods: Monitoring
Data monitoring	21a	13	Composition of data monitoring committee (DMC); summary of its role and reporting structure; statement of whether it is independent from the sponsor and competing interests; and reference to where further details about its charter can be found, if not in the protocol. Alternatively, an explanation of why a DMC is not needed
	21b	12	Description of any interim analyses and stopping guidelines, including who will have access to these interim results and make the final decision to terminate the trial

Harms	22	12	Plans for collecting, assessing, reporting, and managing solicited and spontaneously reported adverse events and other unintended effects of trial interventions or trial conduct
Auditing	23	12	Frequency and procedures for auditing trial conduct, if any, and whether the process will be independent from investigators and the sponsor
			Ethics and dissemination
Research ethics approval	24	2	Plans for seeking research ethics committee/institutional review board (REC/IRB) approval
Protocol amendments	25	12	Plans for communicating important protocol modifications (eg, changes to eligibility criteria, outcomes, analyses) to relevant parties (eg, investigators, REC/IRBs, trial participants, trial registries, journals, regulators)
Consent or assent	26a	6	Who will obtain informed consent or assent from potential trial participants or authorised surrogates, and how (see Item 32)
	26b	6	Additional consent provisions for collection and use of participant data and biological specimens in ancillary studies, if applicable
Confidentiality	27	13	How personal information about potential and enrolled participants will be collected, shared, and maintained in order to protect confidentiality before, during, and after the trial
Declaration of interests	28	18	Financial and other competing interests for principal investigators for the overall trial and each study site
Access to data	29	14	Statement of who will have access to the final trial dataset, and disclosure of contractual agreements that limit such access for investigators
Ancillary and post-trial care	30	19	Provisions, if any, for ancillary and post-trial care, and for compensation to those who suffer harm from trial participation

Dissemination policy	31a	15	Plans for investigators and sponsor to communicate trial results to participants, healthcare professionals, the public, and other relevant groups (eg, via publication, reporting in results databases, or other data sharing arrangements), including any publication restrictions
	31b	15	Authorship eligibility guidelines and any intended use of professional writers
	31c	15	Plans, if any, for granting public access to the full protocol, participant-level dataset, and statistical code
Appendices			
Informed consent materials	32	Available	Model consent form and other related documentation given to participants and authorised surrogates
Biological specimens	33	14	Plans for collection, laboratory evaluation, and storage of biological specimens for genetic or molecular analysis in the current trial and for future use in ancillary studies, if applicable

*It is strongly recommended that this checklist be read in conjunction with the SPIRIT 2013 Explanation & Elaboration for important clarification on the items. Amendments to the protocol should be tracked and dated. The SPIRIT checklist is copyrighted by the SPIRIT Group under the Creative Commons "Attribution-NonCommercial-NoDerivs 3.0 Unported" license.

Chapter 7
Discussion

7.1 Summary of aims

This thesis investigated different aspects of the prostate cancer diagnostic and radiation-related therapeutic pathway, including the role of MRI radiomic analysis for prediction of prostate tumour hypoxia (Chapter 2), the utility of MRI-derived radiomic and hypoxia gene signatures in predicting biochemical recurrence after prostate radiotherapy (Chapter 3), the impact of longitudinal radiomic feature changes within organs at risk during MRI-guided prostate radiotherapy (Chapter 4), the evidence base underpinning use of salvage radiotherapy for retreatment of locally recurrent prostate cancer (Chapter 5), and the design of a prospective clinical trial to elucidate the best radiotherapy modality for prostate reirradiation (Chapter 6).

The sections in this chapter will summarise each study, and the limitations and potential future work are discussed.

7.2 Prediction of prostate tumour hypoxia using pre-treatment MRI-derived radiomics: preliminary findings (Chapter 2)

7.2.1 Summary

This study explored the utility of models based on RFs extracted from T2W whole prostate gland magnetic resonance imaging (MRI) and clinical features for the prediction of prostate tumour hypoxia compared to an externally validated hypoxia gene signature (training = 156, test = 39). The study cohort consisted of 195 consecutive patients undergoing radiotherapy at two oncology centres with histologically confirmed high-risk prostate cancer. Six different machine learning models (ridge regression, random forest, elastic net, k-nearest neighbour (KNN), support vector machine (SVM), and least absolute shrinkage and selection operator (LASSO)) were trained and tuned using five-fold cross-validation stratified around hypoxia status (normoxia or hypoxia) with 25 repeats.

The best performing model based on mean AUC derived from the ROC curve was tested on the unseen test set. This was a ridge regression model which selected five radiomic features including logarithm grey level size zone matrix large area emphasis (GLSZM LAE) and four wavelet transformed features. Wavelet transformed features are when low- (L) or high-pass (H) filters are applied to the volumetric images, resulting in eight different

decomposed volumes of images which can be labelled as LLL, LLH, LHL, LHH, HLL, HLH, HHL and HHH. For example, LLH means the images have been transformed by using the low-pass filters on the X and Y axis, and a high-pass filter on the Z-axis. The four wavelet features selected by the model were LLH grey level co-occurrence matrix (GLCM) cluster prominence, HLL GLCM maximal correlation coefficient (MCC), HLH first-order median and HHH GLCM MCC. No clinical features were selected despite integrating all clinical variables into the model. The radiomic model had a mean training validation AUC of 0.71 (SD 0.10) and outperformed the clinical model which had a mean training validation AUC of 0.60 (SD 0.08). The AUC on the unseen test set was 0.69 (95% CI 0.55-0.83).

7.2.2 Limitations

As described in Chapter 2, there are a number of limitations to the study:
Manual segmentation was used which is arduous and time consuming even for experienced radiologists and can impact on the reproducibility and robustness of radiomic studies, however to ensure feature robustness was appropriately tested, a proportion of cases were re-segmented and interclass correlation coefficient (ICC) used to exclude (non-reproducible) features with high intra-observer variation (if ICC < 0.8). A discretisation method was chosen based on the combination of voxel size and bin number, 1 and 256 respectively, that had the largest number of robust radiomic features. Using this method does not consider whether radiomic features with little variation are actually robust and if they actually improve overall model performance. Both variation and robustness of radiomic features need to be considered.

Genomic profiling and imaging were performed over several years, scanner technology and imaging protocols have evolved in the interim; imaging data used were all acquired on 1.5 Tesla (T) scanners and many did not incorporate functional imaging sequences as this was not routine at the time of the initial imaging acquisition. Including MRI scans from two different centres acquired on a range of different scanners with varied acquisition parameters could be considered a limitation as there is a chance for random errors/ noise to be present within the model from the heterogeneous imaging acquired. Paradoxically however using this "real-world" dataset across two oncology centres may improve the generalisability of the prediction model.

Similarly, the transcriptomic data were generated from small historic biopsy specimens which has its own limitations. The genomics of tumour hypoxia are highly complex, involving increased genomic instability and gene-level mutations involving several oncogenes and tumour suppressor genes[1]. Using one specific gene signature may be

oversimplifying this process, however a pragmatic approach to radiogenomic model creation is required, given the scarcity of combined clinical, pathological, genomic and imaging datasets.

Only T2W MR images were used to develop radiomic models and whole prostate segmentations were used to extract radiomic features as not all cases had a visible tumour on the anatomical imaging, and it was not possible to match the site of the biopsy taken which is what was used to generate the gene signature.

7.2.3 Future work

Convolutional neural networks (CNNs) have shown promise in segmentation of the whole prostate gland, prostate zonal anatomy and tumours [2]. Training CNNs remains challenging without verified ground truth image data given that biopsy data is limited, particularly with regards to spatial location, an issue encountered in the study described in Chapter 2. Another potential limitation of CNNs is the lack of transparency of how networks reach a decision, which could impact on the trust and acceptance amongst clinicians and ultimately patients who are the end users that would be affected if such AI tools translate into routine clinical use. A recent review on the acceptance of artificial intelligence (AI) amongst healthcare professionals highlighted safety as one of the most important factors, for example AI systems addressing more complex tasks, such as surgical robots, were perceived as less reliable, more risky and therefore less trustworthy[3]. In situations where an AI tool provides a treatment recommendation that differs from a clinician's expectations, the explainability component allows verification as to whether the parameters considered by the AI tool make sense from the clinical perspective [4]. Explainable models must be able to quantify why certain predictions are made[5]. For example, Selvaraju et al. proposed a novel gradient-weighted class activation mapping (Grad-CAM) method for visualising important components of an image in the model decision-making process [6]. This technique, which was applied to images of animals, used spatial information preserved through convolutional layers to understand which parts of an input image are most important for a classification decision, which could also be applied to medical imaging. The output of the Grad-CAM method is a class discriminative localisation map (or heat map) which highlights the most important pixels of a particular class and offers greater clarity on which aspects of the imaging give the most predictive information. This helps with explainability of the AI tool for clinicians and patients by providing a visual representation of how different imaging features contributed to the final risk assessment. By using these tools appropriately, explainable AI could enhance patient experience by

making them better informed and more knowledgeable about their health condition.

The next step is to compare hypoxia radiomics signatures with specialised MR-imaging methods developed to visualise hypoxia in prostate tumours. Intravoxel incoherent motion (IVIM) is a technique than can detect the imbalance between oxygen consumption and supply and has been shown to provide quantifiable measurements which correlate with pimonidazole-staining used to identify hypoxia on histopathological specimens[7]. It would be beneficial for future studies to establish a reproducible method of mapping the location of biopsy samples from the index lesion to the prostate MRI to allow direct correlation of imaging features with pathological and genomic findings. Combining biological samples such gene signatures with quantitative functional MRI should help to provide a more comprehensive understanding of the hypoxia phenotype and lead to more informed treatment decisions in prostate cancer. Oxygen-enhanced MRI (OE-MRI) is an emerging technique offering a practical tool to assess oxygenation in normal tissues and tumours with excellent spatial resolution compared to other imaging modalities such as positron emission tomography (PET), which requires specialist radiochemistry, expensive radiopharmaceuticals and local expertise that are a barrier to clinical translation [8]. OE-MRI can measure the change in longitudinal relaxation rate (R1) of blood and tissues following inhalation of 100% oxygen or carbogen [9]. Inhaled oxygen molecules dissolve in blood plasma and interstitial fluid resulting in an increase in R1 (ΔR1) via a paramagnetic contrast effect [10]. Including OE- MRI in multiparametric assessment of prostate cancer has been shown to be feasible and sheds further light into the biology of the tumour microenvironment [11]. OE-MRI also offers the opportunity to monitor tumour oxygenation on hybrid imaging systems that combine real-time MRI with radiotherapy delivery. MRI Linear Accelerator (MRI-LINAC) systems can facilitate personalised biology-guided adaptive radiotherapy (BiGART) by targeting hypoxic tumours through dose painting or other techniques [12]. The clinical translation of these novel sequences from diagnostic MRI systems to MRI-LINAC systems has been shown to be feasible and have demonstrated excellent repeatability in the imaging hypoxia biomarkers, showing promise for guiding future clinical trials [13].

As different MRI sequences reflect diverse aspects of tumour biology, combining other analytical techniques, including radiomics, might provide complimentary information with a higher predictive value for early treatment response. Further testing in larger prospective cohorts is required in the first instance. Standardisation of MRI protocols across institutions would also assist to improve reproducibility [14]. Better understanding of temporal changes in visible and quantifiable (radiomic) imaging

features is also required as these may differ between patients and even within the tumour of the same patient. In addition, the relevance of observed radiomic or other quantitative MRI metric changes in relation to treatment outcomes, such as survival, biochemical recurrence or toxicity, needs to be more comprehensively studied to confirm if these could be utilised as predictive imaging biomarkers in the future.

7.3 Adding MRI radiomics and hypoxia gene signature scores to clinical variables improves prediction of biochemical recurrence-free survival after prostate radiotherapy (Chapter 3)

7.3.1 Summary

This experiment investigated the potential utility of combining radiomic features extracted from pre-treatment MRI, hypoxia-associated gene signature information and clinical data for predicting biochemical recurrence free survival (BCRFS) after radiotherapy in a twin centre cohort of men with prostate cancer. 187 patients were included from 2 centres. The combined clinical-radiomics-hypoxia model (c-index 0.73 [0.68-0.75]) and clinical-radiomics model (c-index 0.72 [0.68-0.74]) performed equally well and outperformed the clinical-only (c-index 0.67 [0.62-0.70]) and clinical-hypoxia (c-index of 0.68 [0.62-0.69) models. The selected features of the combined clinical-radiomics model included age, International Society of Urological Pathology (ISUP) grade, tumour stage, tumour volume, radiotherapy modality and wavelet-derived radiomic features.

Akaike Information Criterion (AIC) was used to compare performance of the models since this provides a method to balance goodness of fit of a model with its complexity or the number of parameters used. The smaller the AIC statistic the better the model fit. When comparing the AIC of the combined models back with the clinical only model (null model), the inclusion of radiomics improved the model ($p=0.013$), whereas the inclusion of hypoxia-associated gene signature did not ($p=0.079$), unless it was also combined with the radiomics ($p=0.005$). Based on AIC, the overall best-fit model was the combined clinical, radiomic and hypoxia model (AIC=536.79).

The conclusion from this preliminary work was that adding pre-treatment MRI-derived radiomic features to clinical variables improves the accuracy of predicting BCRFS after prostate radiotherapy, with or without the addition of hypoxia gene signature.

7.3.2 Limitations

As this was a retrospective study, the MRI data acquired was historic, mostly biparametric and acquired from several different MR scanners across multiple institutions where patients had been referred from before prior to their radiotherapy treatment at one of two oncology centres (Leeds Cancer Centre and The Christie). MRI-based radiomics features are highly sensitive to acquisition and reconstruction parameters that affect the arbitrary intensity values generated on the MR image[15,16]. It was necessary to apply an image normalisation step to the image data in order to reduce variation in imaging appearances caused by these differences in imaging protocols, equipment, and acquisition parameters. In addition, ComBat harmonisation, was further applied to the extracted radiomic feature data in order to pool all the radiomic data without it being negatively impacted by multiple sources/ scanners, whilst maintaining the biological information and ensuring comparability between centres. There is a risk that applying ComBat results in the loss of the original physical meaning of harmonised radiomic features due to the data being manipulated in order to account for all samples and if externally validating an MRI-based radiomic signature in a new cohort of patients, ComBat would need to be re-applied on all available data[17].

Only T2W MR imaging was available for all the included study patients due to the historic MRIs available. Functional imaging sequences such as diffusion weighted imaging (DWI) which measures underlying tumour cell density and water diffusion provides additional information on the cellular microenvironment and would add to the prognostic information offered by the T2W sequence, which is mainly used for detailing anatomy [7]. A radiomics signature derived from DWI outperformed a model using T2W MRI-derived radiomic features for predicting survival in cervical cancer patients [18]. In prostate cancer, a combined DWI and T2W survival prediction model outperformed models using only one of these sequences when predicting 3-year progression-free survival [19]. Future prostate radiomic models would further benefit from adding in these functional sequences.

Only one hypoxia-associated gene signature was used which has its own limitations as the Ragnum signature is essentially a combination of genes whose expression is correlated with pimonidazole, another hypoxia biomarker [20]. As this gene signature requires expression profiling platforms measuring relative mRNA abundance, it is affected by the biopsy sample preservation technique (e.g. fresh-frozen or FFPE), age of the FFPE blocks and by technical batch effect which limits comparison of these hypoxia scores between different institution cohorts.

7.3.3 Future work

Biopsy-derived gene expression signatures show promise as prognostic hypoxia biomarkers and a number of signatures have been developed and validated on different patient cohorts. These signatures are processed from small tissue samples taken from only a small part of a tumour which may fail to characterise the full extent of the disease given the presence of multi-focal tumours and intra-tumoural heterogeneity and differences in gene expression between tumours or parts of the tumour that also impact on molecular information. It is also important to note that the majority of prostate biopsies taken in this study were not MRI-targeted biopsies which is now current practice, and there is a chance that clinically significant cancers were missed as the PROMIS trial found over half of clinically significant cancers seen on MRI were missed with a standard transrectal biopsy undertaken without MRI-guidance [21]. Samples taken now are likely to be more representative of tumour behaviour with MRI visible prostate lesions generally more aggressive, larger in size and correlated with higher histological grade [22]. There is an increasing shift towards an MRI-guided approach to prostate cancer care. Recently, the ReIMAGINE study further highlighted the potential role and advantage of MRI in screening for prostate cancer, over other tests such as PSA. After identifying that one in six screened men, out of 303 patients, had a prostate lesion on MRI, the study found that two in three men with a positive MRI and more than half of the men with significant cancer on biopsy had a PSA $<$3 ng/mL [23]. A larger MRI-led approach to screening may be warranted to investigate if this could reduce prostate cancer mortality and reduce overdiagnosis.

Dedicated hypoxia-imaging offers an opportunity to visualise changes throughout the entire prostate gland and facilitate longitudinal measurements to be performed, for example to monitor treatment response. One way to indirectly assess hypoxic changes in the prostate is by measuring perfusion and vascular changes because hypoxia results in increased expression of pro- and anti-angiogenic factors leading to the formation of abnormal and disorganised vascular networks [24]. Dynamic contrast-enhanced (DCE) MRI is an established method for imaging perfusion and permeability in prostate cancer [25]. In the pre-clinical setting, DCE-MRI has been shown to detect naturally occurring and treatment-induced tumour hypoxia, and predict hypoxia-associated radiation response and hypoxia-induced metastasis, in pancreatic and cervical cancer and melanoma [26]. Clinical studies of using DCE-MRI for measuring prostate tumour hypoxia are limited, with only one pilot study involving six patients who had in vivo MR imaging prior to radical prostatectomy [27]. Hypoxia-related gene signatures were used as surrogates of ground truth for hypoxia. The MRI sequences included DCE-MRI as well as T2W imaging, DWI and blood oxygen-level dependent (BOLD) imaging.

Textural features were also extracted. In the correlation analysis, six quantitative MRI features including the Ktrans metric from DCE-MRI were correlated with the hypoxia gene expressions, and 28 textural features extracted from the T2W image were also correlated. A further subanalysis was performed to validate the results observed in the initial correlation analysis. Immunohistochemistry staining was performed using the hypoxia marker glucose transporter 1 (GLUT-1). Pearson correlation coefficients were calculated on a voxel level between all the candidate MRI features and GLUT-1 IHC which found that the only significantly correlated imaging features to be 16 of the T2W textural features and none of the quantitative MRI metrics. This study also identified several hypoxia-related genes that were strongly associated with quantitative MRI metrics including several genes related to cellular structure and tissue development such as P4HA2, DDIT4, SERPINE1 and VEGFA. Overall, the associations between quantitative MRI and gene signatures offers potential to develop combined imaging, radiomic and genomic signatures that could be tested in larger prospective cohorts [7,28, 29,30, 31].

7.4 Exploratory Study of Bladder and Rectum Radiomic Feature Changes Following External Beam Radiation Therapy Delivered on a Magnetic Resonance Imaging Linear Accelerator (MRI-LINAC) (Chapter 4)

7.4.1 Summary

The ability to detect changes in the organs at risk during prostate radiotherapy may facilitate better prediction of toxicity symptoms and help with patient management. In this exploratory study, the aim was to design a robust and reproducible approach to assessing rectal and bladder wall changes in MRI-based longitudinal radiomic features (RFs) across a course of treatment in men undergoing MRI-guided radiotherapy for prostate cancer. 21 men were included, 10 receiving conventional fractionation external beam radiotherapy (EBRT) (60Gy in 20 fractions over four weeks) and 11 receiving stereotactic ablative radiotherapy (SABR) (36.25Gy in 5 fractions over two weeks) respectively. Changes between EBRT and SABR were also compared. All patients were scanned and treated on the 1.5T Unity MRI-LINAC (Elekta AB, Stockholm, Sweden) at The Christie Hospital (Manchester, UK).

We demonstrated a feasible approach to measuring the longitudinal RF changes in the organs at risk during and following prostate radiotherapy which provides opportunities for

future research in this area. Statistically significant changes ($p<0.05$) were seen in the EBRT cohort in 6 rectal RFs as early as fraction 10 over the population. Different RF trends were observed in the EBRT bladder group across 5 time points in patients with and without GU toxicity. Fewer longitudinal changes in the radiomic profiles were observed in the SABR group.

7.4.2 Limitations

This was a small case series of only 21 patients, not designed or powered to identify statistically significant changes within treatment or toxicity subgroups. The majority of patients who experienced acute toxicity had grade 1 toxicity with only three patients having more than grade 1 toxicity. The nature of this study was exploratory and limited conclusions can be drawn about the role of longitudinal radiomics in predicting toxicity at this stage. It serves as hypothesis generating research that can facilitate more extensive data collection with a longer duration of follow-up to allow for late toxicity information to be collected. Late toxicity occurs in approximately 10% and any future work would likely need larger patient numbers.

One of the technical limitations was the choice of using a 2 mm uniform contraction of the rectal contour to define the rectal wall as this may still have included material from within the rectal lumen given the variable appearance of the rectum ranging from a fully collapsed structure to a distended rectum with gas or luminal contents. The bladder thresholding technique used could also have included surrounding peri-vesical fat or bladder contents however for the purposes of radiomic feature extraction, only the manually contoured bladder wall volumes were used.

7.4.3 Future work

There is an opportunity to further validate this toxicity radiomic signature in a larger external dataset by using the paired imaging and clinical outcome data available from the Multi-OutcoMe EvaluatioN of radiation Therapy (MOMENTUM) study [28]. This is a prospective international registry, which is an academic-industrial partnership between seven hospitals and industry partner Elekta who produce the 1.5T Unity MRI-LINAC (Elekta AB, Stockholm, Sweden). In addition to toxicity, the expanded dataset with long-term follow-up will allow for correlation of these longitudinal radiomic changes to additional clinical outcomes including late toxicity i.e., occurring more than 3 months after completion of RT and tumour control. Only first-order RFs were included in this initial analysis which focuses on the distribution of voxel intensities however second-order features such as shape or texture will be analysed in future.

Measuring tissue responses during a radiotherapy course using routinely collected MR imaging, and potentially radiomic feature analysis, could enable further personalisation and adaptation of treatment based on identifying patients at higher risk of toxicity or patients who have tumours that are responding poorly to treatment. Future work can also use dose-surface mapping to further understand the relationship between anatomical radiation dose, OAR tissue response and toxicity symptoms.

In addition to the OAR, the prostate can be assessed longitudinally using the MRI-LINAC particularly with the advent of using quantitative MRI sequences. DCE-MRI has a defined role in the diagnostic pathway for prostate cancer however the need for MRI contrast agent injections, limits its role for daily treatment response monitoring which could be achieved with the MRI-LINAC platforms. One alternative sequence to DCE-MRI is intravoxel incoherent motion (IVIM) imaging, a technique based on DWI which was mentioned in an earlier section. Using different diffusion weighting (b-values), both the intravascular water movement or perfusion and extravascular water molecule diffusion can be quantified using apparent diffusion coefficient (ADC) [29]. Using an IVIM model, the DW-MR signal from the intravascular water molecules transported via the blood can be separated from the signal from the extravascular water diffusion[29]. This enables the calculation of a fractional blood volume (fBV) and integrating fBV with ADC allows for the indirect assessment of hypoxia by effectively calculating oxygen consumption and supply leading to the development of consumption and supply-based hypoxia (CSH) imaging [7,30,31]. A study correlating pre-operative CSH prostate imaging with pimonidazole stained prostatectomy specimens further validated the robustness and biological rationale for CSH imaging[7]. A study of 43 patients with prostate cancer treated on the 1.5T MRI-LINAC had IVIM measurements at every treatment fraction (20 in total) [32]. The IVIM diffusion coefficient metric of the tumour increased over the course of treatment, while it remained stable in the non-cancerous prostate, highlighting a potential to discover IVIM metrics that could predict treatment response at an earlier time point.

7.5 Salvage Reirradiation Options for Locally Recurrent Prostate Cancer: A Systematic Review (Chapter 5)

7.5.1 Summary

A systematic review of literature evaluating the oncological and toxicity outcomes following salvage brachytherapy (BT) and external beam radiation therapy (EBRT) in locally radiorecurrent prostate cancer was performed. Thirty nine studies comprising

1967 patients were included (28 BT and 11 EBRT). In 35 studies (90%), the design was single centre and/or retrospective and no randomised prospective studies were found. Only one third of studies included Patient Reported Outcome Measures (PROMs). All EBRT studies used stereotactic body radiation therapy (SBRT). Twelve BT studies used low dose-rate BT (LDR-BT) only, 11 used high dose-rate BT (HDR-BT) only, 4 used LDR-BT or HDR-BT and one used pulsed-dose rate only.

This systematic review found that both salvage HDR-BT and SBRT provided similar biochemical control and low rates of late GU and GI toxicity. Salvage LDR-BT however had reports of higher late GU/GI toxicity. Prospective randomised trials directly comparing HDR-BT with SBRT and assessing PROMs as well as cancer control outcomes in the setting of prostate reirradiation are needed.

7.5.2 Limitations

The overall quality of the included reirradiation studies was low largely due to missing or unreported data and inconsistencies in reporting of outcome and toxicity data. The majority of studies were non-comparative retrospective case series with differences in baseline patient demographics, primary and/or salvage treatments, reported endpoints and use of androgen deprivation therapy (ADT). The treatment fractionation schedules and delivery approach were also highly variable. A meta-analysis was therefore not conducted to quantitatively compare the studies.

Only one third of studies in the systematic review reported PROMs therefore the impact of reirradiation on quality of life was not well assessed, particularly with SBRT where only one of the eleven included studies evaluated PROMs outcomes. It is likely that the true rates of toxicity experienced by patients were underestimated by only using clinician reported tools [33]. The Consolidated Standards of Reporting Trials Patient Reported Outcome (CONSORT-PRO) extension in 2013 addressed how to best report PROs in clinical trials and studies and meta-analyses found trials using PROs as a primary endpoint were associated with more favourable PRO reporting highlighting the attention that is required to improve collection of PROMs[34,35]. Brachytherapy radiotherapy trials were associated with better PROM reporting [35].

Using validated PROM questionnaires such as the Expanded Prostate Cancer Index (EPIC) tool may help to identify patients most at risk of significant toxicity from salvage therapies by finding those who already have baseline GU and GI symptoms. Integrating longitudinal PROM assessments into future clinical trials is important to ascertain the time-dependent nature of treatment toxicity onset/resolution after treatment [33,36].

7.5.3 Future work

This systematic review highlighted and reinforced the need for a future prospective randomised trial comparing BT and EBRT. It has informed the EBRT and HDR-BT dose fractionation approach for a prospective trial. This has directly led to the development of the RO-PIP trial which was discussed in Chapter 6.

Since the systematic review was undertaken, there have been further publications on salvage RT for recurrent prostate cancer. A single centre retrospective study of 20 patients found the two-year progression-free survival (PFS) rate to be 81.5% [37]. In addition, the study showed that prostate reirradiation delayed the need for ADT for 12–39 months which helped preserve patient quality of life. Reirradiation was well tolerated and all completed their treatment. No grade 3 toxicity was reported. Study limitations were heterogenous patient characteristics including variable irradiation of the pelvis, previous hormonal therapy, and the presence of lymph node disease in 20% of patients. The patients in this study also had no pathological confirmation of local recurrence and diagnosis was based on PET and MRI imaging. A further multicentre retrospective study of MRI-guided SBRT (n=18) treated with a total dose ranging from 25 to 40 Gy in 5 fractions reported no grade 2 acute GU toxicity events and 22.2% acute GI toxicity events, with a one-year local control rate of 88.9% [38]. As with the majority of studies included in this systematic review, this study was affected by the small patient cohort size given that only centres with capabilities to deliver MRI-guided RT were included. Further limitations were the heterogeneous range of prescription RT doses and the limited follow-up period. Ultimately, these issues limit the conclusions that can be drawn about the effectiveness and toxicity of salvage BT and SBRT. Prospective trials with clear entry criteria and standardised treatment protocols are still needed to validate the toxicity and long-term clinical outcomes associated with the salvage treatment of locally recurrent prostate cancer.

7.6 Reirradiation Options for Previously Irradiated Prostate cancer (RO-PIP): Feasibility study investigating toxicity outcomes following reirradiation with stereotactic body radiotherapy (SBRT) versus high-dose-rate brachytherapy (HDR-BT) (Chapter 6)

7.6.1 Summary

The reirradiation options for previously irradiated prostate cancer (RO-PIP) trial is the first randomised control trial that aims to determine the feasibility of recruitment to a

trial randomising patients to salvage HDR-BT or SBRT and provide prospective data on patient recorded toxicity outcomes that will inform a future phase III trial. As this trial has a 2 year recruitment window from the point at which the final recruitment site has opened, followed by a 2 year follow-up period, it will continue after the completion of my PhD.

At the point of writing up this thesis, 4 patients had been recruited over a period of 10 months since the first site opened, although all 3 sites have only been open for 3 months.

7.6.2 Limitations

Due to the feasibility design of the study, it was not powered to assess for differences in outcome between SBRT and HDR-BT arms. Delays were experienced between the trial receiving ethical approval to the opening of the trial at the 3 sites with over 6 months between the first and the final site opening. This has affected the screening and recruitment of potential trial patients. The RO-PIP Trial timelines are highlighted in Figure 7.1.

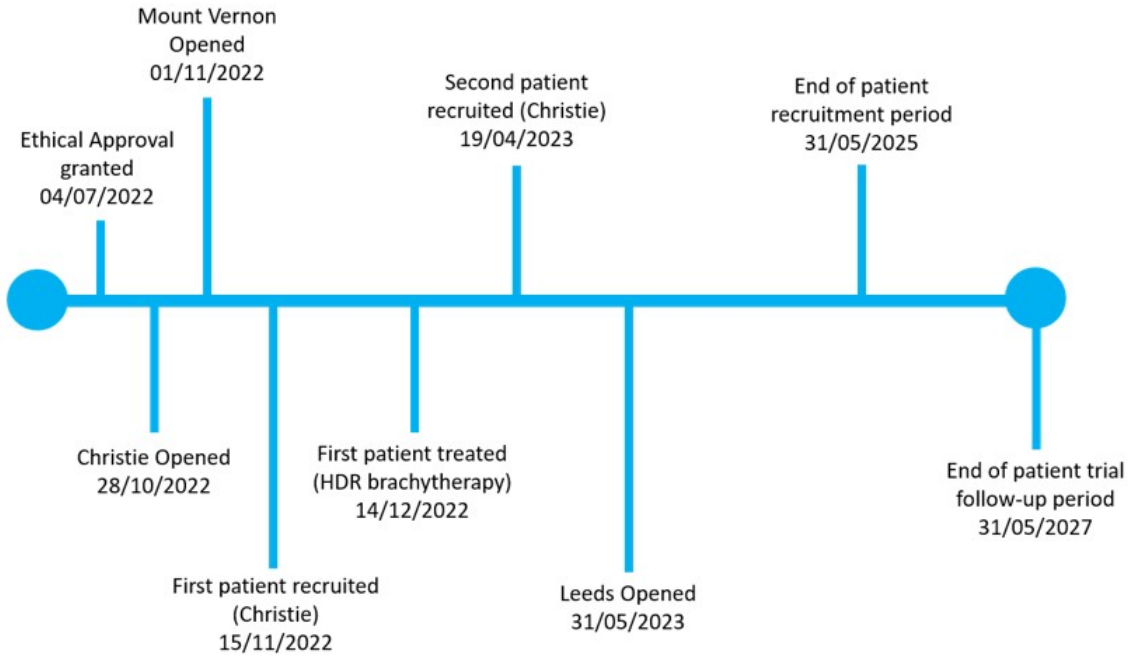

Figure 7.1 Current RO-PIP Trial Timelines

To date the main reasons that potential screened trial patients were not eligible was due to delays in awaiting further investigations e.g. PSMA PET-CT, failure to meet the inclusion criteria pre-salvage prostate specific antigen (PSA) or general anaesthetic or thrombosis concerns.

After feedback from the study sites about recruitment after the first 6 months of trial opening, it was decided that amendments to the study inclusion/ exclusion criteria would be required to increase the pool of potential participants. The criteria amended included removing the exact pre-salvage radiotherapy PSA cut off of less than 50 ng/ml as some patients may be very close to this threshold but only slightly over and should still be offered treatment. Inclusion criteria 7 has been amended from 'biochemical recurrence' to 'recurrence' to reflect that all patients would have biopsy-confirmed local recurrence anyway (standard of care). Finally, inclusion criteria 15 has been amended so there is greater flexibility for androgen deprivation therapy (ADT) to be given at the discretion of the treating oncologist. None of these changes have any implications on the patient or participants already on the study. The specification for treatment duration of the 2 fraction HDR-Brachytherapy arm has also been amended (the two treatments can be performed 1 day to 2 weeks apart) to allow more flexibility between treatment technique at participating sites and enable more patients to be recruited. The amendment was granted by the Health Research Authority on 8th June 2023 and implemented at all sites.

7.6.3 Future work

At completion, this study will determine the feasibility of recruitment to a prostate reirradiation trial with different RT treatment arms. If it were to be feasible to recruit patients then a phase 3 trial would be designed that would be powered to assess the difference in oncological and toxicity outcomes between the two treatments. Even if the trial was not feasible, the study will help in setting up a standardised radiotherapy treatment protocol, including dose fractionation and delivery for salvage prostate radiotherapy that would help inform future multicentre studies.

The translational work in this study will seek to further understand the role of MR imaging in the global hypoxia assessment of the prostate tumour and whole gland following radiotherapy. The addition of intravoxel incoherent motion (IVIM), dynamic contrast-enhanced (DCE) imaging and blood oxygenation level dependent (BOLD) sequences into the imaging protocol will allow for a comprehensive assessment of perfusional and cellular changes after radiotherapy. These imaging changes will be correlated to the pre-radiotherapy biopsy derived hypoxia-associated gene signature and cytokine/ proteomic response to enhance our understanding of local and systemic impact of radiotherapy.

7.7 Future perspectives and considerations

Innovation and rapid technological developments in medicine, including artificial intelligence and genome sequencing, have led to the emergence of radiogenomics, a new state-of-the-art computational field that has the potential to change the practice of personalised medicine [39].

Chapter 2 demonstrated the feasibility of using features derived from anatomical T2W MRI for predicting prostate tumour hypoxia compared to a pimonidazole validated hypoxia-associated gene signature. Given that hypoxia is linked to metastatic disease and radioresistance, there is an opportunity to improve treatment of hypoxic prostate tumours. Recent approaches to safely increase radiation doses to the dominant intraprostatic lesions has shown promising results, with the aim of overcoming the effects of hypoxia, an approach called biologically adapted radiotherapy[40]. This relies on an MRI-guided approach and tumour hypoxia mapping. There is an opportunity to develop a radiogenomic approach to identify the most hypoxic or aggressive tumours using routinely acquired multiparametric MRI. Future work requires correlation of radiogenomic signatures with hypoxia MRI sequences such as IVIM and OE-MRI [7,10].

Preliminary results integrating either radiomics or biopsy-based hypoxia-associated gene signatures into clinical prediction models have demonstrated improved accuracy of predicting survival and disease progression [19,20,41]. Chapter 3 investigates how these imaging-based and genomic biomarkers relate to each other in prostate cancer and their combined impact on survival outcomes to understand how to fully exploit any synergistic potential. In cervical cancer, using a multifactorial biomarker that incorporates both imaging and gene expression signatures gave better prediction of progression free survival [42]. Future testing of a combined imaging and genomic model in external datasets is vital to show whether this is generalisable and has a role in future clinical decision making. Before radiomic signatures can be tested in a clinical trial setting, a reproducible pipeline must be established including standardisation of image acquisition, pre-processing, analysis and data mining processes [43]. Current radiomics approaches largely use basic intensity, shape and textural features extracted from a region of interest however integrating more functional information into a radiogenomic signature, e.g. derived from quantitative MRI or PET, would help to develop more biologically meaningful parameters [43]. Incorporating a radiogenomic signature with a deep learning model would also allow it to be deployed in trials, with studies in gastrointestinal and brain tumours demonstrating the potential of using such approaches, with further roles in predicting response to immunotherapy as well [44–47].

The lack of predictive biomarkers for radiation-related toxicity and morbidity is a major unmet need in modern radiation therapy. Chapter 4 demonstrates a feasible approach to measuring the longitudinal radiomic feature changes in the pelvic organs at risk (bladder and rectum) during MRI-guided prostate radiotherapy which provides opportunities for future research in this area to identify metrics for measuring tissue responses during radiotherapy that can aid treatment adaptation and optimisation.

Better understanding the landscape of prostate reirradiation is a key priority, with regards to patient selection and choice of radiotherapy technique. Chapter 5 systematically reviewed published literature which overall was of low quality with missing or unreported data on both clinical and toxicity outcomes, along with a lack of standardised treatment techniques and dose fractional schedules. This work did reveal that the best evidence to date for reirradiation and salvage treatment was for HDR-BT or EBRT and reinforced the need for a future prospective randomised trial comparing these. This led to the design of a prospective feasibility study (Chapter 6) which is ongoing and should provide data on patient recorded toxicity outcomes that will inform a future phase III trial.

7.8 Conclusions

This thesis has addressed several aspects of prostate cancer non-surgical treatment pathway, by exploring advanced imaging analysis to predict tumour hypoxia, combining radiomic and hypoxia-associated gene signature information with clinical data to guide more accurate outcome prediction, identifying potential imaging markers of radiation toxicity, evaluation of the optimal radiation treatment modality for reirradiation and provisionally assessed the potential for imaging to assist with biologically adapted radiotherapy in the future. The relationship between MRI biomarkers and tumour hypoxia has been studied to better understand how this biological phenomenon can be predicted non-invasively using imaging and the integration of clinical data with imaging and genomic information to better predict how patients respond to radiotherapy treatment. Systematically reviewing the prostate reirradiation literature highlighted the need for prospective comparative studies comparing salvage brachytherapy with EBRT for locally recurrent prostate cancer and this led to the design of the RO-PIP study which will evaluate HDR-BT with EBRT in a randomised control trial setting. It is hoped the completion of this trial, the first of its kind, will help inform the future of salvage prostate reirradiation and provide useful information on the side effect profile of these treatments including the impact on quality-of-life assessments. I have gained

useful experience in setting this trial up, including liaising with different institutions and stakeholders such as working with Leeds Clinical Trials Unit and initiating translational collaborations with the Manchester Cancer Research Centre Biobank to facilitate prostate sample processing and storage which will enable future research evaluating the impact of radiotherapy on hypoxia-associated gene signatures. The protocol development, completion and submission of the ethics application for a multi-centre study will be invaluable experience for future trials with which I am involved with. The retrospective imaging and hypoxia biomarker work has also helped inform the design of the prospective trial which includes novel MRI sequences designed to better understand the hypoxic changes within the prostate and tumour, and how these are altered by radiotherapy treatment. This should help guide future translational research and offer opportunities to design imaging biomarker driven prostate radiotherapy trials.

7.9 References

1. Bhandari V, Hoey C, Liu LY, Lalonde E, Ray J, Livingstone J, *et al.* Molecular landmarks of tumor hypoxia across cancer types. Nat Genet. 2019 Feb 14;51(2):308–18.

2. Gunashekar DD, Bielak L, Hägele L, Oerther B, Benndorf M, Grosu AL, *et al.* Explainable AI for CNN-based prostate tumor segmentation in multi-parametric MRI correlated to whole mount histopathology. Radiation Oncology. 2022 Dec 2;17(1):65.

3. Lambert SI, Madi M, Sopka S, Lenes A, Stange H, Buszello CP, *et al.* An integrative review on the acceptance of artificial intelligence among healthcare professionals in hospitals. NPJ Digit Med. 2023 Jun 10;6(1):111.

4. Amann J, Blasimme A, Vayena E, Frey D, Madai VI. Explainability for artificial intelligence in healthcare: a multidisciplinary perspective. BMC Med Inform Decis Mak. 2020 Dec 30;20(1):310.

5. Barredo Arrieta A, Díaz-Rodríguez N, Del Ser J, Bennetot A, Tabik S, Barbado A, *et al.* Explainable Artificial Intelligence (XAI): Concepts, taxonomies, opportunities and challenges toward responsible AI. Information Fusion. 2020 Jun;58:82–115.

6. Selvaraju RR, Cogswell M, Das A, Vedantam R, Parikh D, Batra D. Grad-CAM: Visual Explanations from Deep Networks via Gradient-Based Localization. In: 2017 IEEE International Conference on Computer Vision (ICCV). IEEE; 2017. p. 618–26.

7. Hompland T, Hole KH, Ragnum HB, Aarnes EK, Vlatkovic L, Lie AK, *et al.* Combined MR Imaging of Oxygen Consumption and Supply Reveals Tumor Hypoxia and Aggressiveness in Prostate Cancer Patients. Cancer Res. 2018 Aug 15;78(16):4774–85.

8. Dewhirst MW, Birer SR. Oxygen-Enhanced MRI Is a Major Advance in Tumor Hypoxia Imaging. Cancer Res. 2016 Feb 15;76(4):769–72.

9. O'Connor JPB, Jackson A, Buonaccorsi GA, Buckley DL, Roberts C, Watson Y, *et al.* Organ-specific effects of oxygen and carbogen gas inhalation on tissue longitudinal relaxation times. Magn Reson Med. 2007 Sep;58(3):490–6.

10. O'Connor JPB, Boult JKR, Jamin Y, Babur M, Finegan KG, Williams KJ, *et al.* Oxygen-Enhanced MRI Accurately Identifies, Quantifies, and Maps Tumor Hypoxia in Preclinical Cancer Models. Cancer Res. 2016 Feb 15;76(4):787–95.

11. Zhou H, Hallac R, Yuan Q, Ding Y, Zhang Z, Xie XJ, *et al.* Incorporating Oxygen-Enhanced MRI into Multi-Parametric Assessment of Human Prostate Cancer. Diagnostics. 2017 Aug 24;7(3):48.

12. van Houdt PJ, Yang Y, van der Heide UA. Quantitative Magnetic Resonance Imaging for Biological Image-Guided Adaptive Radiotherapy. Front Oncol. 2021 Jan 29;10.

13. Dubec MJ, Buckley DL, Berks M, Clough A, Gaffney J, Datta A, *et al.* First-in-human technique translation of oxygen-enhanced MRI to an MR Linac system in patients with head and neck cancer. Radiotherapy and Oncology. 2023 Jun;183:109592.

14. Kooreman ES, van Houdt PJ, Keesman R, Pos FJ, van Pelt VWJ, Nowee ME, *et al.* ADC measurements on the Unity MR-linac – A recommendation on behalf of the Elekta Unity MR-linac consortium. Radiotherapy and Oncology. 2020 Dec;153:106–13.

15. Um H, Tixier F, Bermudez D, Deasy JO, Young RJ, Veeraraghavan H. Impact of image preprocessing on the scanner dependence of multi-parametric MRI radiomic features and covariate shift in multi-institutional glioblastoma datasets. Phys Med Biol. 2019 Aug 21;64(16):165011.

16. Moradmand H, Aghamiri SMR, Ghaderi R. Impact of image preprocessing methods on reproducibility of radiomic features in multimodal magnetic resonance imaging in glioblastoma. J Appl Clin Med Phys. 2020 Jan 27;21(1):179–90.

17. Da-ano R, Masson I, Lucia F, Doré M, Robin P, Alfieri J, *et al.* Performance comparison of modified ComBat for harmonization of radiomic features for multicenter studies. Sci Rep. 2020 Jun 24;10(1):10248.

18. Zheng R ru, Cai M ting, Lan L, Huang XW, Yang YJ, Powell M, *et al.* An MRI-based radiomics signature and clinical characteristics for survival prediction in early-stage cervical cancer. Br J Radiol. 2022 Jan 1;95(1129).

19. Jia Y, Quan S, Ren J, Wu H, Liu A, Gao Y, *et al.* MRI radiomics predicts progression-free survival in prostate cancer. Front Oncol. 2022 Aug 30;12.

20. Ragnum HB, Vlatkovic L, Lie AK, Axcrona K, Julin CH, Frikstad KM, *et al.* The tumour hypoxia marker pimonidazole reflects a transcriptional programme associated with aggressive prostate cancer. Br J Cancer. 2015 Jan 2;112(2):382–90.

21. Ahmed HU, El-Shater Bosaily A, Brown LC, Gabe R, Kaplan R, Parmar MK, *et al.* Diagnostic accuracy of multi-parametric MRI and TRUS biopsy in prostate cancer (PROMIS): a paired validating confirmatory study. The Lancet. 2017 Feb;389(10071):815–22.

22. Norris JM, Simpson BS, Parry MA, Allen C, Ball R, Freeman A, *et al.* Genetic Landscape of Prostate Cancer Conspicuity on Multiparametric Magnetic Resonance Imaging: A Systematic Review and Bioinformatic Analysis. Eur Urol Open Sci. 2020 Jul;20:37–47.

23. Moore CM, Frangou E, McCartan N, Santaolalla A, Kopcke D, Brembilla G, *et al.* Prevalence of MRI lesions in men responding to a GP-led invitation for a prostate health check: a prospective cohort study. BMJ Oncology. 2023 Aug 21;2(1):e000057.

24. Nagy JA, Chang SH, Dvorak AM, Dvorak HF. Why are tumour blood vessels abnormal and why is it important to know? Br J Cancer. 2009 Mar 24;100(6):865–9.

25. Berman RM, Brown AM, Chang SD, Sankineni S, Kadakia M, Wood BJ, *et al.* DCE MRI of prostate cancer. Abdom Radiol (NY). 2016 May;41(5):844–53.

26. Gaustad JV, Hauge A, Wegner CS, Simonsen TG, Lund K V, Hansem LMK, *et al.* DCE-MRI of Tumor Hypoxia and Hypoxia-Associated Aggressiveness. Cancers (Basel). 2020 Jul 20;12(7).

27. Sun Y, Williams S, Byrne D, Keam S, Reynolds HM, Mitchell C, *et al.* Association analysis between quantitative MRI features and hypoxia-related genetic profiles in prostate cancer: a pilot study. Br J Radiol. 2019 Dec;92(1104):20190373.

28. de Mol van Otterloo SR, Christodouleas JP, Blezer ELA, Akhiat H, Brown K, Choudhury A, *et al.* The MOMENTUM Study: An International Registry for the Evidence-Based Introduction of MR-Guided Adaptive Therapy. Front Oncol. 2020 Sep 7;10.

29. Le Bihan D, Breton E, Lallemand D, Aubin ML, Vignaud J, Laval-Jeantet M. Separation of diffusion and perfusion in intravoxel incoherent motion MR imaging. Radiology. 1988 Aug;168(2):497–505.

30. Bäuerle T, Seyler L, Münter M, Jensen A, Brand K, Fritzsche KH, *et al.* Diffusion-weighted imaging in rectal carcinoma patients without and after chemoradiotherapy: a comparative study with histology. Eur J Radiol. 2013 Mar;82(3):444–52.

31. Federau C, Maeder P, O'Brien K, Browaeys P, Meuli R, Hagmann P. Quantitative measurement of brain perfusion with intravoxel incoherent motion MR imaging. Radiology. 2012 Dec;265(3):874–81.

32. Kooreman ES, van Houdt PJ, Keesman R, van Pelt VWJ, Nowee ME, Pos F, *et al.* Daily Intravoxel Incoherent Motion (IVIM) In Prostate Cancer Patients During MR-Guided Radiotherapy—A Multicenter Study. Front Oncol. 2021 Aug 13;11.

33. Chen RC, Chang P, Vetter RJ, Lukka H, Stokes WA, Sanda MG, *et al.* Recommended Patient-Reported Core Set of Symptoms to Measure in Prostate Cancer Treatment Trials. JNCI: Journal of the National Cancer Institute. 2014 Jul;106(7).

34. Efficace F, Fayers P, Pusic A, Cemal Y, Yanagawa J, Jacobs M, *et al.* Quality of patient-reported outcome reporting across cancer randomized controlled trials according to the CONSORT patient-reported outcome extension: A pooled analysis of 557 trials. Cancer. 2015 Sep 15;121(18):3335–42.

35. Fabian A, Domschikowski J, Letsch A, Schmalz C, Freitag-Wolf S, Dunst J, *et al.* Use and Reporting of Patient-Reported Outcomes in Trials of Palliative Radiotherapy. JAMA Netw Open. 2022 Sep 22;5(9):e2231930.

36. Skolarus TA, Dunn RL, Sanda MG, Chang P, Greenfield TK, Litwin MS, *et al.* Minimally Important Difference for the Expanded Prostate Cancer Index Composite Short Form. Urology. 2015 Jan;85(1):101–6.

37. Cozzi S, Finocchi Ghersi S, Bardoscia L, Najafi M, Blandino G, Alì E, *et al.* Linac-based stereotactic salvage reirradiation for intraprostatic prostate cancer recurrence: toxicity and outcomes. Strahlentherapie und Onkologie. 2023 Jun 2;199(6):554–64.

38. Boldrini L, Romano A, Chiloiro G, Corradini S, De Luca V, Verusio V, *et al.* Magnetic resonance guided SBRT reirradiation in locally recurrent prostate cancer: a multicentric retrospective analysis. Radiation Oncology. 2023 May 22;18(1):84.

39. Rosenstein BS, West CM, Bentzen SM, Alsner J, Andreassen CN, Azria D, *et al.* Radiogenomics: Radiobiology Enters the Era of Big Data and Team Science. International Journal of Radiation Oncology*Biology*Physics. 2014 Jul;89(4):709–13.

40. Her EJ, Haworth A, Sun Y, Williams S, Reynolds HM, Kennedy A, *et al.* Biologically Targeted Radiation Therapy: Incorporating Patient-Specific Hypoxia Data Derived from Quantitative Magnetic Resonance Imaging. Cancers (Basel). 2021 Sep 29;13(19):4897.

41. Yang L, Roberts D, Takhar M, Erho N, Bibby BAS, Thiruthaneeswaran N, *et al.* Development and Validation of a 28-gene Hypoxia-related Prognostic Signature for Localized Prostate Cancer. EBioMedicine. 2018 May;31:182–9.

42. Fjeldbo CS, Hompland T, Hillestad T, Aarnes EK, Günther CC, Kristensen GB, *et al.* Combining imaging- and gene-based hypoxia biomarkers in cervical cancer improves prediction of chemoradiotherapy failure independent of intratumour heterogeneity. EBioMedicine. 2020 Jul;57:102841.

43. Fournier L, Costaridou L, Bidaut L, Michoux N, Lecouvet FE, de Geus-Oei LF, *et al.* Incorporating radiomics into clinical trials: expert consensus endorsed by the European Society of Radiology on considerations for data-driven compared to biologically driven quantitative biomarkers. Eur Radiol. 2021 Aug 25;31(8):6001–12.

44. Bibault JE, Giraud P, Housset M, Durdux C, Taieb J, Berger A, *et al.* Deep Learning and Radiomics predict complete response after neo-adjuvant chemoradiation for locally advanced rectal cancer. Sci Rep. 2018 Aug 22;8(1):12611.

45. Ning Z, Luo J, Li Y, Han S, Feng Q, Xu Y, *et al.* Pattern Classification for Gastrointestinal Stromal Tumors by Integration of Radiomics and Deep

Convolutional Features. IEEE J Biomed Health Inform. 2019 May;23(3):1181–91.

46. Shboul ZA, Alam M, Vidyaratne L, Pei L, Elbakary MI, Iftekharuddin KM. Feature-Guided Deep Radiomics for Glioblastoma Patient Survival Prediction. Front Neurosci. 2019 Sep 20;13.

47. Castello A, Castellani M, Florimonte L, Urso L, Mansi L, Lopci E. The Role of Radiomics in the Era of Immune Checkpoint Inhibitors: A New Protagonist in the Jungle of Response Criteria. J Clin Med. 2022 Mar 21;11(6):1740.

Appendix A Ethics approval

Ymchwil Iechyd a Gofal Cymru
Health and Care Research Wales

NHS
Health Research Authority

Dr Ann Henry
Leeds Cancer Centre
St James's University Hospital
Beckett Street
LS9 7TFN/A

Email: approvals@hra.nhs.uk
HCRW.approvals@wales.nhs.uk

04 July 2022

Dear Dr Henry

HRA and Health and Care Research Wales (HCRW) Approval Letter

Study title:	**Reirradiation Options for Previously Irradiated Prostate cancer (RO-PIP): Feasibility randomised clinical trial investigating toxicity outcomes following reirradiation with ultra-hypofractionated external beam radiotherapy vs. high dose rate brachytherapy**
IRAS project ID:	**297060**
REC reference:	**21/YH/0305**
Sponsor	**University of Leeds**

I am pleased to confirm that **HRA and Health and Care Research Wales (HCRW) Approval** has been given for the above referenced study, on the basis described in the application form, protocol, supporting documentation and any clarifications received. You should not expect to receive anything further relating to this application.

Please now work with participating NHS organisations to confirm capacity and capability, in line with the instructions provided in the "Information to support study set up" section towards the end of this letter.

How should I work with participating NHS/HSC organisations in Northern Ireland and Scotland?
HRA and HCRW Approval does not apply to NHS/HSC organisations within Northern Ireland and Scotland.

If you indicated in your IRAS form that you do have participating organisations in either of these devolved administrations, the final document set and the study wide governance report (including this letter) have been sent to the coordinating centre of each participating nation. The relevant national coordinating function/s will contact you as appropriate.